UNIVERSITY OF OKLAHOMA

GRADUATE COLLEGE

A STUDY ON UNSATURATED SOIL-GEOTEXTILE INTERFACE STRENGTH USING MULTI-SCALE LABORATORY TESTS

A DISSERTATION

SUBMITTED TO THE GRADUATE FACULTY

in partial fulfillment of the requirements for the

Degree of

DOCTOR OF PHILOSOPHY

By

DANIAL ESMAILI
Norman, Oklahoma
2014

Downloaded from SHAREOK. Persistent Handle URL: https://hdl.handle.net/11244/13643

A STUDY ON UNSATURATED SOIL-GEOTEXTILE INTERFACE STRENGTH USING MULTI-SCALE LABORATORY TESTS

A DISSERTATION APPROVED FOR THE
SCHOOL OF CIVIL ENGINEERING AND ENVIRONMENTAL SCIENCE

BY

_____
Dr. Kianoosh Hatami, Chair

_____
Dr. Gerald A. Miller

_____
Dr. Amy B. Cerato

_____
Dr. Musharraf Zaman

_____
Dr. Kurt Gramoll

© Copyright by DANIAL ESMAILI 2014
All Rights Reserved.

ACKOWLEDGMENTS

I would like to express my deepest gratitude to my advisor, Dr. Kianoosh Hatami for his valuable discussions and revisions of the materials contained in this Dissertation. Special thanks to my committee members, Dr. Miller, Dr. Cerato, Dr. Zaman and Dr. Gramoll for their precious comments that helped improve the quality of this work and completion of the Dissertation. I would also like to thank my parents and friends. They were always supporting me and encouraging me with their best wishes. I would like to acknowledge the faculty and staff of the School of Civil Engineering and Environmental Science, Mrs. Audre Carter, Mrs. Brenda Clouse, Ms. Molly Smith and Mrs. Susan Williams and funding and support from the Oklahoma Department of Transportation (ODOT), the Oklahoma Transportation Center (OkTC) and TenCate Geosynthetics for this study. Appreciation is also expressed to Dr. Jim Nevels and Mr. Dale Hokett for their valuable help with locating desired soil samples for this study. Contributions of Mr. Michael Schmitz at the Fears Structural Laboratory, Dr. Christopher Ramseyer and undergraduate students: Brandi Dittrich, John Tucker, Kyle Olson, Carlos Chang, Thai Dinh, Jesse Berdis, Chase W. Iddings, Jeremiah C. Kayiza, and Owen D. Watley in this project are also acknowledged.

TABLE OF CONTENT

ABSTRACT		xv
CHAPTER 1	INTRODUCTION	1
1.1.	Background	1
1.2.	Theory	4
1.3.	Extended Mohr-Coulomb Envelope	6
CHAPTER 2	LITERATURE REVIEW	8
2.1.	Pullout and Interface Shear Tests	8
2.2.	MSE Wall and Reinforced Embankment Tests	17
CHAPTER 3	MULTI-SCALE PULLOUT AND INTERFACE SHEAR TESTS	34
3.1.	Large-Scale Pullout Tests	40
3.1.1.	Test Equipment	41
3.1.2.	Test Procedure	42
3.1.2.1.	Processing of the Soil	42
3.1.2.2.	Placement of Soil in Pullout Box	44
3.1.2.3.	Pullout Tests and Dismantling of the Test Setup	45
3.2.	Small-Scale Tests	45
3.2.1.	Small-Scale Pullout Tests	47
3.2.2.	Interface Shear Tests	48
CHAPTER 4	REDUCED-SCALE REINFORCED EMBANKMENT TESTS	49
4.1.	Test Equipment	56
4.2.	Test Procedure	57
4.2.1.	Processing of the Soil	57
4.2.2.	Construction of Embankment Models	60
4.2.3	Loading of Model Embankments and Dismantling of the Test Setup	62
CHAPTER 5	FULL-SCALE REINFORCED EMBANKMENT TESTS	64
5.1.	Test Box	67
5.2.	Test Procedure	69
5.2.1.	Construction of Embankment Model	71
5.2.2.	Loading of Embankment	77
CHAPTER 6	INSTRUMENTATION	80
6.1.	Suction Sensors	80
6.1.1.	Fredlund Sensors	80
6.1.2.	PST-55 Psychrometers	83
6.1.3.	Filter Paper	85
6.1.4.	WP4 Potentiometer	88
6.2.	Soil Moisture Sensors	89
6.3.	Earth Pressure Cells (EPC) and Tactile Sensors	90
6.4.	Piezometers and Glass Beads	91
6.5.	Wire Potentiometers (WPT) and Linear Variable Differential Transformers (LVDT)	92
6.6.	Instrumentation Plan	93
6.6.1.	Large-Scale Pullout Tests	93
6.6.2.	Reduced-Scale Embankments	94
6.6.3.	Full-Scale Embankments	96
CHAPTER 7	LABORATORY RESULTS OF PULLOUT AND INTERFACE SHEAR TESTS	100
7.1.	Large-Scale Pullout Tests	100
7.1.1.	Water Content and Suction	100

7.1.2.	Reinforcement Strain and Interface Strength	105
7.2.	Small-Scale Pullout Tests	118
7.3.	Small-Scale Interface Shear Tests	122
CHAPTER 8	LABORATORY RESULTS OF REDUCED-SCALE EMBANKMENT TESTS	126
8.1.	Soil Gravimetric Water Content and Suction	126
8.2.	Load-Settlement Data	131
8.3.	Strain Distributions	143
CHAPTR 9	RESULTS OF FULL-SCALE REINFORCED EMBANKMENT TEST AND SLOPE STABILITY ANALYSIS	149
9.1.	Gravimetric Water Content (GWC) and Density of Embankment Soil	149
9.2.	Load-Settlement and EPC Data	153
9.3.	Embankment Deformation	156
9.4.	Slip Surface and Strain in Geotextile Reinforcement Layers	158
9.5.	Slope Stability Analysis	164
9.5.1.	Stability Analysis using GSTABL	164
9.5.2.	Stability Analysis using FLAC/SLOPE	166
9.6.	Results	167
9.6.1.	Embankment Model at OMC-2%	167
9.6.2.	Embankment Model at OMC+2%	173
CAHPTER 10	INPLICATION OF STUDY RESULTS TO DESIGN: MOISTURE REDUCTION FACTOR	176
CHAPTER 11	CONCLUSIONS AND RECOMMENDATIONS	181
11.1.	Conclusions	181
11.2.	Recommendations for Future Work	183
CHAPTER 12	REFERENCES	185
APPENDIX I	PRELIMINARY STABILITY ANALYSIS FOR REDUCED-SCALE AND LARGE-SCALE EMBANKMENT MODELS	194

LIST OF FIGURES

Figure 1.1.	A failed embankment in US Route 62, Chickasha, Oklahoma	1
Figure 3.1.	Excavation pit where soil samples were taken from the failed slope in Chickasha, OK	34
Figure 3.2.	Gradation curve of Chickasha soil. Note: the vertical broken line shows the location of #200 sieve	35
Figure 3.3.	Compaction test results for Chickasha soil used in pullout and interface tests	37
Figure 3.4.	SWCC for Chickasha soil using WP4 Potentiometer	38
Figure 3.5.	GWC vs. total suction for Chickasha soil on semi-log plot (pF is the base 10 logarithm of the suction expressed in cm of water)	39
Figure 3.6.	One of the pullout test boxes at the OU Fears laboratory	42
Figure 3.7.	Soil processing equipment at the OU Fears laboratory, (a, b) soil processors, (c) soil mixer	43
Figure 3.8.	(a) Sealed buckets containing processed soil before placing in the pullout box, (b) soil samples in the oven to determine their moisture content	44
Figure 3.9.	(a) Sealed compacted soil at the end of large-scale pullout box setup, (b) Geotextile specimen at the mid-height of the pullout box	45
Figure 3.10.	Small-scale pullout tests in Chickasha soil using a DST machine	47
Figure 4.1.	Soil sampling locations on U.S. Route 62 Chickasha, OK; (a) cross section 2770, (b) cross section 2780, and (c) cross sections 2790 and 2800	51
Figure 4.2.	Gradation curves for the soil samples taken from CS 2780 (different depths) as compared to that of the Chickasha soil (failed embankment slope used in pullout and interface tests). Note: The vertical broken line shows the location of #200 sieve	52
Figure 4.3.	SWCC for the test soil using WP4 Potentiometer as compared to the original soil from a failed embankment in Chickasha, OK. Note: Red dashed lines show the OMC-2% and OMC+2% lines for the test soil	54
Figure 4.4.	Compaction test results for clay (i.e. CS 2780) as compared to the original Chickasha soil	55
Figure 4.5.	Test box and self-reacting loading frame fabricated for the reduced-scale reinforced embankment tests	57
Figure 4.6.	Soil processing for reduced-scale embankment tests using a crusher-sifter machine	58
Figure 4.7.	(a) Mixing of soil to reach target gravimetric water content, (b) sealed buckets containing processed soil before constructing the model embankment in the test box	59
Figure 4.8.	(a) Sealing of model embankments during construction to preserve their water content, (b) trimmed slope of the model embankment before applying the footing loading on the top	61
Figure 4.9.	Placing the hydraulic cylinder at the center of footing and	62

reaction beam in embankment tests
Figure 5.1. Soil deposit at Fear laboratory for full-scale reinforced embankment tests 65
Figure 5.2. (a) Gradation curve from sieve analysis and hydrometer tests on sand, (b) Maximum dry unit weight and OMC of sand from modified proctor test. Note: Dashed line in 'a' indicates the location of Sieve# 4 66
Figure 5.3. Test box and loading frame fabricated for the full-scale reinforced embankment tests; (a) mounting the loading frame, (b) ramp for transporting soil to the test box using front loader 69
Figure 5.4. Preparing the soil for full-scale embankment test constructed at OMC-2%: (a) Taking GWC sample for oven-drying method, (b) Mixing the soil with SUPER GEL-X and water, (c) Covering the mixed soil to reach equilibrium before placing inside the test box 71
Figure 5.5. (a) Placement of the soil in the test box, (b) Compaction of the prepared soil 72
Figure 5.6. (a) Location of moisture and density samples in each compacted lift using a reference grid, (b) Tube sampling for density measurement, (c) Rubber balloon method for density measurement; Note: All dimensions in (a) are in "mm". 74
Figure 5.7. Covering the embankment with tarp and plastic sheet to avoid losing moisture content and reach moisture equilibrium 75
Figure 5.8. (a) Trimming the embankment's facing, (b) Locations of reference plates on the slope 76
Figure 5.9. Preparing loading beam for the test. (a) Leveling off under the beam, (b) Moving the beam to the test box using forklift, and (c) Location of loading beam from the embankment crest 78
Figure 5.10. Hydraulic cylinders and load cells used for embankment test 79
Figure 6.1. Fredlund sensors placed in a calibration bucket to measure matric suction of the Chickasha soil 81
Figure 6.2. Schematic cutaway section indicating the locations of Fredlund sensors in the calibration bucket 82
Figure 6.3. Soil suction versus GWC for Chickasha soil from Fredlund sensors. Note: The vertical lines indicate the mean values of measured GWC in each test 82
Figure 6.4. (a) A PST 55 sensor submerged in NaCl solution; (b) Sensor calibration setup 84
Figure 6.5. Variation of GWC and total suction for Chickasha soil from filter paper tests 87
Figure 6.6. WP4 Water Potentiometer equipment (soil samples in sealed cups are shown in the inset) 88
Figure 6.7. Piezometer placed in the 2nd lift of the model embankment to measure possible changes in the soil pore water pressure 91
Figure 6.8. LVDT used to measure facing deformation of reduced-scale embankments 92
Figure 6.9. Schematic diagram of the large-scale pullout test box setup (not 93

to scale). Notes: (1) Black and white circles represent the locations of PST-55 sensors and soil samples for the WP4 sensor, respectively; (2) The distance between the sensors and the interface is 25 mm; (3) The sleeves above and below the geotextile layer are 200 mm wide

Figure 6.10. (a) Wire-line extensometers attached to the geotextile reinforcement (the numbers in the figure indicate the extensometer number and distance from the tail end of the geotextile); (b) Earth pressure cell placed on the top of the soil in the pullout test box 94

Figure 6.11. Instrumentation plan for reduced-scale reinforced embankment tests; (a) cross sectional view, (b) plan view. Note: (1) numbers in bracket in (a) indicate the numbers of each sensors used in each test. (2) H, V, P and C in (a) stand for “horizontal”, “vertical”, “plan view” and “cross-sectional view”. (3) The distances between WP #1-WP #2 and WP #5-WP #6 are 65 mm and those between all other WPs are 90 mm. (4) datum for the reported elevations is the bottom of the test box. (5) All dimensions are in “mm”, (6) Dimensions and locations of sensors are not in scale 96

Figure 6.12. (a) WPTs installed at the back of the test box to measure geotextile local displacements, (b) WPT used for footing settlement measurements 97

Figure 6.13. Instrumentation plan for full-scale reinforced embankment test; Note: (1) All dimensions are in “mm”, (2) Length of reinforcement layers throughout the embankment is uniform and equal to 1500 mm, (3) WPs were attached at an equal distance over the length of each reinforcement, (4) Dimensions and locations of sensors are not in scale 99

Figure 7.1. Distributions of soil GWC with depth in the pullout box for different pullout test cases. Notes: (1) One soil sample was taken from each bucket to test its GWC value; (2) The number of soil samples from each soil lift in the pullout box is given in Table 7.3 (caption); (3) The horizontal line indicates the target GWC for each test case; (4) The vertical dashed line shows the location of the soil-geotextile interfaces; (5) The mean and COV values reported in the legends are calculated for the fifth layer (i.e. soil-geotextile interface) data only 101

Figure 7.2. Distributions of the soil suction with depth in the pullout box from WP4 at different GWC. The number of soil samples from each soil lift in the pullout box is reported in Table 7.3 103

Figure 7.3. Axial strain distributions in geotextile reinforcement subjected to pullout load from large-scale pullout tests on Chickasha soil at different GWC and overburden pressure values 108

Figure 7.4. Pullout test data and interface strength results from large-scale pullout tests for Chickasha soil at different GWC values: (a)-(c) load-displacement data; (d) failure envelopes for the soil- 111

geotextile interface on frontal plane; (e) failure envelopes for soil-geotextile interface on lateral plane. Note: in (a), dashed line indicates the estimated pullout failure
Figure 7.5. Extended Mohr-Coulomb envelope from large-scale pullout tests 114
Figure 7.6. Pullout parameters for HP370 geotextile from large-scale pullout tests at OMC+2% subjected to 50 kPa overburden pressure: (a)-(b) pullout force versus actuator and extensometer displacement, respectively, (c)-(e) procedure to determine F* and α; Note: In (c), solid and dashed lines indicate actual and interpolated data, respectively. 117
Figure 7.7. Pullout test data and interface strength results from small-scale tests for Chickasha soil and comparison of failure envelopes for soil-geotextile interface at different GWC values: (a)-(c) load-displacement data; (d) failure envelopes for soil-geotextile interface on frontal plane; (e) failure envelopes for soil-geotextile interface on lateral plane. Note: suction values were calculated from the SWCC 120
Figure 7.8. Mohr-Coulomb envelopes for Chickasha soil-geotextile interface from interface shear tests: (a) envelopes on the frontal plane; (b) envelopes 123
Figure 7.9. Extended Mohr-Coulomb envelope from small-scale pullout and interface shear tests 124
Figure 7.10. Comparison of large-scale and small-scale pullout and interface test data 124
Figure 8.1. GWC data within the embankment models constructed with HP570 geotextile reinforcement from oven-drying method and PST-55 psychrometers; (a) Test case at OMC-2%, (b) Test case at OMC and (c) Test case at OMC+2%. Notes: (1) Red dashed line shows the target GWC value, (2) Six (6) samples were taken from each layer to determine an average GWC value before compaction, (3) Three (3) random samples were taken immediately after compaction of 2-3 layers of embankment 128
Figure 8.2. Placement of the sensors before compaction of the layer 129
Figure 8.3. Average GWC data from EC-5 sensors in model embankments constructed with HP570 reinforcement and at different GWC values; (a) OMC-2%, (b) OMC, (c) OMC+2%. Note: The vertical and horizontal lines indicate the time when the loading started and target GWC, respectively. 130
Figure 8.4. Load- settlement data for test soil at different GWC values (OMC-2%, OMC, OMC+2%). Note: For all test cases without distinct failure behavior after the last load-settlement data, the load started to decrease significantly and it was not possible to reach the target value again. 133
Figure 8.5. . Displacements recorded during the embankment tests reinforced with HP370; (a) Lateral displacement of the test box near the top of the embankment, (b) Vertical displacement of the 134

embankment near the footing
Figure 8.6. Horizontal displacements of facing recorded during the embankment tests reinforced with HP570; (a) OMC-2%, (b) OMC (c) OMC+2% 135
Figure 8.7. Comparison of measured and theoretical predicted incremental stresses due to the strip footing loading at selected locations in model embankments reinforced with HP370 (Hatami et al. 2014; Chan, E., 2014): (a) OMC-2% performed on 04/04/2013, (b) OMC performed on 04/22/2013 137
Figure 8.8. Comparison of the measured and theoretical predicted (Boussinesq method) incremental stresses due to the strip footing loading at selected locations in model embankments reinforced with HP570: (a) OMC-2% performed on 11/04/2013, (b) OMC performed on 12/12/2013 and (c) OMC+2% performed on 09/18/2013 139
Figure 8.9. History of incremental earth pressures in the model embankment subjected to footing loading constructed with HP570 at OMC-2% performed on 11/04/2013 141
Figure 8.10. Changes in pore water pressure as recorded by piezometers during surcharge loading (Hatami et al. 2014; Chan, E., 2014): (a) OMC-2% performed on 04/04/2013, (b) OMC performed on 04/22/2013 142
Figure 8.11. Wire-line extensometers attached to geotextile reinforcement to measure geotextile strains 143
Figure 8.12. Failure planes observed in model embankments; (a)-(b) Comparison of failure plane geometries as traced after excavation of failed block at the end of test for model embankments with HP370 and HP570, respectively, (c) Traces of failure planes #1 and #2 in the test case at OMC-2% built with HP370 reinforcement, (d) Front view of failed slope at embankment model reinforced with HP370 and built at OMC-2% after the test 146
Figure 8.13. Failure wedge in the tested model embankments; (a) Front view of the displaced soil block in the test case at OMC, (b) Partially excavated failure wedge for embankment at OMC-2%. 147
Figure 8.14. Strain distributions in the geotextile reinforcement at different model embankments 148
Figure 9.1. Distribution of GWC within the embankment model, (a) Immediately after compaction of each lift, (b) Before placing next lift. Note: Horizontal dashed line indicates target GWC value 150
Figure 9.2. Average GWC data from EC-5 sensors in the large-scale model embankment constructed at OMC-2%; (a) Construction and loading stages, (b) Loading stage only. Note: The vertical and horizontal lines indicate the time when the loading started and the target GWC value, respectively 151

Figure 9.3.	Density data in the model embankment after compaction of each lift	152
Figure 9.4.	Load-settlement response of the large-scale reinforced model embankment constructed at OMC-2%	153
Figure 9.5.	Earth pressure data in the model reinforced embankment constructed at OMC-2%, (a) During construction, (b) During surcharge loading	155
Figure 9.6.	Measured settlements of the embankment top surface near the footing during surcharge loading	156
Figure 9.7.	Facing deformation of embankment constructed at OMC-2% as measured using reference plates, (a) Load-deformation data, (b) Facing profile	158
Figure 9.8.	Failure plane geometry as traced after careful excavation of the failed block at the end of the test. Note: all dimensions are in "mm".	159
Figure 9.9.	Failure wedge for the embankment model tested at OMC-2%; (a) Initiation of slip plane on embankment surface, (b) Excavated part of failure wedge above the fourth layer of geotextile, (c) Continuation of slip plane underneath the fourth geotextile layer and (d) Excavated part of slip plane shown in "c" which slid over the third layer of geotextile	161
Figure 9.10.	(a) Moving construction equipment out of the test box using a forklift, (b) Digging the soil around sensors during the excavation phase after surcharge loading was completed	162
Figure 9.11.	Local displacement of the top (fourth) geotextile layer as measured using 5 wire potentiometers; Note: Black, red, green and blue indicate the footprint of the loading beam at 1st, 2nd, 3rd and 4th geotextile elevations	163
Figure 9.12.	Slope stability analysis of embankment model constructed at OMC-2% using GSTABL: (a) Model geometry, (b) Critical slip surface and factor of safety for reinforced embankment and (c) Critical slip surface and factor of safety for unreinforced embankment	170
Figure 9.13.	Slope stability analysis using FLAC/SLOPE, (a) Embankment geometry (b) Critical slip plane (FS= 1.24)	172
Figure 9.14.	Predicted slip plane and factor of safety for the embankment model constructed at OMC+2% from GSTABL analysis	174
Figure 9.15.	Slip plane and bearing capacity of the embankment model constructed at OMC+2% from GSTABL analysis to reach the factor of safety equal to 1.086. Note: White circles on the facing slope indicate the initiation points of possible slip planes formed within the large-scale embankment in GSTABL model	175
Figure 10.1.	Moisture reduction factor for the woven geotextile in Chickasha soil: (a) Large-scale pullout tests; (b) Small-scale pullout tests; (c) Small-scale interface shear tests	178
Figure 10.2.	Moisture reduction factors for the embankment models	179

constructed with HP370 and HP570 geotextile reinforcement
Figure 10.3. MRF values as a function of soil, geotextile and soil type. Note: The MRF values were determined for the moisture content changes from OMC-2% to OMC+2% (i.e. SC $_{pullout/interface}$: 10.6 to 14.6%; ML $_{pullout/interface}$: 10.7 to 14.7%, CL $_{pullout/interface}$: 16 to 20% and CL $_{embankment}$: 12.9 to 16.9%) 180
Figure A-1. Stability analysis of a 45°- reduced-scale reinforced embankment slope; (a) Model at the end of construction, (b) Slip plane geometry in the embankment with cohesion = 10 kPa and friction angle : 30°, (c) Slip plane geometry in the embankment with cohesion = 30 kPa and friction angle : 5° 195
Figure A-2. Stability analysis of a 69.5°- reduced-scale reinforced embankment slope; (a) Model at the end of construction, (b) Slip plane geometry in the embankment with cohesion = 20 kPa and friction angle : 27° 196
Figure A-3. Stability analysis of a MSE wall and embankment models (cohesion: 60 kPa, friction angle: 25°); (a)-(b) MSE wall at the end of construction and slip plane geometry (uniform vertical geotextile spacing: 150 mm), (c)-(f) Embankment at the end of construction and slip plane geometry (non-uniform vertical geotextile spacing: 100 mm at top and 850 mm at bottom), (g)-(j) Embankment at the end of construction and slip plane geometry (non-uniform vertical spacing: 100 mm at top and 300 mm at bottom) 201
Figure A-4. Modeling outdoor test box in Frame 3-D program, (a) Box dimensions, (b) Box deflections 203

LIST OF TABLES

Table 2.1.	Summarized literature review performed for this study	31
Table 3.1.	Summary of Chickasha soil properties used in pullout and interface tests	35
Table 3.2.	Summary of McKeen (1992) Expansive Soil Classification Methodology	39
Table 3.3.	Physical and mechanical properties of HP370	40
Table 3.4.	Large-scale pullout test parameters	41
Table 3.5.	Small-scale pullout and interface test parameters	46
Table 4.1.	Properties of the soil sample taken from CS 2780 as compared to those of the original Chickasha soil	53
Table 4.2.	Comparison of HP370 and HP570 properties	55
Table 4.3.	Test information for reduced-scale reinforced embankments	56
Table 5.1.	Physical and mechanical properties of blended sand-SUPER GEL-X used in this study	67
Table 6.1.	Total suction for Chickasha soil from filter paper test	86
Table 7.1.	Mean and COV values for the GWC and suction in the fifth layer (in contact with geotextile) in large-scale pullout tests	104
Table 7.2.	Comparison of suction values in Chickasha soil as measured using psychrometers (in-situ) and WP4 (offsite equipment)	104
Table 7.3.	Interface strength properties from large-scale pullout tests in Chickasha soil	112
Table 7.4.	Calculated values of α F^* from large-scale pullout tests in Chickasha soil	115
Table 7.5.	Interface strength properties from small-scale pullout tests	121
Table 7.6.	Summary of the results from all pullout and interface tests performed in this study	125
Table 8.1.	Maximum and failure footing load for embankment models constructed at different GWC	132
Table 9.1.	Reduced-scale pullout test data and MRF values for the large-scale reinforced embankment soil and HP370 geotextile reinforcement at different overburden pressures	165
Table 9.2.	Input parameters used in the GSTABL stability analysis	166
Table 9.3.	Input parameters for FLAC analysis	166
Table A-1.	Results of structural design for outdoor test box	203

ABSTRACT

The performance of marginal soils and their interface with geosynthetic reinforcement can be complex under construction or service loading conditions and may include excessive deformations and loss of strength as a result of wetting. Therefore, design procedures for reinforced soil structures need to take into account the influence of suction on the strength and deformation characteristics of the soil, soil-geosynthetic interface and the resulting factors of safety against failure. Such design provisions are currently not available for reinforced soil structures constructed with marginal soils.

This study presents descriptions and results of multi-scale pullout and interface shear tests on a woven polypropylene (PP) geotextile reinforcement material in a marginal quality soil to develop a moisture reduction factor (MRF) for the pullout resistance equation in the currently available design guidelines. In addition, three (3) 1m-high indoor model embankments and one (1) 1.5 m-high and significantly wider outdoor model reinforced soil embankment were constructed at three different gravimetric water content (GWC) values to study their performance and to determine the MRF value in actual embankment configurations.

All the tests described above were carried out using a lean clay at different gravimetric water content (GWC) values ranging between OMC-2% and OMC+2% and were reinforced with woven polypropylene geotextile reinforcement (OMC: Optimum Moisture Content). The embankment models were instrumented with a total of 67 sensors to measure the soil GWC, matric suction and excess pore pressure,

reinforcement strains, earth pressure, and deformations of the embankment models and the test box during the tests.

Results of the pullout, interface tests and embankment models indicate that the reinforcement interface strength and pullout resistance could decrease significantly as a result of the loss in matric suction (e.g. by 42% in pullout/interface tests and 74% in embankment models). It is concluded that wetting of the soil-geotextile interface during construction or service life of a reinforced soil structure can measurably reduce the interface strength and pullout resistance of the geotextile reinforcement resulting in lower factors of safety for their stability which needs to be accounted for in design. Results of the study will be also useful to estimate the difference in the pullout capacity and interface shear strength of geotextile reinforcement in a marginal soil when placed at different GWC values during construction.

CHAPTER 1

INTRODUCTION

1.1. Background

Oklahoma Department of Transportation (ODOT) and other departments of transportation across the U.S. are faced with a persistent problem of landslides and slope failures along the highways. Repairs and maintenance work due to these failures are extremely costly (i.e. in millions of dollars annually nationwide). In Oklahoma, many of these failures occur in the eastern and central parts of the state due to higher topography and poor soil type (Hatami et al. 2010a,b, 2011). A recent example of these failures is the landslide on the US Route 62 in Chickasha, Oklahoma (Figure 1.1).



Figure 1.1. A failed embankment in US Route 62, Chickasha, Oklahoma

For proper construction or repair of highway slopes and embankments, an ideal solution would be to work with large quantities of coarse-grained, free-draining soils to stabilize

the structures as recommended by design guidelines and specifications for Mechanically Stabilized Earth (MSE) structures in North America (e.g. Elias et al. 2001, Berg et al. 2009). However, coarse-grained soils are not commonly available in Oklahoma and many other parts of the U.S. Consequently, the costs of the fill material and its transportation can be prohibitive depending on the location of the high-quality soil.

One possible solution in such cases would be to use locally available soils as construction materials because they would require significantly less material transportation, fuel consumption and generated pollution compared to using high-quality offsite soils. It has been estimated the fuel costs constitute about 20% of the total costs for transportation of high-quality soil (Ou et al. 1982). On the other hand, commonly available soils in Oklahoma for the construction of reinforced slopes are of marginal quality (e.g., soils with more than 15% fines). Geosynthetic reinforcement can be used to stabilize marginal soils. Using the Mechanically Stabilized Earth technology (MSE) could help reduce the cost of fill material by up to 60% (Keller 1995). However, in order to reinforce earthen structures involving marginal soils, it is important to obtain a satisfactory soil-reinforcement interface performance. The performance of marginal soils and their interface with geosynthetic reinforcement can be complex under construction or service loading conditions and may include strain softening behavior, excessive deformation and loss of strength as a result of wetting.

An important consideration in the design of reinforced soil structures constructed with marginal soils is the possibility of reduction in interface shear strength and/or pullout resistance due to the increase in the soil moisture content (wetting), loss of matric suction and possible development of excess pore water pressure. This can result in

excessive deformations and even failure of the reinforced soil structure. As a result, the design procedures need to take into account the influence of soil moisture content and suction on soil strength, the strength of soil-geosynthetic interface and the resulting factor of safety against failure. Such design provisions are currently not available for reinforced soil structures constructed with marginal soils. Typically, construction materials for reinforced soil structures are tested at moisture content values near optimum (i.e. Optimum Moisture Content - OMC). However, in actual construction, several factors could make the fill moisture content deviate from the design value. Examples include precipitation during construction, groundwater infiltration and development of excess pore water pressure due to compaction. These factors, in addition to seasonal variations of soil moisture content, can significantly reduce the strength of the soil-reinforcement interface and lead to excessive deformations or failure. A primary objective of this study is to develop a moisture reduction factor (MRF) for the pullout resistance and interface shear strength of soil-geotextile interface for the design of reinforced soil structures with marginal soils.

It should be noted that this study is not intended to substitute the need for an adequate and properly located and constructed drainage system in reinforced soil structures and slopes. In addition, quality control and quality assurance in both design and construction of these structures are obviously required. In order for reinforced soil structures with marginal soils to be safe and provide satisfactory performance, a number of crucial factors need to be included in their design and construction including proper drainage systems, quality control during compaction (i.e. placement moisture content and

density), small spacing between reinforcement layers and relatively low construction speed to avert the consequences of loss of suction in the backfill.

1.2. Theory

For internal stability of reinforced soil structures, pullout resistance of the reinforcement, P_r, and interface shear strength of soil and reinforcement (τ) are determined using Equations 1.1 and 1.2, respectively:

$$P_r = F^* \alpha \sigma'_v L_e C \quad (1.1)$$

$$\tau = c_a + (\sigma'_n - u_a) \tan\delta' \quad (1.2)$$

Where:

L_e: Embedment or adherence length in the resisting zone behind the failure surface (m)

C: Reinforcement effective unit perimeter; e.g., C = 2 for strips, grids, and sheets

$L_e\ C$: Total surface area per unit weight of reinforcement in the resistive zone behind the failure surface

$F^* = \tan \delta_{peak}$: Pullout resistance factor

δ_{peak}: Equivalent peak friction angle of the soil-geosynthetic interface (°)

α: A scale effect correction factor to account for a nonlinear stress reduction over the embedded length of highly extensible reinforcements

$\sigma_v^{'}$: Effective vertical stress at the soil-reinforcement interface (kPa)

σ_n: Normal stress on the interface (kPa)

c_a: Interface adhesion at specific suction (kPa)

u_a: Pore air pressure

$\delta^{'}$: The angle of friction between soil and reinforcement with respect to $(\sigma_n^{'} - u_a)$

Pullout tests are typically used to obtain the parameters α and F^* for different reinforcement materials. The correction factor α depends on the extensibility and the length of the reinforcement. For extensible sheets (i.e., geotextiles), the recommended value of α is 0.6 (Berg et al. 2009). The parameter F^* (especially in reinforcement types such as geogrids and welded wire mesh) includes both passive and frictional resistance components (e.g., Palmeira 2004, Abu-Farsakh et al. 2005, Berg et al. 2009).

The hypothesis of this study is that changes in matric suction and gravimetric water content due to wetting of the soil-reinforcement interface could significantly influence the interface strength and the reinforcement pullout capacity as determined from Equations 1.1 and 1.2. Depending on the type of failure in reinforced soil structures (i.e. pullout failure or sliding over the length of reinforcement), a moisture factor, μ(ω), needs to be included in the above equations to account for the influence of gravimetric water content and suction on the unsaturated soil-reinforcement interface strength (Equation 1.3 and 1.4):

$$P_{rOMC+2\%} = [F^{*} \alpha \, \sigma'_{v} \, L_e \, C]_{OMC-2\%} \, \mu(\omega) \quad (1.3)$$

$$\tau_{OMC+2\%} = [c_a + (\sigma_n^{'} - u_a) \, tan\delta']_{OMC-2\%} \, \mu(\omega) \quad (1.4)$$

The main objective of this study was to determine moisture reduction factors from multi-scale interface and embankment tests for use in stability analysis of reinforced soil walls and slopes. A series of moisture reduction factors has been produced for a selection of Oklahoma soils and two different woven geotextile reinforcement materials as described in detail in this dissertation. However, the methodology and discussions described herein can be used for a wider selection of soils and reinforcement materials in order to account for the influence of the soil gravimetric water content and suction on the soil-reinforcement interface strength and stability of reinforced soil structures involving marginal soils.

1.3. Extended Mohr-Coulomb Envelop

The shear strength of an unsaturated soil depends on two stress variables: net normal stress ($\sigma_n - u_a$) and soil matric suction ($u_a - u_w$) (Fredlund et al. 1978). Net normal stress is the difference between the total stress and pore air pressure, and the matric suction is the difference between the pore air and the pore water pressures. This theory is also valid for dry and saturated soil conditions. Miller and Hamid (2005) proposed the following equation to determine the shear strength of unsaturated soil-structure interfaces:

$$\tau = C'_a + (\sigma_n - u_a) \, tan \, \delta' + (u_a - u_w) \, tan \, \delta^b \quad (1.5)$$

Where:

$C_a^{'}$: Adhesion intercept

u_w: Pore water pressure

δ^b: The angle of friction between soil and reinforcement with respect to suction $(u_a - u_w)$

In the case of an unsaturated soil, Mohr circles representing failure conditions correspond to a 3D failure envelope, where the shear stress (τ) is the ordinate and the two stress variables are the abscissas $(\sigma_n - u_a)$ and $(u_a - u_w)$. The locations of the Mohr circles in the third dimension are functions of matric suction $(u_a - u_w)$. The planar surface formed by these two stress variables is called the extended Mohr-Coulomb failure envelope.

CHAPTER 2

LITERATURE REVIEW

A survey of related literature was carried out for this study and salient findings are summarized in this section.

2.1. Pullout and Interface Shear Tests

Palmeira (1987) performed a series of direct shear and pullout tests to investigate the interaction between sand and reinforcement. The results showed that the reinforcement caused a significant increase in the shear resistance as compared to unreinforced sand. It was also observed that when the reinforcement direction coincides with the direction of minor principal strain, shear strains in the central region were limited. The results showed that the friction on the front wall of the box in pullout tests could severely affect pullout test results.

Chua et al. (1993) carried out pullout tests on silty sand and clay with geogrid. Their results indicated that the degree of saturation had a significant influence on the soil-reinforcement interface strength in both soils. The interface strength in wet silty sand (SP) and clay (CL) was reduced by as much as 50% and 25%, respectively, compared to the values in relatively dry conditions.

Adanur et al. (1994) investigated the effects of normal pressure and strain rate on pullout capacity of three woven and four non-woven geotextiles in different granular soils. The study concluded that for woven geotextiles at the slow test rate, the peak

pullout capacity occurred at the higher displacement. The results also showed that the woven fabric's ultimate strength and displacement at failure increased as the test displacement rate decreased. It was also observed that the fine particle soils had higher soil/non-woven fabric cohesion components and lower frictional components as compared to coarser soils.

Interface frictional characteristics of non-woven geotextiles buried in Sabkha (a problematic soil in Arabian Gulf) and sand was studied by Muhammad Ali (1999). The pullout tests showed that the strength of Sabkha decreased as the moisture content of the reinforced soil matrix increased. The results also indicated that the geotextile with high tensile strength resulted in a large pullout force as the interface was sand-geotextile-sand, while the Sakhba-geotextile-sand interface led to maximum pullout force for the least extensible geotextile.

Ellithy and Gabr (2000) performed a series of direct shear test on kaoline clay to study the effect of compaction moisture on geomembrane-clay interface strength. Their results indicated that in both unconsolidated undrained and consolidated undrained direct shear tests, the interface shear strength decreased by 60% and 37%, respectively, as the water content increased from dry side of optimum (i.e. 28%) to wet side of optimum (i.e. 32%).

Goodhue et al. (2001) carried out small-scale direct shear tests, large-scale multistage interface shear tests and pullout tests using foundry sands reinforced with three geosynthetics (i.e., geotextile, geogrid and geomembrane) to investigate interaction mechanisms between soil and geosynthetics. It was observed that bentonite content of

the sands did not affect the interface friction angle for both as-compacted and drained conditions. The effect of fines content on interface adhesion depended on the drainage condition and the type of geosynthetic. For the drained condition, the interface adhesion decreased slightly with increasing the fines content, while the as-compacted interface showed an increase in adhesion with increasing fine content.

Ling et al. (2001) studied the interaction between plastic soils (i.e., with the plastic limit of 35% to 100%) and a polyvinyl chloride geomembrane with a smooth or textured surface using a direct shear apparatus under as-compacted conditions. The results indicated that the interface adhesion and angle of friction increased for plasticity index up to 70% and then started decreasing. It also was reported that for peak strength the adhesion was larger as compared to the residual strength and it was reversed for the angle of friction. The results also indicated that at the residual strength, the smooth and textured surfaces of the geomembrane showed little difference.

Hossain and Inoue (2002) performed a series of laboratory pullout tests using geosynthetic and wire mesh to evaluate the soil-reinforcement interaction mechanisms. The results showed that the pullout stress increased with displacement and normal stress. The results also showed that the vertical displacement increased with an increase in horizontal displacement, especially at higher normal pressures. The results also indicated that for soil structure with clay, the use of geosynthetic is more suitable than wire mesh.

Mohiuddin (2003) analyzed soil-geosynthetic interactions in a marginal soil using laboratory and field pullout tests on different geotextiles and geogrids. The study

concluded that the coefficient of interaction was higher in high strength geogrids as compared to weaker geogrids. The study showed that the coefficient of interaction increased as the confining pressure and geotextile length decreased. According to Mohiuddin (2003), the maximum average shear stress happened in the frontal part of the fabric and decreased along the length of the fabric.

Interaction properties of geosynthetic in a marginal silty clay soil were studied by Farrag and Morvant (2004). Field and laboratory pullout tests were carried out on four types of geogrids and three types of geotextiles to investigate the effects of geosynthetic length and confining pressure. Pullout tests in the field indicated that pullout capacity increased with an increase in specimen length and confining pressure.

Lee and Bobet (2005) carried out pullout tests in clean sand, 5% silty sand, 10% silty sand, 15% silty sand and 35% silty sand under both drained and undrained conditions using steel inclusions. Their results showed that reinforcement pullout capacity for all overburden pressures decreased significantly under undrained conditions due to development of excess pore pressures in the soil subjected to rapid loading. In addition, undrained tests resulted in smaller initial stiffness values, and the maximum pullout capacity occurred at smaller displacements when compared to otherwise identical drained tests. Lee and Bobet (2005) found that the reinforcement pullout capacity consistently decreased as the silt content of the sand increased.

Niemiec (2005) investigated the soil-geosynthetic interface properties for three different soil types (i.e., sand, silt and clay) and three geosynthetic materials using direct shear and pullout tests. The results showed that moisture content, geosynthetic type, normal

stress and soil properties had effects on soil-geosynthetic interface behavior. The direct shear test results indicated that the friction angle for the sand-geosynthetic interface was close to that of the sand-sand interface and was not affected by the tensile strength of the geosynthetic. The pullout test results showed that shear stress values increased with increases in normal stress. Also, the pullout test data showed that the interface friction angle increased as the tensile strength of the geosynthetic increased and the clay content of the soil decreased. The research also indicated that the failure shear stress decreased as the clay content of the soil increased.

Zornberg and Kang (2005) carried out a study on the pullout capacity of geosynthetic reinforcement with in-plane drainage capability for marginal soils. They compared the pullout behavior of a nonwoven geotextile and a geogrid with and without drainage capability. Their results indicated that reinforcement materials with in-plane drainage capability provided a significantly higher pullout capacity as compared to those without drainage function.

Abu-Farsakh et al. (2007) performed an extensive laboratory testing program using a large direct shear test apparatus to investigate the effect of soil moisture content and dry density on cohesive soil-geosynthetic interface strength. Four different soils were reinforced with three different geogrids and a woven geotextile. The results showed that the increase in soil moisture content or decrease in dry density caused an appreciable reduction in interface shear strength.

Sharma et al. (2007) conducted a series of laboratory tests to measure unsaturated soil-geomembrane interface shear strength parameters. A miniature pore-pressure transducer

was installed at a silty sand-geomembrane interface to record suction during the shearing process. The results indicated that the soil suction contributed to the mobilization of shear stress at the interface at low normal stress because the suction caused the effective normal stress to be higher than total stress, resulting in a higher interface shearing strength. However, at higher normal stresses, the shearing process was governed only by the magnitude of the total normal stress.

Bergado et al. (2008) performed pullout tests to evaluate the interface parameters of reinforced silty sand and weathered clay with geotextile and compared the results with the assumption of uniform shear stress distribution. The results showed that the distributions of shear stress along the interface were highly non-uniform. Hence, the conventional interpretation methods based on uniform shear stress distribution assumption would not yield the correct parameters for soil-geotextile interface. The research concluded that the conventional method underestimated both shear stiffness and shear strength at the soil-geotextile interface.

Chandrakaran et al. (2008) conducted pullout tests to evaluate the frictional and bearing resistance of woven geotextiles based on the spacing of yarns in warp and weft directions. The results showed that the spacing of warp and weft yarns influenced both interface friction and passive resistance. It was also observed that the contribution to total pullout resistance of warp yarns was higher than the weft yarns.

Subaida et al. (2008) performed a series of laboratory tests on the woven coir geotextiles to examine the interface properties of geotextile in sand. The results of direct shear tests on coir geotextile in sand indicated that at lower overburden pressures (e.g.

100 kPa), the geotextile-sand interface resistance was up to 70% more than the soil shear strength, while at higher normal stresses the values obtained were not consistent. The pullout tests data showed that the tensile strength of geotextile and the relative size of mesh opening to particle size of fill material governed the pullout resistance of geotextile. Their results showed that the pullout resistance of open meshed geotextile was more in fine-grained sand as compared to that in coarse-grained sand because of good interlocking and bearing resistance.

Chadi and Milind (2009) conducted vertical pullout tests (VPT) to measure peak interface friction angle and adhesion between soil and planar geosynthetic products. The results were compared with those parameters obtained from a conventional direct shear test apparatus. The comparison showed that the peak interface parameters measured using VPT were within 12% of the values obtained from direct shear tests.

Hamid and Miller (2009) studied the shearing behavior of an unsaturated low-plasticity fine-grained soil using a modified direct shear test apparatus in which the matric suction of the soil specimen was controlled. Their results showed that the matric suction contributed to the peak shear strength of unsaturated interfaces but did not influence their post-peak shear strength. However, variations of net normal stress affected both the peak and post-peak shear strength values.

Liu et al. (2009) performed a series of direct shear tests on sand and various types of geogrids to evaluate the contributions of geogrid's transverse ribs to the interface shear. The test results showed that the interface shear strength of sand and geogrid was considerably higher than that of sand-geotextile interfaces. Also, shear displacement-

strength response of the interfaces indicated that the transverse ribs provided approximately 10% of the overall sand-geogrid interface resistance and this contribution was positively correlated with the tensile strength and the stiffness of geogrid ribs, but was negatively correlated with the percent open area of the geogrid.

Anubhav (2010) conducted a series of direct shear tests to examine the shear stress-displacement behavior of sand-geotextile interfaces. The results indicated that peak interface shear strength in sand-coarse textured geotextile was significantly higher (i.e. up to 35%) than that of fine textured geotextile. The results also showed that the shear displacement at peak shear strength increased with normal stress.

Hatami et al. (2010a,b) performed a series of large-scale pullout tests and small-scale pullout/interface shear tests to investigate the effects of interface soil moisture content on pullout capacity of a geotextile in Minco silt. The results indicated that the pullout capacity decreased as the soil moisture content increased and the greatest interface strength was obtained in soil compaction at 2% below optimum moisture content (OMC).

Lopes and Silvano (2010) investigated the interface behavior in direct shear and pullout tests. The study concluded that the ratio of shear stress to vertical stress at the maximum pullout force at the interface of geosynthetic with the full plane contact area with the soil were lower than those for the sliding movement at the interface. The results also showed that characteristics of the soil-geosynthetic interface in pullout, when the geosynthetic had a full plane contact with the soil, could not be obtained from the results of direct shear tests.

Khoury et al. (2011) used a modified direct shear apparatus to study the effect of soil suction on soil-geotextile interface behavior. Results of the study indicated that the peak shear strength of the soil-geotextile interface increased nonlinearly with soil suction. The study showed that increasing soil suction and net normal stress led to increases in the interface peak shear strength. Also, the increase in suction reduced the horizontal displacement at peak shear strength. The tests indicated that the increase in soil suction resulted in higher interface adhesion but no change in interface friction angle with regards to net normal stress.

Lawson et al. (2013) performed a series of laboratory pullout tests on sandy backfill and steel reinforcement used for MSE walls. Their results showed that relative compaction could significantly impact pullout resistance of high adherence (HA) strips so that a slight drop in compaction would dramatically reduce the pullout resistance of strip. The data also indicated that the pullout resistance factor (F*) was independent of reinforcement length and transverse and longitudinal bar spacings could significantly influence pullout resistance of welded steel grids.

Sayeed et al. (2014) conducted a series of large-scale direct shear tests on non-woven geotextile and sand to determine interfacial shear characteristics at different normal stress values. Their results showed that the interface friction angle of sand-geotextile was in the range of internal friction angle of medium dense sand particles. It was also observed that non-woven geotextile consisted of pure polypropylene (PP) fibers had higher initial shear stiffness compared to Jute-polypropylene hybrid non-woven geotextile. However, the contact efficiencies ($\tan\delta/\tan\emptyset$), (where $\tan\delta$ implies the

friction coefficient between sand-geotextile while tanØ is the friction coefficient for sand sliding on sand) of either geotextiles with sand were similar.

2.2. MSE Wall and Reinforced Embankment Tests

Huang et al. (1994) tested a series of reinforced and unreinforced sand slopes subjected to footing loading. Their results showed that the bearing capacity of the footing increased when reinforcement layers were placed within the active wedge. They also found that the bearing capacities and failure patterns of the reinforced slopes was dependent on the arrangement of reinforcement members.

Liu et al. (1994) studied the performance of a geogrid-reinforced cohesive soil test embankment over a period of seven (7) years. The observations showed that the tensile strains in the geogrid and the horizontal strains in the cohesive fill were essentially uniform and comparatively small (i.e. less than 0.8 %) for the bottom half (i.e. 6 m) of the embankment during construction. After the embankment was constructed beyond the first 6 m up to the full height, the slope started to deform significantly and tensile strains increased to a maximum of 2.8% and 2.0% in the uniaxial and biaxial geogrid sections, respectively. Liu et al. (1994) found that reinforcement strains varied from zero at the slope surface to a maximum value before decreasing at locations deeper into the fill. They also observed that the fill and the foundation exhibited their greatest settlements only after the final stage (i.e. 6 m) of the construction was completed.

Adams et al. (1997) conducted large-scale model footing load tests on a frictional soil reinforced with geogrids and geocells. In their study, they varied factors such as the number of reinforcement, reinforcement spacing, soil density, reinforcement type and the depth of the first reinforcement layer. Their results showed that geosynthetic reinforcement could increase the ultimate bearing capacity (BC) of shallow spread footings by a factor of 2.5.

Lee et al. (1999) studied the influence of geotextile reinforcement and the thickness of sand layer on ultimate bearing capacity and settlement behavior of a footing supported on soft clay overlaid by granular fill (sand). Their results showed that the foundation bearing capacity increased with the ratio of sand layer thickness to footing width up to 0.8 (which was called the optimum thickness of the sand layer). Their study also showed that the use of a geotextile reinforcement layer at the interface between the sand and clay significantly improved the footing bearing capacity and decreased its settlement.

Lee and Manjunath (2000) examined the influence of geosynthetic reinforcement on the bearing capacity of footings on sloped embankments. Their study confirmed that the load-settlement behavior and ultimate bearing capacity of the footing could be significantly improved as the reinforcement layer was installed in an optimum location within the slope. Their test data indicated that the optimum depth of reinforcement layer was 0.5 times the width of the footing (B). The study also showed that when the distance between the footing and the slope crest was less than five times the width of the footing (5B), the footing bearing capacity decreased as the slope angle increased and the footing distance from the slope edge decreased. Beyond 5B, the bearing capacity of

the footing was found to be practically independent of the distance between the footing and the slope.

Cassidy et al. (2002) described a work-hardening plasticity theory model for the behavior of rigid circular footing on carbonate sand. They utilized a series of tests on loose carbonate sand to verify its suitability for this soil type and conditions. The model made use of the force resultants and the corresponding displacements of footing and allowed prediction of response for any load or displacement combinations.

Bathurst et al. (2003) studied the performance of reinforced and unreinforced slopes under a strip footing load. Their study showed that an increase in the reinforcement length and stiffness increased the ultimate load capacity of the strip footing. Their results also indicated that the bearing capacity of the reinforced embankment was up to two times as large as that of an otherwise identical unreinforced embankment.

Kumar and Saran (2003) carried out several tests on closely spaced strip and square footings resting on geogrid-reinforced sand to study the influence of footing spacing and reinforcement size and continuity of reinforcement on the bearing capacity and rotation of the footing. Their results showed a significant improvement in bearing capacity and settlement of strip footings when continuous reinforcement layers were used in the models. However, the improvement in the case of square footings was found to be rather insignificant. Their data showed that both strip and square footings experienced less tilting when continuous reinforcement was placed in the soil.

Zhang et al. (2003) evaluated the effect of synthetic fibers and non-woven geotextile reinforcements on the stability of clay embankments. Their results showed that every

unit increase in moisture content led to 3% decrease in shear strength of the reinforced soil. The study concluded that fiber reinforcement could compensate for the loss of soil shear strength caused by increases in soil moisture content. The results also indicated that repairing failed slopes with the nonwoven geotextile can decrease repetitive surface failures in slopes of highly plastic soils.

Bueno et al. (2005) studied the field performance of retaining walls reinforced with non-woven geotextiles. A series of nonwoven geotextile-reinforced soil structures was built and instrumented to measure face displacement, vertical settlement of backfill and horizontal displacement within reinforcements. The study also showed that the Finite Element Method could be a useful tool to predict the response of structures reinforced with geosynthetic.

Mofiz et al. (2005) carried out a field instrumentation program to measure the matric suction in a granite residual soil slope. Tenisometers were used to measure the soil matric suction and it was concluded that matric suction increased the soil shear strength. They also observed that the change in matric suction was greatest near the ground surface and decreased with depth.

Sitharam et al. (2005) performed a series of laboratory loading tests on a circular footing placed on a geocell-reinforced clay to investigate the influence of the geocell layer depth and the width and height of the geocell on the foundation bearing capacity. Their test results showed that using geocell reinforcement layer could improve the bearing capacity of soft clay by a factor of 4.8 as compared to unreinforced clay. Their

results also indicated that a sufficiently deep and wide geocell could also decrease the swelling of the soft clay significantly.

Kato and Kohashi (2006) monitored the deformations of a slope and were able to capture its failure following continuous rainfall using optical fiber sensors. They concluded that optical fiber sensors are sufficiently accurate to measure and monitor slope deformations in the field.

Sako et al. (2006) performed numerical analyses to investigate the failure mechanism of unsaturated soil slopes due to increases in saturation. Their results showed that the slope failure was preceded by a rapid increase in the pore water pressure. It was also observed that as the soil became more saturated, the factor of safety against slope failure decreased.

Zhan et al. (2006) studied the effect of rainfall infiltration on soil-water interaction in an unsaturated expansive soil slope. Tensiometers, thermal conductivity sensors, vibrating wire earth pressure cells and inclinometers were used to measure the soil matric suction, water content, earth pressure and deformations of the slope. ThetaProbe is an in-situ sensor which measures the volumetric moisture content of the soil by measuring its dielectric constant. The measured changes are converted to a millivolt signal which is proportional to the soil moisture content (or GWC). Zhan et al.'s results indicated that the horizontal displacement and pore water pressure within the slope increased with rainfall. The data showed that the horizontal stress also increased with swelling pressure.

Briaud (2007) performed a study on ultimate bearing capacity of footings in sand to find out the shortcomings in the bearing capacity equation through load test data. He concluded that there was no scale nor embedment effect on the normalized load-settlement curve, which was a plot of the mean pressure under footing normalized to a soil strength parameter versus the settlement divided by the footing width. Their study showed that the general bearing capacity equation is appropriate for sands with a soil shear strength which increases linearly with depth and should not be used for any other soil including the profile of constant shear strength with depth.

Cerato and Lutenegger (2007) investigated the scale effects on the bearing capacity of shallow foundations in granular materials. Their test results showed that the bearing capacity factor (N_γ) for square and circular footings depends on the footing width or diameter (as applicable). Their data indicated that N_γ decreased with footing size but increased with the relative density of the sand. They also found that scale effects were more important for dense sands.

Dash et al. (2007) performed a series of laboratory tests to investigate the behavior of geocell-reinforced sand beds under strip loading. The study showed that the strain in geocell wall is largest at the center and much smaller in the extended portions outside the footing width. The authors also concluded that the geocell mattress behaved as a subgrade composite beam under the footing loading and for deeper mattress the deep beam effect becomes more predominant.

Hossain and Sakai (2007) studied the effect of water content on the behavior of geogrid-reinforced clayey backfill. The tests were performed at the range of water content

between 6% and 33% and normal stress of 48 kPa to 192 kPa. Their results at the moisture content of 32.5% showed that the pullout strength of geogrid increased from 75 kPa to 150 kPa with the increase in the normal stress. The study also showed that the maximum difference in pullout strength as a result of a difference in water content happened at the lowest normal stress and its value for the test constructed at 6.6% water content was 2.3 times as large as the strength at the water content of 32.5%.

Kumar et al. (2007) performed a series of tests on a strip footing rested on a reinforced layered sand to determine its ultimate bearing capacity. The foundation consisted of a strong sand layer overlying a low bearing capacity sand deposit. They observed that replacing the top 1B-thick layer of the weak soil (B is the strip footing width) with well graded sand reinforced with 2 to 4 layers of geogrid reinforcement could increase the ultimate bearing capacity of footing up to 4 times and reduced the footing settlement.

Tohari et al. (2007) carried out a series of tests on laboratory-scale soil slopes to investigate the effects of rainfall on slope failure. The dominant failure mode was found to be a shallow noncircular slip surface after formation of a seepage zone near the slope toe. Tohari et al. found that although the zones of localized failure reached a saturated state, the major part of the unstable soil slope was unsaturated.

Yoo et al. (2007) evaluated the pullout capacity and drainage properties of three types of geosynthetics (i.e. a geogrid, a geotextile and a composite reinforcement) in a weathered granite backfill which contained a significant amount of fines between 25% and 33%. From the results of their pullout tests and finite difference analysis, they concluded that tensile resistance and deformation of the geosynthetic reinforcement was

improved when the material included drainage properties, i.e. composite reinforcement such as geogrids was used in combination with geotextiles with good drainage capability.

Germer et al. (2008) investigated the effect of saturation on the development of failure processes within a soil slope. Their results showed that the slope could sustain 20% more load to reach failure when the shear band had negative pore pressure as compared to the case where the shear band was below the ground water level.

Thanapalasingam and Gnanendran (2008) performed a numerical analysis to study the effects of using multiple layers of reinforcement and to determine the most effective layout for reinforced slopes. The study indicated that the locations and spacing of the reinforcement layers are key factors to improve the load-displacement response of footing on a slope.

Bilgin and Kim (2010) investigated the effect of reinforcement length on wall deformation at different soil conditions. The results indicated that the reduction in reinforcement length from 0.7H to 0.4H (H: height of the wall) could increase the wall deformation and reinforcement load more than 80% and up to 20%, respectively. The study also showed that an increase in soil friction angle from 30° to 42° could reduce the maximum wall deformation up to 50%.

Castelli and Motta (2010) used a limit equilibrium method to find the threshold distance (i.e. d/B in which d is the footing distance from the slope crest and B is the footing width) at which the influence of the slope on the footing bearing capacity would be negligible. Their results indicated that the d/B value increased with the soil friction

angle varying from d/B= 1 for an undrained condition to d/B= 6 for the soil with a friction angle equal to 40˚.

Georgiadis (2010) studied the undrained bearing capacity of a strip footing on a slope as a function of the footing width, its distance from the slope and the slope height using the finite element method. Their results indicated that three different failure modes could occur depending on the height of slope relative to the footing width. Their study also indicated that the undrained bearing capacity of the footing increased with its distance from slope.

Shiau et al. (2011) used the Finite Element Method to find a critical strength ratio which separates two types of failures in the stability analysis of cohesive slopes (i.e. bearing capacity failure vs. slope failure). Their results showed that if $C_u/\gamma B$ is greater than a critical value which is proportional to H/B (i.e. height of slope/footing width), the slope will be stable otherwise it would experience a global slope failure.

Sawwaf and Nazir (2012) studied the behavior of an eccentrically loaded ring footing on a geogrid-reinforced compacted sand which overlaid loose sand. Their test results showed that the behavior of the ring footing considerably improved as the thickness and relative density of compacted sand layer increased. Their investigation also confirmed that using geosynthetic reinforcement could reduce the required thickness of compacted sand and/or lead to increased bearing capacity of the footing.

Gill et al. (2013) performed a series of large-scale footing tests on geogrid reinforced coal ash slope to study the effect of number of reinforcement and edge distance of footing from slope crest on load bearing capacity of slope. Their results showed that

increasing the number of reinforcement layers improved the bearing pressure of footing as well as the stiffness of foundation bed. However, the bearing capacity ratio became less significant while the number of geogrids used in the slope exceeded 3. The data also indicated that the edge distance of footing had a significant effect on the load bearing capacity of unreinforced and reinforced ash slope. Also, the authors showed that the bearing capacity of footing increased with an increase in the edge distance up to 3B (B: footing width) and beyond that the improvement became insignificant.

Hossain et al. (2013) investigated the influence of intensity and duration of rainfall on slope constructed on expansive clay using numerical simulations. The results of study showed that the factor of safety against slope failure dropped from 2.13 to 1.3 after 7 days rainfall. The results also indicated that long-duration and low intensity rainfall had more adverse effect than short-duration and high-intensity rainfall in unsaturated slopes constructed on low permeability expansive clays.

Hsu et al. (2013) constructed several silty sand slopes to investigate the effect of infiltration on slope stability. Their results showed that the failure was initiated at toe of slope after 28 hours due to infiltration and lower matric suction and led to retrogressive failure along the slope after 57, 98 and 102 hours of rain.

Kawamura et al. (2013) constructed a series of small-scale volcanic slopes and then a large-scale slope (i.e. H: 5 m, W: 2 m and L: 12 m) with the same soil to investigate the failure mechanism and to monitor the slopes performance. The results confirmed that the depth of failed wedge due to rainfall was deeper for the 45°-slope compared to 65° one. It was also observed that the first collapse in both slopes was generated at the toe

of slope and then, the second failure was induced with the increase in water level for each slope irrespective of its angle. The authors also concluded that the evaluation of soil moisture content was significant for evaluation of slope stability in all seasons.

Keskin and Laman (2013) performed a series of laboratory tests to evaluate the influences of footing setback from the slope crest, slope angle and relative density of sand on the ultimate bearing capacity of strip footings. Their study showed that the ultimate bearing capacity increased with the setback distance and relative density of the sand but it decreased with the slope angle. Their results also indicated that at a setback distance of 5 times the width of the footing, the bearing capacity of the footing practically approached that of the same footing on a level ground.

Kim and Lee (2013) studied the effect of rainfall on the stability of unsaturated weathered granite slope in Korea. Results of their analysis indicated that the slope with higher initial suction had greater initial factor of safety and the failure happened later than that with lower initial suction. The data also confirmed that the slope with higher saturated permeability was more vulnerable to rainfall-induced landslide as compared to that with lower saturated permeability. The study also showed that the slope constructed at wetting soil water characteristic curve (SWCC) reached failure earlier than that placed at drying SWCC.

Shivashankar and Jayaraj (2013) performed a series of laboratory bearing capacity tests to investigate the influence of reinforcement on strength improvement and settlement reduction of reinforced granular bed overlying weak soil. The results indicated that the improvement of bearing capacity depended on the thickness of granular bed, magnitude

of reinforcement prestress, direction of prestress and number of layers of reinforcement. Their results showed that for the granular bed with the thickness of B (B: width of footing) and uniaxially prestressed single reinforcement layer, the bearing capacity ratio (BCR) increased until the prestress reached 2% and beyond that the BCR reduced. While the reinforcement was biaxially prestressed, BCR was maximum at 1% prestress. In the cases with granular bed of thickness of 2B, BCR increased with prestress in both biaxial and uniaxial. In granular bed of thickness of B and 2B with two layers of reinforcement, the maximum BCR was attained at the prestress of 2% and 3%, respectively.

Yoo (2013) performed a numerical investigation on the effect of rainfall on the performance of reinforced soil wall. The results showed that a geosynthetic reinforced soil wall backfilled with marginal soil could experience significant increases in wall displacement and reinforcement load leading to slope instability. It was also observed that the wall displacement increased continuously up to 90 mm at the end of construction at the location of 1/3 H (H: wall height) from the base. It was concluded that the reinforcement load tended to increase during rainfall with a maximum increase of 8 KN/m.

Bilgin and Mansour (2014) performed a parametric analysis to study the effect of reinforcement types on the required minimum reinforcement length in mechanically stabilized earth (MSE) walls. The parameters included wall height, reinforcement vertical spacing, soil and foundation properties and they used geotextiles, geogrids, metal strips and metal bar mats as the reinforcement materials. Results indicated that the

reinforcement type affected the required minimum reinforcement lengths as well as the governing failure mode. The reinforcement type had a significant effect on the required minimum reinforcement length for relatively shorter wall heights and the effect decreased as the wall height increased. Their results also showed that the required length of reinforcement increased for external failure modes (i.e. overturning, eccentricity, sliding and bearing capacity) as the unit weight and friction angle of backfill soil increased and decreased, respectively. However, the pullout failure was not affected by the change in backfill soil unit weight. Their results also confirmed that the effect of reinforcement type on the reinforcement length was minimal when the reinforcement vertical spacing was small. However, the effect was significant when the reinforcements were placed at 0.8 m vertical spacing. The effect of reinforced soil was also investigated by authors and they concluded that an increase in its unit weight decreased the required reinforcement length for all external failure modes and had slight effect in pullout mode.

Kibria et al. (2014) studied the effects of soil reinforcement on excessive movement of a MSE wall backfilled with frictional soil in Texas using numerical Finite Element method. Numerical analysis results showed that the reinforcement stiffness did not have noticeable effect in 4 m high wall compared to 8 and 12 m high. Their data indicated that, while the reinforcement stiffness increased from 250 to 42000 KN/m at 1H reinforcement length (H: wall height), the horizontal movement of the wall varied from 74 to 29 mm. The study also showed that an increase in reinforcement length/height (L/H) ratio from 0.5 to 1 caused a 70%, 72.5% and 44.2% reduction in horizontal movement of 12-m, 8-m and 4-m wall, respectively.

Riccio et al. (2014) monitored the performance of a block-faced geogrid wall built using fin-grained soil as backfill. The results indicated that the induced stress due to soil compaction influenced the reinforcement tension. The data showed that the friction mobilization at the soil-block interface and backfill vertical stress transferred to the blocks and the loads in block facing reduced the tension mobilized in reinforcements. The data from inclinometers indicated that lateral movements increased from the bottom of the wall to top and the maximum deflection was 1.5% of the wall's height at the end of construction.

Yang et al. (2014) monitored the performance of a 17-m high two-tiered geogrid reinforced soil wall backfilled with granular soil-rock mixture under gravity load after construction. The authors monitored horizontal earth pressures at the back of facing, strains in reinforcement layers and lateral facing displacement at the toes and top of the wall. Their results showed that the large particles in the backfill reduced the bond strength between backfill and geogrid in localized regions. The displacement data also indicated that the post-construction displacement of reinforced wall was small (i.e. 0.3% H; H: height of wall) and this lateral movement was due to backfill-reinforcement slippage and time-dependent properties of soil.

The above literature review is summarized and classified in Table 2.1 based on the type of tests carried out and observations made in each study. It can be concluded that only a few studies have been performed on unsaturated soil-geosynthetic interface to examine the influence of matric suction on strength properties. Additionally, none of them included an extensive series of multi-scale laboratory tests to quantify the reduction in

pullout and interface shear strength of soil with geotextile due to an increase in as-compacted moisture content, which is the focus of this study.

Table 2.1. Summary of literature review performed in this study

Author(s)	Type of test	Type of soil	Major finding
Palmeira (1987)	Interface/Pullout	Sand	wall friction affected pullout results
Chua et al. (1993)	Pullout	Sand/clay	wetting of soil reduced interface strength by 50%
Adanur et al. (1994)	Pullout	Granular	reduction in pullout rate increased strength of fabric
Ali (1999)	Pullout	Sand	moisture content decreased interface strength
Ellithy and Gabr (2000)	Interface	Clay	strength decreased by 60% from dry to wet side of OMC
Goodhue et al. (2001)	Interface/pullout	Sand	fines content and drainage condition influenced adhesion
Ling et al. (2001)	Interface	Plastic	adhesion increased for PI values up to 70 and then decreased
Hossain and Inoue (2002)	Pullout	Clay	geosynthetics were more suitable than wire mesh for soil structure with clay
Mohiuddin (2003)	Pullout	Marginal	peak strain was observed in the fabric front end and decreased toward the tail end
Farrag and Morvant (2004)	Pullout	Clay	pullout capacity increased with fabric length and confining pressure
Lee and Bobet (2005)	Pullout	Sand	pullout capacity decreased as silt content of sand increased
Niemiec (2005)	Interface/pullout	Sand	Interface strength was greater for stronger fabrics
Zornberg and Kang (2005)	Pullout	Marginal	in-plane drainage increased pullout capacity
Abu-Farsakh et al. (2007)	Interface	Cohesive	shear strength decreased at higher moisture contents
Sharma et al. (2007)	Interface	Sand	suction at low normal stress increased shear strength
Bergado et al. (2008)	Pullout	Sand/clay	shear stress along the interface was non-uniform
Chandrakaran et al. (2008)	Pullout	-----	spacing of warp and weft yarns influenced passive resistance
Subaida et al. (2008)	Interface/pullout	Sand	fine-grained sands produced larger pullout resistance than coarse-grained sands
Chadi and Milind (2009)	Pullout	----	Peak interface parameters from VPT were 12% of interface properties from DST
Hamid and Miller (2009)	Interface	Fine-grained	Matric suction contributed to the interface strength
Liu et al. (2009)	Interface	Sand	sand -geogrid interface strength was greater than that of sand-geotextile interface
Anubhav (2010)	Interface	Sand	Peak interface strength was higher in coarse textured geotextile than that of fine textured geotextile
Hatami et al. (2010a,b)	Pullout	Marginal	pullout capacity decreased as moisture content increased

Table 2.1 (Cont'd). Summary of literature review performed in this study

Author(s)	Type of test	Type of soil	Major finding
Lopes and Silvano (2010)	Interface/pullout	------	soil-geosynthetic properties in pullout differs from those from interface tests
Khoury et al. (2011)	Interface	Sil-Co-Sil	interface shear strength was higher at higher suctions
Lawson et al. (2013)	Pullout	Sand	degree of compaction could impact pullout resistance of fabric
Sayeed et al. (2014)	Interface	Sand	pure PP fibers had higher shear stiffness than Jute-PP hybrid
Huang et al. (1994)	Embankment	Sand	bearing capacity of slope was dependent on reinforcement arrangement
Liu et al. (1994)	Embankment	Cohesive	strains in embankment increased up to 2.8% during construction
Lee and Manjunath (2000)	Embankment	----	Beyond 5B, bearing capacity was independent of setback distance
Bathurst et al. (2003)	Embankment		bearing capacity of reinforced embankment was twice as large as unreinforced model
Zhang et al. (2003)	Embankment	Clay	1% increase in moisture content led to 3% decrease in shear strength
Mofiz et al. (2005)	Embankment	Granite	matric suction increased the soil shear strength
Kato and Kohashi (2006)	Embankment	-----	Optical fiber sensors are accurate for measuring slope deformations
Zhan et al. (2006)	Embankment	Expansive	horizontal stress increased with swelling pressure
Dash et al. (2007)	Embankment	Sand	strain in geocell was largest at center and smaller outside footing
Germer et al. (2008)	Embankment		slope with negative pore pressure sustained 20% more load
Tohari et al. (2007)	Embankment	------	dominant failure due to rainfall was a shallow noncircular slip
Gill et al. (2013)	Embankment	Coal ash	bearing capacity of footing increased with setback distance up to 3B and beyond that the improvement became insignificant
Hossain et al. (2013)	Embankment	clay	factor of safety against slope failure dropped from 2.13 to 1.3 after 7 days of rainfall
Hsu et al. (2013)	Embankment	Sand	failure was initiated at toe of slope after 28 hours due to water infiltration and reduced matric suction
Kawamura et al. (2013)	Embankment	Volcanic	depth of failed wedge due to rainfall was deeper for the 45° slope as compared to a 65° slope
Keskin and Laman (2013)	Embankment	Sand	bearing capacity increased with the setback distance and relative density of the sand but it decreased with the slope angle
Kim and Lee (2013)	Embankment	-------	slope with higher saturated permeability was more vulnerable to rainfall-induced landslide as compared to that with lower saturated permeability
Adams et al. (1997)	Bearing capacity	Frictional	reinforcement could increase ultimate bearing capacity by a factor of 2.5
Lee et al. (1999)	Bearing capacity	Sand	bearing capacity increased with ratio of sand thickness to footing width
Sitharam et al. (2005)	Bearing capacity	Clay	geocell layer could improve bearing capacity by a factor of 4.8
Cerato and Lutenegger (2007)	Bearing capacity	Granular	N_γ decreased with footing size but increased with relative density

Table 2.1 (Cont'd). Summary of literature review performed in this study

Author(s)	Type of test	Type of soil	Major finding
Kumar et al. (2007)	Bearing capacity	Sand	replacing weak soil with reinforced sand increased bearing capacity by a factor of up to 4
Sawwaf and Nazir (2012)	Bearing capacity	Sand	geosynthetic reinforcement reduce thickness of compacted sand and led to increased BC of footing
Shivashankar and Jayaraj (2013)	Bearing capacity	Granular	improvement of bearing capacity depended on the thickness of granular bed and magnitude of reinforcement prestress
Hossain and Sakai (2007)	MSE	Clay	pullout strength increased 2.3 times at lower water content
Yoo et al. (2007)	MSE	Weathered granite with fine content	tensile resistance of fiber improved with drainage properties
Bilgin and Kim (2010)	MSE	------	reduction in reinforcement length below L/H = 0.7 increased wall deformation
Yoo (2013)	MSE	------	reinforcement load tended to increase during rainfall with a maximum increase of 8 kN/m
Riccio et al. (2014)	MSE	Fine-grained	lateral movement increased from bottom of wall toward the top and deflection was 1.5% of wall height at end of construction
Yang et al. (2014)	MSE	Granular	post-construction displacement of reinforced wall was small and this lateral movement was due to backfill-reinforcement slippage and time-dependent properties of soil
Cassidy et al. (2002)	Numerical bearing capacity	Sand	prediction of rigid footing response for any load or displacement
Kumar and Saran (2003)	Numerical bearing capacity	----	improvement in bearing capacity footing with continuous reinforcement
Bueno et al. (2005)	Numerical MSE	----	FEM could be useful to predict response of reinforced structures
Sako et al. (2006)	Numerical slope	-------	factor of safety against slope failure decreased as soil became saturated
Briaud (2007)	Numerical bearing capacity	Sand	general bearing capacity equation is not valid for sands with constant shear strength
Thanapalasingam and Gnanendran (2008)	Numerical slope	------	spacing of reinforcement layers influenced bearing capacity of slope subjected to footing load
Castelli and Motta (2010)	Numerical slope	------	ratio of footing setback to footing width, at which the effect of slope on BC was negligible, increased with soil friction angle
Georgiadis (2010)	Numerical slope	------	undrained bearing capacity of footing increased with its distance from slope
Shiau et al. (2011)	Numerical slope	------	for a slope to be stable, the $C_u/\gamma B$ should be greater than a critical value
Bilgin and Mansour (2014)	Numerical MSE	------	reinforcement type had significant effect on required minimum reinforcement length for short walls
Kibria et al. (2014)	Numerical MSE	------	horizontal facing movement varied between 74 and 29 mm for models with reinforcement stiffness ranging between 250 and 42000 kN/m

CHAPTER 3

MULTI-SCALE PULLOUT AND INTERFACE SHEAR TESTS

The soil used in the pullout and interface shear tests was a lean clay found on US Route 62 in Chickasha, OK (Figure 3.1). In this study, the soil is referred to as the Chickasha soil. Physical and mechanical soil property tests were carried out on the soil samples in general accordance with ASTM D1140 to determine the fines content and ASTM D422 for sieve analysis and hydrometer test. A series of direct shear tests (ASTM D3080) was carried out on the soil at three different GWC values (i.e. OMC-2%, OMC and OMC+2%) and at a rate of 0.06 mm/min to determine its shear strength parameters (i.e. c' and $\emptyset'$). The results are given in Figure 3.2 and Table 3.1. According to the Unified Soil Classification System (USCS) and AASHTO, the soil is classified as CL and A-6, respectively.



Figure 3.1. Excavation pit where soil samples were taken from the failed slope in Chickasha, OK

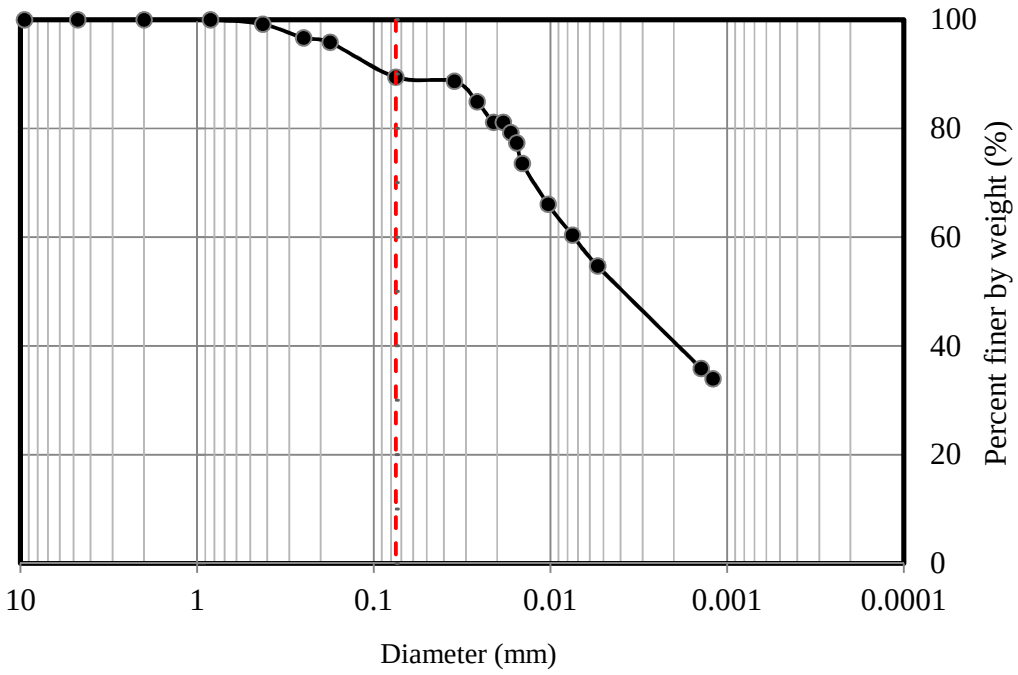

Figure 3.2. Gradation curve of Chickasha soil. Note: The vertical broken line shows the location of #200 sieve.

Table 3.1. Summary of Chickasha soil properties used in pullout and interface tests

Property (Lean clay)	***Value***
Liquid Limit (%)	38
Plastic Limit (%)	20
Plasticity Index (%)	18
Specific Gravity	2.75
Gravel (%)	0
Sand (%)	10.6
Silt (%)	49.4
Clay (%)	40
Maximum Dry Unit Weight, kN/m^3	17.3
Optimum Moisture Content (%)	18
Cohesion at OMC-2%, OMC and OMC+2% (kPa)	42.6, 29.3, 20.4
Friction angle at OMC-2%, OMC and OMC+2% (°)	29.6, 27.3, 27.1

Four compaction tests (one standard, two Harvard miniature, and one modified proctor test) were carried out on the Chickasha soil to determine the values of the soil maximum dry unit weight and optimum moisture content more accurately. Figure 3.3 shows the compaction test data and a series of theoretical curves of the soil dry unit weight versus moisture content for different degrees of saturation. These curves show different values of degree of saturation at maximum dry unit weight that were obtained from Equation 3.1:

$$\gamma_d = \left(\frac{G_s}{1+\frac{\omega G_s}{S}}\right) \gamma_w \qquad (3.1)$$

Where:

G_s: Specific gravity

ω: Moisture content

S: Degree of saturation

γ_w: Water unit weight

γ_d: Soil dry unit weight

The curves corresponding to S = 1, 0.9 and 0.8 are shown as the zero air void line (ZAVL - representing the minimum void ratio attainable at a given moisture content), 10% AVL and 20% AVL, respectively (Budhu, 2000). The air void lines in Figure 3.3 were determined from Equation 3.1. To plot the ZAVL, the soil saturation was set to unity (S = 1). Then, having specific gravity for Chickasha soil from Table 3.1 (G_s = 2.75) and water unit weight (γ_w= 10 kN/m^3), the dry unit weight (γ_d) was calculated at

different moisture content (ω) values. This procedure was repeated to obtain the 10% and 20% air void lines. Based on the results of all compaction tests, the best values for the maximum dry unit weight and optimum moisture content were chosen as γ_{dmax} = 17.3 kN/m^3 and OMC = 18%, respectively.

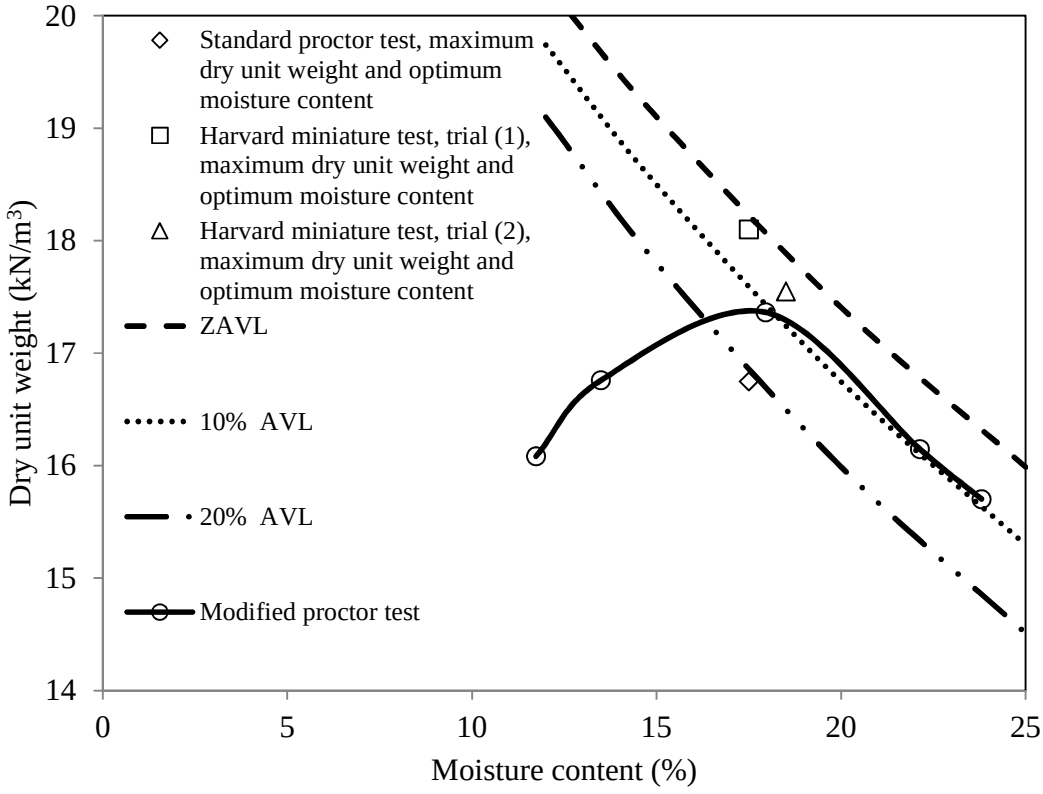

Figure 3.3. Compaction test results for Chickasha soil used in pullout and interface tests

Seventeen (17) 300-gram samples of Chickasha soil were prepared at different moisture content values. Approximately 100 grams of each sample was used to measure its moisture content using the oven-drying method. The rest of the soil was used to make a 40 mm (diameter) by 6 mm (height) sample for the WP4 equipment at the same dry unit weight as was used in the laboratory pullout tests (See section 6.1.4 for descriptions on

WP4 and sample preparation). Figure 3.4 shows the Soil-Water Characteristic Curve (SWCC) for Chickasha soil that was obtained through WP4 tests.

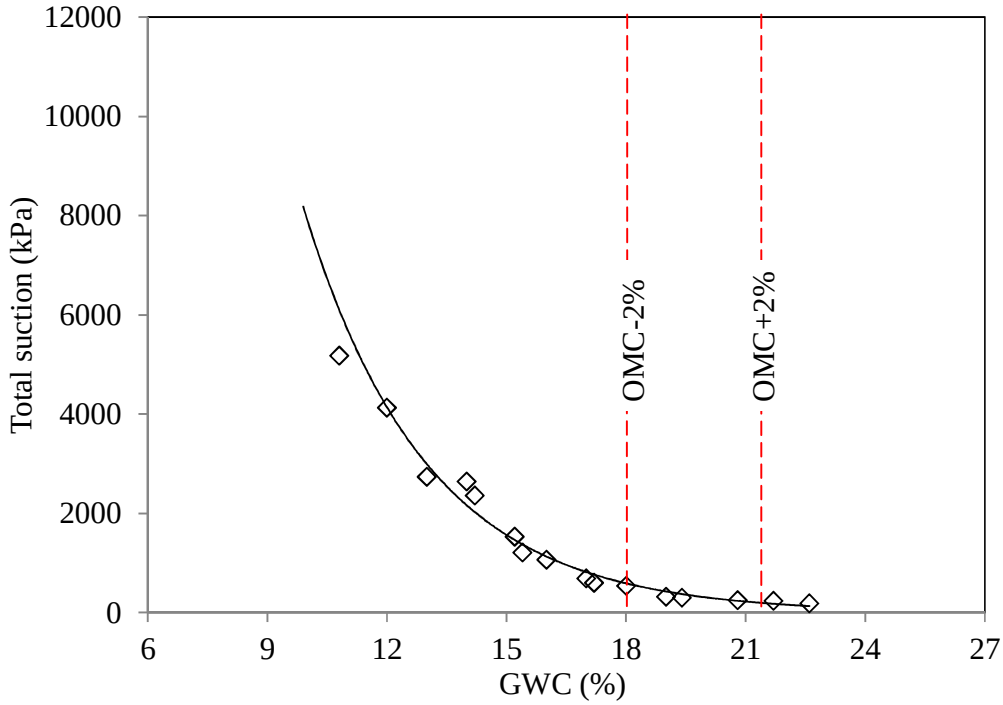

Figure 3.4. SWCC for Chickasha soil using WP4 Potentiometer

Results shown in Figure 3.4 indicate that the total suction in Chickasha soil varies between 300 kPa and 1200 kPa for the range of moisture contents between OMC-2% and OMC+2%. This range of soil suction is consistent with the values that can be found in the literature for lean clay (Cardoso et al. 2007, Nam et al. 2009).

Analysis of WP4 results also allowed us to determine whether or not Chickasha soil is classified as an expansive clay. For this purpose, a procedure called McKeen analysis was used. In the McKeen's classification methodology for expansive soils the slope of

the SWCC in a semi-log plot is used to determine a parameter called the ‘‘total suction-water content index’’. The swelling potential of expansive soils is qualitatively classified (e.g. ‘‘low’’ or ‘‘high’’) based on the magnitude of the total suction-water content index (Table 3.2) (McKeen 1992). Figure 3.5 shows a plot of the gravimetric moisture content vs. total suction for the Chickasha soil.

Table 3.2. Summary of McKeen (1992) Expansive Soil Classification Methodology

Category	***Slope***	c_h	H_c ***(%)***	***Expansion***
I	> 0.17	-0.027	10	Special case
II	0.1 – 0.17	-0.227 to -0.12	5.3	High
III	0.08 – 0.1	-0.12 to -0.04	1.8	Moderate
IV	0.05 – 0.08	-0.04 to 0	-	Low
V	< 0.05	0	-	Non-Expansion

Note: c_h and H_c are the suction-compression index and vertical movement, respectively as computed by McKeen (1992).

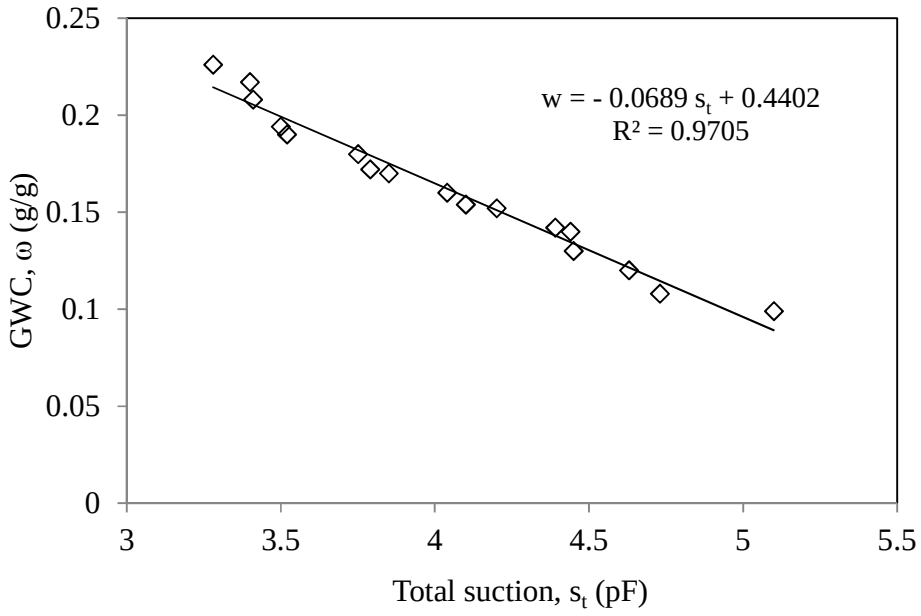

Figure 3.5. GWC vs. total suction for Chickasha soil on semi-log plot (pF is the base 10 logarithm of the suction expressed in cm of water)

According to Table 3.2 and Figure 3.5, since the slope of the graph is less than 0.08, Chickasha soil is classified under category IV indicating that its expansive tendency is low.

A woven polypropylene (PP) geotextile (Mirafi HP370) was used in the pullout and interface shear tests carried out in this study, with the properties as given in Table 3.3.

Table 3.3. Properties of HP370 woven geotextile

Property	***ASTM test method***	***Unit***	***Maximum average Roll Value HP370***	
			MD	CD
Tensile strength (at ultimate)	D4595	kN/m	52.5	47.3
Tensile strength (at 5% strength)	D4595	kN/m	21.9	22.8
Factory seam strength	D4884	kN/m	24.6	
Permeability	D4491	cm/sec	0.05	
Permittivity	D4491	sec^{-1}	0.52	
Apparent opening size (AOS)	D4751	mm	0.6	

3.1. Large-Scale Pullout Tests

A series of large-scale pullout tests were carried out in Chickasha soil and Mirafi HP370 woven geotextile. These tests were carried out at three different moisture content values OMC-2%, OMC and OMC+2% (Table 3.4). The differences in the magnitude of geotextile pullout resistance among these cases were used to determine a moisture reduction factor (MRF = $\mu(\omega)$) in Equation 1.3 and 1.4 to account for the loss of reinforcement pullout resistance due to increased moisture content. The tests for each

moisture content value were carried out at three different overburden pressures as given in Table 3.4.

Table 3.4. Large-scale pullout test parameters

Test information	
Soil	Chickasha soil
Geosynthetic reinforcement	Mirafi HP370, woven PP
Overburden pressure, kPa	10 , 20, 50
GWC	OMC-2%, OMC, OMC+2%

3.1.1. Test Equipment

The nominal dimensions of the large-scale pullout test box used in this study (Figure 3.6) are 1800 mm (L) × 900 mm (W) × 750 mm (H). The size of the box and its basic components, including metal sleeves at the front end exceed the minimum requirements of the ASTM D6706 test protocol (ASTM 2010). The boundary effects were further minimized by lining the walls of the test box with plastic sheets. The large pullout test equipment has a 100 mm bore, 450 mm stroke hydraulic cylinder with a high precision servo-control system. A surcharge assembly including an airbag and reaction beams on the top of soil surface was used to apply overburden pressures up to about 50 kPa on the soil-reinforcement interface. The pullout load on the reinforcement specimen was applied using a 90 kN, servo-controlled hydraulic actuator. In the pullout tests carried out in this study, only one half of the box length (i.e. 900 mm) was used.

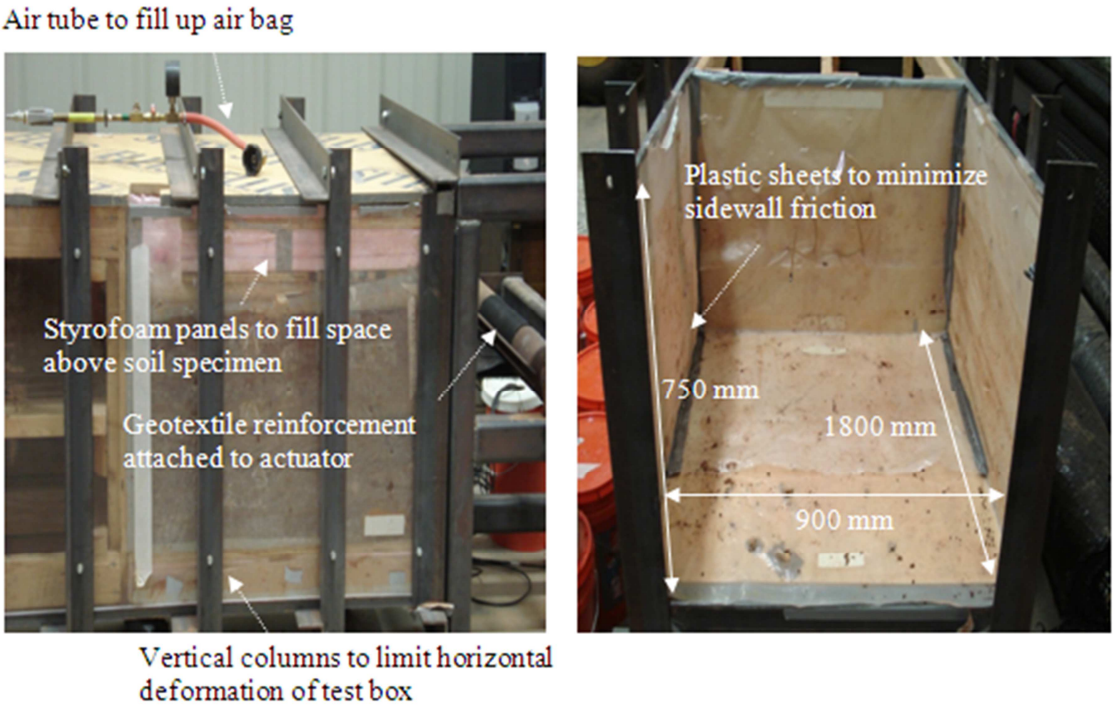

Figure 3.6. One of the pullout test boxes at the OU Fears laboratory

3.1.2. Test Procedure

3.1.2.1.Processing of the Soil

After the soil was transported from the borrow site (Figure 3.1) to the Fears lab, the clayey soil was air dried and broken into small pieces using two soil processors (Figure 3.7a,b). Afterwards, the soil was passed through a #4 sieve in a 7-tray Gilson screen shaker. Next, the soil was mixed with water to reach the desired moisture content for each test (Figure 3.7c). This procedure took approximately 5 to 7 days depending on the initial soil moisture content. The wet soil was stored in thirty five to forty 25 kg-buckets and was sealed for more than 24 hours to reach moisture equilibrium. The soil moisture

content in each bucket was measured using the oven drying method (Figure 3.8). The above procedure was repeated for every test.



(a) (b)



(c)

Figure 3.7. Soil processing equipment at the OU Fears laboratory, (a, b) Soil processors, (c) Soil mixer



(a) (b)

Figure 3.8. (a) Sealed buckets containing processed soil before placing in the pullout box, (b) Soil samples in the oven to determine their moisture content

3.1.2.2.Placement of Soil in the Pullout Box

The pullout box was lined with plastic sheets to preserve the soil moisture content and to minimize the friction between the soil and the sidewalls during each test. Next, the soil was placed and compacted in the test box in nine 50-mm lifts. The soil was compacted to 95% of its maximum dry unit weight (i.e. γ_d = 16.4 kN/m^3). The compaction for each layer took approximately 1 hour. The instrumented geotextile was placed at the mid-height of the box. The pullout box containing compacted soil at its target moisture content was sealed with plastic sheets on the top (Figure 3.9). In all pullout tests, a rectangular block of Styrofoam with dimensions of 900 mm (W), 457 mm (H) and 140 mm (T) was used in front of the soil specimen, which in addition to the 200 mm-wide metal sleeves, helped further minimize the influence of front boundary condition on the soil-geotextile interface.



(a) (b)

Figure 3.9. (a) Sealed compacted soil at the end of large-scale pullout box setup, (b) Geotextile specimen at the mid-height of the pullout box

3.1.2.3.Pullout Test and Dismantling of the Test Setup

The pullout phase of the test usually took between 1 and 2 hours depending on the overburden pressure and target soil moisture content. The pullout force was applied on the geotextile reinforcement at a target displacement rate of 1 mm/min according to the ASTM D6706 test protocol. After the test was completed and the reinforcement underwent pullout failure, the test assembly was carefully dismantled. First, the surcharge assembly was removed from the top of the box and the soil was carefully excavated from the box. It usually took about 4 to 5 hours to carefully dig the entire soil out of the test box. All together, a complete test required 45 to 50 hours of hands-on operation including soil processing, mixing and setting up the box, 24 to 48 hours as equilibrium time for suction sensors and 1 to 2 hours to run the pullout test.

3.2. Small-Scale Tests

In addition to large-scale pullout tests, a series of small-scale pullout tests and interface shear tests were performed to develop a better understanding of the influence of soil

moisture content on marginal soil-geotextile interfaces using a multi-scale laboratory testing approach. The small-scale tests were carried out on the same soil used in the large-scale pullout tests. In addition, these tests were carried out at the same soil moisture contents (OMC-2%, OMC and OMC+2%), unit weight (i.e. 95% of maximum dry unit weight from standard Proctor test) and overburden pressure magnitudes (10 kPa, 20 kPa and 50 kPa) as those in the large-scale pullout tests (Table 3.5)**.**

Table 3.5. Small-scale pullout and interface test parameters

Test information	***Chickasha Soil***
Type of small-scale test	Pullout, Interface shear
Geosynthetic reinforcement	Mirafi HP370, woven PP
Overburden pressure, kPa	10 , 20, 50
Moisture content	OMC-2%, OMC, OMC+2%

Pullout tests and interface shear tests were carried out using the direct shear testing (DST) equipment at the OU Geotechnical Testing Laboratory. The soil in both tests was placed in a 60 mm × 60 mm square test cell that was supplied with the test equipment. A rectangular block of Styrofoam with the dimensions 60 mm (W), 23 mm (H) and 9 mm (T) was used in the small-scale pullout tests in front of the soil specimen to provide a compressible boundary condition similar to that in the large-scale pullout box. A 20 mm (W) × 40 mm (L) geotextile specimen was used in each pullout test. The linear scale factor between the small-scale and large-scale pullout tests was 1:15. In the pullout tests, the geotextile specimen was pulled out of a fixed test cell filled with Chickasha clay at a speed of 0.06 mm/min (i.e. 1/15 of 1 mm/min nominal rate at large

scale). In the direct shear tests, the lower box of the DST machine was pushed laterally at a speed of 0.06 mm/min to apply a shear load on the soil-geotextile interface.

3.2.1. Small-Scale Pullout Tests

Pullout tests were carried out in Chickasha soil at OMC-2%, OMC and OMC+2% (Figure 3.10). Clay was prepared for small-scale pullout tests using the same process as was followed for the large-scale tests: The clay was first processed, then passed through #4 sieve in a 7-tray Gilson screen shaker and mixed with water to reach the target moisture content and its moisture content was measured using the oven drying method preceding and following each test. The bottom half of the 60 mm × 60 mm test cell was filled with four layers of Chickasha soil at target moisture content and each layer was compacted to 3 mm. The geotextile specimen was attached to a custom-made clamp mounted on the test box and was embedded 40 mm inside the test cell. A U-shape metal spacer was used to maintain a gap within the pullout slot to prevent any frictional contacts within the test cell frame during the pullout process. The top half of the box was filled with 4 more layers of clay, each compacted to 3 mm thickness.

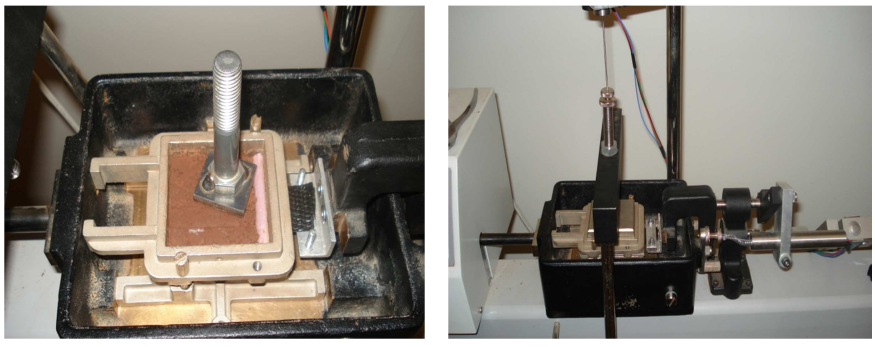

Figure 3.10. Small-scale pullout tests in Chickasha soil using a DST machine

3.2.2. Interface Shear Tests

A series of interface shear tests was carried out on the HP370 woven geotextile with Chickasha soil at different moisture content values to determine the Chickasha soil-geotextile interface properties (interface adhesion and friction angle). Filler aluminum panels were placed in the bottom half of the test cell in the DST machine. A geotextile specimen was attached to an aluminum panel and placed on the top in the bottom half of the test cell. The top half of the test cell was filled with four layers of Chickasha soil each of which was 3 mm thick after compaction.

CHAPTER 4

REDUCED-SCALE REINFORCED EMBANKMENT TESTS

A significant amount of soil (on the order of 5 cubic yards) from the Chickasha highway slope failure site (Figure 3.1) was required for the reduced-scale embankment tests. Obviously, it was not feasible to collect such amount of soil at the Chickasha highway embankment site. Therefore, the Web Soil Survey (WSS) online utility was used and four alternative sources of soil near the Chickasha site were identified that indicated properties similar to those of the embankment soil. A trip was made to the area near the Chickasha highway embankment site by the research group and met up with Dr. Jim Nevels to inspect the sites closely and take some soil samples. The soil that was used originally in the construction of the embankment is categorized as McLain Series which is primarily a thick layer of silty clay material (weathered loamy alluvium). The locations where the soil samples were taken are marked with red stars in Figure 4.1. These areas are located on U.S. Route 62 at cross section numbers 2770, 2780, 2790 and 2800. The soil samples were taken from depths between 170 mm and 1270 mm below the ground surface and were transported to the soils laboratory at OU for testing and classification.


E1320 Rd
N2780 Rd
E1320 Rd
Grady
OK
N2770 Rd
N2760 Rd
Boundary St
2nd St
1st St
Main St
Olive St
Railroad St
62

(a)


N2785 Rd
E1320 Rd
Grady
OK
N2760 Rd
E1330 Rd
62

(b)



(c)

Figure 4.1. Soil sampling locations on U.S. Route 62 Chickasha, OK; (a) Cross section 2770, (b) Cross section 2780, and (c) Cross sections 2790 and 2800

Physical and mechanical soil property tests were carried out on the soil samples taken from the four candidate cross sections identified near the borrow source locations in Chickasha (i.e. CS 2770, 2780, 2790 and 2800) in general accordance with ASTM D1140 and ASTM D422 to determine the soil gradation and fines content. The laboratory test results showed that the liquid limit (LL), plastic limit (PL) and the plasticity index (PI) values of the soil located at CS 2780 (i.e. 39, 22 and 17, respectively) were comparable with those of the Chickasha soil at the roadway embankment site (i.e. LL=38, PL=20 and PI=18). Figure 4.2 shows the gradation curves from sieve analysis and hydrometer tests for the soil samples taken from different depths at the CS 2780 location. The soil from this borrow source is classified as CL and

A-6 according to the Unified Soil Classification System (USCS) and AASHTO, respectively, which is the same as the soil from the failure site. Table 4.1 shows a comparison of the soil properties for the sample from CS 2780 as compared to those of the Chickasha soil at the failed embankment site.

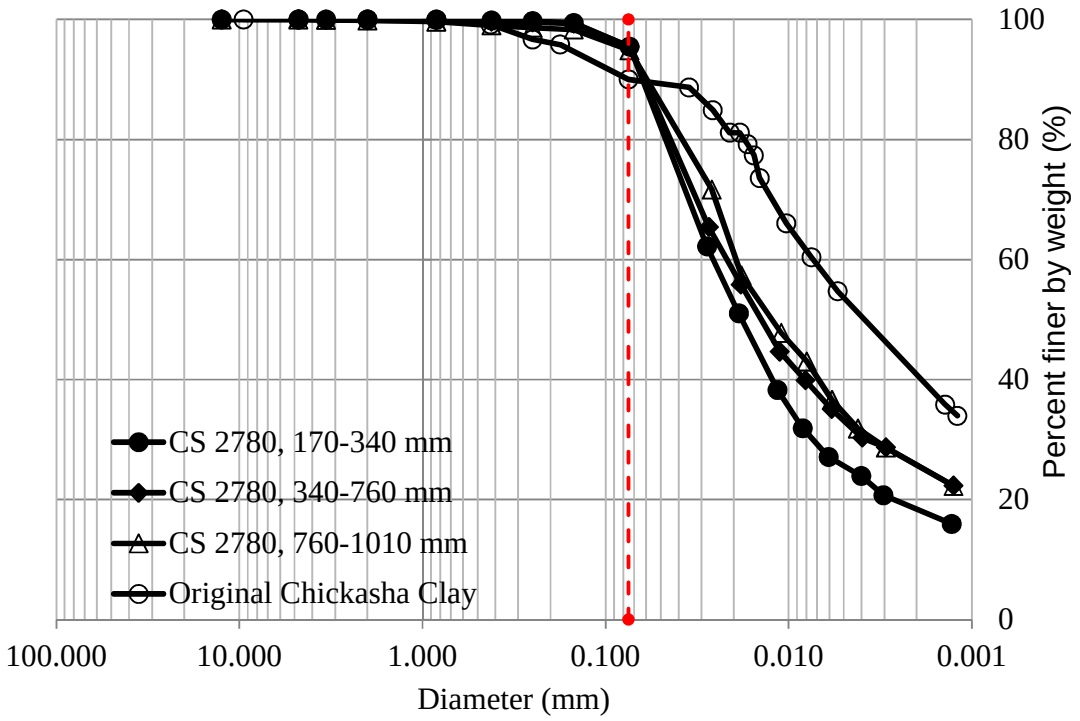

Figure 4.2. Gradation curves for the soil samples taken from CS 2780 (different depths) as compared to that of the Chickasha soil (failed embankment slope used in pullout and interface tests). Note: The vertical broken line shows the location of #200 sieve.

Table 4.1. Properties of the soil sample taken from CS 2780 as compared to those of the original Chickasha soil

Property	***Chickasha soil***	***CS 2780***
Liquid Limit (%)	38	39
Plastic Limit (%)	20	22
Plasticity Index (%)	18	17
Sand (%)	10.6	4.8
Silt (%)	49.4	69.2
Clay (%)	40	26
Maximum Dry Unit Weight, kN/m^3	17.3	18.8
Optimum Moisture Content (%)	18	14.9
Cohesion at OMC-2%, OMC and OMC+2% (kPa)	42.6, 29.3, 20.4	33.1, 20.7, 15.9
Friction angle at OMC-2%, OMC and OMC+2% (°)	29.6, 27.3, 27.1	35.3, 34.2, 34.0

Figure 4.3 shows the SWCC for the test soil (from the CS2780 borrow source) that was obtained through WP4 tests as compared to the original (i.e. failed embankment) Chickasha soil. A modified proctor test was carried out on the CS 2780 soil to determine the values of its maximum dry unit weight and optimum moisture content (Figure 4.4).

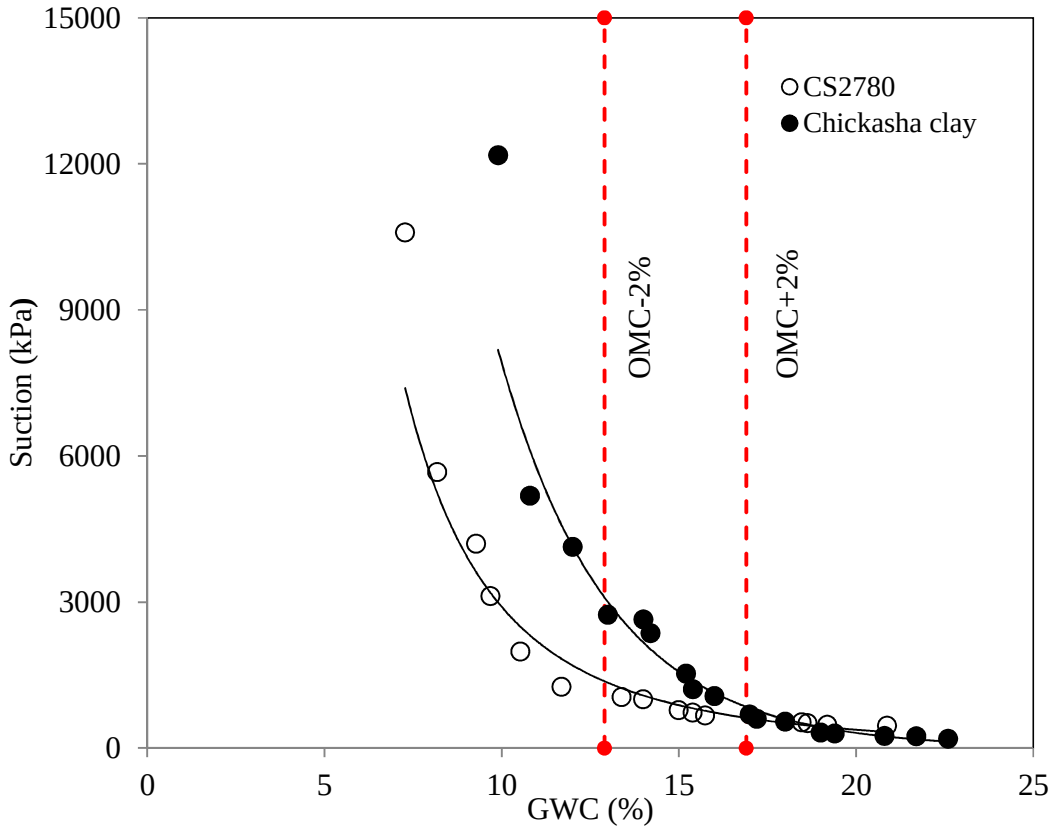

Figure 4.3. SWCC for the test soil using WP4 Potentiometer as compared to the original soil from a failed embankment in Chickasha, OK. Note: Red dashed lines show the OMC-2% and OMC+2% lines for the test soil

The woven polypropylene (PP) geotextile, Mirafi HP570, was used as the single-layer reinforcement in the embankment models. Table 4.2 compares the properties of HP370, used in the earlier study by Hatami et al. (2014), and HP570, used in this study, and their interface with CS 2780 lean clay.

Table 4.2. Comparison of HP370 and HP570 geotextile properties

Property	***ASTM test method***	***Unit***	***Maximum average Roll Value***	
			HP370[(1)]	***HP570***
			MD	MD
Tensile strength (at ultimate)	D4595	kN/m	52.5	70
Tensile strength (at 5% strength)	D4595	kN/m	21.9	35.0
Factory seam strength	D4884	kN/m	24.6	43.8
Permeability	D4491	cm/sec	0.05	0.05
Permittivity	D4491	sec^{-1}	0.52	0.4
Apparent opening size (AOS)	D4751	mm	0.6	0.6
Soil-geotextile interface property				
Interface adhesion at OMC-2%, OMC and OMC+2%	D5321	kPa	17.9, 12.4, 11.7	13.0, 11.9, 10.1
Interface friction angle at OMC-2%, OMC and OMC+2%	D5321	(°)	27.8, 24.9, 21.8	13.2, 12.8, 12.4

[(1)]The results of reduced-scale embankment tests with HP370 are reported in a recent study by Hatami et al. (2014)

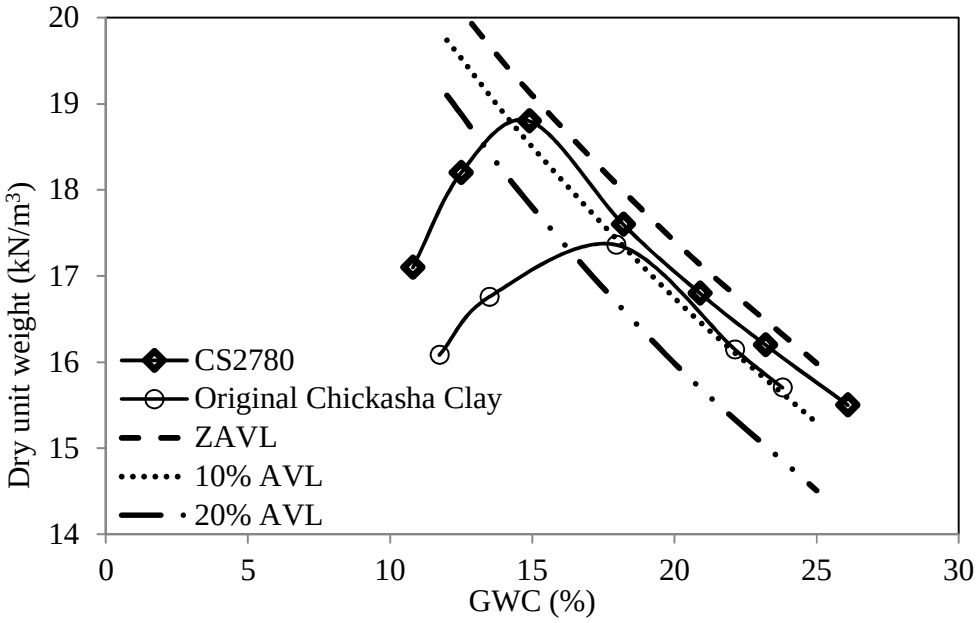

Figure 4.4. Compaction test results for clay (i.e. CS 2780) as compared to the original Chickasha soil

The model embankments were constructed and surcharge load tested at three different GWC values equal to OMC-2%, OMC and OMC+2% (Table 4.3).

Table 4.3. Test information for reduced-scale reinforced embankments

Test information	
Soil	Silty clay
Geosynthetic reinforcement	Mirafi HP370 and HP570, woven PP
Moisture content	OMC-2%, OMC, OMC+2%

4.1. Test Equipment

A 2000 mm (L) × 750 mm (W) × 1200 mm (H) portable embankment test box with an integrated loading frame was fabricated for the tests carried out in this study. In this configuration, the self-reacting loading frame of the test station was mounted on the test box itself as opposed to the strong floor (Figure 4.5). A main advantage of this design was that the test station would not be restricted to any particular location within the laboratory where a strong floor would have to be available. In addition, the loading frame was designed so that it could be mounted on the top of the test box at several designated locations to allow for flexibility in testing scenarios in the current and future projects. The sidewalls of the test box were lined with of 30-mm-thick polycarbonate glass panels so that the embankment deformations (including the formation of slip plane) could be monitored and measured. The steel columns and the thickness of the polycarbonate glass panels were designed so that the sidewalls of the text box would be essentially rigid when the embankment models were subjected to surcharge loading.



Figure 4.5. Test box and self-reacting loading frame fabricated for the reduced-scale reinforced embankment tests

4.2. Test Procedure

4.2.1. Processing of the Soil

After the soil was transported from the borrow site in CS 2780, Chickasha OK to the Fears lab at OU, the silty clay soil was air dried and broken into small pieces. Afterwards, the soil was passed through a #4 sieve using a Royer shredder and sifter machine (Figure 4.6). Next, the soil was mixed with water to reach the target GWC value for each test (Figure 4.7a). The wet soil was stored in one hundred and forty (140) 25kg-buckets and was sealed for more than 24 hours to reach moisture equilibrium

(Figure 4.7b). The soil gravimetric water content (GWC) in each bucket was measured using the oven drying method. The above procedure was repeated for every test.



Figure 4.6. Soil processing for reduced-scale embankment tests using a crusher-sifter machine



(a)



(b)

Figure 4.7. (a) Mixing of soil to reach target gravimetric water content, (b) Sealed buckets containing processed soil before constructing the model embankment in the test box

4.2.2. Construction of Embankment Models

The model embankments were designed with a facing slope of 69.5 degrees from horizontal. This was the steepest slope that could be used in the category of reinforced soil slopes (e.g. Berg et al 2009) to instigate larger deformations in the models in order to be able to detect differences in the performances of different models for the available loading capacity of the test equipment. Before constructing the model embankments in the test box, its side walls were lined with thin clear sheets of plexiglass to protect the polycarbonate glass panels against scratches during soil placement and compaction. Next, the soil was placed and compacted in the test box in five 100-mm lifts followed by nine 50-mm lifts. Preliminary testing and numerical simulation had indicated that the geometry of the failure plane would be contained within the upper half of the embankment models which would also exhibit significantly larger deformation as compared to its lower region (Appendix I). This allowed the bottom half of the embankment models to be constructed with larger lifts to expedite the otherwise time-consuming construction process without adversely impacting the performance of the model embankments relative to the study objectives. The soil was compacted to 85% and 95% of its maximum dry unit weight (i.e. γ_{dmax} = 18.8 kN/m^3) within the 100-mm and 50-mm lifts, respectively. The compaction for each layer took approximately 2 hours. The instrumented geotextile layer was placed about 180 mm below the embankment surface. The embankments were not meant to be reinforced models. Rather, they provided a single-reinforced soil mass to verify or modify MRF values from earlier interface tests in an embankment configuration

The test box containing compacted soil at its target gravimetric water content was sealed with plastic sheets on the top for a few days until the moisture and suction sensors inside the embankment reached equilibrium with their surrounding soil. Figure 4.8a shows covering the embankment with plastic sheet during construction to preserve its moisture content. Afterwards, the facing slope was trimmed to complete the construction stage before the model was subjected to surcharge loading (Figure 4.8b).



(a)



(b)

Figure 4.8. (a) Sealing of model embankments during construction to preserve their water content, (b) Trimming slope of the model embankment before applying the footing loading on the top

4.2.3. Loading of Model Embankments and Dismantling of the Test Setup

The loading phase of the embankment tests typically took between 6 and 10 hours depending on the gravimetric water content of the embankment soil. The strip footing was placed on the embankment 320 mm away from the embankment crest. The bottom of the footing was covered with sandpaper to simulate a rough counterface (e.g. a concrete bridge abutment). A 22-ton, 150-mm stroke hydraulic cylinder (Enerpac Model 506) was used to apply a vertical line load on embankment via the strip footing. It was made sure that the hydraulic cylinder was placed precisely at the center of footing and the reaction beam to avoid unexpected tilting of the strip footing (Figure 4.9). The vertical load was applied statically in 140 kg increments after it was observed at each load step that the rate of footing settlement had been reduced to less than 0.05 mm/min following the application of the load. The loading continued until a clear and continuous failure surface was started from the top of the embankment and extended to the slope.

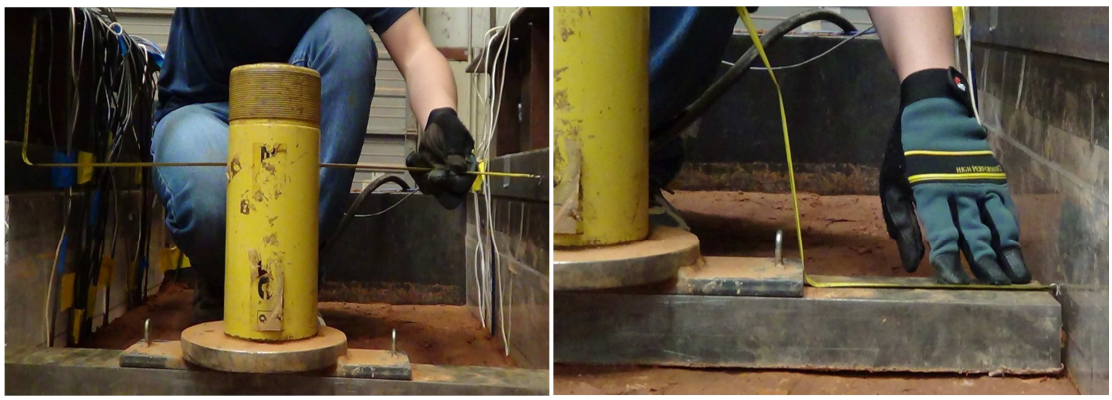

Figure 4.9. Placing the hydraulic cylinder at the center of footing and reaction beam in embankment tests

After the test was completed and the embankment failed, the test assembly was carefully dismantled. First, the surcharge assembly was removed from the top of the box and the soil in failure zone was carefully excavated out of the box. It typically took between 8 and 10 hours to carefully dig the entire soil out of the test box and remove all the sensors buried within the embankment. Altogether, a complete test required approximately 65 to 70 hours of hands-on operation including processing and mixing of the soil, construction and instrumentation of the model embankment in the test box, 36 to 48 hours as equilibrium time for moisture and suction sensors and 8 to10 hours to run the surcharge loading test.

CHAPTER 5

FULL-SCALE REINFORCED EMBANKMENT TEST

The experience with Chickasha clay in the pullout and reduced-scale embankment tests (Chapters 3 and 4) indicated that its mixing, processing and compaction for large-scale experiments would be time-consuming and therefore it would not be a practical soil for the significantly larger outdoor test. Additionally, the soil becomes stiff at lower water contents resulting in reduced influence of reinforcement on the embankment behavior. Therefore, it was decided to look for a more suitable marginal soil in the Norman-OKC area to study the soil-reinforcement interface performance. After communications with selected ODOT field offices and local contractors, a source of soil was identified from excavations in a recently completed I-35/Main Street Interchange project in Norman, OK. Several samples were brought to the OU Soils laboratory and tested to determine the soil gradation, Atterberg limits, Proctor compaction curve and suction values at different gravimetric water contents (GWC). The Liquid Limit (LL), Plastic Limit (PL) and Plasticity Index (PI) of the soil samples were found to be 18.3, 16.7 and 1.6, respectively. The target range of PI values for a suitable range of matric suction and plastic behavior was between 4 and 10. Therefore, it was decided to mix the soil sample with a high-grade sodium bentonite (SUPER GEL-X) to produce a soil mix with desired ranges of matric suction and plasticity index. Several portions of SUPER GEL-X were blended with the soil sample and it was eventually determined that a mixture of 98% soil and 2% SUPER GEL-X would produce a desired mix with PI = 7.8 and 500-900 kPa of suction for the GWC values within the range between 8.1% and 12.1%.

Subsequently, 40 cubic meters of the soil from the I-35/Main St. project and twenty five 22-kg bags of SUPER GEL-X were obtained and transported to the Fears laboratory to prepare and process for the large-scale embankment test (Figure 5.1).



Figure 5.1. Soil deposit at Fear laboratory for full-scale reinforced embankment tests

A series of sieve analysis, hydrometer tests and modified proctor tests were conducted on the blended soil with 2% SUPER GEL-X and the results are shown in Figure 5.2. The soil is classified as SC according to the Unified Soil Classification System (USCS) and its physical and mechanical properties are summarized in Table 5.1.

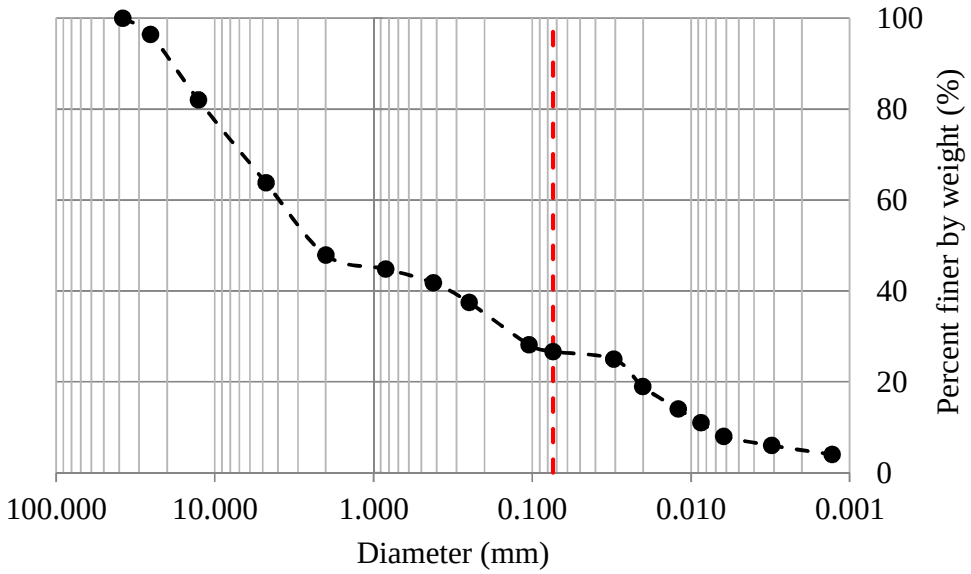

(a)

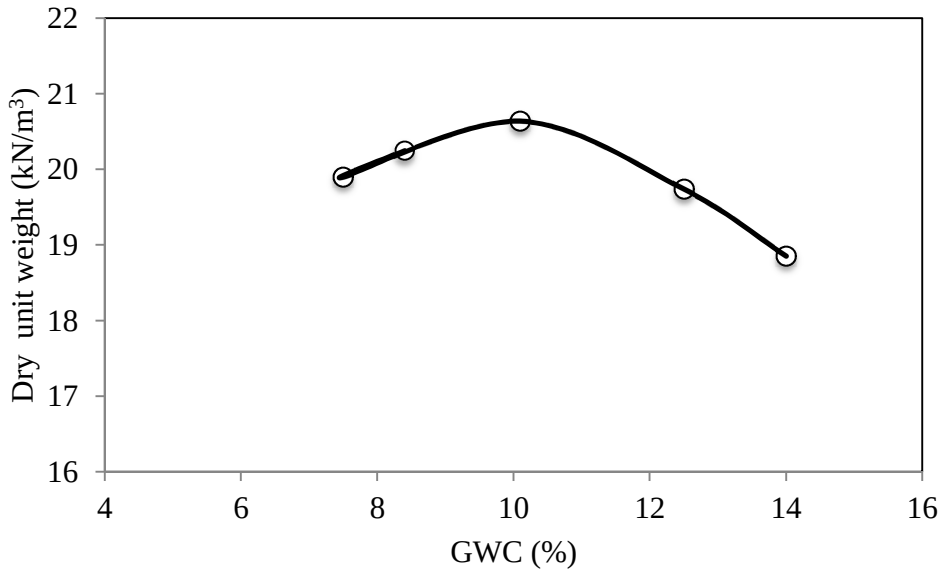

(b)

Figure 5.2 (a) Gradation curve from sieve analysis and hydrometer tests on sand, (b) Maximum dry unit weight and OMC of sand from modified proctor test. Note: Dashed line in 'a' indicates the location of Sieve# 4.

Table 5.1. Physical and mechanical properties of blended sand-SUPER GEL-X used in this study

Property	
Liquid Limit (%)	24.7
Plastic Limit (%)	16.9
Plasticity Index (%)	7.8
Specific Gravity	2.65
Gravel (%)	36.2
Sand (%)	37.1
Silt (%)	21.7
Clay (%)	5
Maximum Dry Unit Weight, kN/m^3	20.6
Optimum Moisture Content (%)	10.1
Cohesion at OMC-2% and OMC+2% (kPa)	12.2, 10.8
Friction angle at OMC-2% and OMC+2% (°)	37.5, 34.3

The full-scale reinforced embankment was constructed with the HP370 geotextile as the reinforcement layers. The properties of HP370 woven geotextile is shown in Table 3.3. The model embankment was constructed and surcharge load tested at GWC value equal to OMC-2%.

5.1. Test Box

Different design alternatives were initially explored for the full-scale test unit including a steel test box, an embankment pit and a reinforced concrete test box which was selected as the final design alternative (Appendix I). This selection was made considering the project needs (e.g. to minimize deformation tolerance of the testing unit) and value as a long-term investment for future projects. The reinforced concrete

design alternative of the outdoor testing unit was finalized for this study and it was designed by Dr. Ramseyer, P.E. (Director of the Fears Laboratory) as shown in Figure 5.3. The nominal dimensions of the test box are 5 m (L) × 3 m (W) × 2.8 m (H). All the walls are 0.3-m thick with the exception of the walls which the base plates are mounted to, which are 0.45-m thick. The loading frame was mounted on the test box together with two 180-ton hydraulic cylinders purchased from Enerpac company (Figure 5.3a). The access earth ramp also was built to facilitate the transportation of processed soil to the test box for embankment construction (Figure 5.3b).



(a)



(b)

Figure 5.3. Test box and loading frame fabricated for the full-scale reinforced embankment tests; (a) Mounting the loading frame, (b) Ramp for transporting soil to the test box using front loader

5.2. Test Procedure

After the soil was transported from I35-main interchange project, Norman OK to the Fears lab at OU, the required clayey sand for every two lifts was spread on the ground and 5 samples were taken from the bottom, top and middle of the soil to determine the initial GWC values. 2% of SUPER GEL-X and water was added to the sand and mixed using a tiller at the back of tractor to reach the target GWC value (i.e. OMC-2%). Then, the moisture samples were taken from the prepared soil to check how close the GWC was to the target value (i.e. 8.1%). Figure 5.4 shows the procedure of preparing the soil to be placed in the test box in the next day.



(a)





(b)



(c)

Figure 5.4. Preparing the soil for full-scale embankment test constructed at OMC-2%: (a) Taking GWC sample for oven-drying method, (b) Mixing the soil with SUPER GEL-X and water, (c) Covering the mixed soil to reach equilibrium before placing inside the test box

5.2.1. Construction of Embankment Model

Before constructing the embankment model in the test box, its side walls were painted to possibly reduce the friction between concrete and soil embankment during the test. The soil was placed and compacted in the test box in eleven (11) 150-mm lifts and to the target value of 95% of its maximum dry unit weight (i.e. γ_d = 20.6 kN/m^3). The compaction of each layer was conducted using a Chicago pneumatic rammer (Model 9662) and stayed consistent throughout the embankment (Figure 5.5).



(a)



(b)

Figure 5.5. (a) Placement of the soil in the test box, (b) Compaction of the prepared soil

The embankment was reinforced with four (4) layers of instrumented geotextile with the uniform spacing of 300 mm. Compaction of each layer took approximately 45 minutes and oven-drying method, tube sampling and rubber balloon method (ASTM D2167) was used to determine the as-compacted GWC and dry unit weight/compaction degree of each lift at seven (7) different locations (Figure 5.6). Figure 5.6a shows the geogrid used as a reference point to take consistent sampling all over the embankment. The compacted soil inside the test box was covered with a heavy duty tarp every day before leaving the site to preserve moisture content of the soil (Figure 5.7).

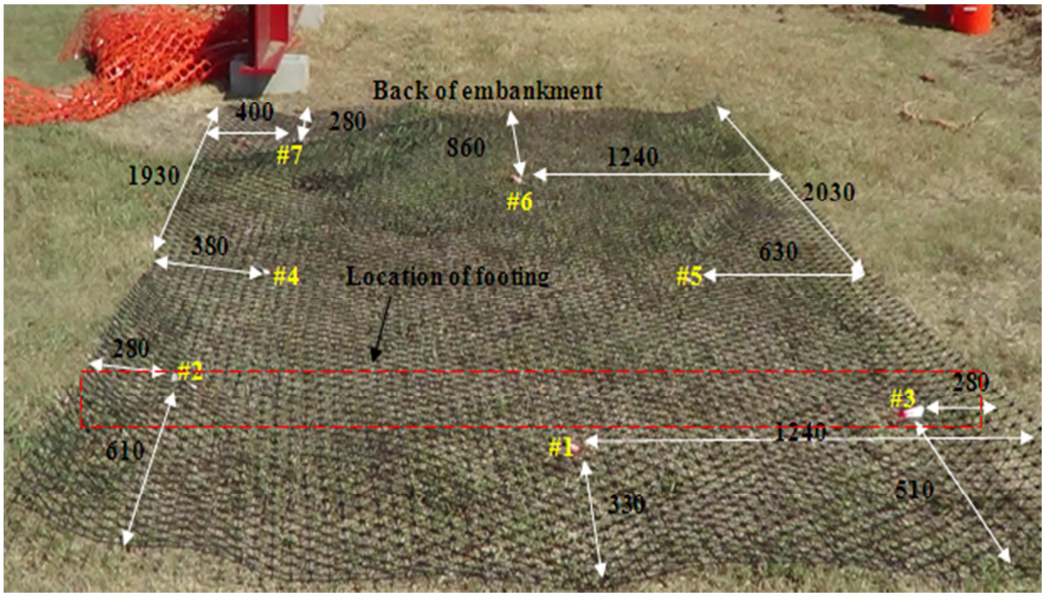

(a)



(b)



(c)

Figure 5.6. (a) Location of moisture and density samples in each compacted lift using a reference grid, (b) Tube sampling for density measurement, (c) Rubber balloon method for density measurement. Note: All dimensions in (a) are in "mm".



Figure 5.7. Covering the embankment with tarp and plastic sheet to avoid losing moisture content and reach moisture equilibrium

After the embankment was fully constructed, the facing slope was trimmed to complete the construction stage before the model was subjected to surcharge loading. Then, eight

(8) 25-mm square plates were installed into the embankment's facing as the reference points to monitor the slope deformation during the loading stage (Figure 5.8).



(a)

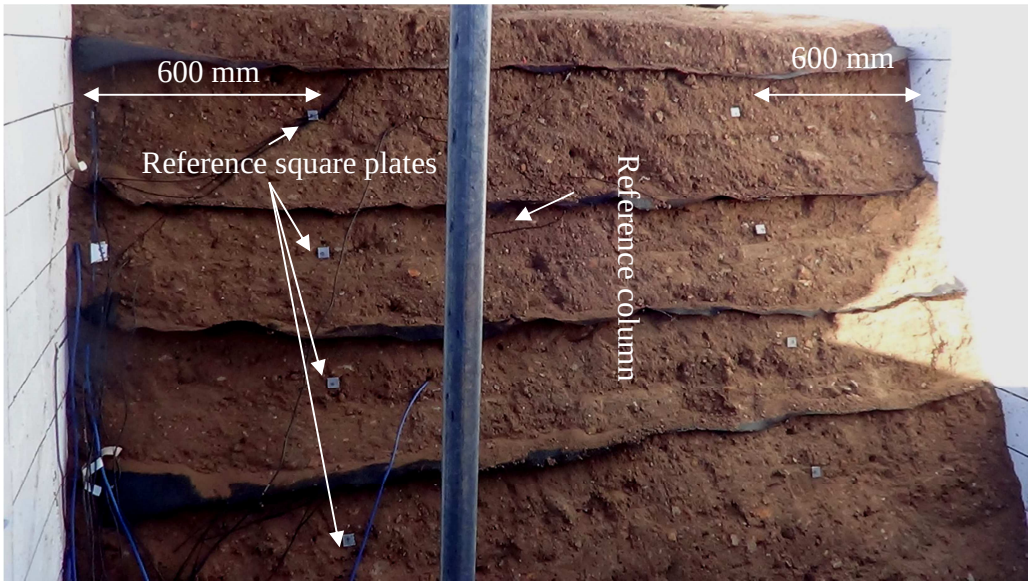

(b)

Figure 5.8. (a) Trimming the embankment's facing, (b) Locations of reference plates on the slope

5.2.2. Loading of Embankment

The location of loading beam was first leveled on the embankment to prevent its possible rotation during loading. Then, the beam was moved to the test box using a forklift and it was placed on the embankment at 355 mm away from the crest (Figure 5.9). The load cells were calibrated and placed on the loading beam and were tied to the reaction beam using two long chains to keep them on place after the embankment failed. The surcharge load on embankment was applied using two 200-ton, 300-mm stroke hydraulic cylinder (Enerpac Model CLRG-20012) and an Enerpac Pump Electric, Model ZU4420SB, was used to apply the static load (Figure 5.10). The loading stage continued until a clear and continuous slip surface was started from the top of the embankment and extended to the slope.



(a)



(b)



(c)

Figure 5.9. Preparing loading beam for the test. (a) Leveling off under the beam, (b) Moving the beam to the test box using forklift, and (c) Location of loading beam from the embankment crest



Figure 5.10. Hydraulic cylinders and load cells used for embankment test

CHAPTER 6

INSTRUMENTATION

In this study, several different sensors were studied and examined to find suitable methods for measurement of soil suction, gravimetric water content, earth pressure, embankment deformation and geotextile strain as described in the following sections:

6.1. Suction Sensors

6.1.1. Fredlund Sensors

The thermal conductivity of a porous medium increases with its moisture content. The thermal conductivity of a standard porous (e.g. ceramic) block in equilibrium with the surrounding soil can be used to measure the moisture content of the ceramic block, which in turn, is dependent on the matric suction of the surrounding soil (Perera et al. 2004). The concept described above makes it possible to calibrate the thermal conductivity of Fredlund sensors against the matric suction in the surrounding soil.

Samples of the Chickasha soil (refer to Table 3.1 for soil properties) were placed and compacted in a test bucket to examine the performance of our three available Fredlund thermal sensors in measuring soil suction (Fredlund et al. 2000, Perera et al. 2004). Five tests were carried out using these sensors. For each test, the bucket was filled with a sample of Chickasha soil in three lifts which were compacted to 95% of its maximum dry unit weight similar to the target compaction level in the pullout tests. Once each lift

was compacted, a cylindrical core was excavated within the soil to place the Fredlund sensor. The soil was then backfilled around the sensor and compacted (Figure 6.1).



Figure 6.1. Fredlund sensors placed in a calibration bucket to measure matric suction of the Chickasha soil

The positions of the three sensors in the bucket are schematically shown in Figure 6.2**.** After taking suction readings and finishing each test, soil samples were taken from the areas around each sensor to measure their moisture content. The waiting time between consecutive readings for sensors was 24 hours to equilibrate with the surrounding soil. This procedure was repeated on the soil placed in the bucket at different moisture content values. The resulting Soil Water Characteristic Curves (SWCC) from Fredlund sensors are plotted in Figure 6.3.

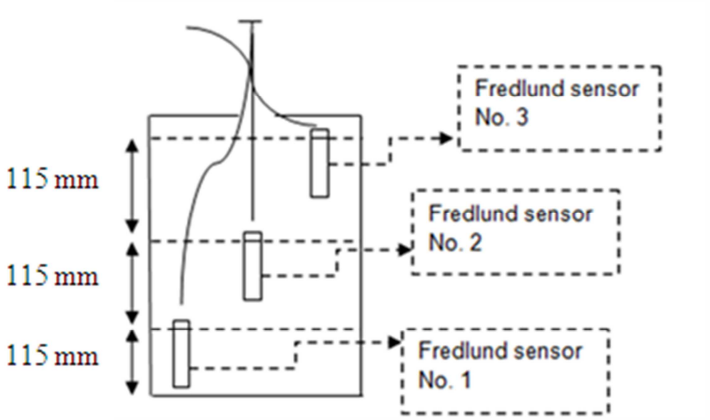

Figure 6.2. Schematic cutaway section indicating the locations of Fredlund sensors in the calibration bucket

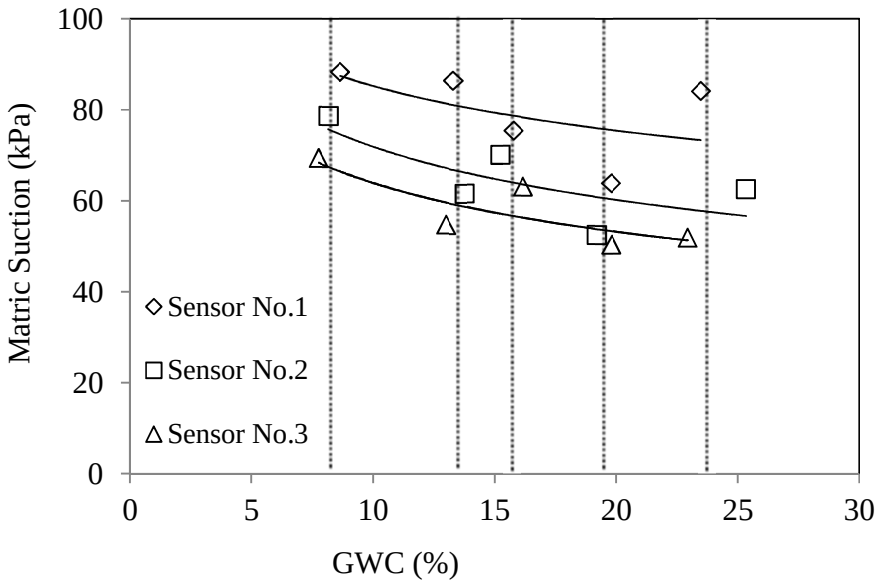

Figure 6.3. Soil suction versus GWC for Chickasha soil from Fredlund sensors. Note: The vertical lines indicate the mean values of measured GWC in each test.

The data in Figure 6.3 show a reasonable trend of reduction in the soil suction at higher moisture contents. However, the scatter in data is significant. Moreover, the range of suction values is significantly lower than what is expected for Chickasha soil (i.e. on the order of 1000 kPa on the dry side of optimum) as measured using WP4 equipment (see section 6.1.4). A possible reason for the above shortcomings is that the Fredlund sensors need to be in complete contact with the backfill soil to function properly. Extra care was taken to compact the soil as best as possible around the sensors after they were placed in the cavities in the calibration bucket. However, due to the small amount of soil that needed to be compacted and space limitations around the sensors, achieving proper compaction without disturbing the intact soil around the hole proved to be challenging. Results in Figure 6.3 indicate that readings from these sensors could be very sensitive to the placement procedure. Therefore, it was decided to search for other suction/moisture sensors for this study.

6.1.2. PST 55 Psychrometers

PST 55 is an in-situ psychrometer which can measure soil total suctions up to 5000 kPa. Under vapor equilibrium conditions, water potential of its porous cup is directly related to the vapor pressure of the surrounding air. This means that the soil water potential is determined by measuring the relative humidity of the chamber inside the porous cup (Campbell et al. 1971). PST 55 psychrometers are much smaller than Fredlund sensors and are commonly used in geotechnical research projects. PST 55 Psychrometer sensors can lose their factory calibration over time. Therefore, in this study they were calibrated

using a 1000 mmol/kg NaCl solution before using them in the large-scale pullout tests. Figure 6.4 shows a snapshot of the calibration setup and procedure for these sensors.

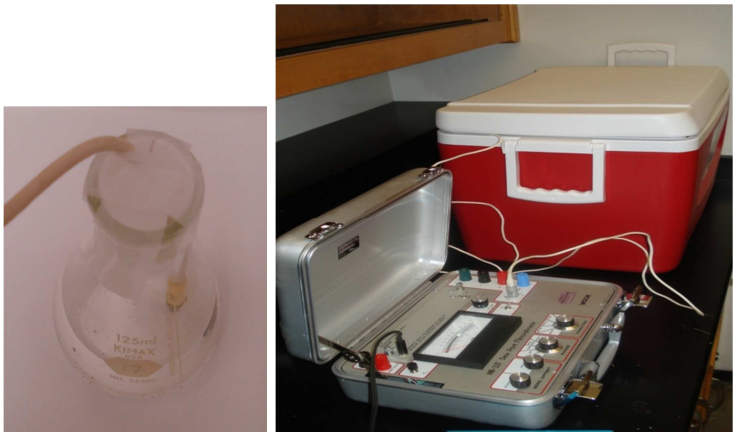

(a) (b)

Figure 6.4. (a) A PST 55 sensor submerged in NaCl solution; (b) Sensor calibration setup

The data logger shown in Figure 6.4b was used to read the water potential of the NaCl solution samples, and the ice chest provided a controlled temperature and moisture environment for the calibration of the sensors. The sensors were submerged in NaCl solutions and kept in the ice chest for about 2 hours to reach equilibrium (Wescor Inc. 2001). Then, each sensor was connected to the data logger (one at a time) and the water potential of the control NaCl solution was read in microvolts (μV). Four Psychrometer sensors were calibrated to be utilized in this study.

6.1.3. Filter Paper

In-contact and non-contact filter paper techniques are used to measure the soil matric and total suction values, respectively. In the in-contact filter paper technique, water content of the initially dry filter paper increases due to a flow of water in liquid form from the soil to the filter paper until the two media come into equilibrium with each other. After equilibrium is established, the water content of the filter paper is measured. Then, by using the appropriate filter paper calibration curve, the soil matric suction is estimated. In the non-contact technique, the dry filter paper is suspended above a soil specimen in a sealed container for water vapor equilibrium between the filter paper and the soil specimen at a constant temperature. The vapor space above the soil specimen acts as a true semi-permeable membrane which is only permeable to water vapor but not to ions from the pore-water. The separation between the filter paper and the soil by a vapor barrier limits water exchange to the vapor phase only and prevents solute movement. Therefore, in this technique, the total suction is measured. After equilibrium, the filter paper is removed and water content of the filter paper determined as quickly as possible. Then, by using the appropriate filter paper calibration curve, the soil total suction is estimated (Pan et al. 2010).

Chickasha soil samples were prepared at OMC-2% and OMC+2% moisture contents to predict maximum and minimum suction levels in our pullout tests (See Table 3.1 for soil properties). The filter paper test method was used as an alternative means to measure the soil matric suction as per the ASTM D5298-10 test standard (ASTM 2010). Each soil sample was cut into two halves with smooth surfaces. A circular piece of Whatman filter paper with the diameter d = 42 mm was placed between two larger

papers (d = 55 mm). All three papers were sandwiched between the two soil halves which were then taped together. The entire assembly was placed in a jar. To measure total suction, a piece of geogrid was placed on the top of the taped soil specimen and two large filter papers were placed on the top. The geogrid provided a suitable and convenient way to leave a small gap between the unsaturated soil sample and the filter paper assembly. Next, the jar lid was put back on and labeled with the information on the soil sample. The jar was placed in a well-insulated container for suction equilibrium and its temperature was monitored and recorded. This process was repeated for all other samples (Table 6.1).

Table 6.1. Total suction in Chickasha soil from filter paper tests

Measured Suction	***OMC-2%***				***OMC+2%***			
	Top FP		***Bottom FP***		***Top FP***		***Bottom FP***	
----------	*Test (1)*	*Test (2)*	*Test (1)*	*Test (2)*	*Test (1)*	*Test (2)*	*Test (1)*	*Test (2)*
Log kPa	4.25	4.15	4.23	3.99	3.82	3.85	3.78	3.88
Suction (kPa)	17,820	14,060	17,060	9,750	6,620	7,060	5,960	7,530
Ave. Suction (kPa)		14,670				6,790		

Note: [(1)]Two tests were carried out at each target moisture content (OMC-2% and OMC+2%). [(2)] FP stands for Filter Paper

According to Table 6.1, since the difference between the two suction values in the repeat trials of nominally identical samples is less than 0.5 Log kPa (ASTM D5298-10), the results are acceptable and no results should be discarded. Therefore, the mean value of total suction for each of the OMC-2% and OMC+2% cases for the Chickasha soil is given in the last row of Table 6.1. Results of Table 6.1 are plotted in Figure 6.5.

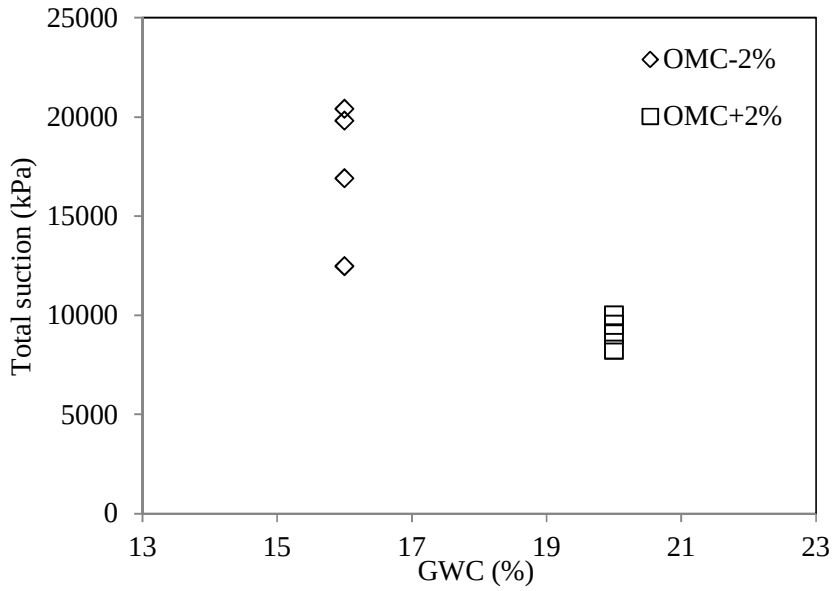

Figure 6.5. Variation of GWC and total suction for Chickasha soil from filter paper tests

Although the results in Figure 6.6 show a reasonable trend of lower total suction at higher moisture content values, the measured values of total suction for Chickasha soil are significantly higher than what is expected (see section 6.1.4). There are three critical parameters that must be considered in order to achieve reasonable results from filter paper tests. First, this test method requires an extremely clean lab environment. Second, the test should be carried out at constant temperature and relative humidity. Third, the weights of the filter papers need to be measured immediately after the samples reach

equilibrium. Failure to adhere to any one of these requirements could result in significant errors in the measured results.

6.1.4. WP4 Potentiometer

The WP4 equipment measures the soil total suction. It consists of a sealed block chamber equipped with a sample cup, a mirror, a dew point sensor, a temperature sensor, an infrared thermometer and a fan (Figure 6.6). The soil sample is placed in the sample cup and brought to vapor equilibrium with the air in the headspace of the sealed block chamber. At equilibrium, the water potential of the air in the chamber is the same as the water potential or suction of the soil sample. Please refer to chapters 3 through 5 for SWCC of soils tested in this study using WP4.



Figure 6.6. WP4 Water Potentiometer equipment (soil samples in sealed cups are shown in the inset)

The WP4 samples are placed in sealed disposable cups (Figure 6.6). Before testing each soil sample using WP4, a salt solution of known water potential (0.5 molal KCl in H_2O) is used to calibrate the WP4 sensor. For each test, the sample is placed inside the WP4 sample drawer and is allowed to reach temperature equilibrium with the equipment

internal chamber. Then, the knob on the tray is turned to the “READ” position to read the water potential of the soil sample. The magnitude of the soil total suction is recorded once the displayed reading stabilized at a constant value.

Based on previous experience with different methods of determining the soil suction as described earlier in this section, psychrometers were found to be the most suitable for in-situ testing and WP4 as the most suitable laboratory equipment to determine the soil suction in this study.

6.2. Soil Moisture Sensors

The capabilities of several different sensors were examined to measure GWC in the embankment soil based on the past experience in pullout and interface shear tests and the available literature. Example sensors surveyed in the literature included models 5-TE, EC-5, 10-HS, 5-TM, Hydra probe, SM-300 and Theta probe. Major factors that were the focus of this study included the sensor size, measuring range, precision and cost. The objective was to look for the smallest sensor that would operate over a wide range of GWC values and would be suitable for different types of soils. Based on the specifications and capabilities reported in the literature and prior experience, the EC-5 sensors were chosen to measure the GWC in the embankment models. EC-5 sensors are capable of continuous reading of the soil volumetric water content which is related to the GWC through the following relationship:

$$\theta_v = \omega \times \frac{\rho_d}{\rho_w} \qquad (6.1)$$

Where:

θ_v: Volumetric water content (VWC)

ω: GWC

ρ_d: Dry density of the soil

ρ_w: Density of water

The EC-5 sensors were installed in the vicinity of the soil-reinforcement interface to monitor changes in the soil GWC value in that part of the embankment models before, during and after each test. Also, HS2P moisture sensor from Campbell Scientific was utilized as a quick method for measurement of VWC in full-scale embankment models to verify the readings obtained from EC-5 sensors.

6.3. Earth Pressure Cells (EPC) and Tactile Sensors

Earth pressure cells (EPC) (i.e. Geokon model 4800 and Model 4810) were used to measure the vertical and lateral earth pressures inside the embankment models and to verify surcharge loading in pullout box. In addition to the EPC, 40-mm.-diameter free-form tactile pressure sensors (TPS, Sensor Prod 2013) were used to measure earth pressure at various locations in the reduced-scale embankment models. The flexibility and small surface area of the tactile pressure sensors were advantageous in that these attributes helped minimize the influence of their physical presence on the initiation and growth of the failure surface in the embankment models during the embankment models surcharge loading tests. Tactile sensors were found to be impractical in full-scale

embankment tests due to the larger size and angular shape of soil particles and this fact that the sensors might be torn during compaction and loading.

6.4. Piezometers and Glass Beads

Piezometers were installed within the embankment to monitor any possible excess pore water pressure due to loading. Due to their comparatively large size, the piezometers were placed horizontally (Myers and Scofield 2006.) at sufficient distances from the loading beam inside the embankments so that they would not interfere with the stress distribution and embankment deformation during the surcharge loading stage of the test (Figure 6.7). 10-mm.-diameter glass beads were also used inside the embankment models to monitor the internal movements of the embankment soil.



Figure 6.7. Piezometer placed in the 2nd lift of the model embankment to measure possible changes in the soil pore water pressure

6.5. Wire Potentiometers (WPT) and Linear Variable Differential Transformers (LVDT)

Celesco PT101 cable extension position transducers (wire potentiometers) were used to determine the geotextile strains. The PT101 transducer has a precision potentiometric output with a range of 0 to 10 inches and an accuracy of up to 0.1% of full scale. Wire potentiometers were also installed on the strip footing in embankment models to monitor the footing settlement while loading the embankment until failure.

The deformation of the embankment along its facing and top surface was monitored and measured using LVDTs (Figure 6.8). Additional LVDTs were used to measure the lateral deformation of the test box to check the symmetric behavior of the test setup.



Figure 6.8. LVDT used to measure facing deformation of reduced-scale embankments

6.6. Instrumentation Plan

6.6.1. Large-Scale Pullout Tests

A set of PST 55 Psychrometer sensors was placed in rows above and below the soil-geotextile interface to measure the soil suction and moisture content near the soil-reinforcement interface (Figure 6.9).

The geotextile strains and local displacements were measured using four (4) wire-line extensometers attached to different locations along the reinforcement length (Figure 6.11a). A Geokon Earth Pressure Cell (EPC) was used to verify the magnitude of the overburden pressure applied on the soil-geotextile interface using the airbag that was placed on the top of the soil (Figure 6.10b).

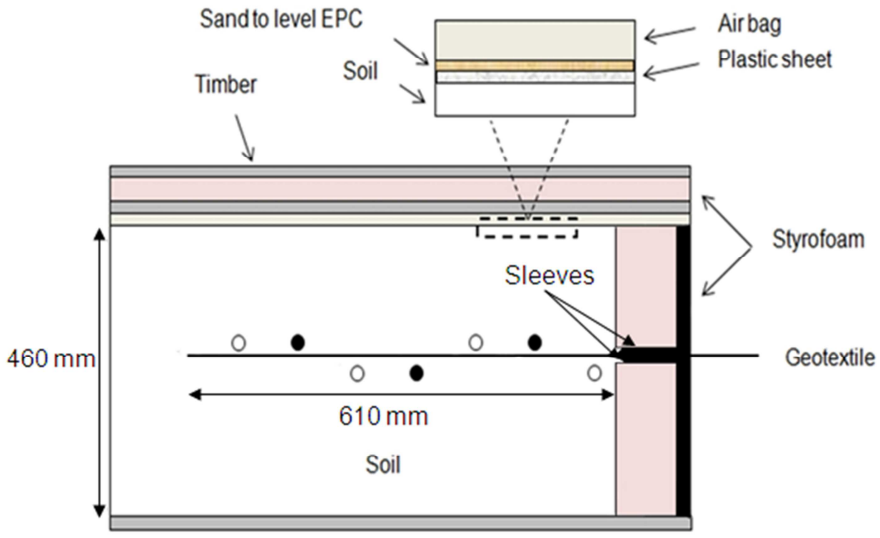

Figure 6.9. Schematic diagram of the large-scale pullout test box setup (not to scale). Notes: (1) Black and white circles represent the locations of PST-55 sensors and soil samples for the WP4 sensor, respectively; (2) The distance between the sensors and the interface is 25 mm; (3) The sleeves above and below the geotextile layer are 200 mm wide

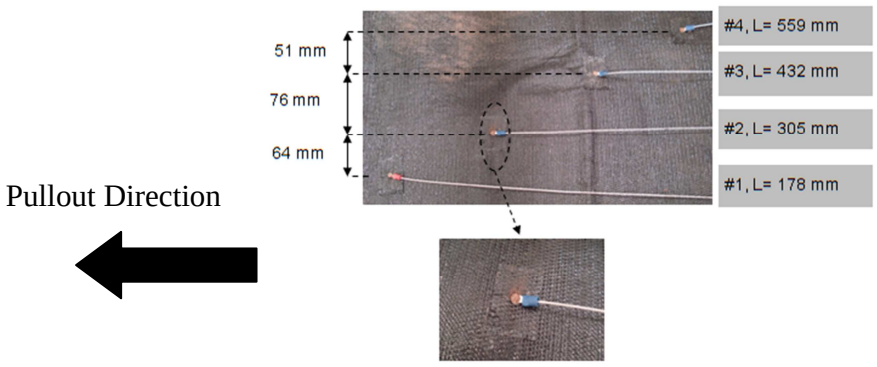

(a)



(b)

Figure 6.10 (a) Wire-line extensometers attached to the geotextile reinforcement (the numbers in the figure indicate the extensometer number and distance from the tail end of the geotextile); (b) Earth pressure cell placed on the top of the soil in the pullout test box

6.6.2. Reduced-Scale Embankments

Figure 6.11 shows the schematic diagram of the instrumentation plan for the reduced-scale embankment tests. Most sensors were place at the top half of embankments and around geotextile layer to better monitor the soil-geotextile interface behavior.

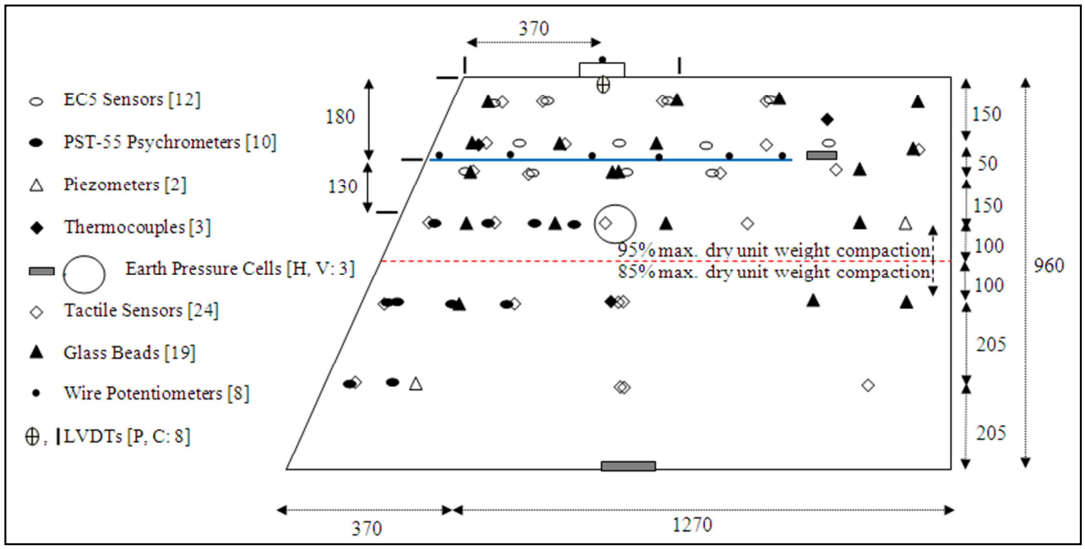

(a)

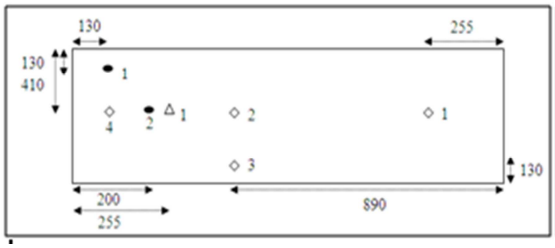

H = 205 mm

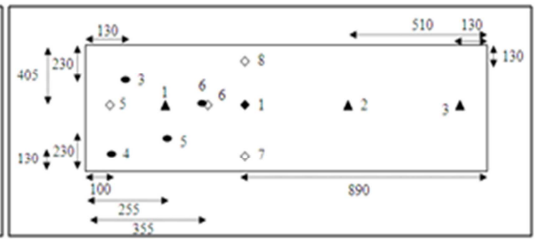

H = 410 mm

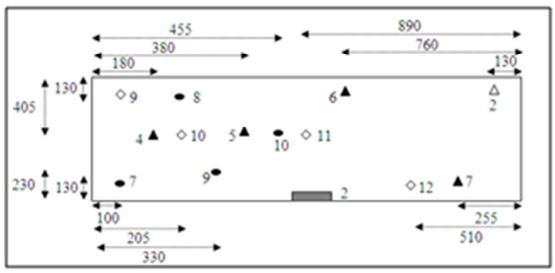

H = 610 mm

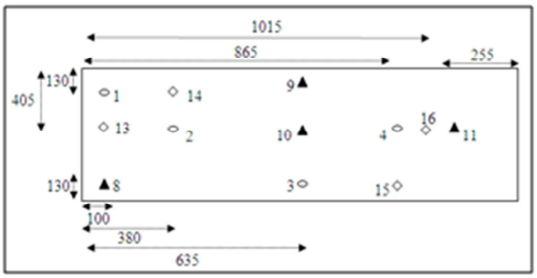

H = 760 mm

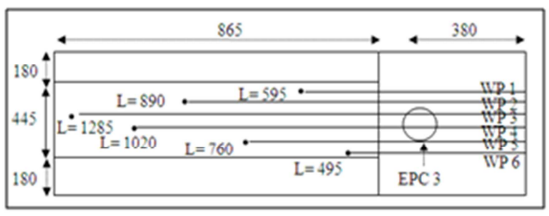

H = 785 mm

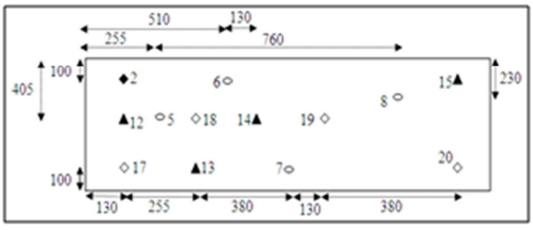

H = 810 mm

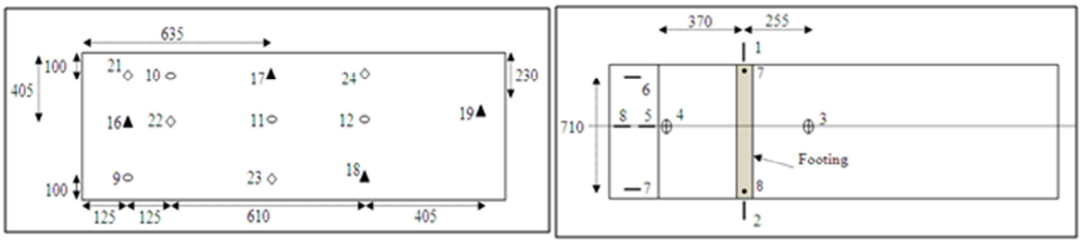

H = 915 mm H = 960 mm

(b)

Figure 6.11. Instrumentation plan for reduced-scale reinforced embankment tests; (a) cross sectional view, (b) plan view. Note: (1) numbers in bracket in (a) indicate the numbers of each sensors used in each test. (2) H, V, P and C in (a) stand for "horizontal", "vertical", "plan view" and "cross-sectional view". (3) The distances between WP #1-WP #2 and WP #5-WP #6 are 65 mm and those between all other WPs are 90 mm. (4) datum for the reported elevations is the bottom of the test box. (5) All dimensions are in "mm", (6) Dimensions and locations of sensors are not in scale.

6.6.3. Full-Scale Embankments

Three (3) EPC sensors and three (3) LVDTs were used in the full-scale embankments to measure the vertical pressure within the embankment and to monitor the vertical deformation of embankment surface near loading beam, respectively. The locations of EPCs were determined based on our initial numerical simulations and they were placed around the presumed failure wedge to give us the appropriate vertical pressure on each reinforcement layer for MRF calculation. Sixteen (16) WPTs were attached to four (4) layers of reinforcements to measure the local displacement and strain of geotextil strips. Two WPTs also were used to measure the footing settlement (Figure 6.12).



(a)

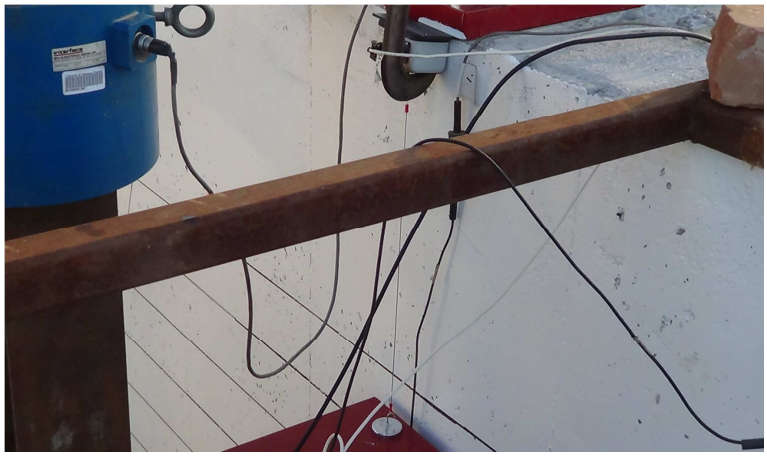

(b)

Figure 6.12. (a) WPTs installed at the back of the test box to measure geotextile local displacements, (b) WPT used for footing settlement measurements

Nine (9) EC-5 sensors were placed near the soil-geotextile interfaces to monitor the GWC during construction and while loading. The lateral deformations of embankment's facing were monitored using observation method by installing references square plates over the height of the embankment. Figure 6.13 shows the details and location of sensors used for this test.

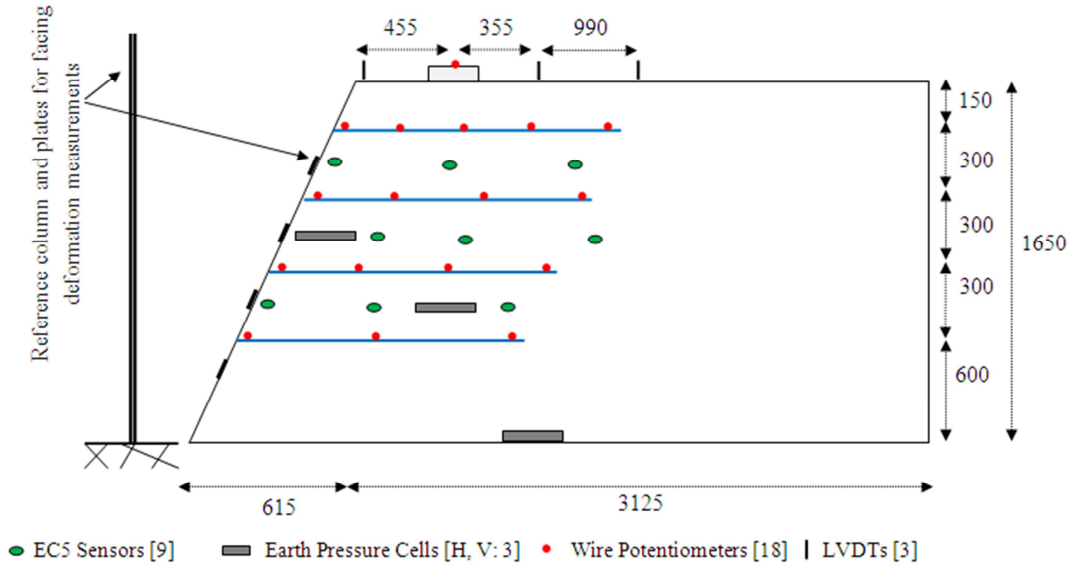

(a)

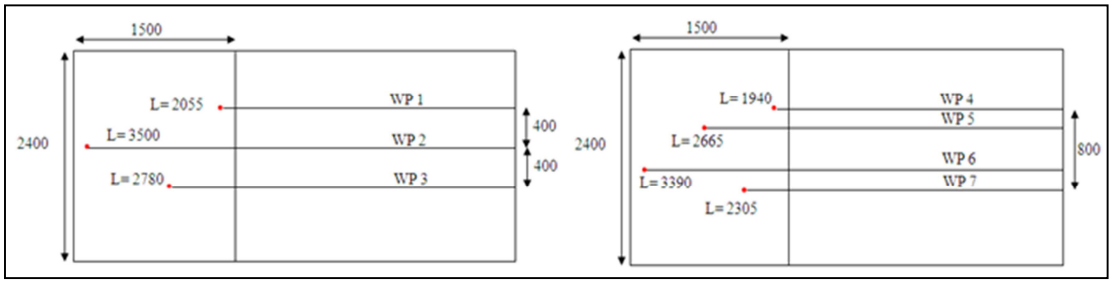

H = 600 mm H = 900 mm

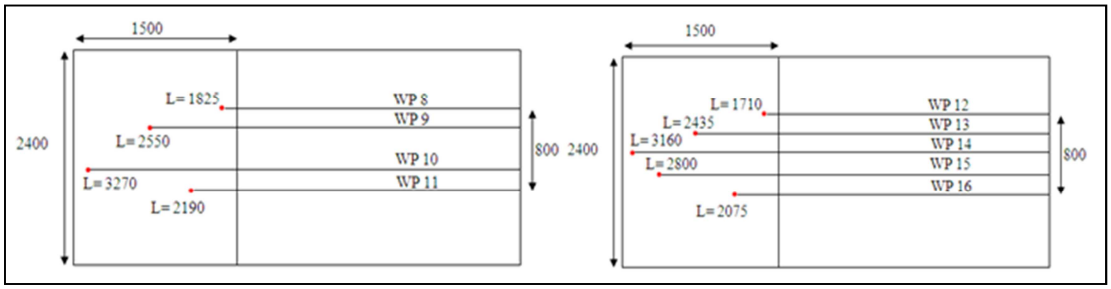

H = 1200 mm H = 1500 mm

(b)

Figure 6.13. Instrumentation plan for full-scale reinforced embankment test; Note: (1) All dimensions are in "mm", (2) Length of reinforcement layers throughout the embankment is uniform and equal to 1500 mm, (3) WPs were attached at an equal distance over the length of each reinforcement, (4) Dimensions and locations of sensors are not in scale.

CHAPTER 7

LABORATORY RESULTS OF PULLOUT AND INTERFACE SHEAR TESTS

7.1. Large-Scale Pullout Tests

7.1.1. Water Content and Suction

Figures 7.1 and 7.2 show distributions of the soil GWC and suction in each layer for the large-scale pullout tests carried out at different GWC under 50 kPa overburden pressure. The mean and Coefficient of Variation (COV) values for these parameters were calculated for the fifth layer (lift) in the pullout box (i.e. for the soil layer in contact with the geotextile reinforcement) to examine the proximity of their as-placed and target values.

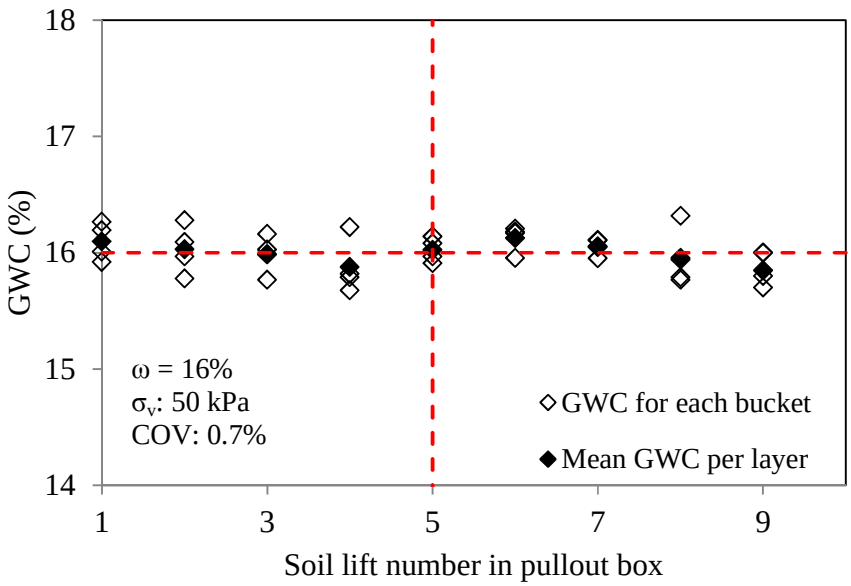

(a)

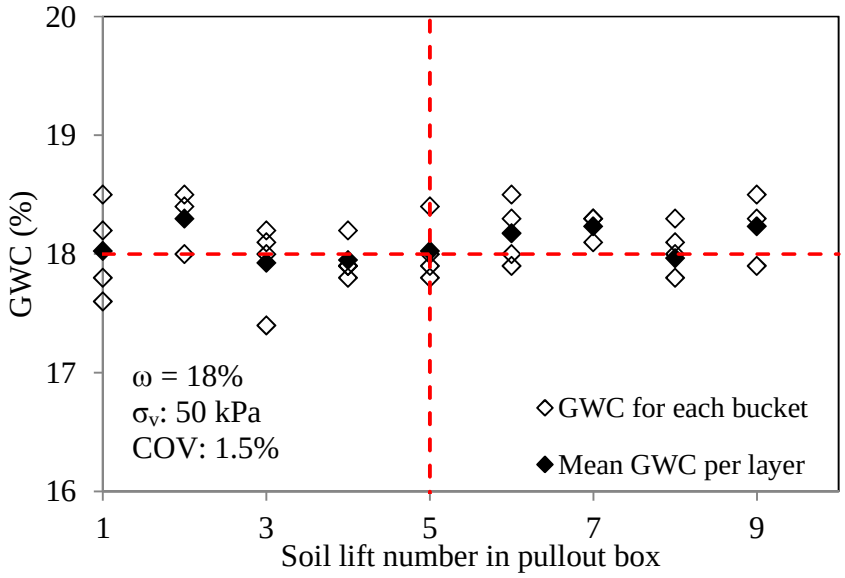

(b)

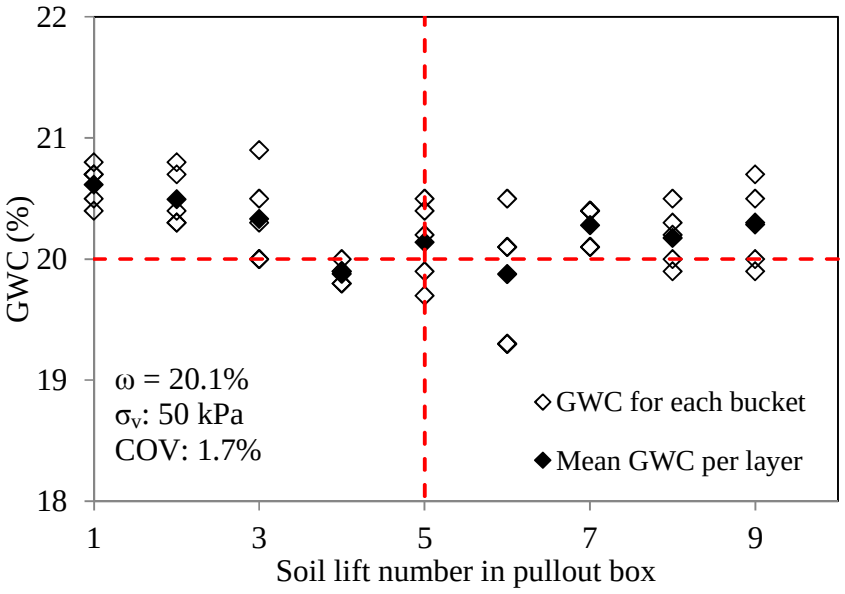

(c)

Figure 7.1. Distributions of soil GWC with depth in pullout box for different pullout test cases. Notes: [1] One soil sample was taken from each bucket to test its GWC value; [2] The number of soil samples from each soil lift in the pullout box is given in Table 7.3 (caption); [3] The horizontal line indicates the target GWC for each test case; [4] The vertical dashed line shows the location of the soil-geotextile interfaces; [5] The mean and COV values reported in the legends are calculated for the fifth layer (i.e. soil-geotextile interface) data only.

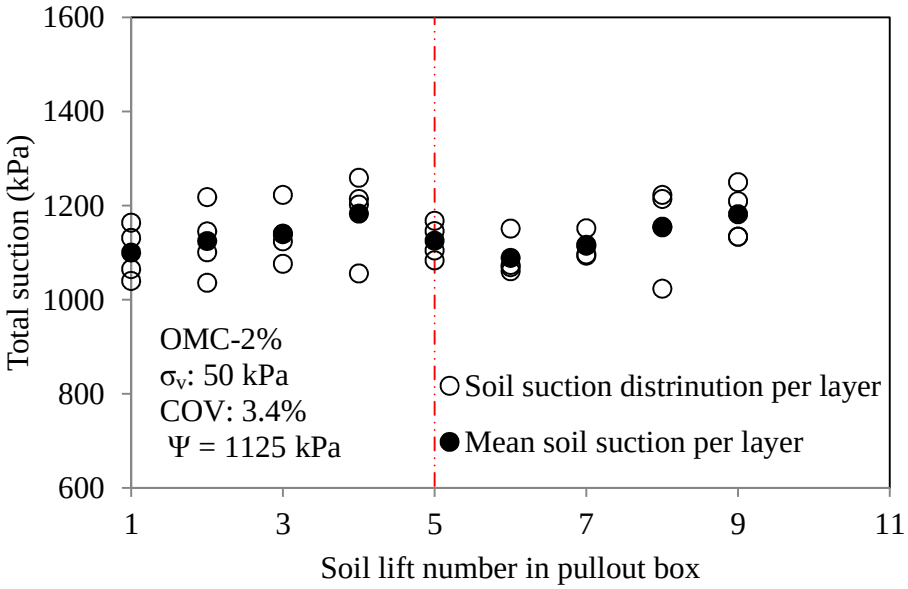
1600
1400
1200
1000
800
600
Total suction (kPa)
OMC-2%
σv: 50 kPa
COV: 3.4%
Ψ = 1125 kPa
Soil suction distrinution per layer
Mean soil suction per layer
1
3
5
7
9
11
Soil lift number in pullout box

(a)

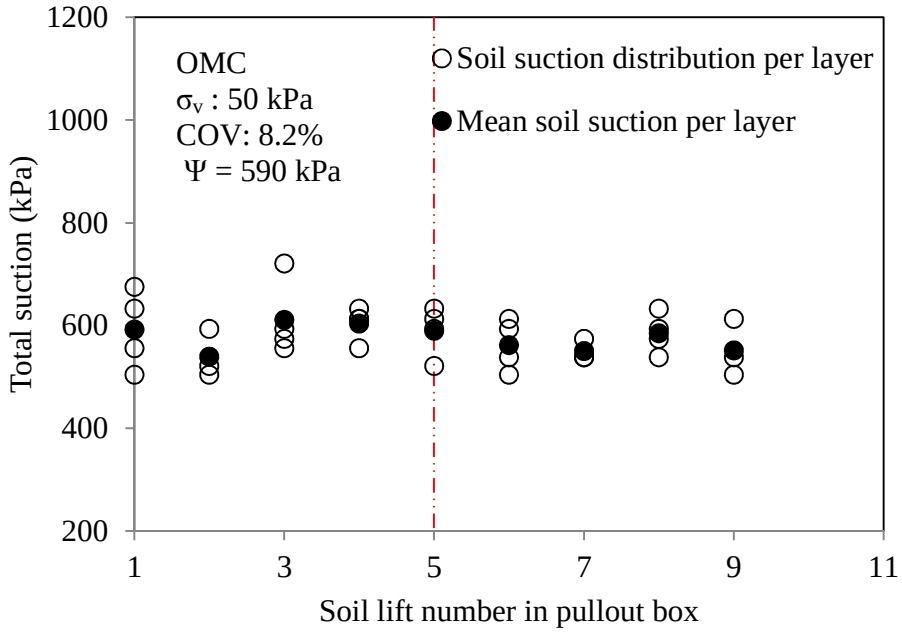
1200
1000
800
600
400
200
Total suction (kPa)
OMC
σv : 50 kPa
COV: 8.2%
Ψ = 590 kPa
Soil suction distribution per layer
Mean soil suction per layer
1
3
5
7
9
11
Soil lift number in pullout box

(b)

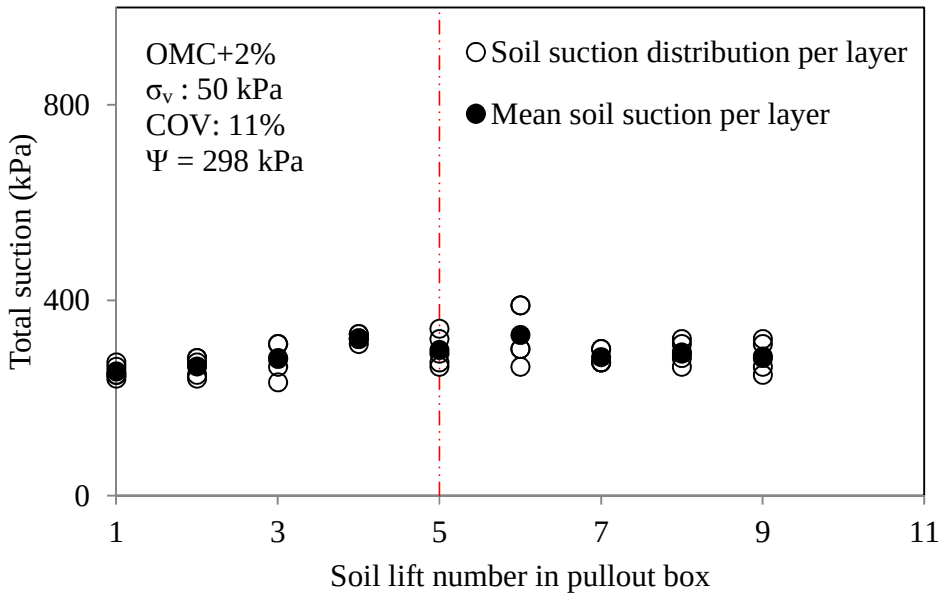

(c)

Figure 7.2. Distributions of the soil suction with depth in the pullout box from WP4 at different GWC. The number of soil samples from each soil lift in the pullout box is reported in Table 7.3.

Table 7.1 shows the mean and COV values for the GWC and suction in the fifth layer in large-scale pullout tests. The accuracy of the soil suction values from the PST-55 psychrometers was also examined by comparing them with the readings from the WP4 potentiometer as shown in Table 7.2. The GWC and suction COV values for all test cases as given in Figures 7 and 8 and Table 7.1 are overall reasonable and indicate that the soil moisture condition was fairly uniform and consistent throughout the large-scale test models.

Table 7.1. Mean and COV values for the GWC and suction in the fifth layer (in contact with geotextile) in large-scale pullout tests

Target ω (%)	σ_n *(kPa)*	*Mean Ψ (kPa)*	$COV_{(\Psi)}$ *(%)*	*Mean ω (%)*	$COV_{(\omega)}$ *(%)*
16 (OMC-2%)	10	1236	7.3	15.7	1.5
	20	1196	5.9	15.8	1.1
	50	1125	3.4	16.0	0.7
18 (OMC)	10	513	5.7	18.5	0.9
	20	570	6.7	18.1	1.1
	50	590	8.2	18.0	1.5
20 (OMC+2%)	10	304	11.2	20.1	1.8
	20	352	9.9	19.6	1.6
	50	298	11.0	20.1	1.7

Table 7.2. Comparison of suction values in Chickasha soil as measured using psychrometers (in-situ) and WP4 (offsite equipment)

Target ω (%)	σ_n (kPa)	Mean Ψ (kPa) WP4 [(1)]	Mean Ψ (kPa) PST-55 [(2)]
16 (OM-2%)	10	1243	921
	20	1200	906
	50	1135	910
18 (OMC)	10	520	488
	20	570	520
	50	580	543
20 (OMC+2%)	10	311	303
	20	360	335
	50	282	310

Notes: [(1)] Mean values were calculated using four undisturbed samples from the fifth layer (in contact with geotextile) for each pullout test; [(2)] Mean values were determined using three PST-55 psychrometers placed in the fifth soil layer.

7.1.2. Reinforcement Strain and Interface Strength

Figure 7.3 shows the strain distributions over the length of geotextile reinforcement at maximum pullout force based on the extensometer results. The strain near the front end of the geotextile reinforcement was calculated by subtracting the displacements measured at the location of Extensometer 1 from those measured at the front end of the geotextile exiting the soil. The displacements at the front end were determined by subtracting the calculated elongation of the in-air portion of the geotextile specimen from the actuator displacement. Results in Figure 7.3 indicate that strains in the geotextile reinforcement are greater at higher overburden pressures and lower GWC values (i.e. higher soil suction).

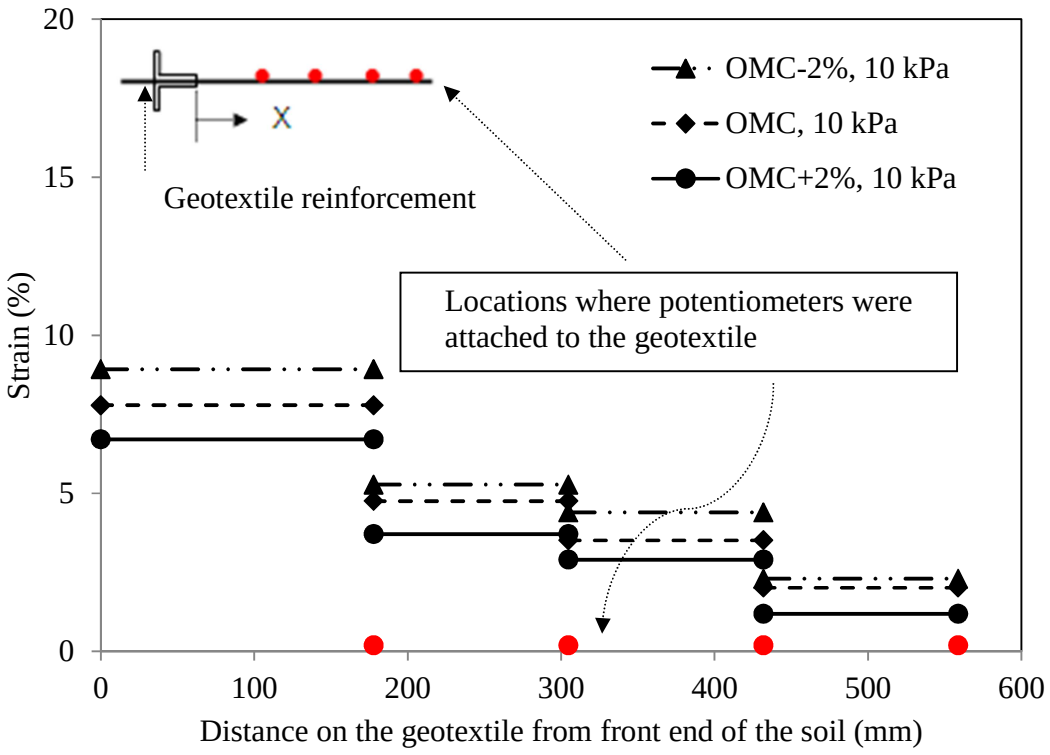

(a)

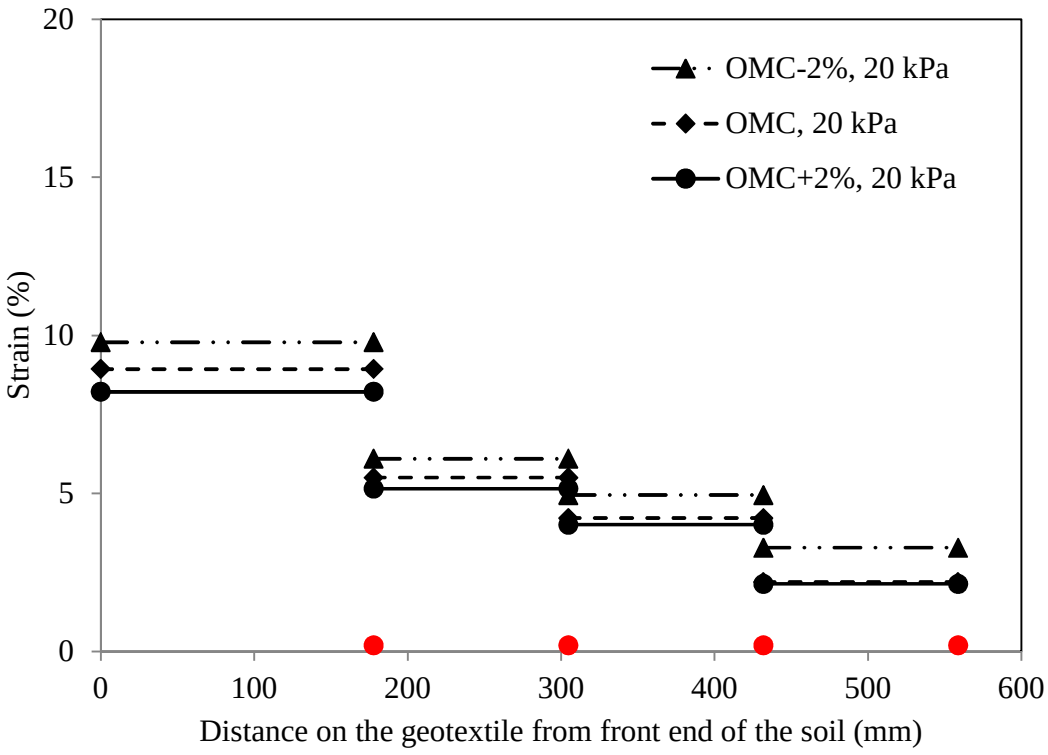
20
15
10
5
0
Strain (%)
0
100
200
300
400
500
600
Distance on the geotextile from front end of the soil (mm)
OMC-2%, 20 kPa
OMC, 20 kPa
OMC+2%, 20 kPa

(b)

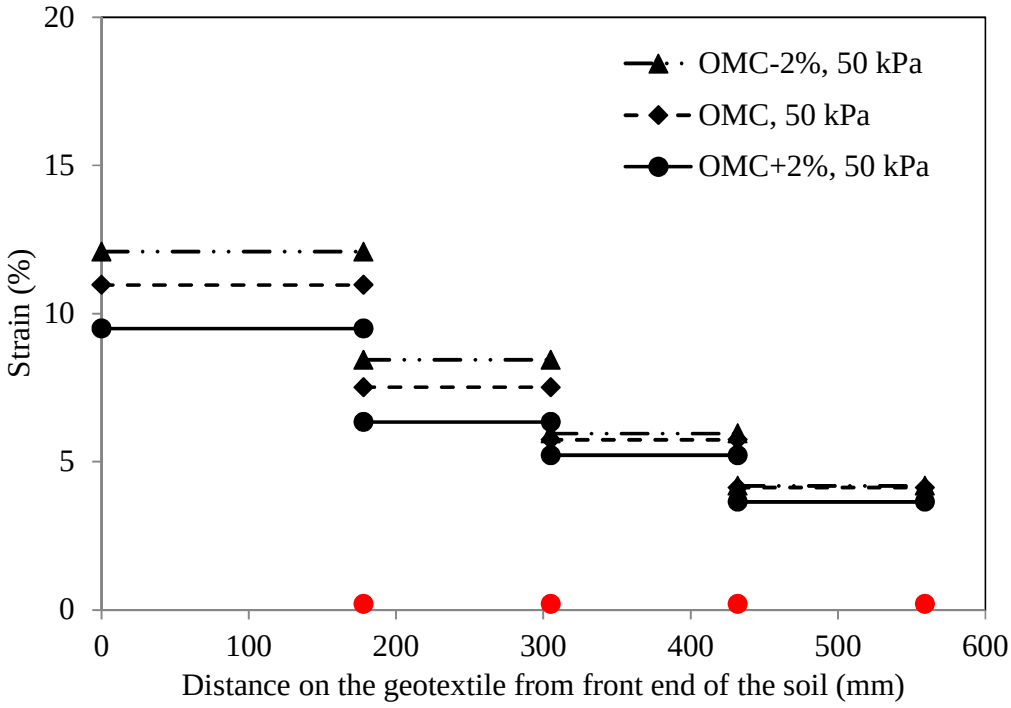
20
15
10
5
0
Strain (%)
0
100
200
300
400
500
600
Distance on the geotextile from front end of the soil (mm)
OMC-2%, 50 kPa
OMC, 50 kPa
OMC+2%, 50 kPa

(c)

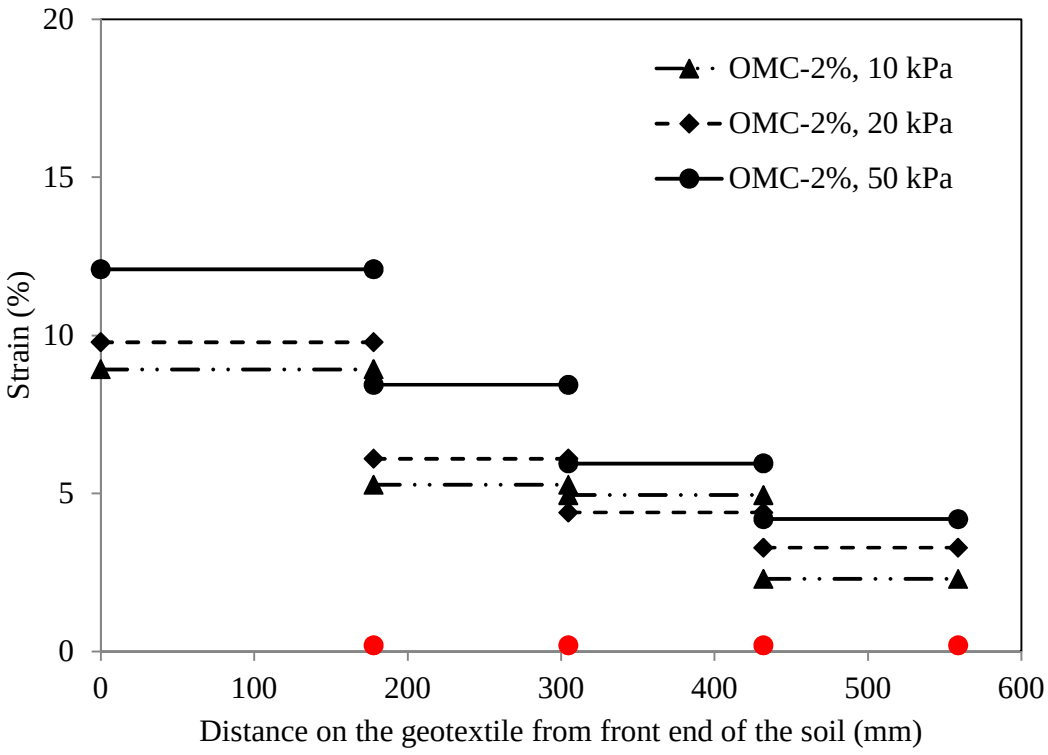
20
15
10
5
0
Strain (%)
0
100
200
300
400
500
600
Distance on the geotextile from front end of the soil (mm)
OMC-2%, 10 kPa
OMC-2%, 20 kPa
OMC-2%, 50 kPa

(d)

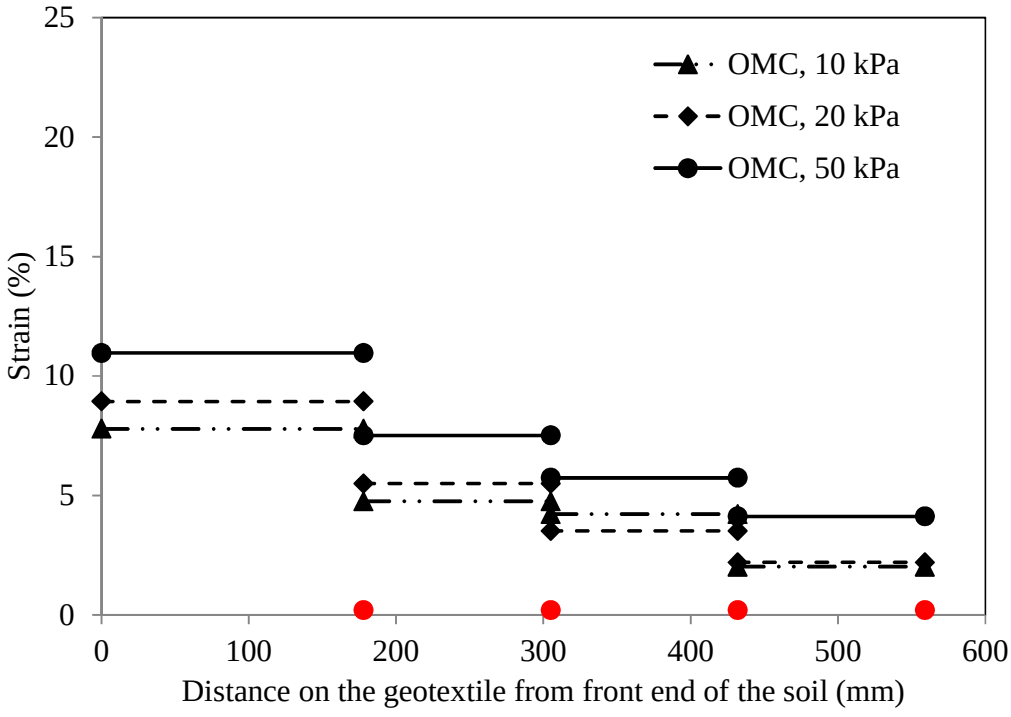
25
20
15
10
5
0
Strain (%)
0
100
200
300
400
500
600
Distance on the geotextile from front end of the soil (mm)
OMC, 10 kPa
OMC, 20 kPa
OMC, 50 kPa

(e)

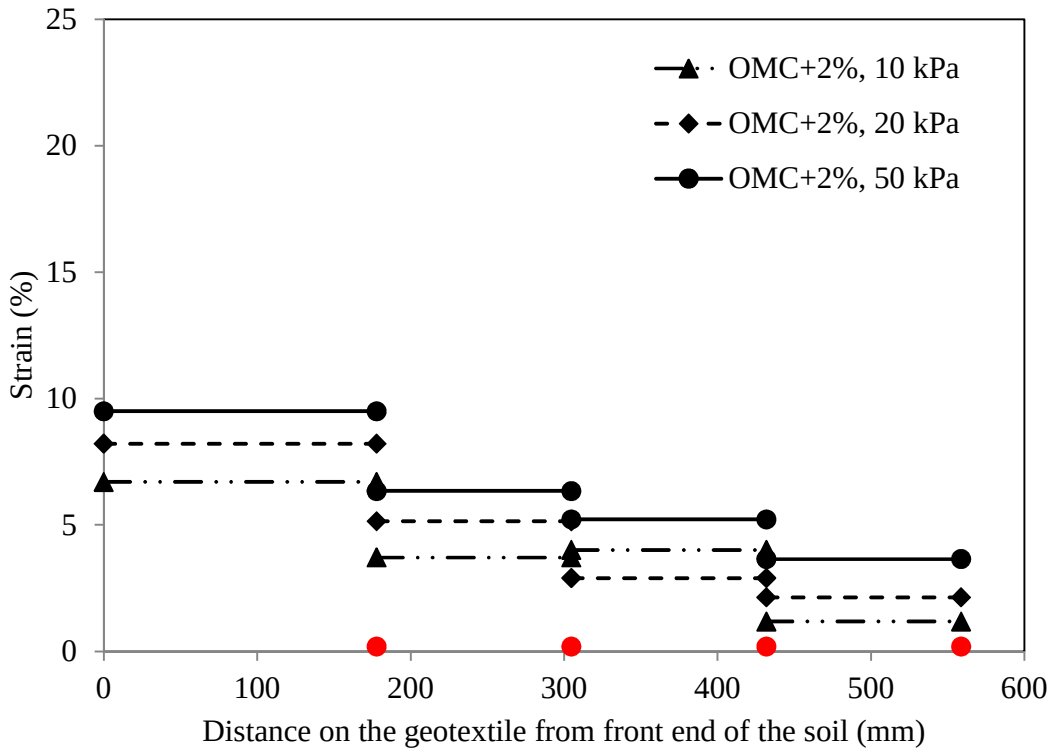

(f)

Figure 7.3. Axial strain distributions in geotextile reinforcement subjected to pullout load from large-scale pullout tests on Chickasha soil at different GWC and overburden pressure values.

Figures 7.4 shows the pullout test data and results of interface shear strength (τ) for the Chickasha soil for different magnitudes of GWC and overburden pressure. The τ values were calculated by dividing the pullout force for each case by the in-soil area of the geotextile specimen (i.e. two times the geotextile area). The target GWC values in the pullout tests include OMC-2% (16%), OMC (18%) and OMC+2% (20%) (see Table 3.1 and 3.2). In Figures 7.4a-c, the measured pullout force is plotted as a function of the actuator displacement. Results shown in Figure 7.4 quantify the increase in the reinforcement pullout resistance in Chickasha soil with overburden pressure for a given GWC value. It should be noted that for the test at OMC-2% subjected to 50 kPa

overburden pressure (Figure 7.4a) it was found that the geotextile had been ruptured before pullout. Therefore, the pullout force at failure was estimated using the trends in the corresponding test data at OMC and OMC+2%. As expected, increasing suction led to a higher maximum reinforcement pullout resistance in otherwise identical test specimens (Figures 7.4d and 7.4e). Results shown in Figure 7.4d indicate that apparent adhesion increases at lower GWC due to higher suction. This observation is consistent with those reported by Khoury et al. (2011) from suction-controlled interface testing of fine-grained soil specimens.

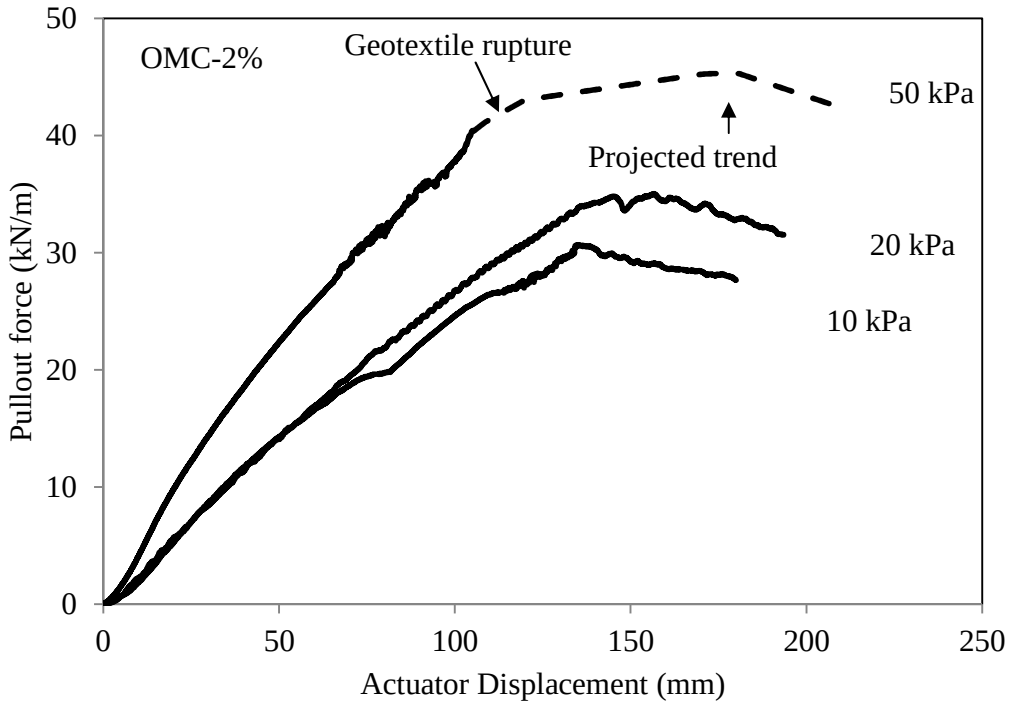

(a)

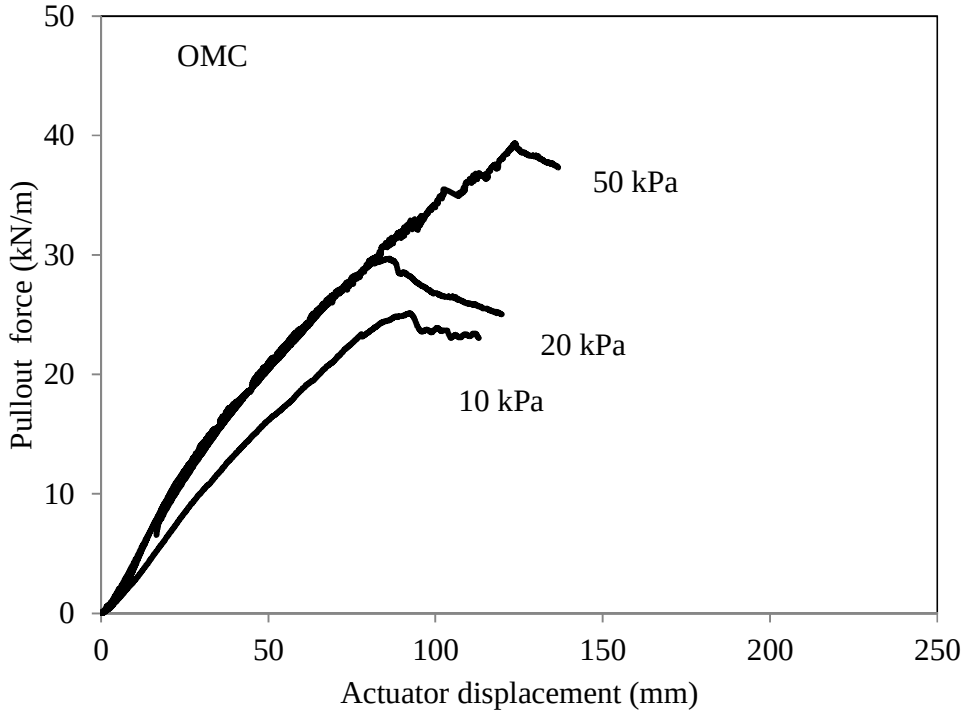
OMC
50 kPa
20 kPa
10 kPa
Pullout force (kN/m)
Actuator displacement (mm)
0
10
20
30
40
50
0
50
100
150
200
250

(b)

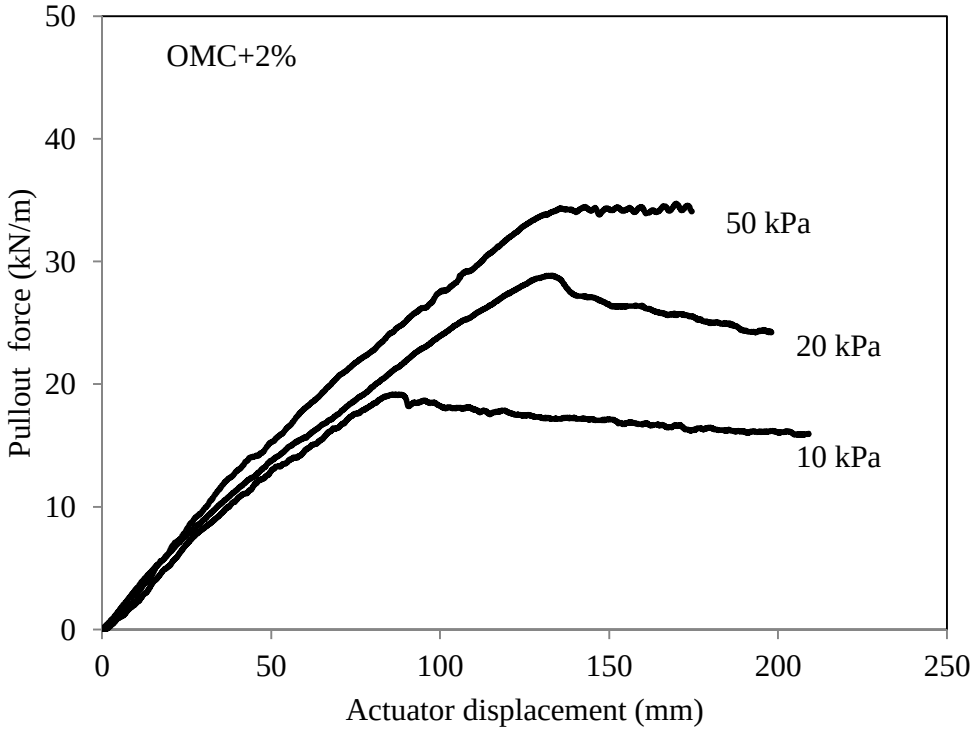
OMC+2%
50 kPa
20 kPa
10 kPa
Pullout force (kN/m)
Actuator displacement (mm)
0
10
20
30
40
50
0
50
100
150
200
250

(c)

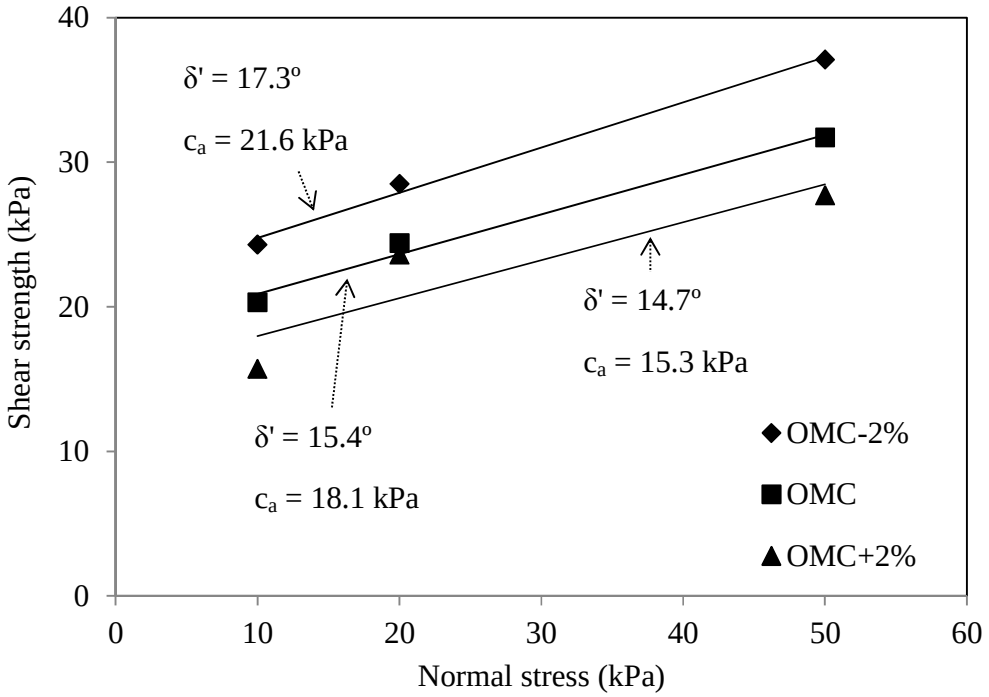

(d)

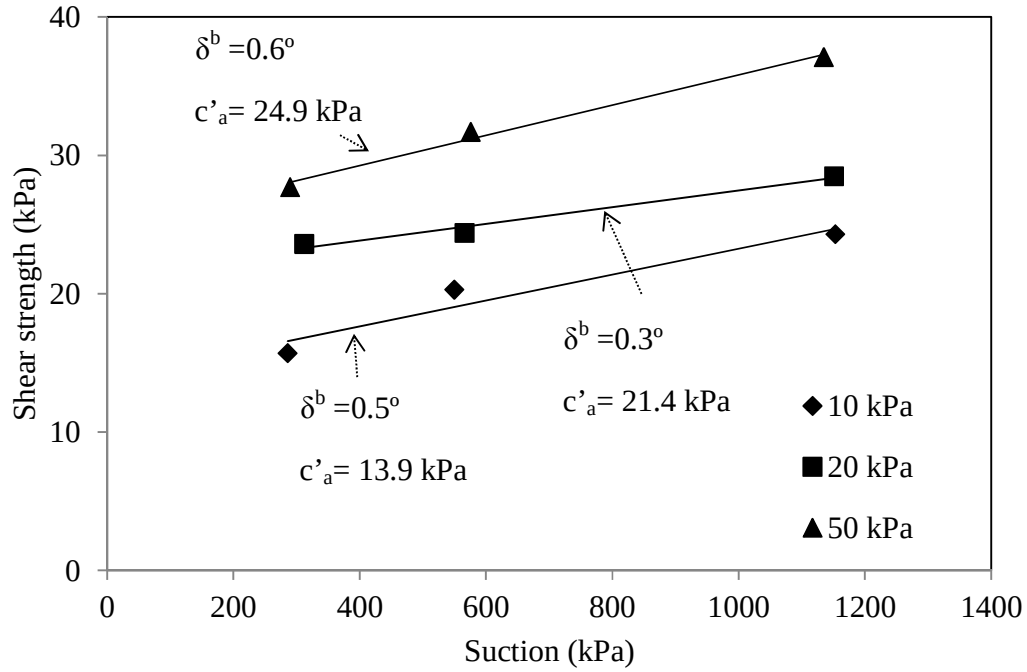

(e)

Figure 7.4. Pullout test data and interface strength results from large-scale pullout tests for Chickasha soil at different GWC values: (a)-(c) load-displacement data; (d) failure envelopes for the soil-geotextile interface on frontal plane; (e) failure envelopes for soil-geotextile interface on lateral plane. Note: in (a), dashed line indicates the estimated pullout failure.

Results shown in Figure 7.4a-d represent the frontal planes of extended Mohr-Coulomb failure envelopes for the soil-geotextile interface at different GWC and suction values. These failure envelopes can be considered to be practically linear for all GWC cases examined. The interface strength results, i.e. the values for the slope (tan δ') and the intercept (c_a) of the failure envelopes on these frontal planes are summarized in Table 7.3. Abu-Farsakh et al. (2007) studied the effect of the GWC on the interaction between three cohesive soils and a woven geotextile reinforcement material. They found that an increase in the molding GWC of the soil from 24% to 33% caused 43% reduction in the interface shear resistance. The data summarized in Table 7.3 are overall consistent with Abu-Farsakh et al.'s observations. For instance, the pullout resistance (P_r) at OMC+2% is between 17% and 35% lower than the corresponding value at OMC-2% depending on the overburden pressure. A smaller confining pressure resulted in a greater reduction in pullout resistance for a given increase in the soil GWC value.

Table 7.3. Interface strength properties from large-scale pullout tests in Chickasha soil

Target ω (%)	σ_n (kPa)	Mean ω (%)[1]	Mean Ψ (kPa)[2]	P_r (kN/m)	τ (kPa)	δ' (°)	C_a (kPa)
16 (OMC-2%)	10	16.0	1153	29.6	24.3	17.3	21.6
	20	16.0	1151	34.8	28.5		
	50	16.0	1135	45.2	37.1		
18 (OMC)	10	18.3	550	24.8	20.3	15.4	18.1
	20	18.2	566	29.7	24.4		
	50	18.1	576	38.7	31.7		
20 (OMC+2%)	10	20.3	286	19.1	15.7	14.7	15.3
	20	20.0	312	28.8	23.6		
	50	20.2	290	33.8	27.7		

Notes: [1] Mean values were calculated using 45 GWC samples for each pullout test (5 samples from each of the nine 2-inch soil lifts); [2] Mean values were determined from SWCC for Chickasha soil based on GWC values determined for each test (i.e. 45 data points).

Results in Figure 7.4e show the failure envelopes of the three-dimensional extended Mohr-Coulomb failure surface on the lateral plane for the soil-geotextile interface as a function of the soil suction. The line intercept and slope represent the effective adhesion at zero overburden pressure (σ_n = 0 kPa) and interface friction angle with respect to suction (δ^b), respectively. The data shown in Figure 7.4e indicate that the interface friction angle with respect to suction for the Chickasha soil-geotextile tested is negligible (it is less than 1°; note the significantly different scales of the horizontal and vertical axes in the figure). These results indicate that as the overburden pressure increases, interface adhesion and consequently, the interface shear strength increases. The extended Mohr-Coulomb envelope in Figure 7.5 shows the variation of the interface shear strength (τ) with the values of soil suction and overburden pressure at the soil-reinforcement interface. Taken together, the results based on the description of soil shear strength using two stress state variables (i.e. soil suction and net normal stress) as presented in Figures 7.4 and 7.5 and Table 7.3 are in good agreement with those reported by Hatami et al. (2010a) and Khoury et al. (2011) on other marginal soils.

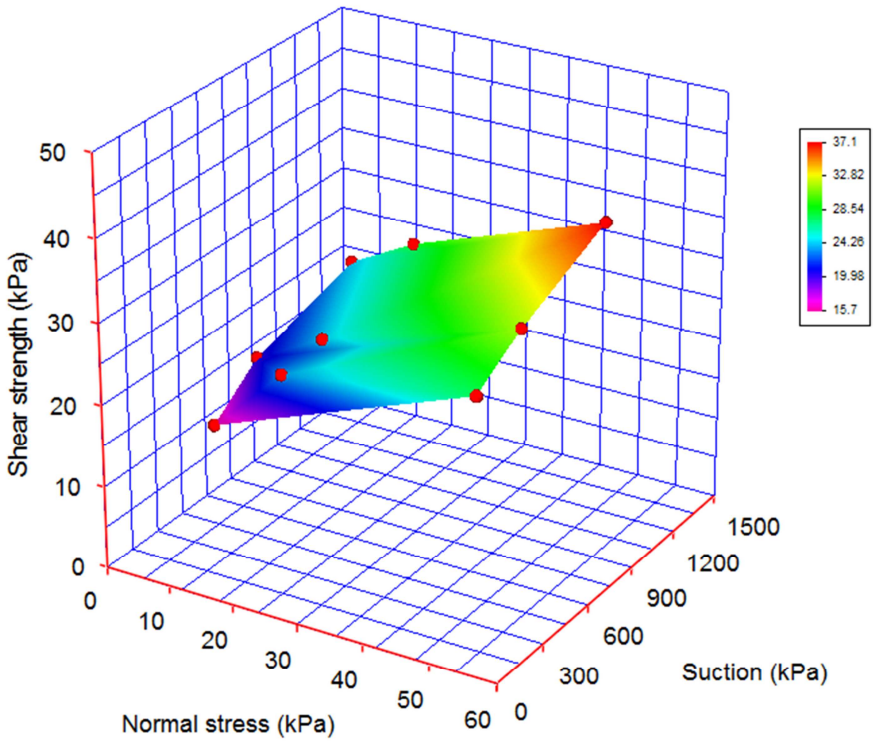

Figure 7.5. Extended Mohr-Coulomb envelope from large-scale pullout tests

Table 7.4 shows α F^* (Equation 1.1) values calculated from all large-scale pullout tests in Chickasha soil. Example calculations for α according to the FHWA guidelines (Berg et. al. 2009) are shown in Figure 7.6. Based on the intersection of the horizontal asymptote with the y-axis, the design value for α from pullout tests in Chickasha soil was found to be 0.5 (Figure 7.6e). This value of α indicates a fairly extensible geotextile material and a linear strain distribution along its length. It is also comparable to the value reported by Hatami et al. (2010a) for the same geotextile material tested in Minco silt (i.e. α = 0.59) and the value α = 0.6 recommended by FHWA for geotextiles (Berg et al. 2009). F* values were calculated using Equation 1.1.

Table 7.4. Calculated values of αF^* from large-scale pullout tests in Chickasha soil

Target ω (%)	σ_n(kPa)	P_r (kN/m)	τ (kPa)	αF*
16 (OMC-2%)	10	29.6	24.3	2.43
	20	34.8	28.5	1.43
	50	45.2	37.1	0.74
18 (OMC)	10	24.8	20.3	2.04
	20	29.7	24.4	1.22
	50	38.7	31.7	0.64
20 (OMC+2%)	10	19.1	15.7	1.57
	20	28.8	23.6	1.18
	50	33.8	27.7	0.56

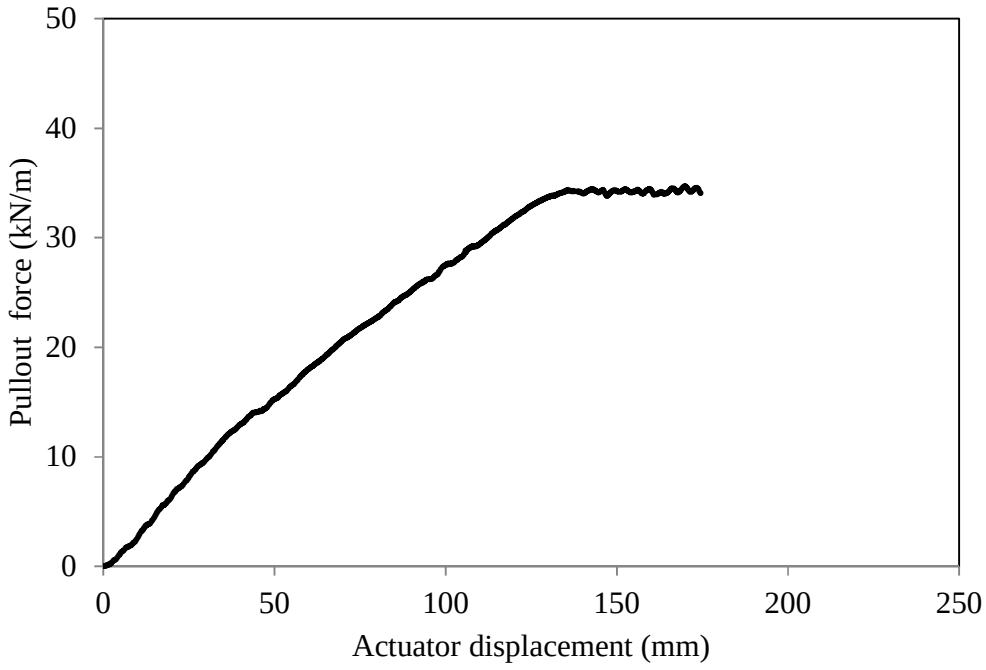

(a)

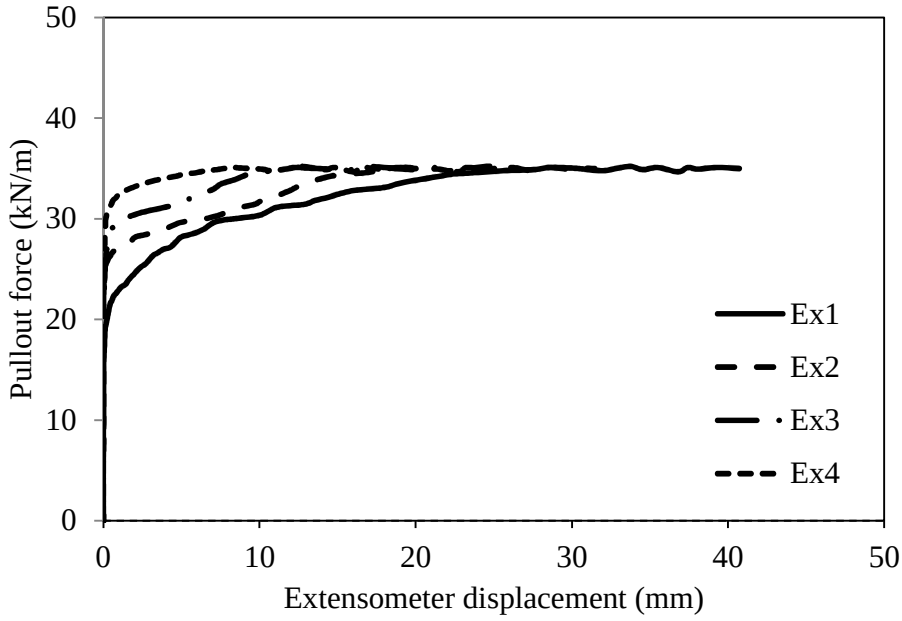
50
40
30
20
10
0
Pullout force (kN/m)
0
10
20
30
40
50
Extensometer displacement (mm)
Ex1
Ex2
Ex3
Ex4

(b)

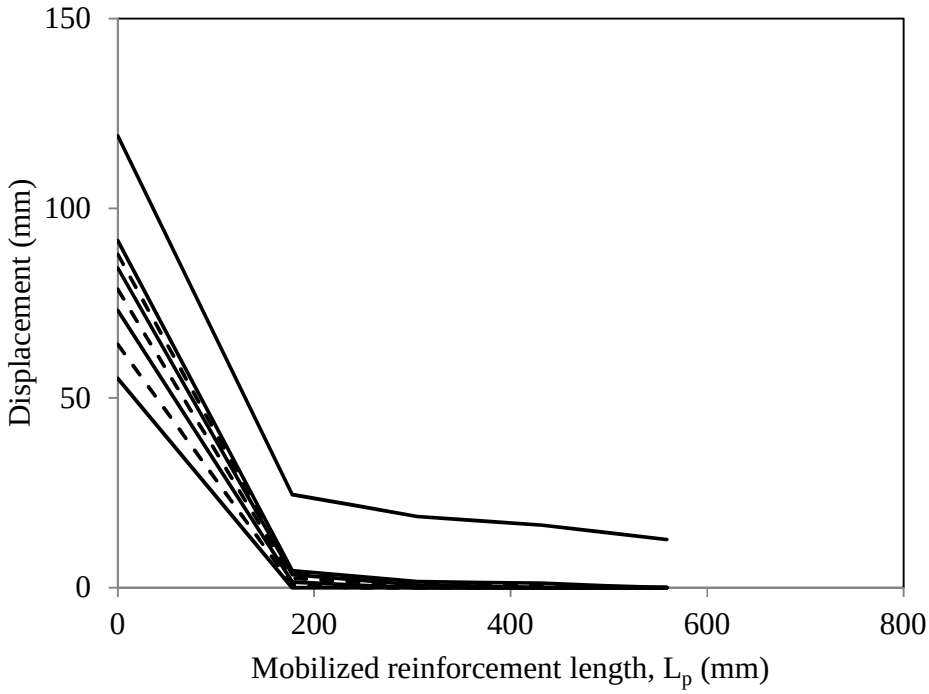
150
100
50
0
Displacement (mm)
0
200
400
600
800
Mobilized reinforcement length, L_p (mm)

(c)

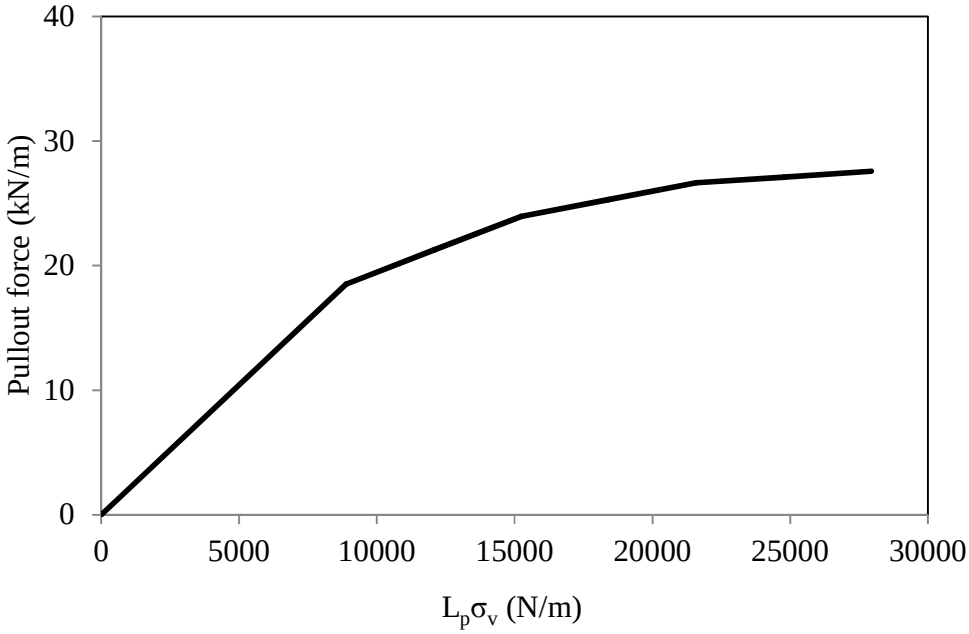

(d)

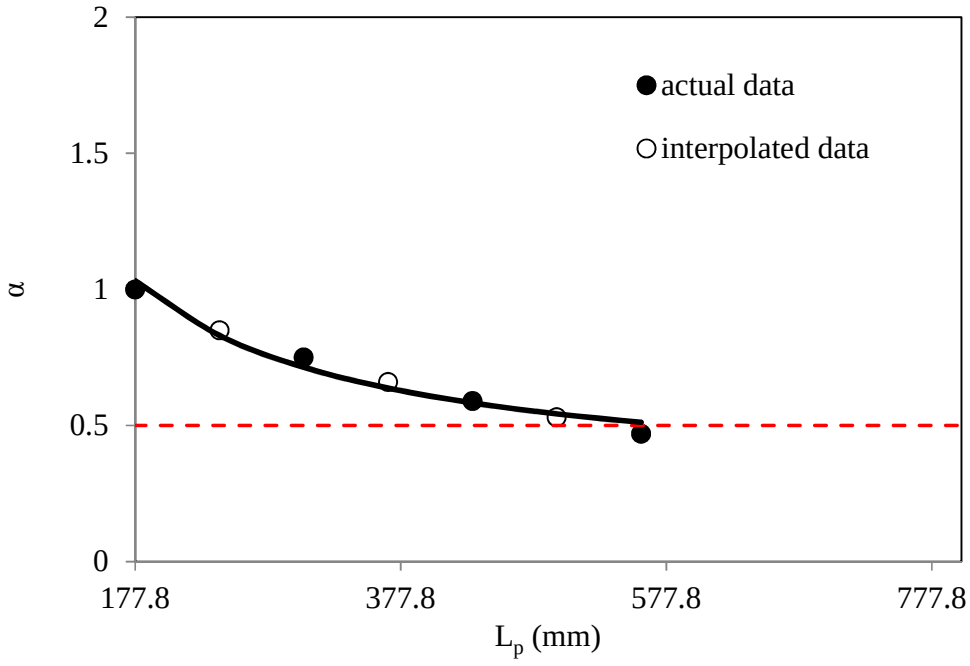

(e)

Figure 7.6. Pullout parameters for HP370 geotextile from large-scale pullout tests at OMC+2% subjected to 50 kPa overburden pressure: (a)-(b) pullout force versus actuator and extensometer displacement, respectively, (c)-(e) procedure to determine F* and α; Note: In (c), solid and dashed lines indicate actual and interpolated data, respectively.

7.2. Small-Scale Pullout Tests

Figure 7.7 shows the plots of pullout force versus actuator displacement for the small-scale pullout tests in Chickasha soil. Soil-geotextile interface strength properties obtained from the small-scale tests are summarized in Table 7.5.

The pullout test results given in Table 7.5 and Figure 7.7 show a clear influence of the soil overburden pressure and GWC on the soil-geotextile interface strength and pullout resistance. It is observed that the pullout force increases with overburden pressure. The interface adhesion contributing to the geotextile pullout resistance decreases by 31% as the soil GWC increases from OMC-2% to OMC+2%. The interface friction angle also decreases by 40% from OMC-2% to OMC+2%. These results are consistent with those obtained by the authors in a previous study on Minco silt (Hatami et al. 2010a,b).

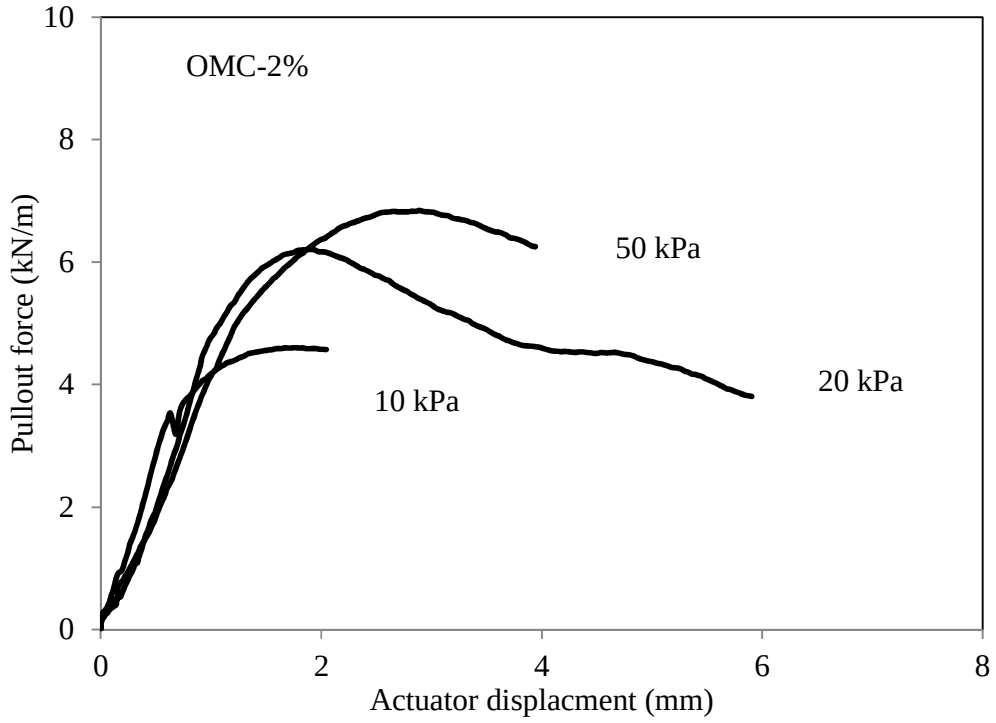

(a)

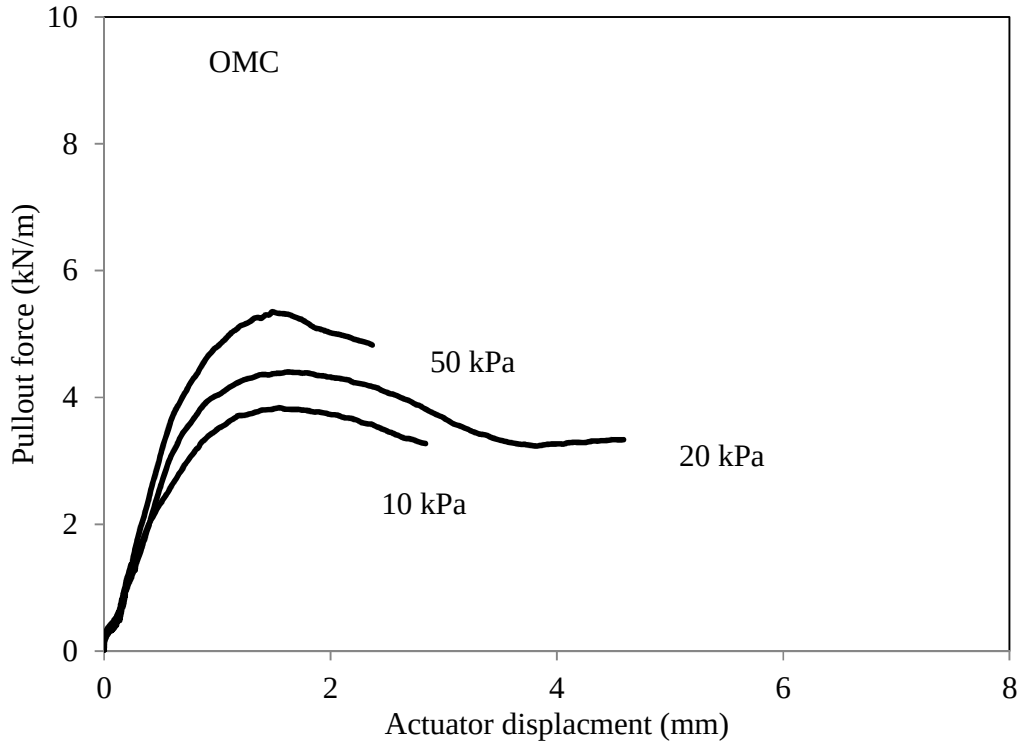
OMC
Pullout force (kN/m)
Actuator displacment (mm)
50 kPa
20 kPa
10 kPa
0
2
4
6
8
10

(b)

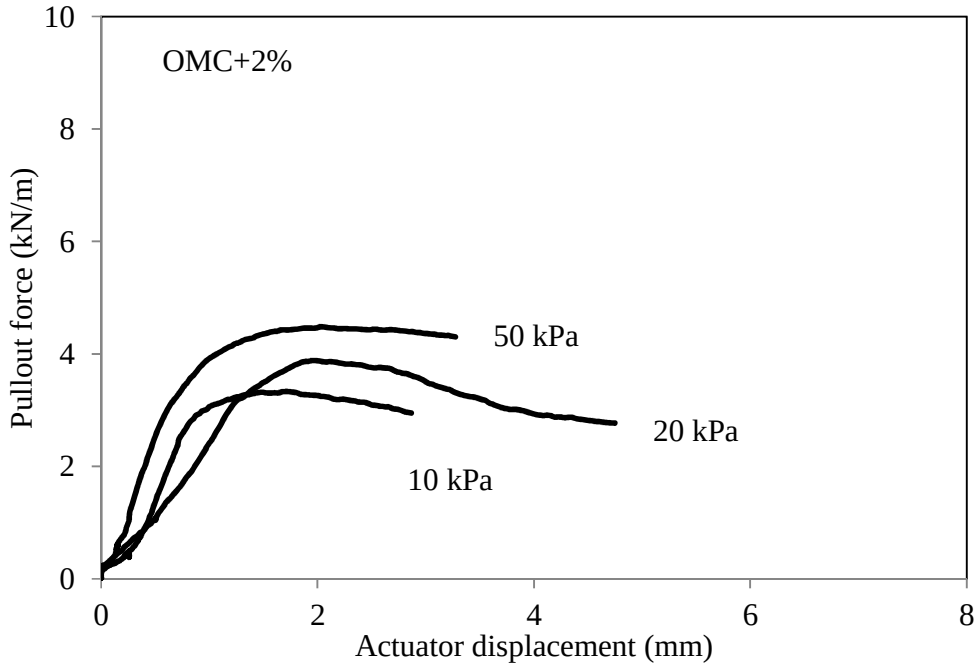
OMC+2%
Pullout force (kN/m)
Actuator displacement (mm)
50 kPa
20 kPa
10 kPa
0
2
4
6
8
10

(c)

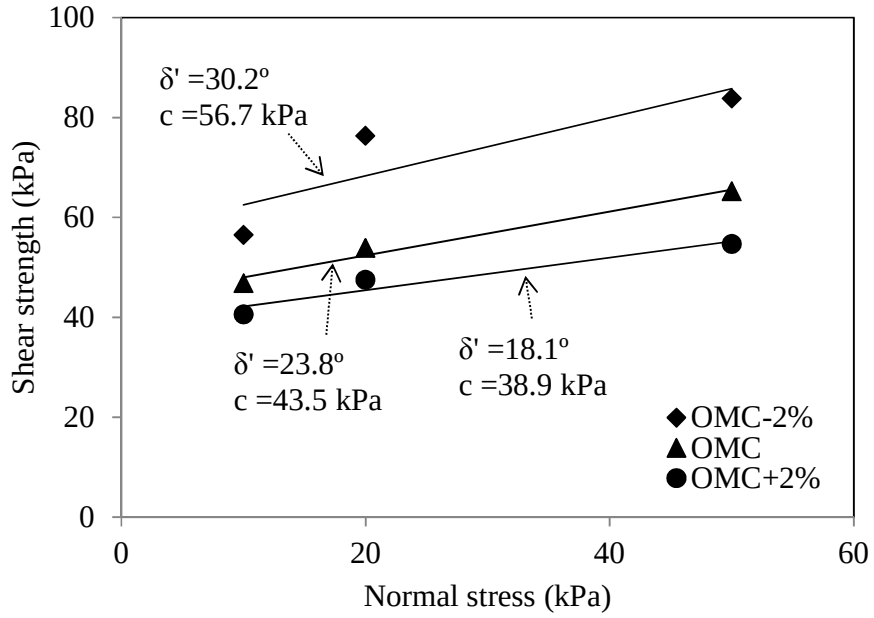

(d)

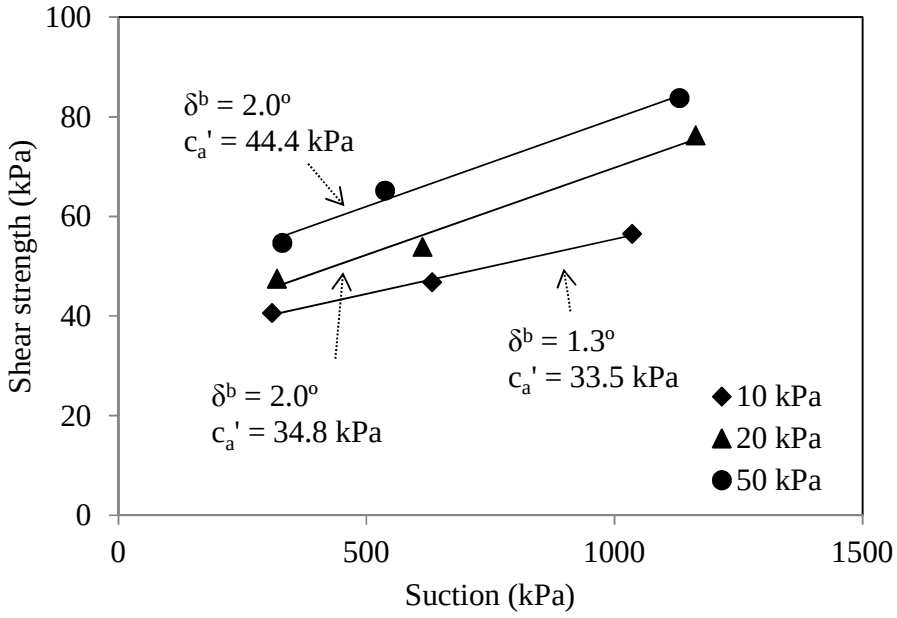

(e)

Figure 7.7. Pullout test data and interface strength results from small-scale tests on Chickasha soil and comparison of failure envelopes for soil-geotextile interface at different GWC: (a)-(c) load-displacement data; (d) failure envelopes on frontal plane; (e) failure envelopes on lateral plane. Note: suction values were calculated from the SWCC.

Table 7.5. Interface strength properties from small-scale pullout tests

Target ω (%)	$\boldsymbol{\sigma_n}$ (kPa)	ω (%)	Ψ (kPa)	τ (kPa)	$\boldsymbol{\delta'}$ (°)	C_a (kPa)
16(OMC-2%)	10	16.3	1036	56.5	30.2	56.7
	20	15.9	1164	76.3		
	50	16.0	1131	83.8		
18 (OMC)	10	17.8	633	46.8	23.8	43.5
	20	17.9	613	53.9		
	50	18.3	538	65.2		
20 (OMC+2%)	10	20.0	310	40.6	18.1	38.9
	20	19.9	320	47.5		
	50	19.8	331	54.7		

Note: Suction values were calculated from the SWCC.

Results in Figures 7.7d and 7.4d indicate that the interface adhesion from both small-scale and large-scale pullout tests depends on the soil GWC and it is consistently larger for greater soil suction values (i.e. lower GWC). These results also indicate that the magnitudes of soil-geotextile interface adhesion from small-scale pullout tests are greater than those from the corresponding large-scale tests. This could be attributed to the smaller size and greater boundary effects in the small-scale tests. Consequently, a calibration (or scale) factor needs to be determined and applied to the small-scale test results before they can be used for practical applications.

The data in Figure 7.7e indicate that the interface shear strength increases with overburden pressure as a result of increase in interface adhesion (c_a'). The results shown in Figure 7.7e indicate that the interface friction angle with respect to suction (δ^b) for the Chickasha soil-geotextile tested is less than 2°.

7.3. Small-Scale Interface Shear Tests

Figure 7.8 shows the Mohr-Coulomb envelopes from interface shear tests at different GWC values. The results show that the soil-geotextile interface strength increases consistently with the overburden pressure and with the soil matric suction. According to Figure 7.8a, the interface friction angle was found to decrease by 15% from OMC-2% to OMC+2%. Results in Figure 7.8b indicate that the interface friction angle with respect to matric suction on the lateral plane is less than 1º, which is consistent with the data from large-scale pullout tests (Figure 10e). Figure 7.9 shows the extended Mohr-Coulomb envelopes from small-scale pullout and interface shear tests. The plots of Mohr-Coulomb envelopes in Figure 7.9 show that the adhesion values calculated from pullout tests are greater which could be attributed to this fact that, in pullout tests, as opposed to the interface shear tests, the geotextile is stretched during the test. This could result in the enlargement of the geotextile openings which, in turn, could allow the fine-grained soil to penetrate into the plane of the geotextile. Similar to geogrids but at a smaller scale, the soil within the openings of the geotextile subjected to overburden pressure could exhibit some passive resistance against the pullout force which could be responsible for the larger adhesion intercept that is observed for the pullout test results as compared to the interface shear data. Table 7.6 and Figure 7.10 summarize the data from all laboratory tests carried out in this study.

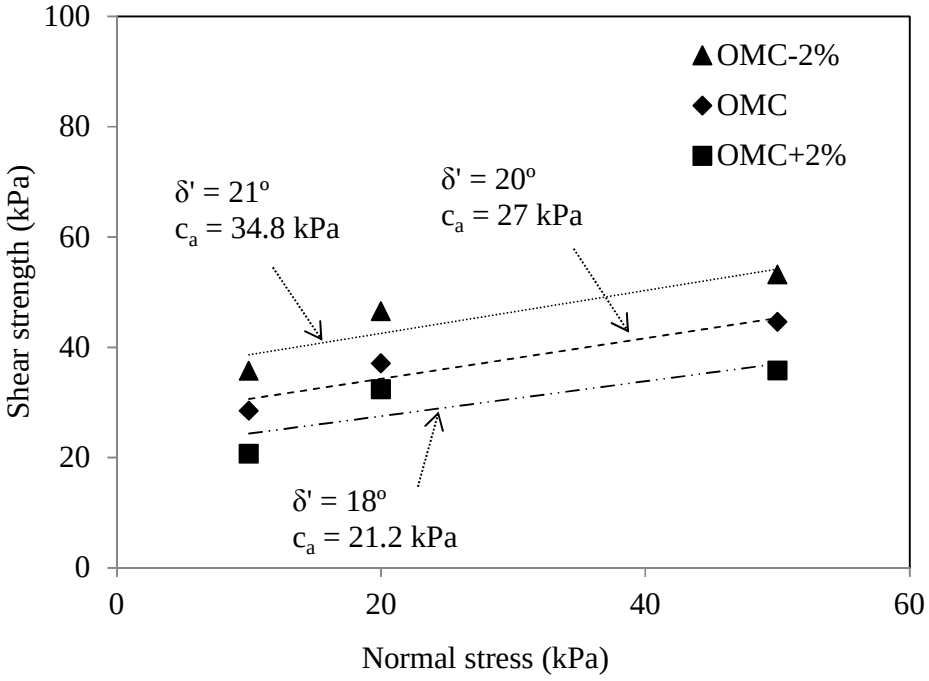

(a)

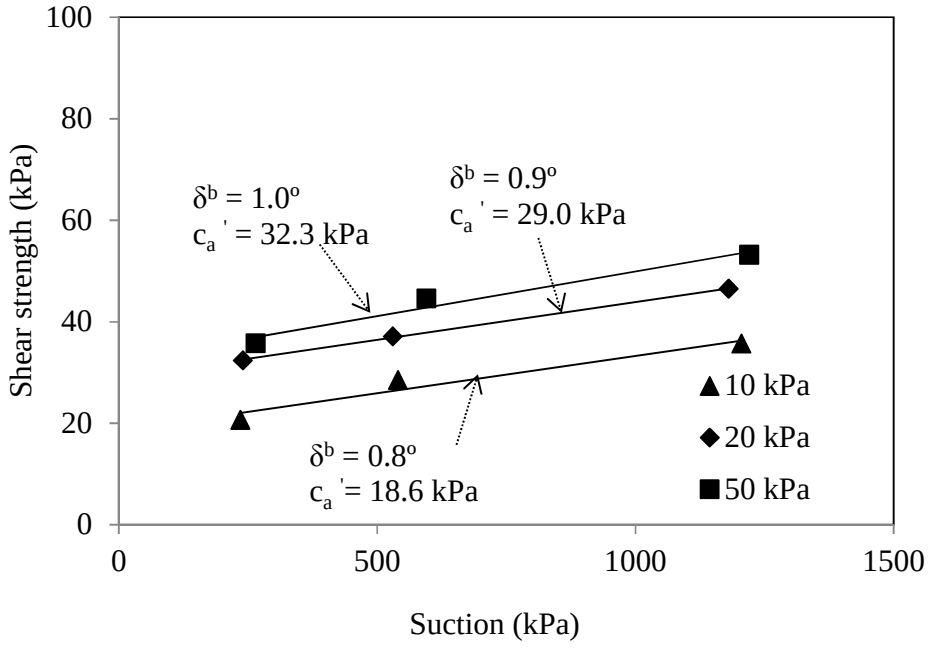

(b)

Figure 7.8. Mohr-Coulomb envelopes for Chickasha soil-geotextile interface from interface shear tests: (a) envelopes on the frontal plane; (b) envelopes on the lateral plane. Note: Suction values were calculated from the SWCC.

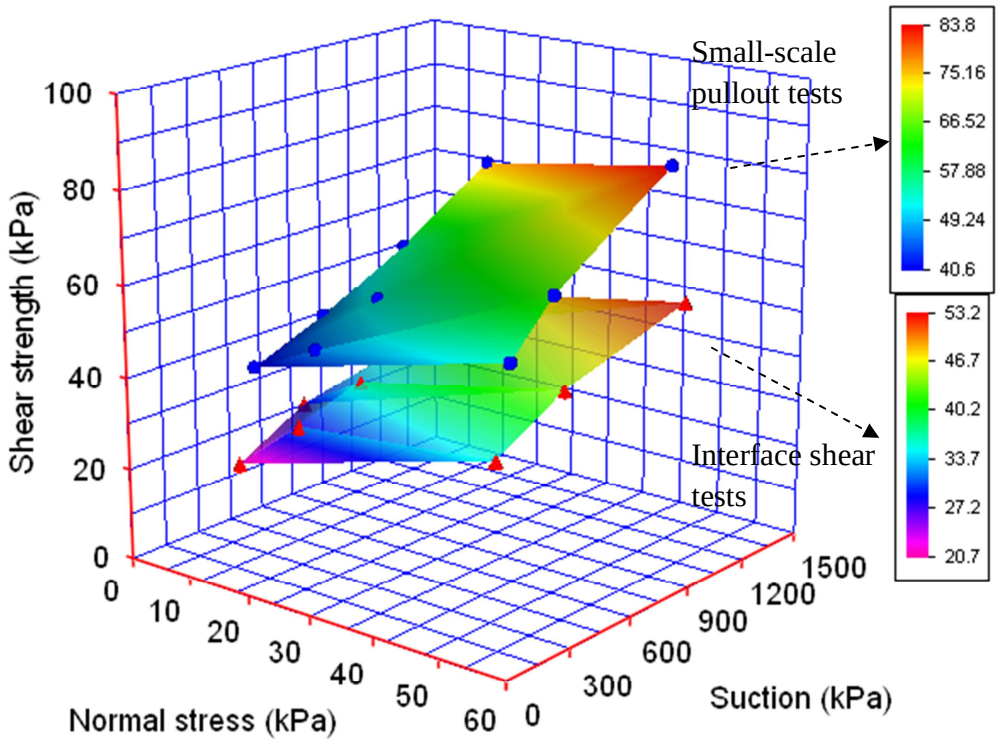

Figure 7.9. Extended Mohr-Coulomb envelope from small-scale pullout and interface shear tests

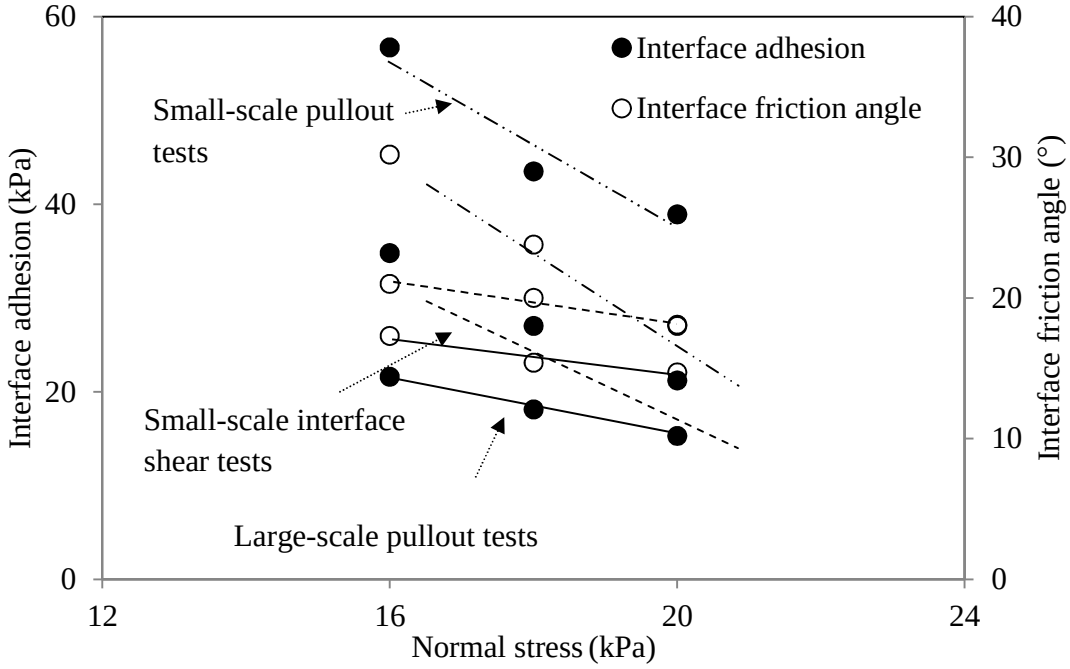

Figure 7.10. Comparison of large-scale and small-scale pullout and interface test data

Table 7.6. Summary of the results from all pullout and interface tests performed in this study

Type of test		Large-scale pullout		Small-scale pullout		Interface shear	
Target ω (%)	σ_n(kPa)	δ' (º)	C_a (kPa)	δ' (º)	C_a (kPa)	δ' (º)	C_a (kPa)
16(OMC-2%)	10	17.3	21.6	30.2	56.7	21.0	34.8
	20						
	50						
18 (OMC)	10	15.4	18.1	23.8	43.5	20.0	27.0
	20						
	50						
20 (OMC+2%)	10	14.7	15.3	18.1	38.9	18.0	21.2
	20						
	50						

CHAPTER 8

LABORATORY RESULTS OF REDUCED-SCALE EMBANKMENT TESTS

8.1. Soil Gravimetric Water Content and Suction

During construction of each embankment model, GWC value of each soil lift was determined by taking 6 soil samples while compaction using oven drying method (ASTM 2216-10). In addition, random soils samples were taken (on the order of 3 from the surface of the soil after each 2-3 layers had been compacted) to measure their GWC values and make sure that the loss of soil water content as a result of the compaction procedure was negligible. Figure 8.1 shows the distributions of soil GWC within the embankment for all test cases carried out in this study. The results are compared with the GWC values obtained from the SWCC (Figure 4.3) and PST-55 psychrometers to examine how close the as-placed values were to the target values.

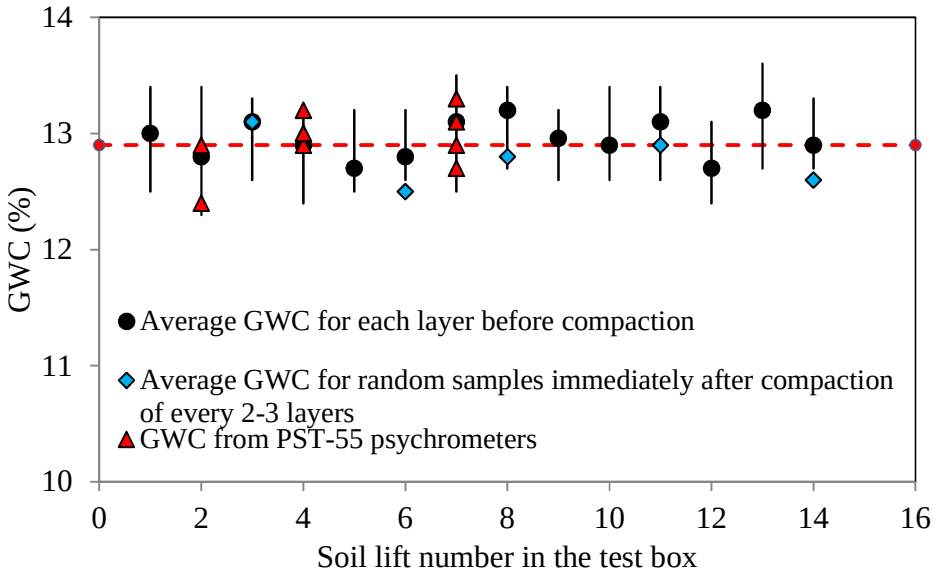
14
13
12
11
10
GWC (%)
0
2
4
6
8
10
12
14
16
Soil lift number in the test box
Average GWC for each layer before compaction
Average GWC for random samples immediately after compaction of every 2-3 layers
GWC from PST-55 psychrometers

(a)

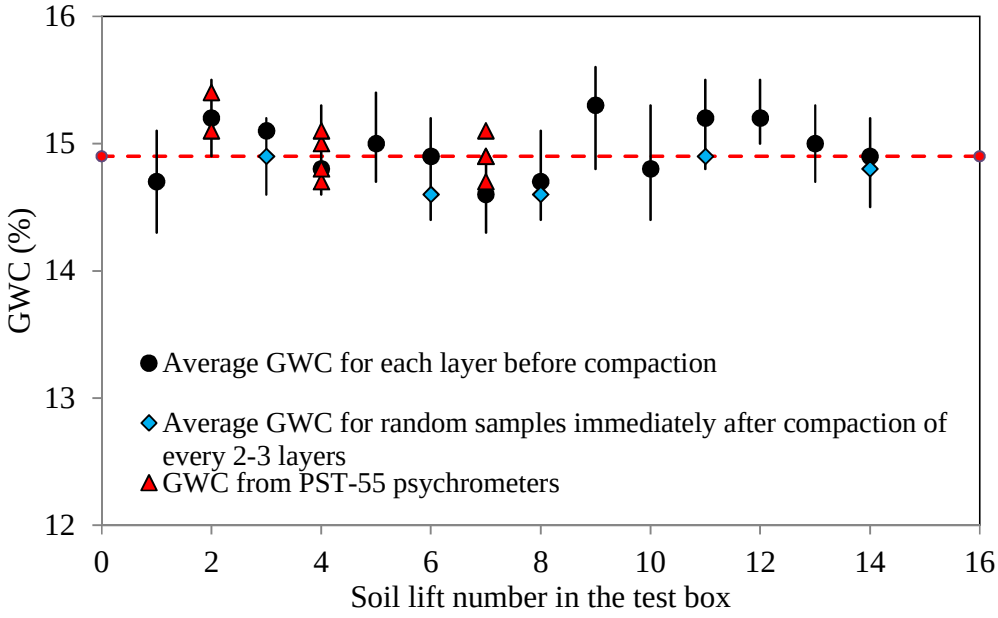
16
15
14
13
12
GWC (%)
0
2
4
6
8
10
12
14
16
Soil lift number in the test box
Average GWC for each layer before compaction
Average GWC for random samples immediately after compaction of every 2-3 layers
GWC from PST-55 psychrometers

(b)

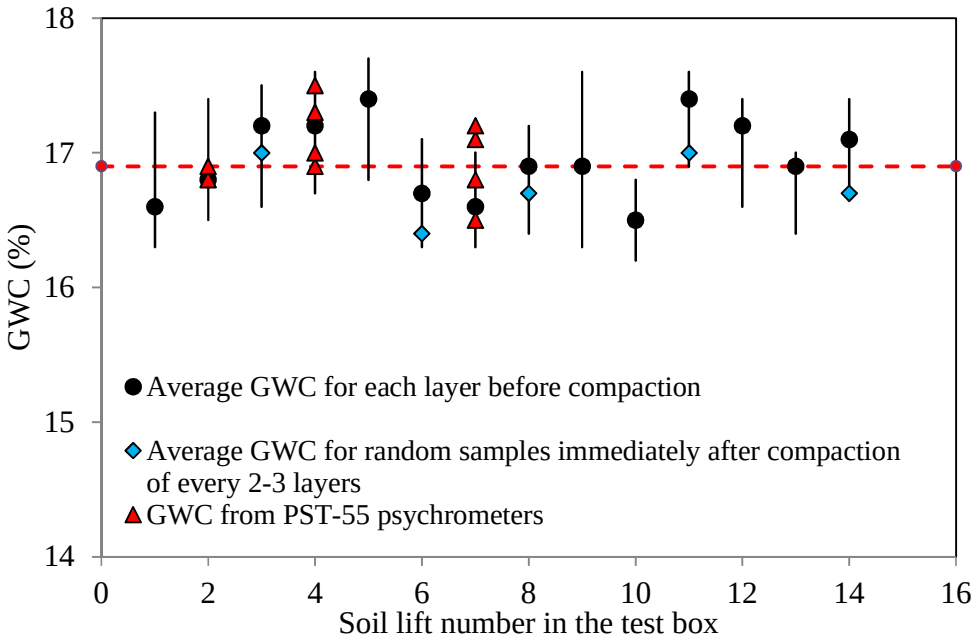

(c)

Figure 8.1. GWC data within the embankment models constructed with HP570 geotextile reinforcement from oven-drying method and PST-55 psychrometers; (a) Test case at OMC-2%, (b) Test case at OMC and (c) Test case at OMC+2%. Notes: [(1)] Red dashed line shows the target GWC value, [(2)] Six (6) samples were taken from each layer to determine an average GWC value before compaction, [(3)] Three (3) random samples were taken immediately after compaction of 2-3 layers of embankment

The EC-5 sensors also were used to monitor the soil water content in the embankments before and after the tests. However, they were only used at the end of construction to find out when the water content in the embankment stabilized before the embankment could be loaded (Figure 8.2). Figure 8.3 shows the data from EC-5 sensors versus time, which indicate that the GWC within the embankment had been stabilized before the loading tests started.

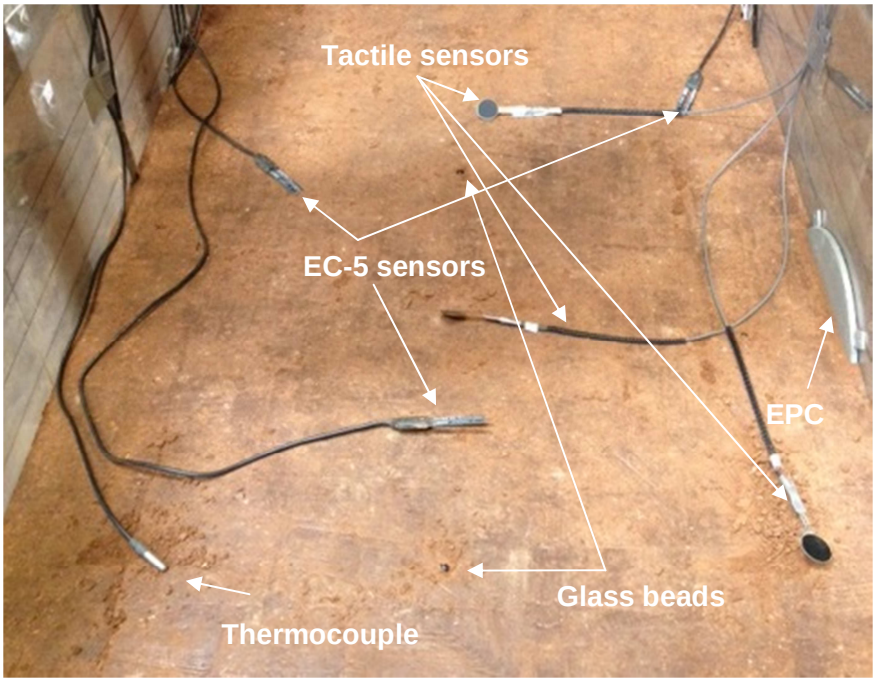

Figure 8.2. Placement of the sensors before compaction of the layer

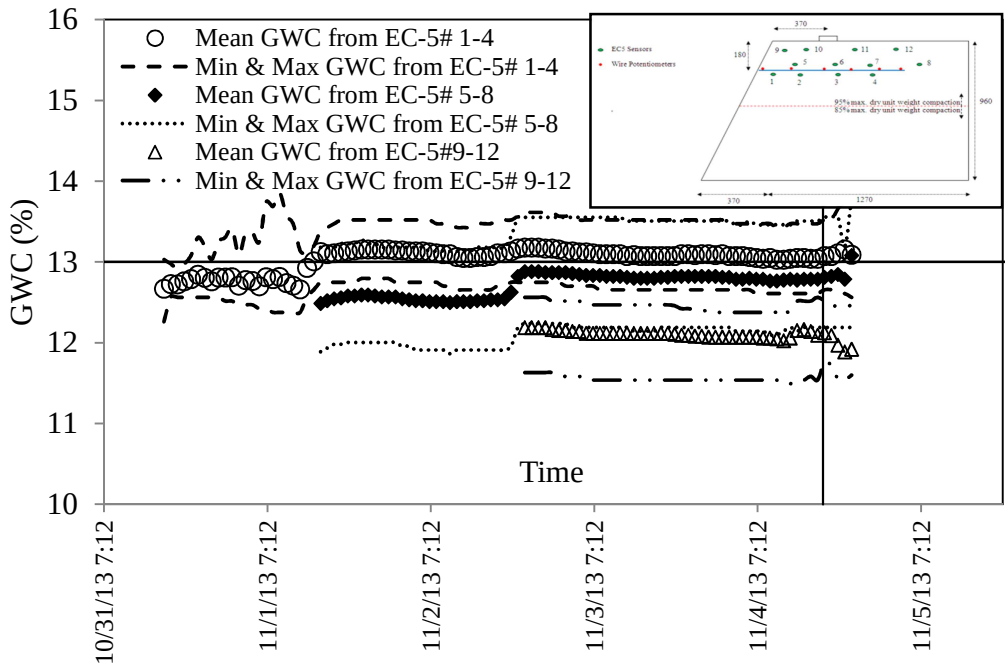

(a)

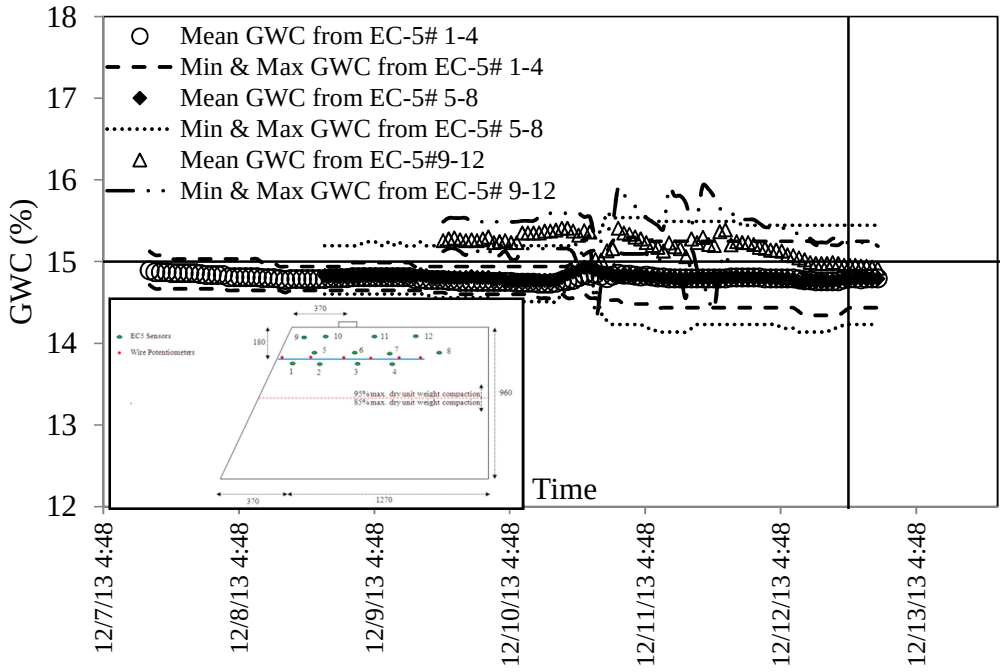

(b)

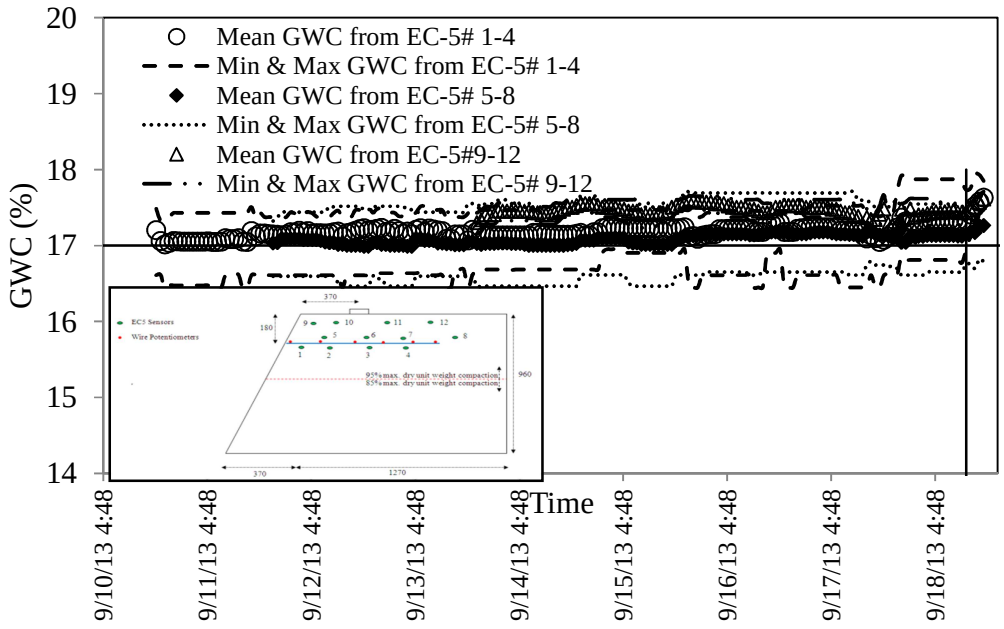

(c)

Figure 8.3. Average GWC data from EC-5 sensors; (a) OMC-2%, (b) OMC, (c) OMC+2%. Note: The vertical and horizontal lines indicate the time when the loading started and target GWC, respectively.

The results in Figure 8.3 show that the soil water content in the model embankments remained essentially constant for nearly all cases during construction and after loading.

8.2. Load- Settlement Data

Figure 8.4 shows the load-settlement data for all three embankment tests built with HP570 geotexile reinforcement as compared to the data from HP370 (Hatami et al. 2014; Chan, E., 2014). The measured compression load is plotted as a function of the strip footing settlement. Failure loads of the embankment models at OMC, OMC+2% for HP370 and OMC-2%, OMC and OMC+2% for HP570 were determined using tangent intersection method (TIM, e.g. Phoon and Kulhawy 2008) as shown in Figure 8.4 for the test case at OMC+2% constructed with HP370 geotextile reinforcement (Table 8.1). Results in Figure 8.4 and Table 8.1 show consistently higher footing bearing capacity in the soil at OMC-2% as compared to the values in the OMC and OMC+2% cases. As expected, increasing suction led to a higher soil bearing capacity in otherwise identical embankment models and the bearing capacity of embankment constructed at OMC+2% and reinforced with HP370 and HP570 woven geotextile is 40% and 33% lower than that of compacted at OMC-2%, respectively.

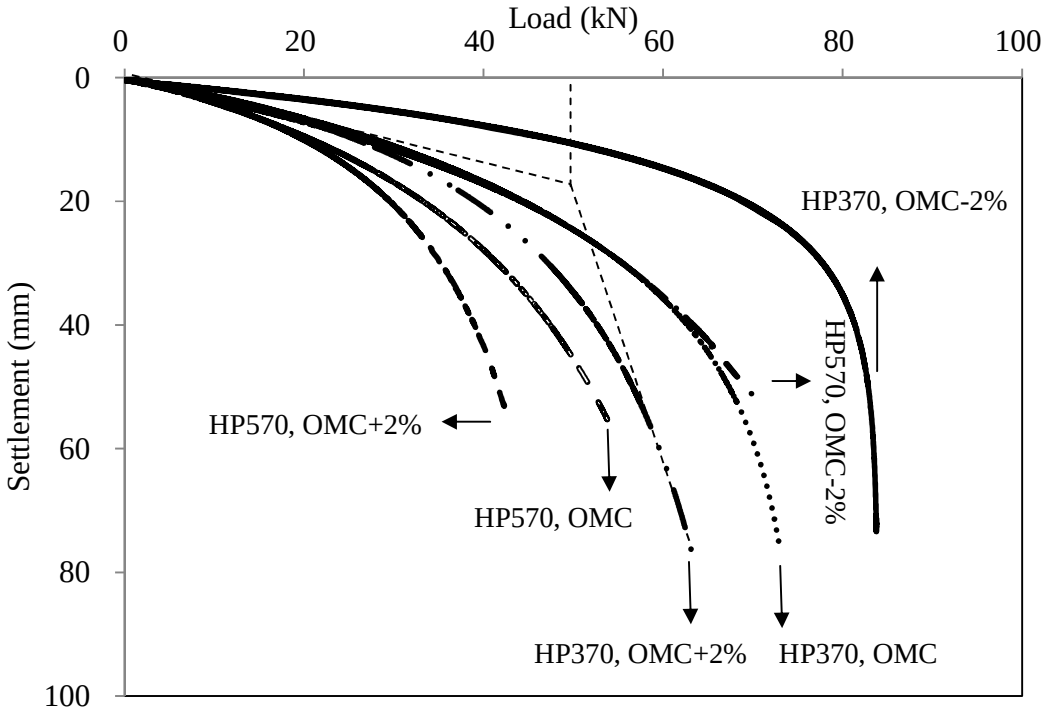

Figure 8.4. Load- settlement data for test soil at different GWC values (OMC-2%, OMC, OMC+2%). Note: For all test cases without distinct failure behavior after the last load-settlement data, the load started to decrease significantly and it was not possible to reach the target value again.

Table 8.1. Maximum and failure footing load for embankment models constructed at different GWC

GWC	**Embankment with HP370 (Hatami et al. 2014; Chan, E., 2014)**			**Embankment with HP570**		
	Max. footing load (kN)	Failure load (kN)	Settlement (mm)	Max. footing load (kN)	Failure load (kN)	Settlement (mm)
12.9%	83.6	83.6	45	69.9	51.0	18
14.9%	73.0	59.0	20	53.8	41.5	20
16.9%	63.1	49.5	18	42.1	34.0	17

Figure 8.5a indicates that the maximum displacement of the test box's wall for the test case at OMC-2% constructed with HP370 is negligible (i.e.0.4 mm) and validate the assumption of rigid side boundaries for the tests. The results in Figure 8.5a also show that the test box performed almost symmetrically while tests since the values recorded by LVDTs 1 and 2 are close to each other (The difference between LVDT 1 and 2 is less than 0.1 mm, depending on the test cases).

Figures 8.5b and Figure 8.6 show the displacement values for the surface of the embankment in the vicinity of the footing and the facing while the embankments were loaded. Results in Figures 8.5b indicate that the soil at the back of footing where LVDT 3 was installed settled before the failure reached in embankment and started to dilate around the ultimate load (Hatami et al. 2014; Chan, E., 2014).

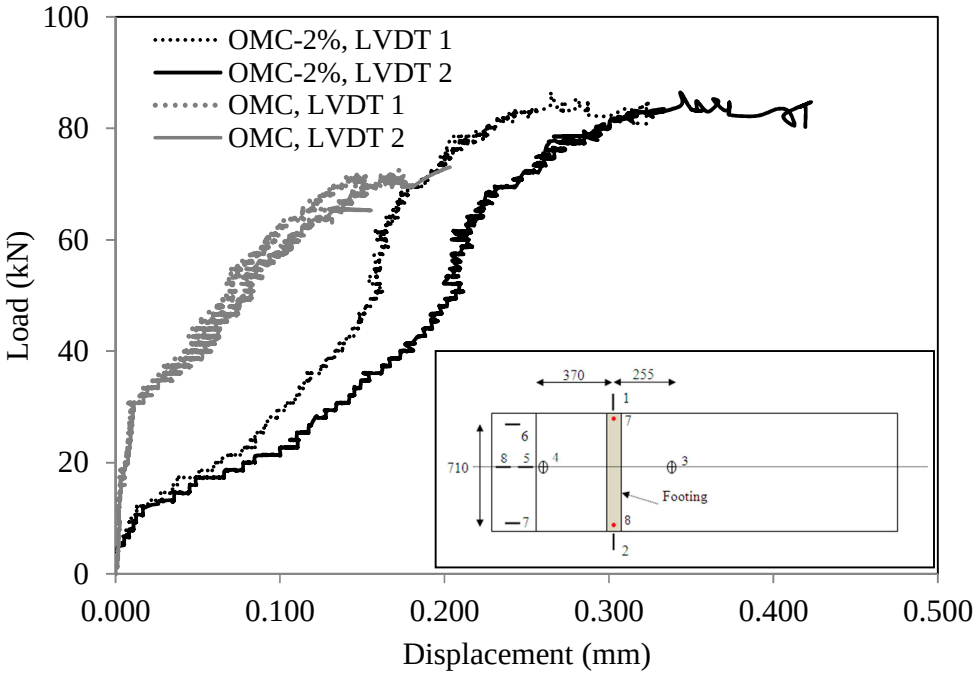

(a)

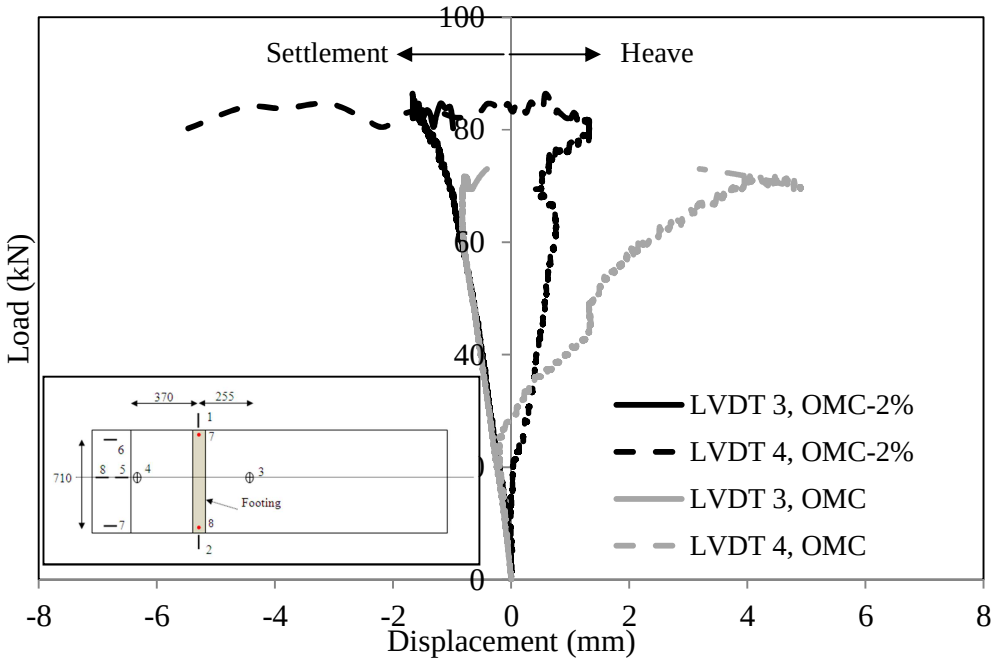

(b)

Figure 8.5. Displacements recorded during the embankment tests reinforced with HP370; (a) Lateral displacement of the test box near the top of the embankment, (b) Vertical displacement of the embankment near the footing

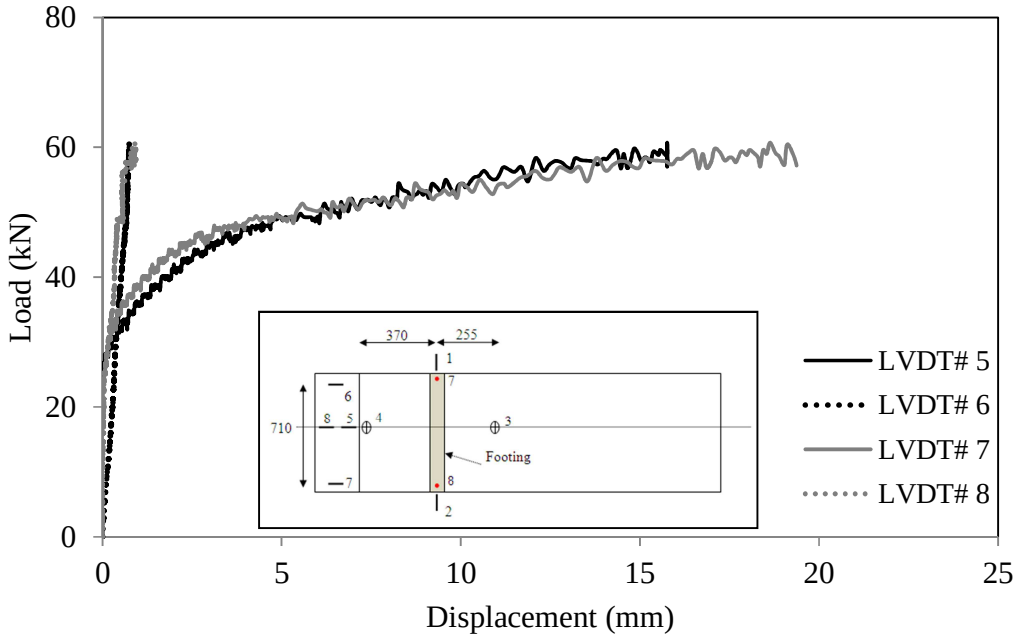

(a)

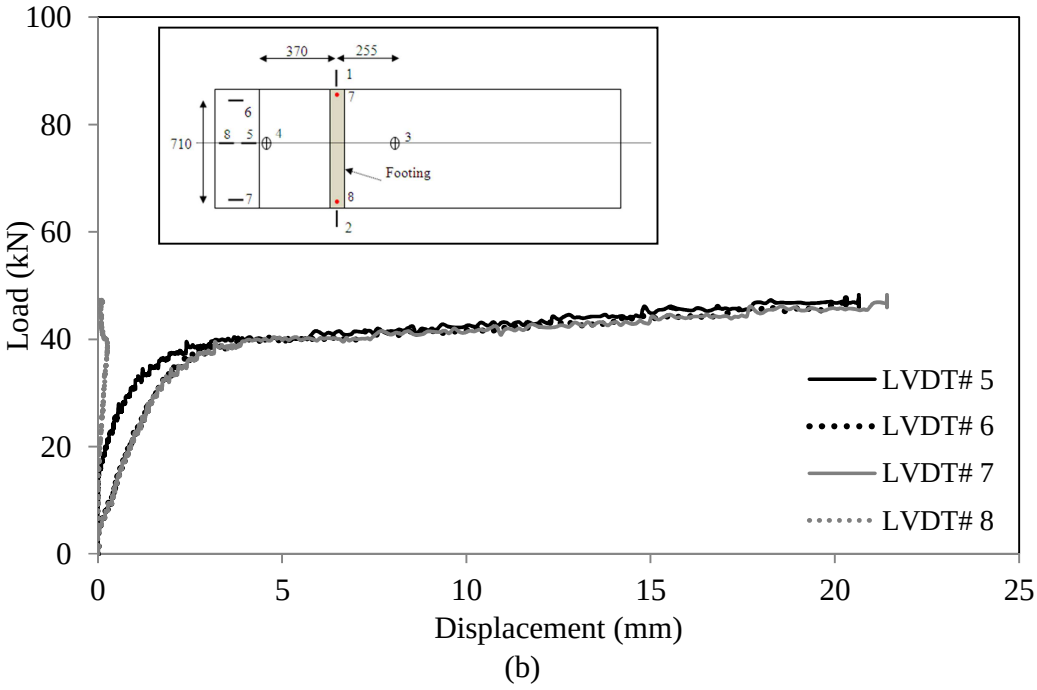

(b)

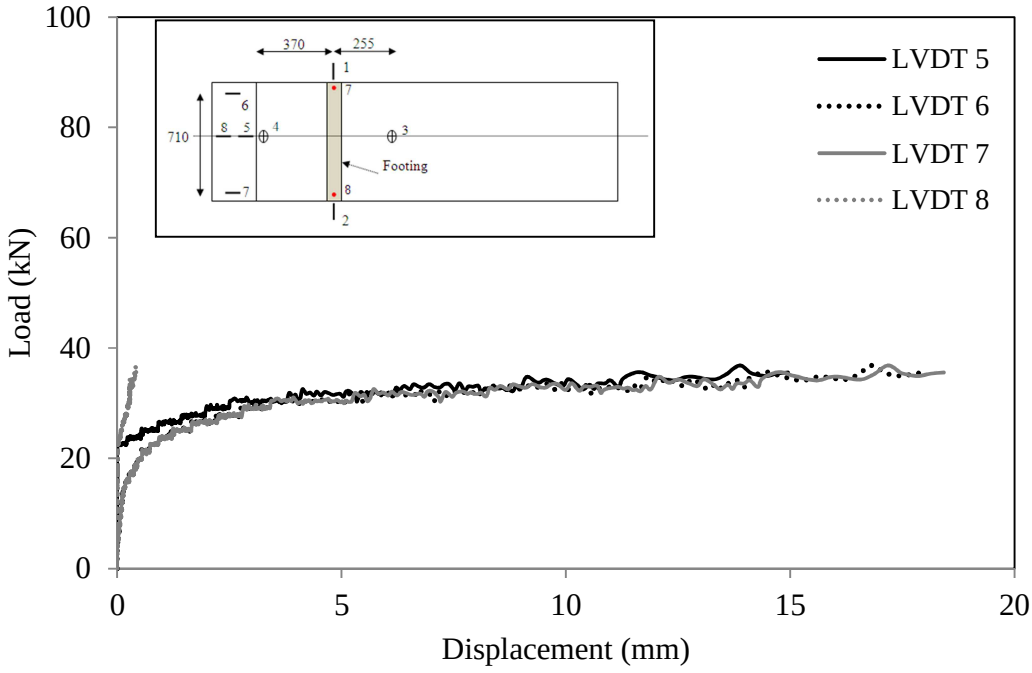

(c)

Figure 8.6. Horizontal displacements of facing recorded during the embankment tests reinforced with HP570; (a) OMC-2%, (b) OMC (c) OMC+2%

LVDT 4 was used to record the crest vertical movement in the model embankments. LVDT 4 results in Figure 8.5b indicate that the embankment crest started to heave once the embankment was subjected to the vertical loading of the strip footing 370 mm away from the crest. The heaving continued throughout the test but started to reverse into settlement when the embankment approached failure. In all embankment models, the failure wedge developed immediately below LVDTs 6 and 7 except in the model reinforced with HP570 built at OMC-2% in which the failure occurred immediately above LVDT 6. In all tests, no detectable movements were observed in the coordinates of the glass beads that were embedded in the embankment models.

The readings from the EPC sensors are shown in Figures 8.7 and 8.8. Boussinesq method (Budhu 2000) was used to compare theoretical predictions of the vertical and horizontal incremental stresses within the embankment due to a line loading (as given in Equations 8.1 and 8.2) with the measured values. With X, Y and Z representing the directions along the running length, width and depth of the model embankments, respectively, the incremental vertical stress in the soil is given by:

$$\Delta\sigma_z = \frac{2qz^3}{\pi(x^2+z^2)^2} \qquad (8.1)$$

Where:

$\Delta\sigma_z$: Increase in vertical stress

q: Vertical line load, lb/in

z, x: Vertical and horizontal distance between the point the stress should be calculated and center of line load

$$\Delta\sigma_y = \frac{2q\vartheta z}{\pi(x^2+z^2)} \qquad (8.2)$$

Where:

$\Delta\,\sigma_y$: Increase in horizontal stress

ϑ: Soil Poisson's ratio

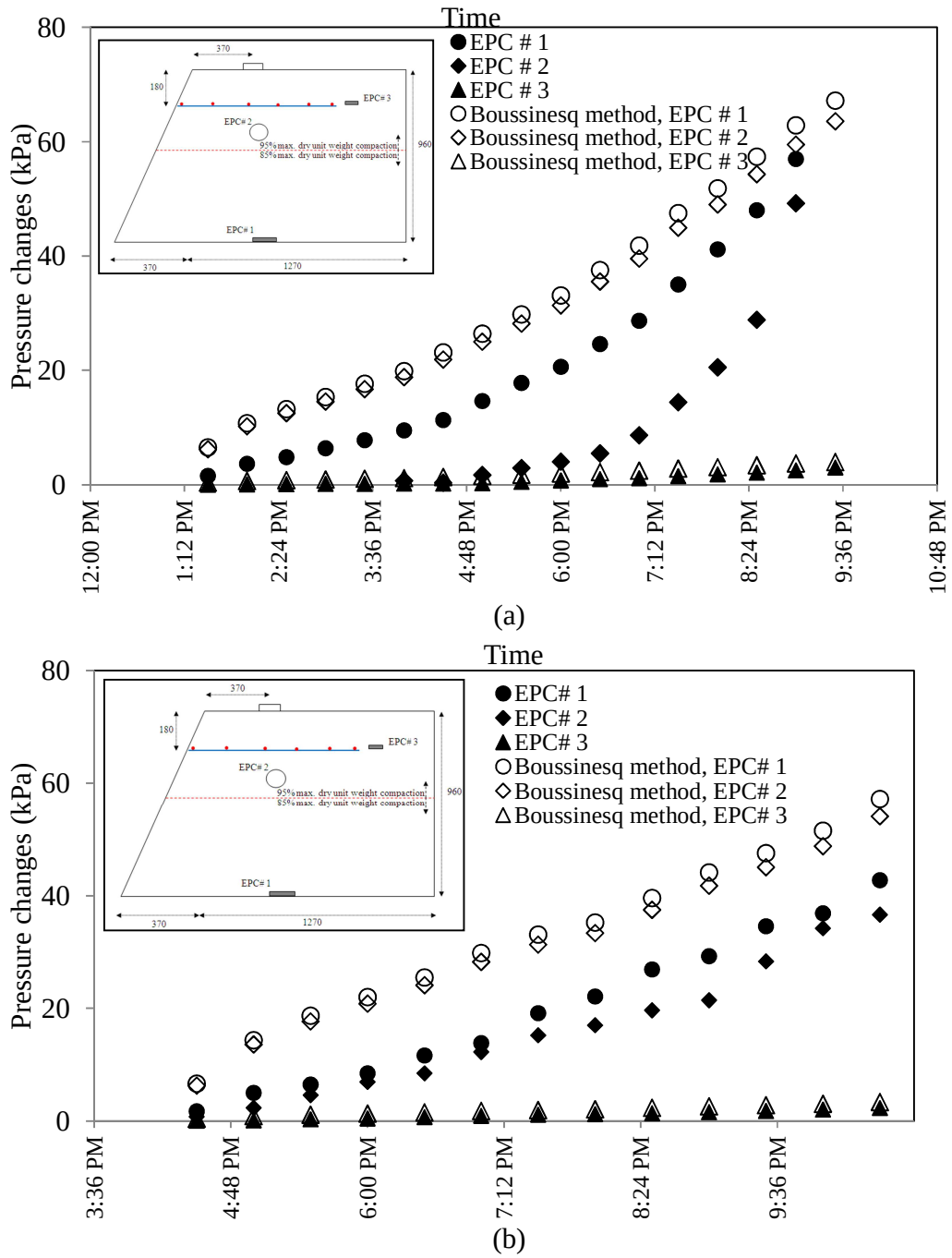

Figure 8.7. Comparison of measured and theoretical predicted incremental stresses due to the strip footing loading at selected locations in model embankments reinforced with HP370 (Hatami et al. 2014, Chan, E., 2014): (a) OMC-2% performed on 04/04/2013, (b) OMC performed on 04/22/2013

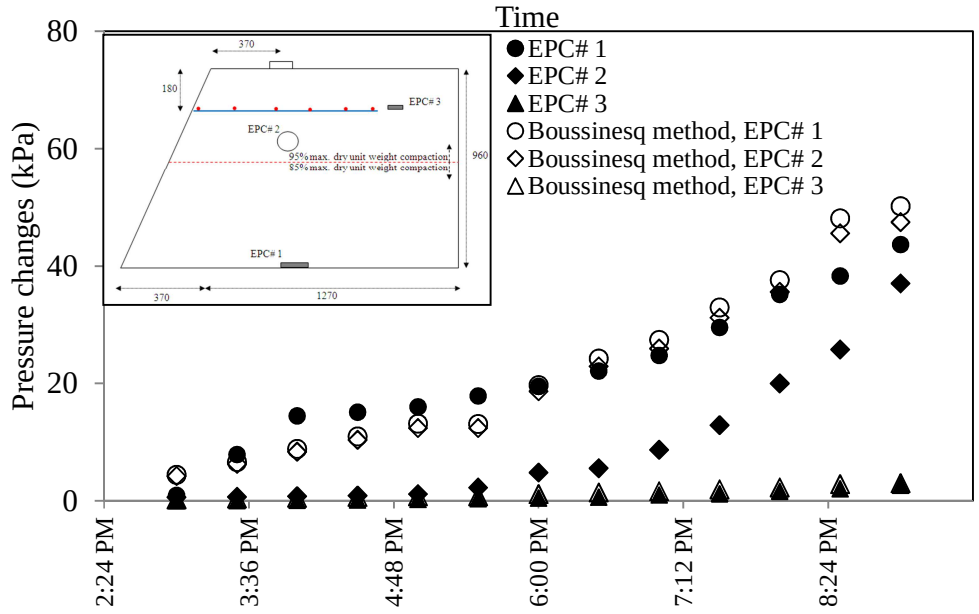
Time
Pressure changes (kPa)
80
60
40
20
0
2:24 PM
3:36 PM
4:48 PM
6:00 PM
7:12 PM
8:24 PM
EPC# 1
EPC# 2
EPC# 3
Boussinesq method, EPC# 1
Boussinesq method, EPC# 2
Boussinesq method, EPC# 3
370
180
960
1270
95% max. dry unit weight compaction
85% max. dry unit weight compaction

(a)

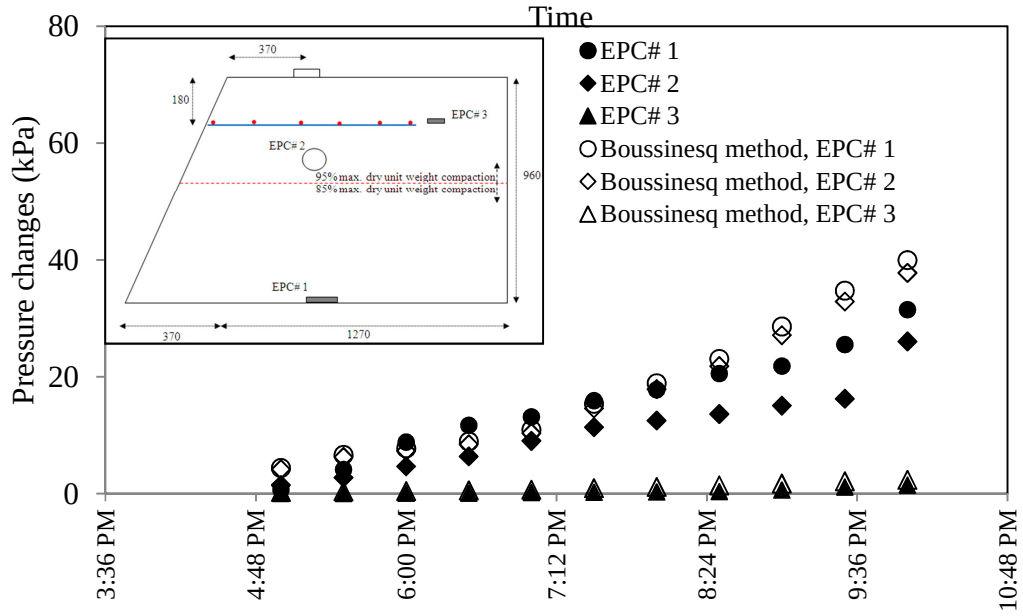
Time
Pressure changes (kPa)
80
60
40
20
0
3:36 PM
4:48 PM
6:00 PM
7:12 PM
8:24 PM
9:36 PM
10:48 PM
EPC# 1
EPC# 2
EPC# 3
Boussinesq method, EPC# 1
Boussinesq method, EPC# 2
Boussinesq method, EPC# 3
370
180
960
1270
95% max. dry unit weight compaction
85% max. dry unit weight compaction

(b)

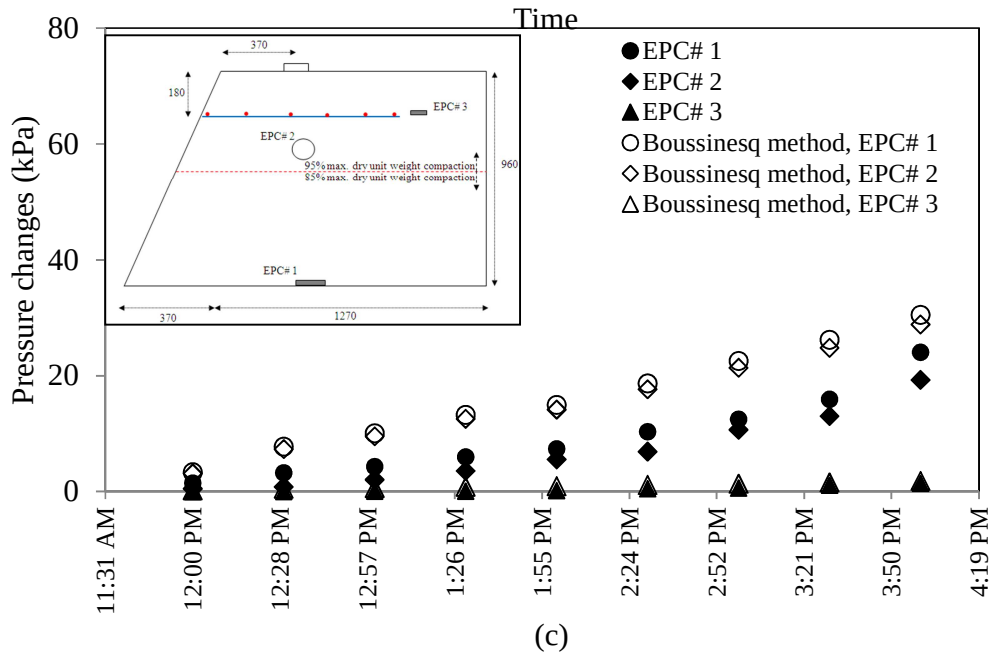

(c)

Figure 8.8. Comparison of the measured and theoretical predicted (Boussinesq method) incremental stresses due to the strip footing loading at selected locations in model embankments reinforced with HP570: (a) OMC-2% performed on 11/04/2013, (b) OMC performed on 12/12/2013 and (c) OMC+2% performed on 09/18/2013

Results shown in Figures 8.7 and 8.8 indicate that the vertical pressures predicted from the Boussinesq equation are greater than the measured values in almost all test cases shown which could be partly attributed to this fact that in contrast to the embankment configuration in the current tests, the Boussinesq method assumes a line load on an elastic and isotropic half space. Another possible reason for the smaller measured earth pressures as compared to the theoretical values is the influence of sidewall boundaries in a limited-width test box. The frictional boundaries invariably present between the embankment soil and the sidewalls transfer a portion of the surcharge load to the walls, resulting in reduced pressures at larger depths as compared to the theoretical values derived for infinitely wide models. Figure 8.9 shows incremental vertical stresses (i.e.

due to footing load only) inside the embankment until failure as recorded by the tactile sensors.

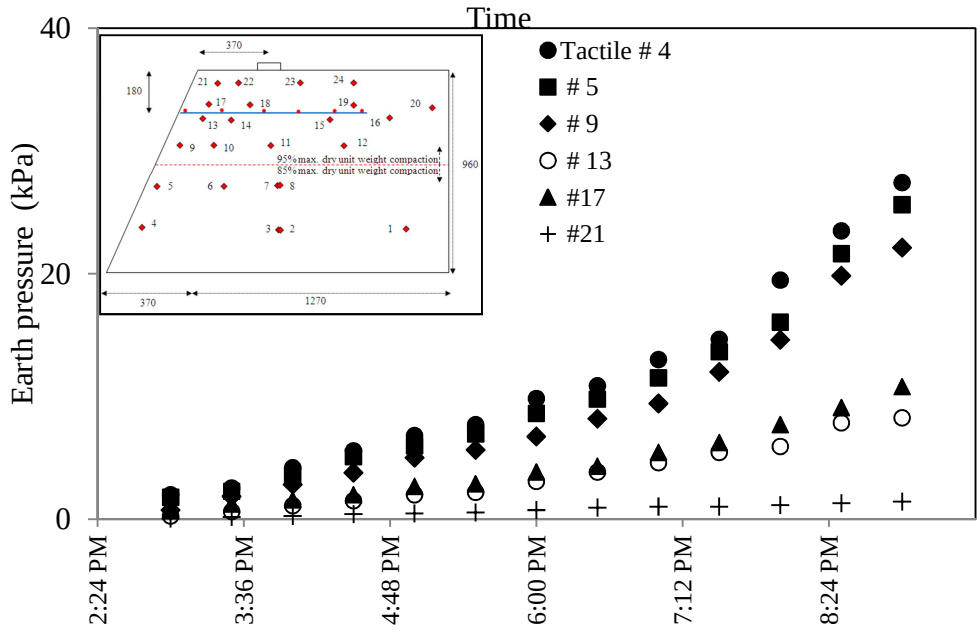

(a)

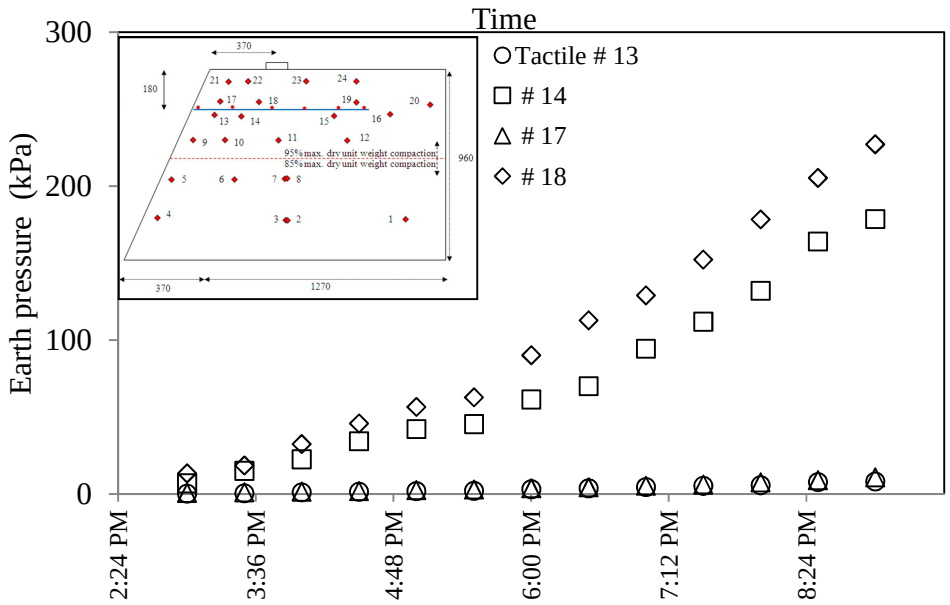

(b)

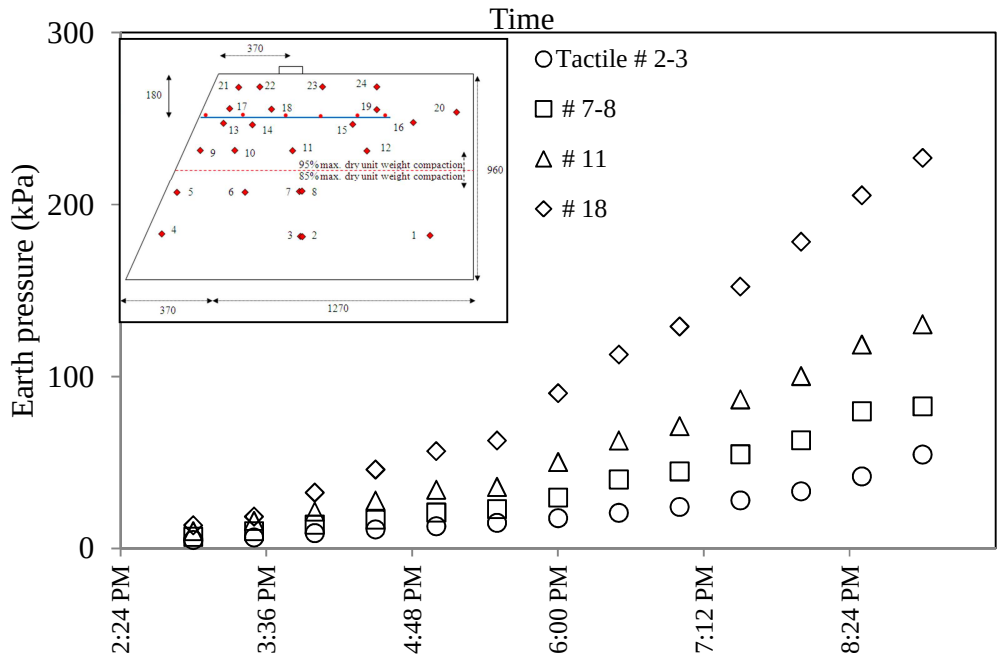

(c)

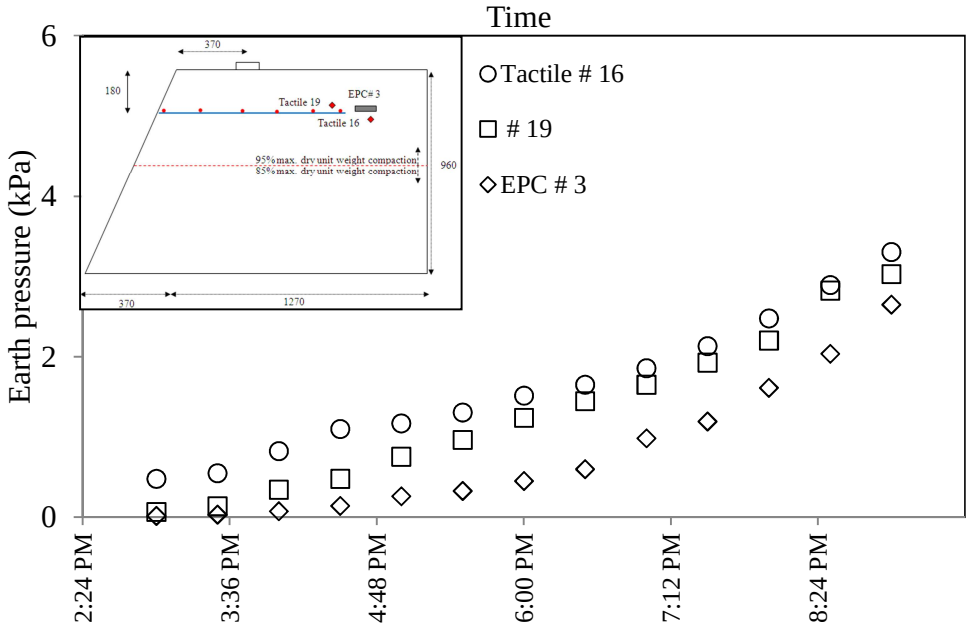

(d)

Figure 8.9. History of incremental earth pressures in the model embankment subjected to footing loading constructed with HP570 at OMC-2% performed on 11/04/2013

Figure 8.10 shows the pore pressure data measured by two piezometers in the embankment constructed with HP370. The results in Figure 8.10a indicate that no positive pore water pressure was developed in the drier model constructed at OMC-2% throughout the testing period. The data for the model embankment at OMC consistently show slightly greater positive pore pressure values. However, their magnitudes remain practically negligible throughout the testing period. Therefore, piezometers were not used for the second series of embankment tests reinforced with HP570 geotextile.

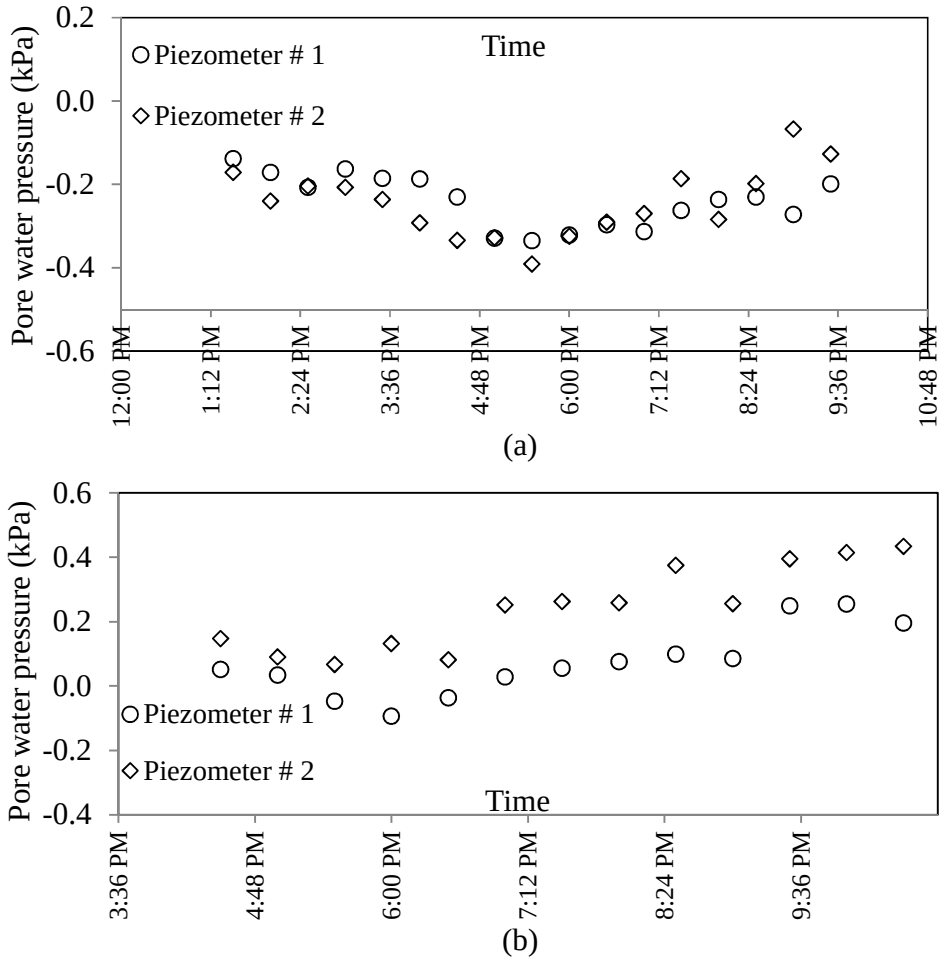

Figure 8.10. Changes in pore water pressure as recorded by piezometers during surcharge loading (Hatami et al. 2014; Chan, E., 2014): (a) OMC-2% performed on 04/04/2013, (b) OMC performed on 04/22/2013

8.3. Strain Distributions

Geotextile strains and local displacements were measured using six (6) wire-line extensometers attached to different locations along the reinforcement length (Figure 8.11). The failure wedge in all six embankment models tested involved a bilinear slip plane that originated from the upstream side of the footing beam on the surface of the embankment and was intercepted by the reinforcement layer, forming a two-part wedge sliding block bracketed by the slip plane and the embankment facing (Figures 8.12 and 8.13). In Figure 8.12, L_{DS} and L_{IS} indicate the length of soil which sheared over the soil and geotextile reinforcement, respectively.

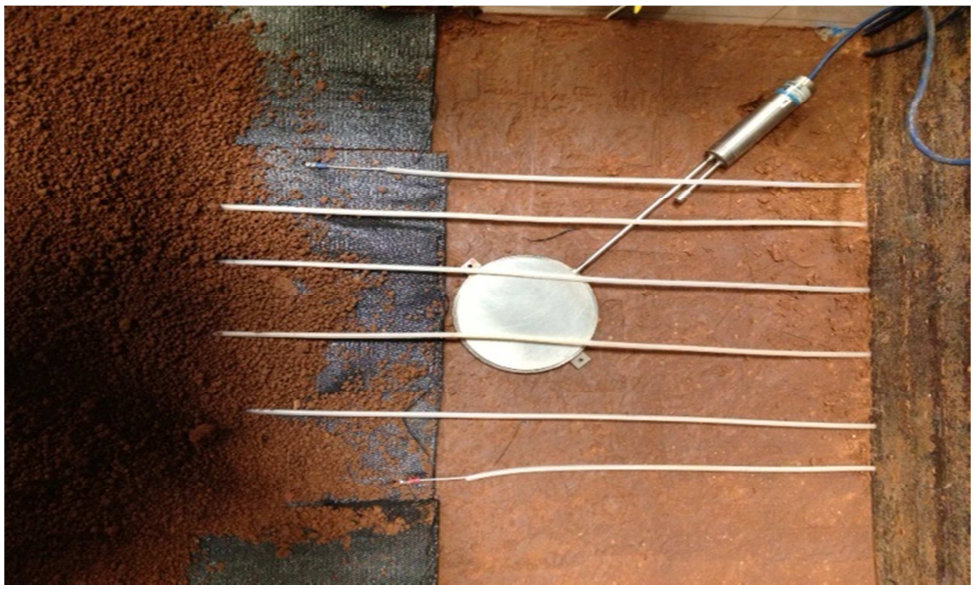

Figure 8.11. Wire-line extensometers attached to geotextile reinforcement to measure geotextile strains

Figure 8.12 shows the failure wedges formed at the end of the surcharge loading stage for the six test cases (i.e. HP370 and HP570 reinforcement at OMC-2%, OMC and OMC+2%). The data shown for each test case are the mean values of failure plane geometries that were traced near both sidewalls of the test box and at the center of the

model (i.e. mean value of three curves along the running length of the slope). It can be observed that in all three embankment models, the primary failure wedge was intercepted by, and slid over the geotextile layer. In the model reinforced with HP370 geotextile and tested at OMC-2%, an additional failure wedge was observed above the geotextile layer (Failure plane #1 in Figure 12c and d). Another failure was observed at the bottom of the facing in the same model embankment which is consistent with significantly larger displacement readings recorded by LVDT #8 (Figure 8.5c). After failure had occurred, the loading assembly was removed. Then, excavation started by carefully removing the soil of the failure wedges. The plexiglass sidewalls helped to trace the failure wedges so that the excavation process does not produce any additional cracks beyond the failure wedges. Figure 8.13b shows the embankment after the failure wedge had been excavated. The geometry of the failure wedges was measured, recorded and plotted in Figure 12. In all the test cases, the failure wedges formed at the back of the footing and propagated until they intercepted the geotextile reinforcement and continued along the soil-geotextile interface as opposed to penetrate through the geotextile. Since there was relatively negligible (i.e. almost zero) movement recorded by WP 6 (tail-end), the failures were defined as a combination of soil shearing and soil-geotextile interface shearing (i.e. without pullout of geotextile). These phenomena could be caused by the size of the embankment model (i.e. reduced-scale). Thus, the footing ultimate bearing capacity was not large enough to generate pullout failure.

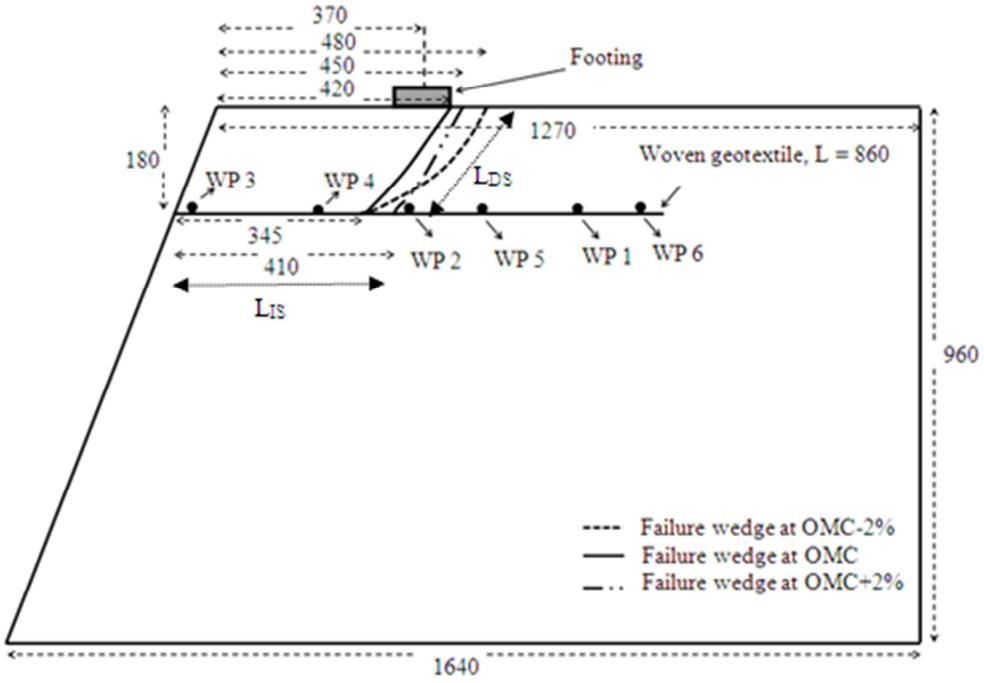
370
480
450
420
Footing
1270
Woven geotextile, L = 860
180
WP 3
WP 4
LDS
345
410
LIS
WP 2
WP 5
WP 1
WP 6
960
Failure wedge at OMC-2%
Failure wedge at OMC
Failure wedge at OMC+2%
1640

(a)

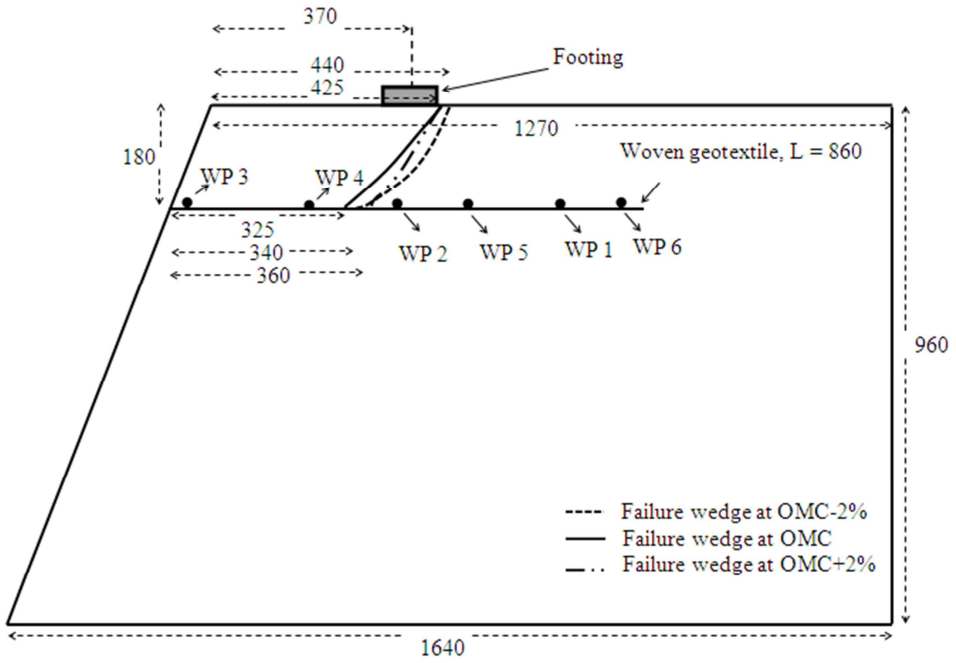
370
440
425
Footing
1270
Woven geotextile, L = 860
180
WP 3
WP 4
325
340
360
WP 2
WP 5
WP 1
WP 6
960
Failure wedge at OMC-2%
Failure wedge at OMC
Failure wedge at OMC+2%
1640

(b)

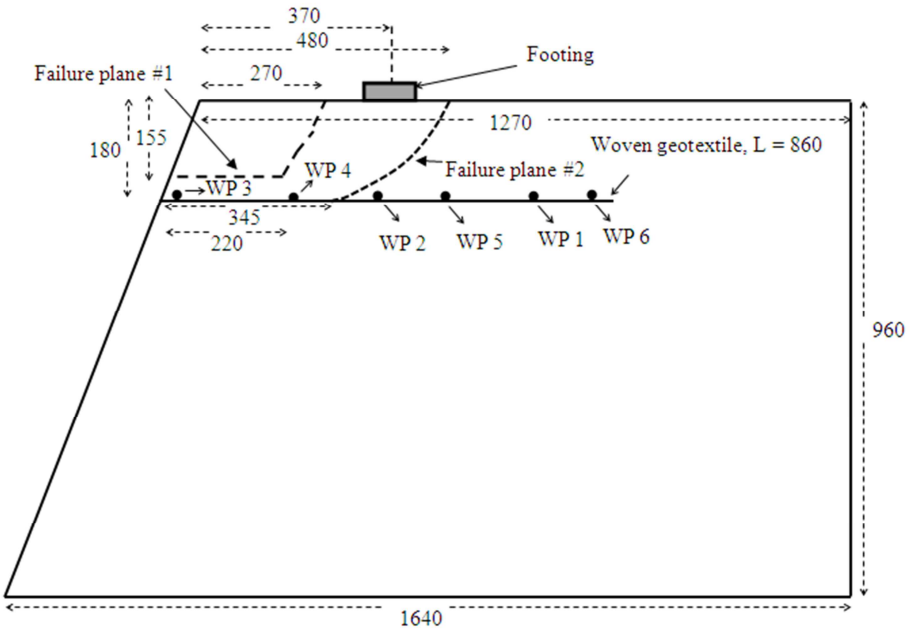

(c)

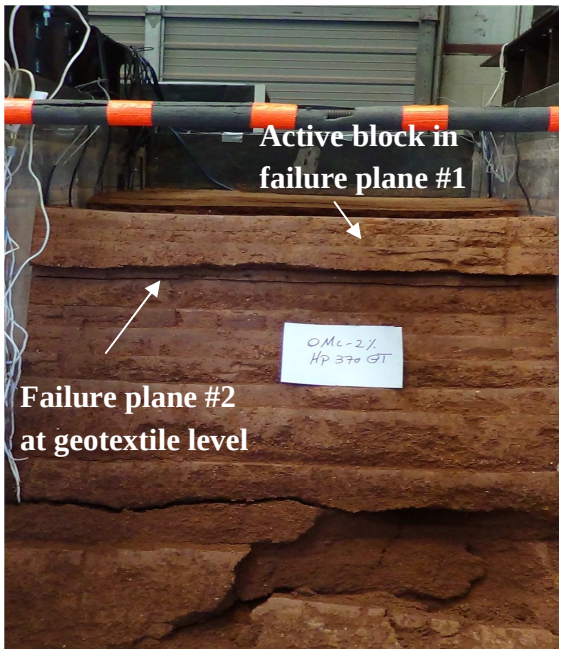

(d)

Figure 8.12. Failure planes observed in model embankments; (a)-(b) Comparison of failure plane geometries as traced after excavation of failed block at the end of test for model embankments with HP370 and HP570, respectively, (c) Traces of failure planes #1 and #2 in test case at OMC-2% built with HP370 reinforcement, (d) Front view of failed slope at embankment model reinforced with HP370 and built at OMC-2% after the test



(a)

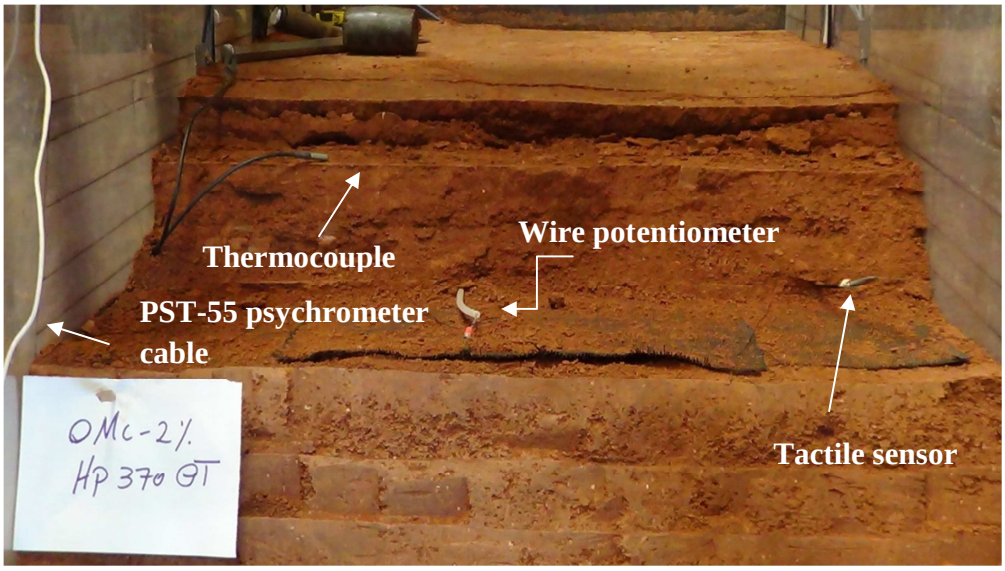

(b)

Figure 8.13. Failure wedge in the tested model embankments; (a) Front view of the displaced soil block in the test case at OMC, (b) Partially excavated failure wedge for embankment at OMC-2%.

Figure 8.14 shows strain distributions over the length of the geotextile reinforcement at the maximum vertical load on the strip footing. Results in Figure 8.14 indicate that the strains in both geotextile reinforcements are greater at higher matric suction and lower gravimetric water content due to greater interface strength properties in a drier soil.

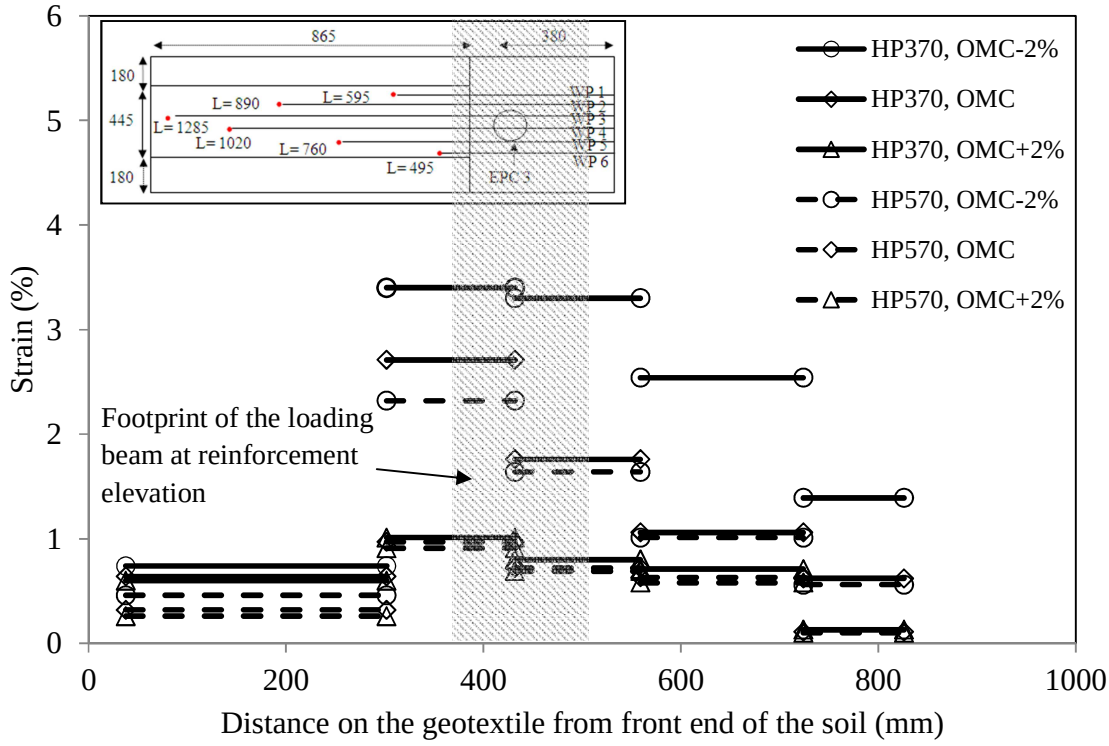

Figure 8.14. Strain distributions in the geotextile reinforcement at different model embankments

CHAPTER 9

RESULTS OF FULL-SCALE REINFORCED EMBANKMENT TEST AND SLOPE STABILITY ANALYSIS

9.1. Gravimetric Water Content (GWC) and Density of the Embankment Soil

GWC value of each soil lift was measured during construction, immediately after compaction and before placing the following lift by taking 7 soil samples from each lift using the oven drying method (ASTM 2216-10). Figure 9.1 shows the distributions of the soil water content within the large-scale model embankment as measured at locations #1 through #7 (Figure 5.7a).

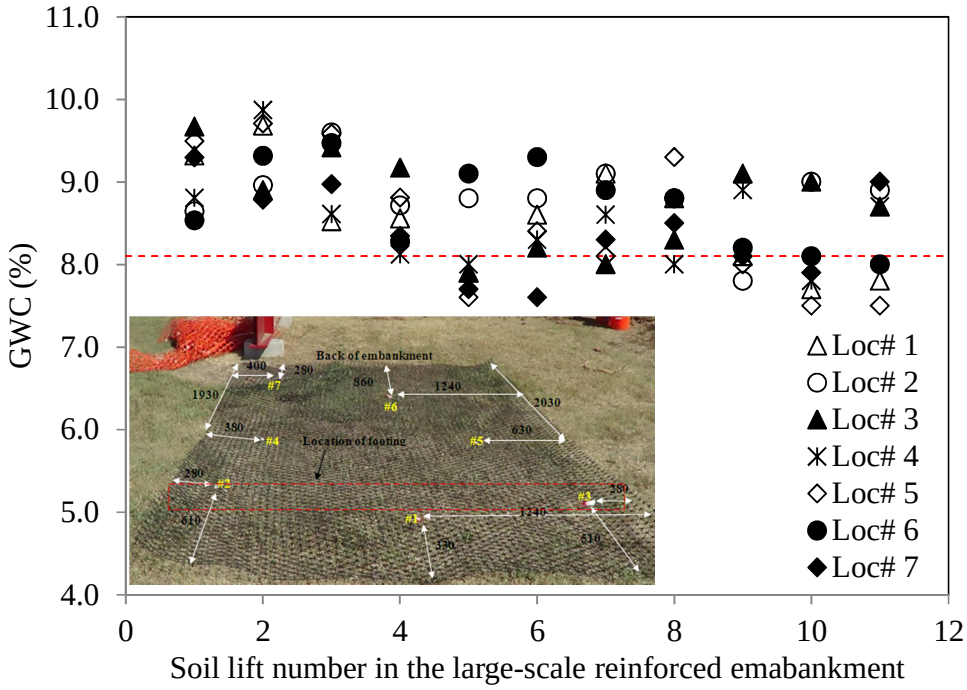

(a)

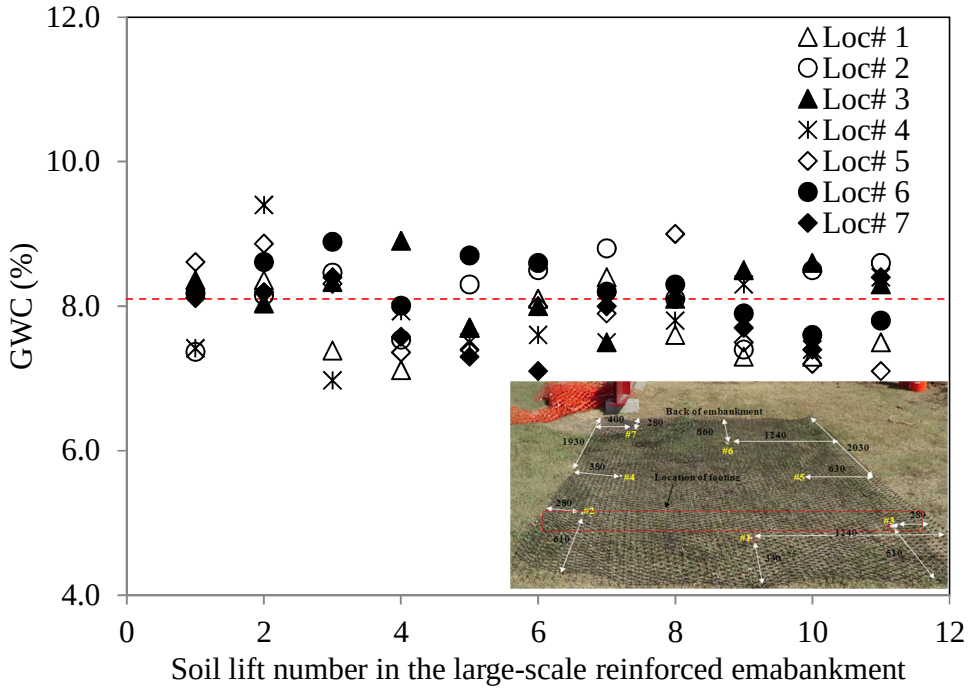

(b)

Figure 9.1. Distribution of GWC within the embankment model, (a) Immediately after compaction of each lift, (b) Before placing next lift. Note: Horizontal dashed line indicates target GWC value.

Nine (9) EC-5 sensors were also used to monitor the soil water content in the embankment during construction and surcharge loading. Figure 9.2 shows the data from the EC-5 sensors which indicates that the GWC within the embankment was practically stable and uniform before the loading phase started.

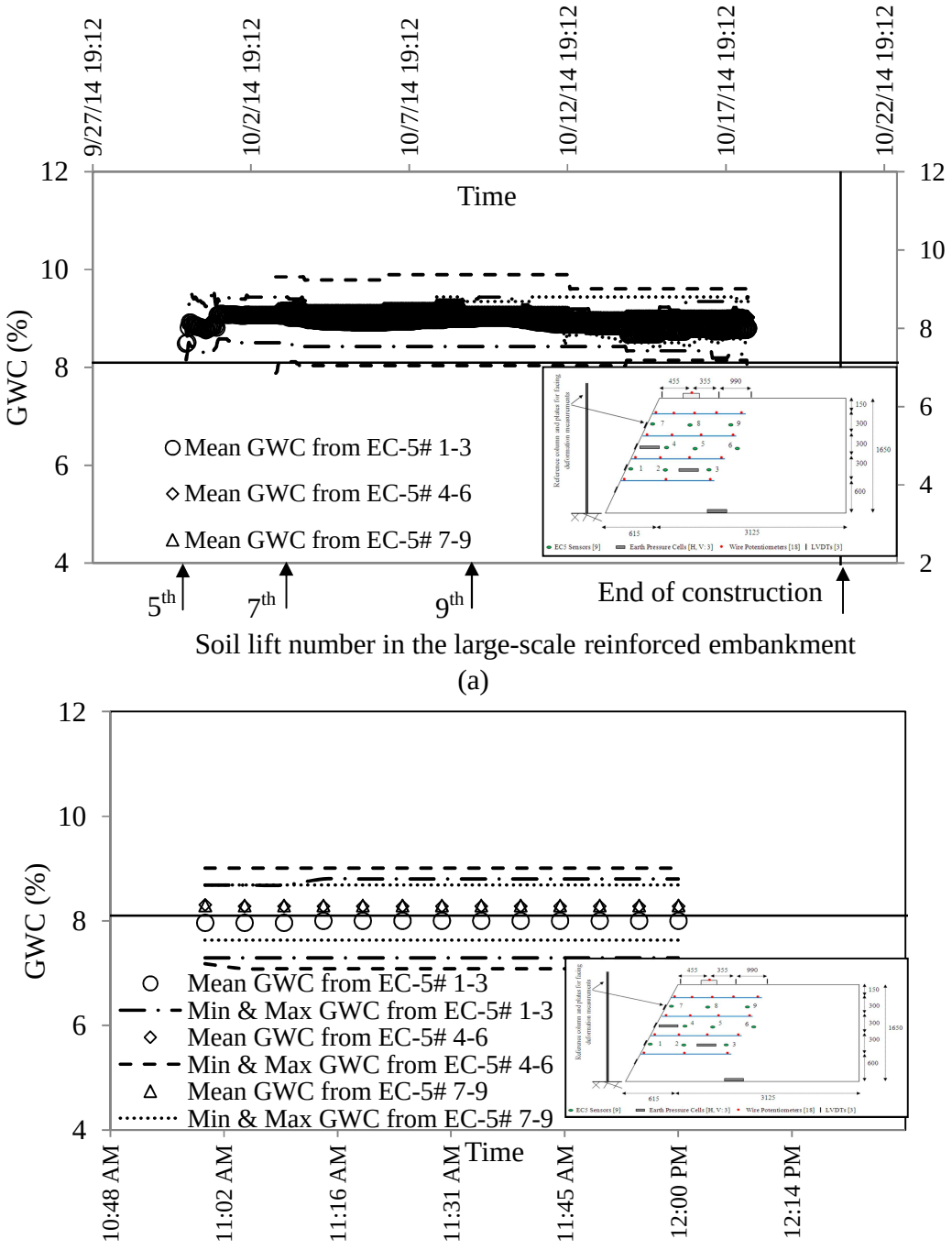

Figure 9.2. Average GWC data from EC-5 sensors in the large-scale model embankment constructed at OMC-2%; (a) Construction and loading stages, (b) Loading stage only performed on 10/18/2014. Note: The vertical and horizontal lines indicate the time when the loading started and the target GWC value, respectively.

Results in Figure 9.2 show that the GWC value in the model embankment remained essentially constant during construction and after loading.

Figure 9.3 shows the variation in the soil density and degree of compaction throughout the embankment using brass tube and rubber balloon methods at locations #1 through #7 as shown in Figure 5.6a. Care was taken to compact each lift with equal amount of energy (i.e. equal passes of compactor equipment). However, measured values for the degree of compaction in Figure 9.3 indicate that the degree of compaction over the entire embankment varied between 85% and 89% (equivalent densities between 1750 and 1840 kg/m^3, respectively). Apart from the natural spatial variation of density throughout the embankment, the observed difference could partly be attributed to possible disturbance of the local soil during sampling.

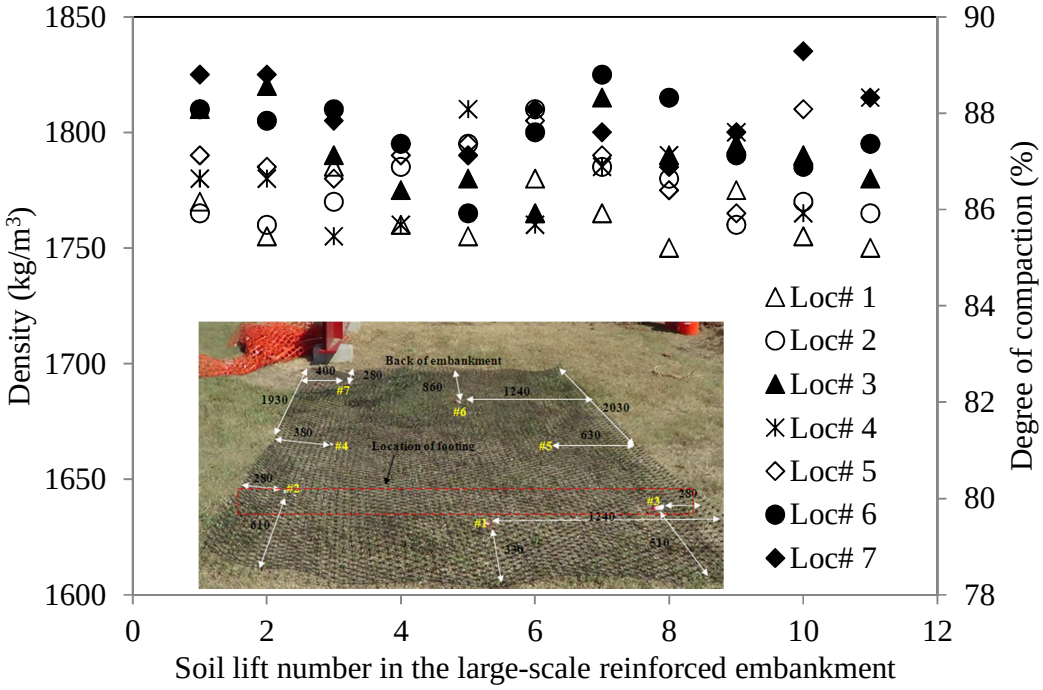

Figure 9.3. Density data in the model embankment after compaction of each lift

9.2. Load-Settlement and EPC Data

Figure 9.4 shows the load-settlement data for the model embankment constructed at OMC-2%. Results indicate that the reinforced embankment showed an essentially linear response up to a total load of 140 kN (285 kPa), followed by a nonlinear performance up to a failure load of 220 kN (450 kPa).

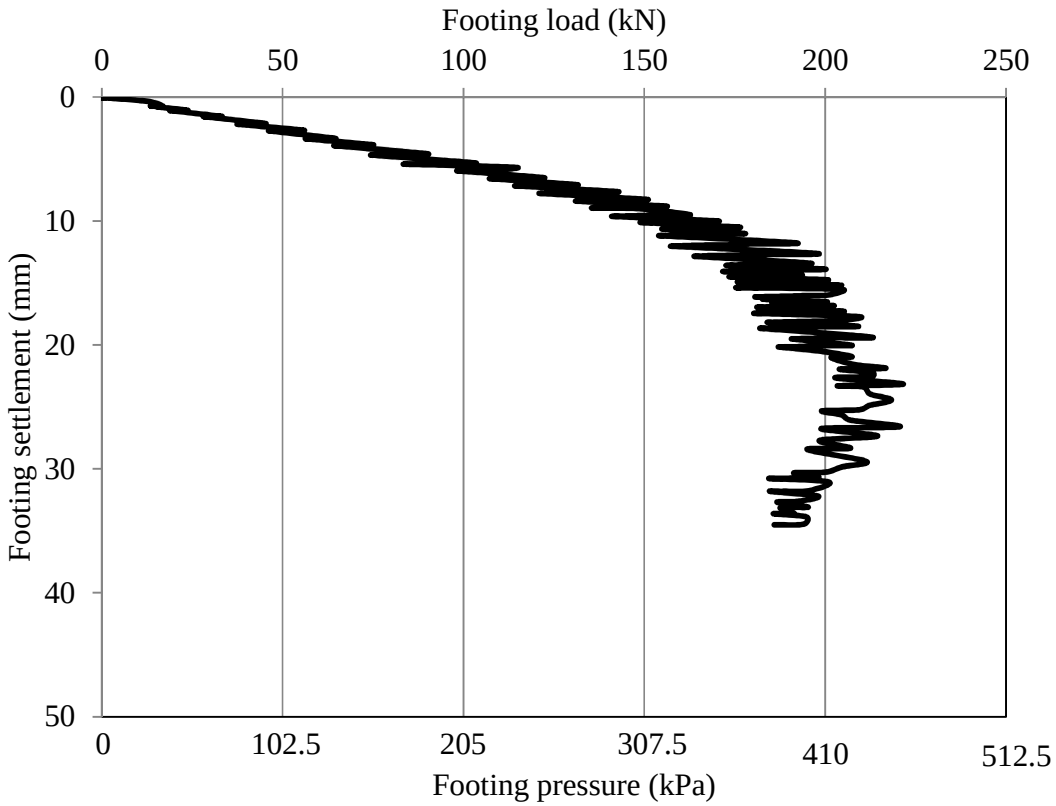

Figure 9.4. Load-settlement response of the large-scale reinforced model embankment constructed at OMC-2%

Figure 9.5 shows the measured (EPC) and predicted (i.e. $\sigma = \gamma z$) earth pressure values within the embankment during the construction and surcharge loading stages. Results in Figure 9.5a indicate that measured earth pressures in all three locations/elevation were significantly greater than the corresponding theoretical values. Additionally, the vertical

pressures did not increase linearly with the number of lifts placed during construction. These observed differences could be attributed to the influences of factors such as the weight and dynamic loading of compaction equipment and construction crew during the construction activity, which resulted in locked-in stresses. It is also observed that the differences between the measured and predicted vertical earth pressures at all locations shown in Figure 9.5a are more significant earlier on during the construction period and decrease toward the end of construction. This can be attributed to the fact that the influence of construction activity on each EPC diminished as more layers of soil were placed over each sensor during construction. The measured vertical earth pressure at the bottom of the embankment from EPC #1 was 38 kPa which is only 20% greater than the corresponding theoretical value. Results in Figure 9.5a also show that the maximum difference in vertical earth pressure at the end of construction due to construction activity was recorded by EPC #2 which is approximately 40% of the measured total earth pressure value. Results shown in Figure 9.5b indicate that maximum recorded earth pressure at failure at mid-height of the slope (EPC #3) is 35 kPa, which is approximately 75% of the values measured by EPC #1 and #2.

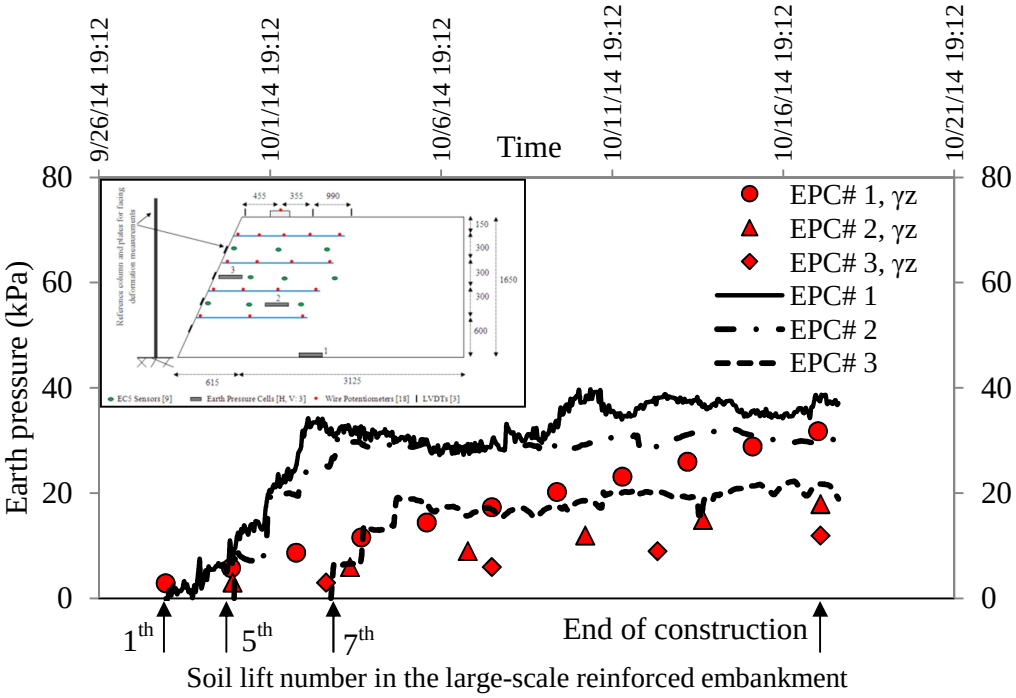

(a)

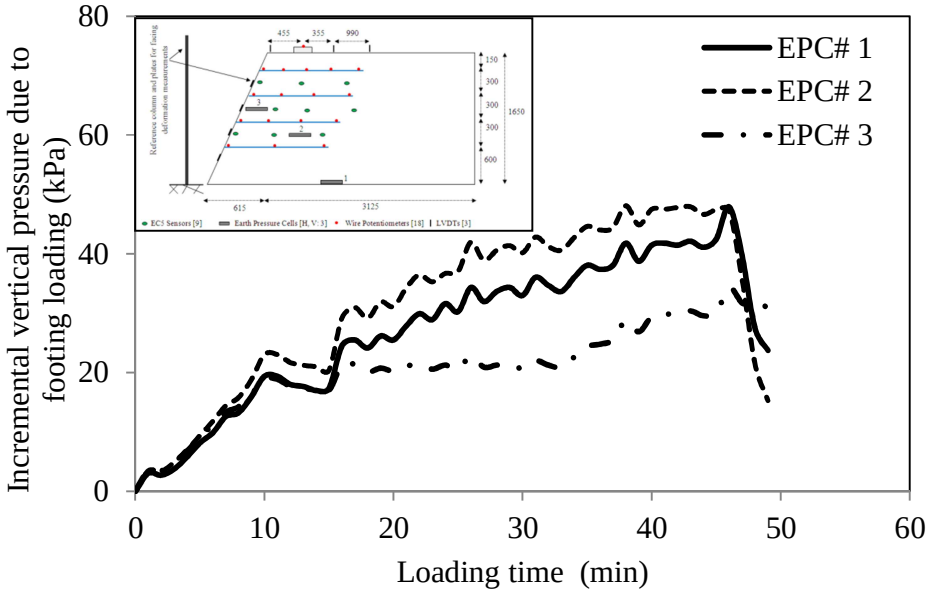

(b)

Figure 9.5. Earth pressure data in the model reinforced embankment constructed at OMC-2%, (a) During construction, (b) During surcharge loading

9.3. Embankment Deformation

Deformation of embankment near footing was measured using LVDTs at 3 different locations as shown in Figure 6.14a. Figure 9.6 shows measured settlements of the embankment top surface during surcharge loading. Results indicate that the embankment surface behind the footing (LVDT 2) settled consistently throughout the loading stage but started to dilate at load levels approaching the failure load. In contrast, LVDT 1 results in Figure 9.6 indicate that the embankment crest started to heave once the embankment was subjected to the strip footing load. The heaving continued throughout the test but started to reverse into settlement when the embankment approached failure. The LVDT 3 data indicates that the vertical displacement of embankment surface just outside the reinforced mass (1325 mm away from the footing center) was negligible (less than 0.1 mm at failure load). The LVDT results are consistent with the data obtained from reduced-scale embankment models (Figure 8.5b).

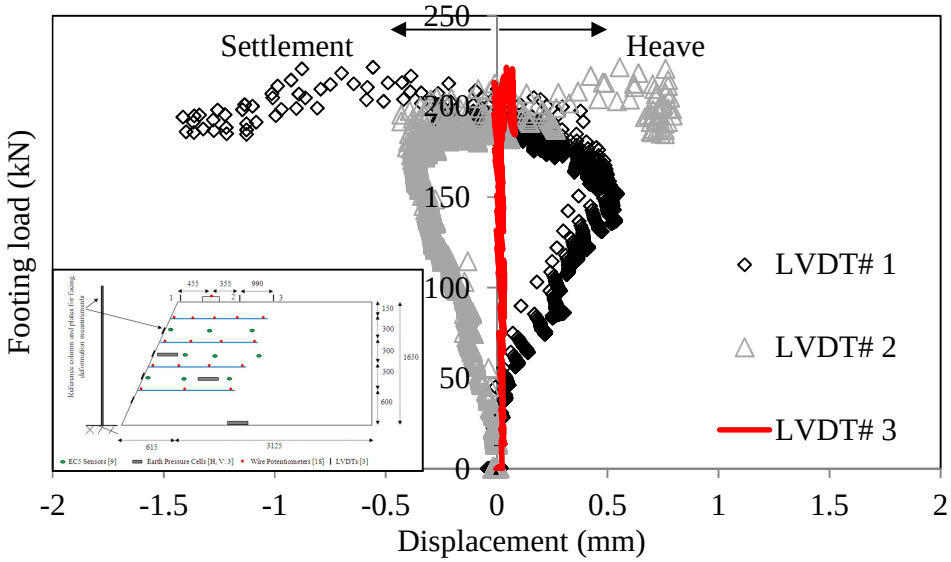

Figure 9.6. Measured settlements of the embankment top surface near the footing during surcharge loading

Figure 9.7 shows the facing displacement of embankment model constructed at OMC-2%. Plates #1, 4, 5 and 8 are the bottom left, top left, bottom right and top right reference plates, respectively, as shown in Figures 5.8b and 6.14a. Two additional plates were mounted at the crest level. However, they fell off the embankment during surcharge loading. Nevertheless, based on observations during the loading stage and the displacement data shown in Figure 9.7, the displacements at the crest of the embankment are expected to be very close to those measured using Plates #4 and #8. Results in Figure 9.7 indicate that a significant horizontal displacement occurred in the embankment slope 150 mm below the top (i.e. 4th) reinforcement layer. The failed block slid between 116 and 146 mm outward on the 3rd geotextile layer as measured using 25- mm square reference plates on both (i.e. left and right) sides of the slope facing (Figure 5.8b).

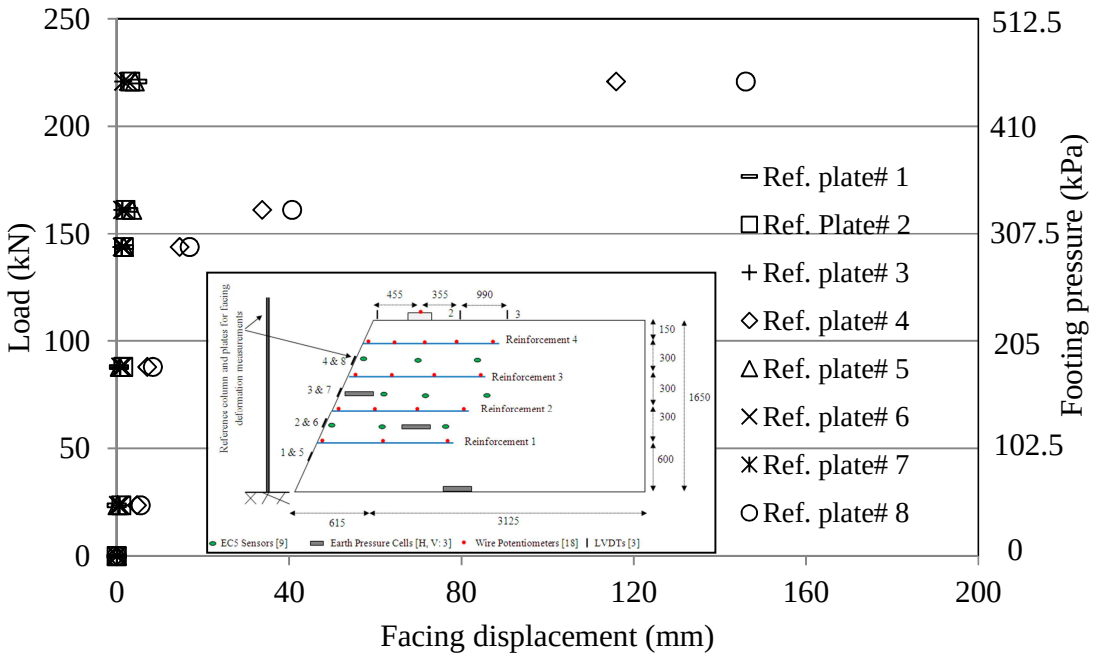

(a)

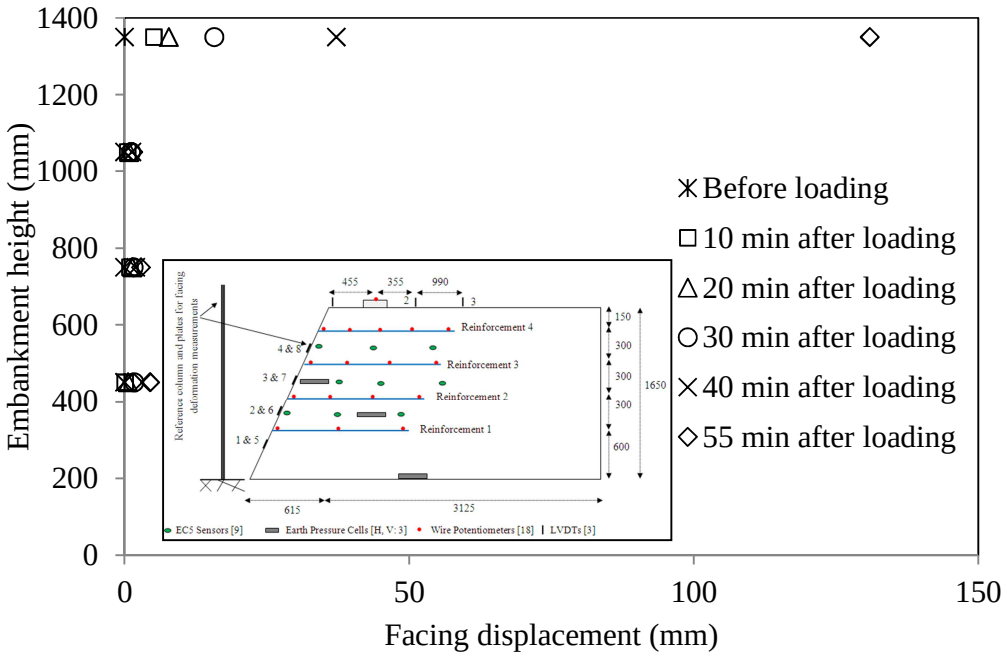

(b)

Figure 9.7. Facing deformation of embankment constructed at OMC-2% as measured using reference plates, (a) Load-deformation data, (b) Facing profile

9.4. Slip Surface and Strain in Geotextile Reinforcement Layers

Figure 9.8 shows traced geometry of the slip plane during embankment excavation after the end of the surcharge loading test. It can be observed that the failure wedge in the reinforced mass originated from the back of the loading beam on the surface of the embankment and was intercepted by the top (4th) geotextile layer and slid over the third geotextile (Figure 9.8 and 9.9).

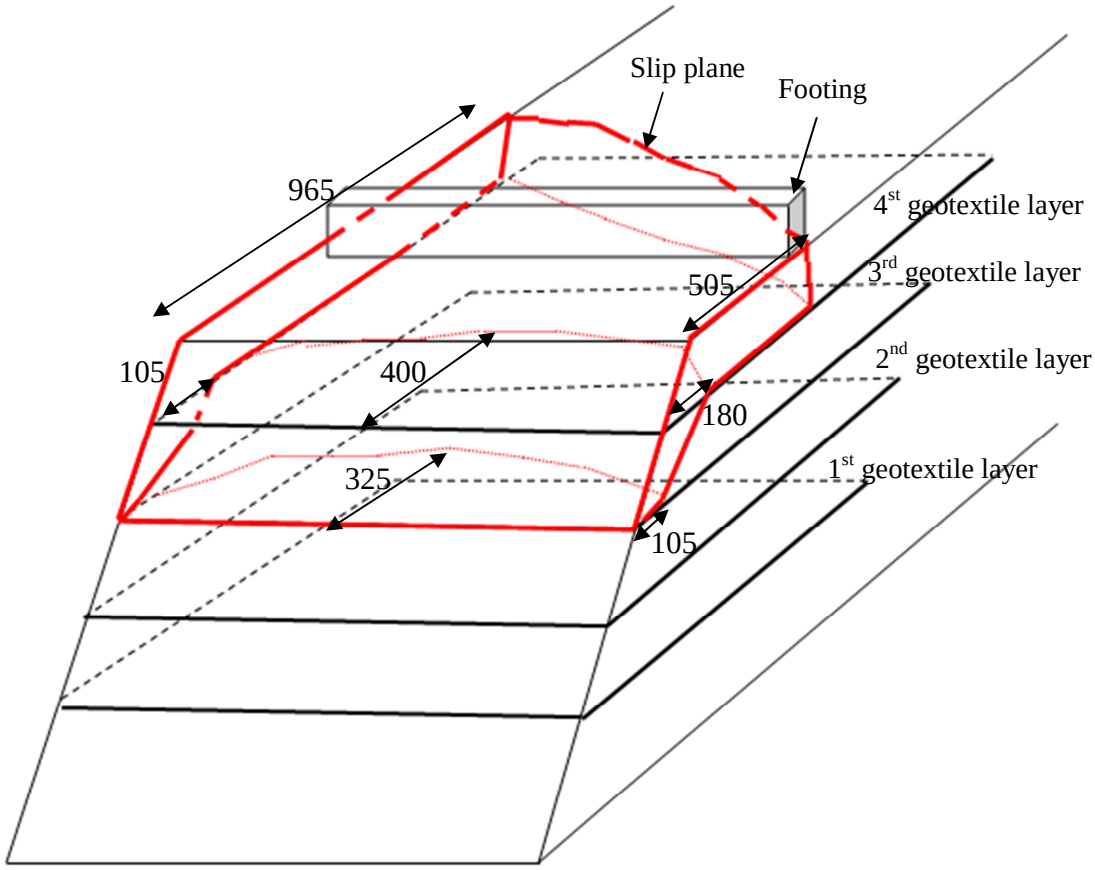

Figure 9.8. Failure plane geometry as traced after careful excavation of the failed block at the end of the test. Note: all dimensions are in “mm”.



(a)



(b)

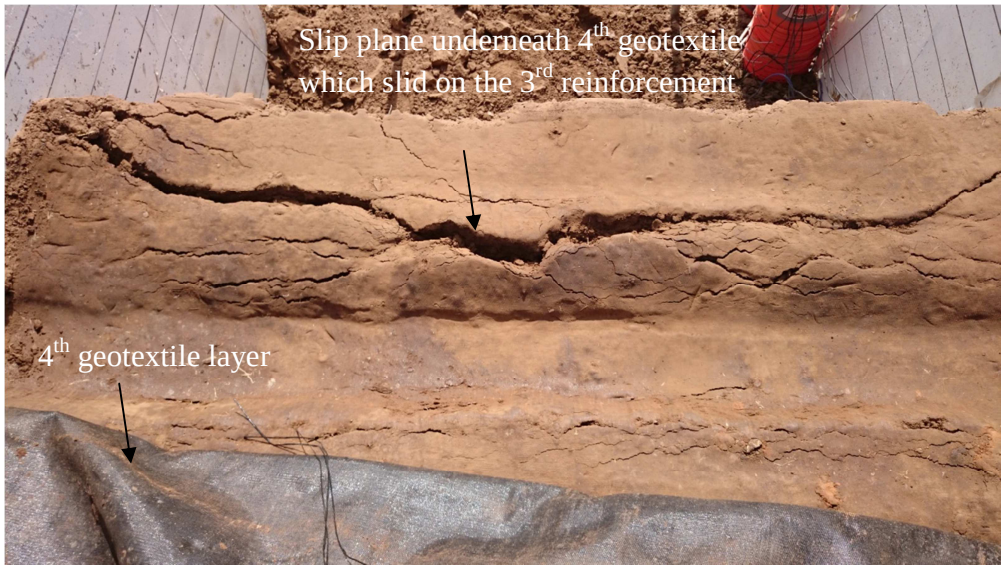
Slip plane underneath 4th geotextile
which slid on the 3rd reinforcement
4th geotextile layer

(c)



(d)

Figure 9.9. Failure wedge for the embankment model tested at OMC-2%; (a) Initiation of slip plane on embankment surface, (b) Excavated part of failure wedge above the fourth layer of geotextile, (c) Continuation of slip plane underneath the fourth geotextile layer and (d) Excavated part of slip plane shown in “c” which slid over the third layer of geotextile

At the end of test, the loading assembly was removed and the construction equipment was moved out of the test box. Afterwards, excavation started by carefully removing the soil within the failure wedge (Figure 9.10).



(a)



(b)

Figure 9.10. (a) Moving construction equipment out of the test box using a forklift, (b) Digging the soil around sensors during the excavation phase after surcharge loading was completed

Figure 9.11a shows local displacements of the top (fourth) geotextile layer and Figure 9.11b shows the corresponding strain distributions at failure load over the length of all reinforcement layers. The results show that the tail end of geotextile (i.e. WP# 12) moved about 5 mm and confirms that the failure happened as a combination of soil shearing, pullout of the top geotextile reinforcement and interface shearing between soil and third geotextile. Results in Figure 9.11b show that the top geotextile reinforcement experienced a maximum strain of 2.4% at the front end which decreased to 0.4% at its tail end. The strain distributions for the top reinforcement layer which experienced pullout are consistent with those from earlier large-scale pullout tests (Figure 7.3).

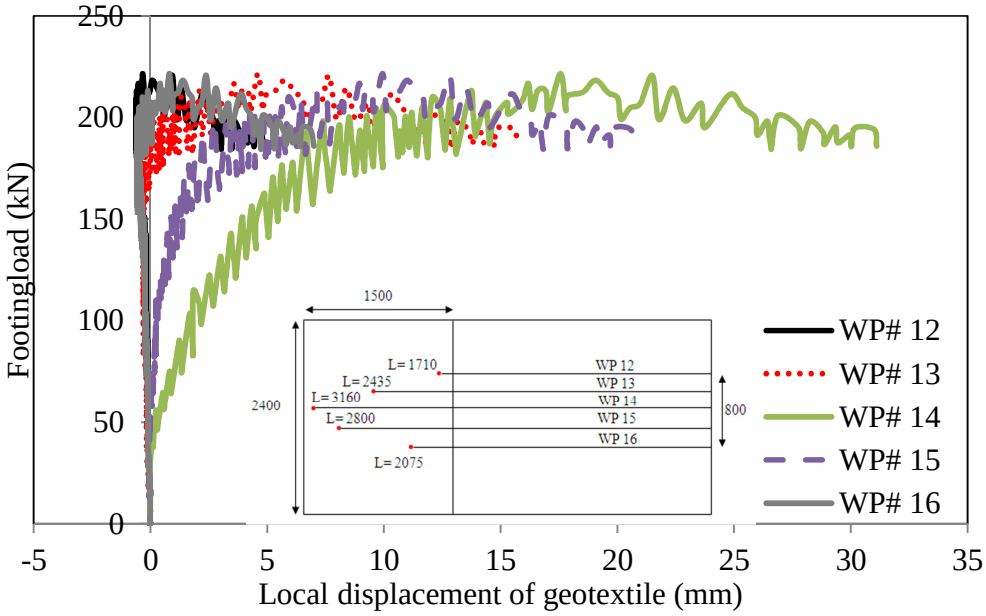

(a)

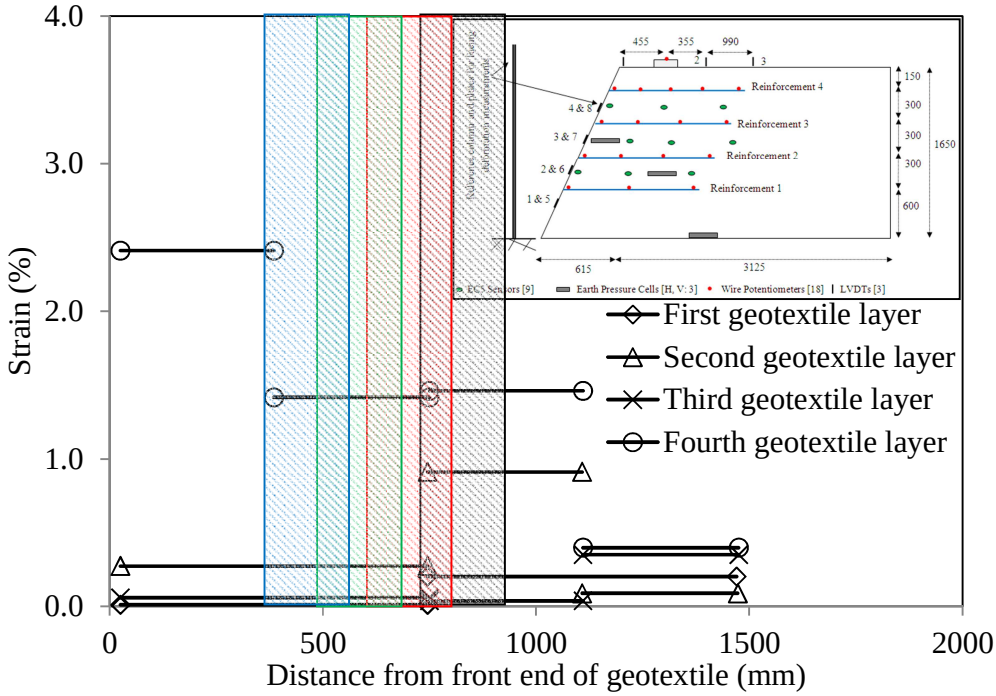

(b)

Figure 9.11. Local displacement of the top (fourth) geotextile layer as measured using 5 wire potentiometers; Note: Black, red, green and blue indicate the footprint of the loading beam at 1st, 2nd, 3rd and 4th geotextile elevations.

9.5. Slope Stability Analysis

Slope stability analysis was carried out using FLAC/SLOPE (Itasca 2005 and GSTABL (Gregory Geotechnical Software 2003) to study the stability of large-scale reinforced embankments in the outdoor testing program. The embankments were modeled at two different GWC values of OMC-2% and OMC+2%. The results for the embankment constructed at OMC-2% were validated using the large-scale outdoor test and ancillary laboratory data (See chapters 5 and 9). The stability of an otherwise identical reinforced embankment constructed at OMC+2% was subsequently predicted using the GSTABL program.

9.5.1. Stability Analysis using GSTABL

A series of slope stability analysis was carried out with GSTABL using Janbu Method of Slices in addition to the General Limit Equilibrium (GLE) and Bishop methods. In contrast to the GLE and Bishop methods which satisfy moment and force equilibriums (the Bishop method does not satisfy horizontal force equilibrium), the Janbu method does not satisfy moment equilibrium and only includes equilibrium of vertical and horizontal inter-slice forces. However, it was found that stability calculations using the Janbu method were more reasonable and comparable to the experimental data in this study.

A series of reduced-scale pullout tests was carried out at different GWC values (i.e. OMC-2% and OMC+2%) and overburden pressures (i.e. 50, 75 and 100 kPa) to determine the pullout capacity of the geotextile reinforcement per unit width (P_r) at different GWC values for GSTABL analysis. Table 9.1 shows the results of pullout

tests on the soil that was used in the large-scale reinforced embankment and HP370 geotextile reinforcement, and the corresponding MRF values.

Table 9.1 Reduced-scale pullout test data and MRF values for the large-scale reinforced embankment soil and HP370 geotextile reinforcement at different overburden pressures

	Force in reduced-scale pullout tests P_{r_rs} (kN/m)		
Test Case	Overburden Pressure, σ_v (kPa)		
----------	50	75	100
OMC-2%	0.9	1.4	1.8
MRF	0.77	0.78	0.78

Table 9.2 shows the input parameters used in the GSTABL stability analysis. The average vertical stress on each reinforcement layer at the laboratory failure load was determined using Boussinesq method (Budhu 2000) and the P_r values were either interpolated or extrapolated from the pullout test results. The P_r values were determined by prorating the reduced-scale pullout capacity values P_{r_rs} by the ratio L_e/L_p in the form:

$$P_r = P_{r_rs} \times L_e/L_p \tag{9.1}$$

where L_e and L_p are the reinforcement embedment lengths in the full-scale reinforced embankment and in the reduced-scale pullout tests (40 mm; see Chapter 3), respectively.

Table 9.2. Input parameters used in the GSTABL stability analysis

Soil			Geotextile				
			-------	1th layer	2th layer	3th layer	4th layer
OMC-2%	γ (kN/m^3)	19.3	P_r (kN/m)	33.8	39.2	46.7	56.4
	c (kPa) φ (°)	12.2, 37.5					
OMC+2%	γ (kN/m^3)	20	P_r (kN/m) [(1)]	26.4	30.5	36.4	44.0
	c (kPa) φ (°)	10.8, 34.3					

(1) P_r values in the embankment at OMC+2% were calculated using the following equation: $P_{r_OMC+2\%} = P_{r_OMC-2\%} \times MRF$

9.5.2. Stability Analysis using FLAC/SLOPE

The embankment model at OMC-2% was also analyzed with FLAC/Slope with input parameters as given in Table 9.3.

Table 9.3. Input parameters for FLAC analysis

Soil			Interface	
OMC-2%	γ (kN/m^3)	19.3	c_a (kPa) δ (°)	8.7, 31.9
	c (kPa) φ (°)	12.2, 37.5		

9.6. Results

9.6.1. Embankment Model at OMC-2%

Figures 9.12a and b show the factor of safety and geometry of failure as obtained from the GSTABL analysis after applying the observed experimental failure pressure (i.e. 450 kPa). Results in Figure 9.12b indicate that the analytical slip plane intercepted the top geotextile layer and slid over the third reinforcement consistent with the observations in the large-scale outdoor test (Figures 9.8 and 9.9). Also, the factor of safety obtained from GSTABL (i.e. FS= 1.086) is reasonably close to unity, indicating impending failure.

In order to quantify the effect of reinforcement on the stability of the embankment, the bearing capacity of unreinforced model for the same factor of safety of 1.086 was analyzed and determined to be 127 kPa, which is 72% smaller than the failure pressure of the reinforced embankment (Figure 9.12c).

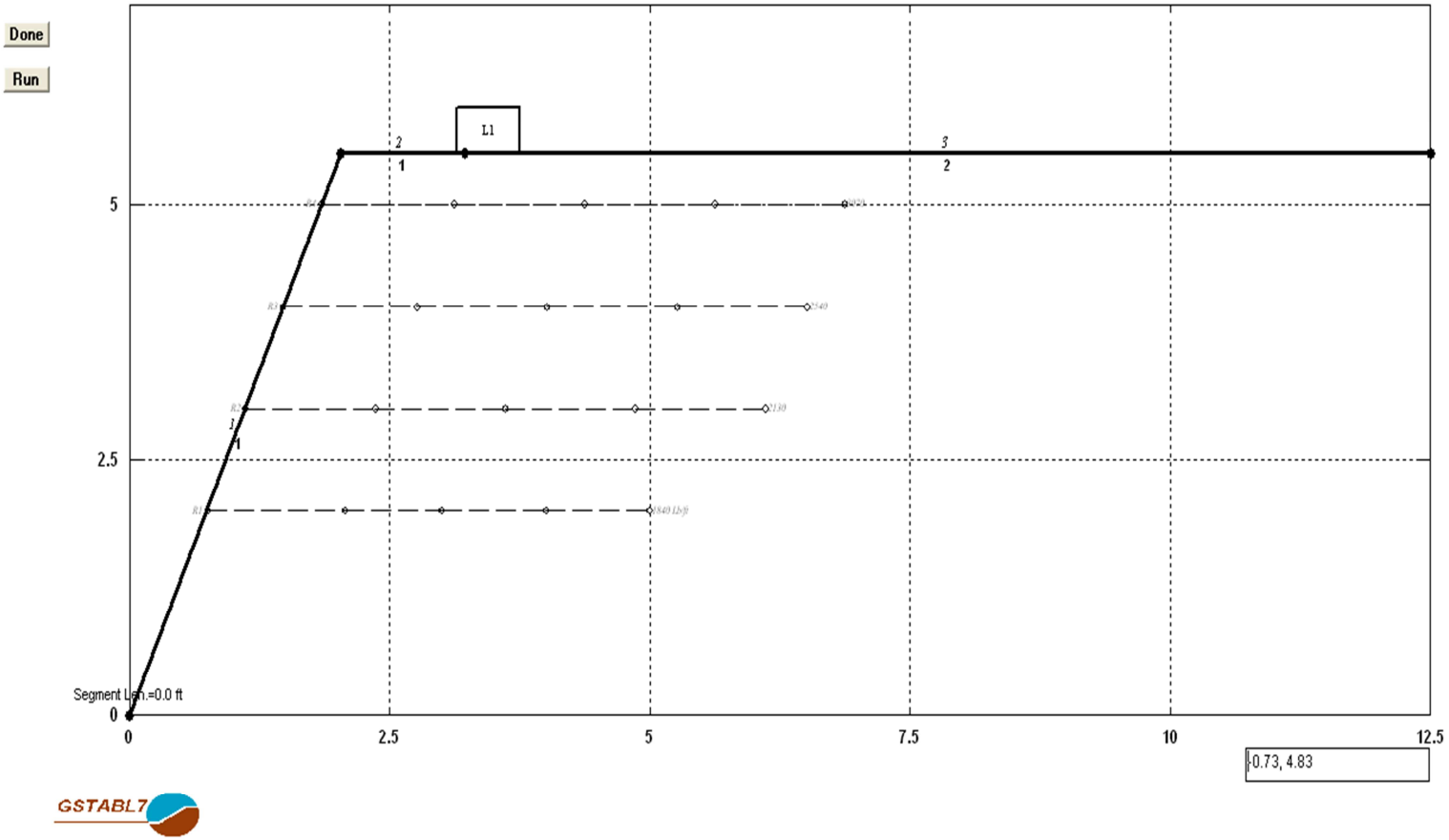
Done
Run
L1
2
1
3
2
5
2.5
0
Segment Length =0.0 ft
0
2.5
5
7.5
10
12.5
-0.73, 4.83
GSTABL7

(a)

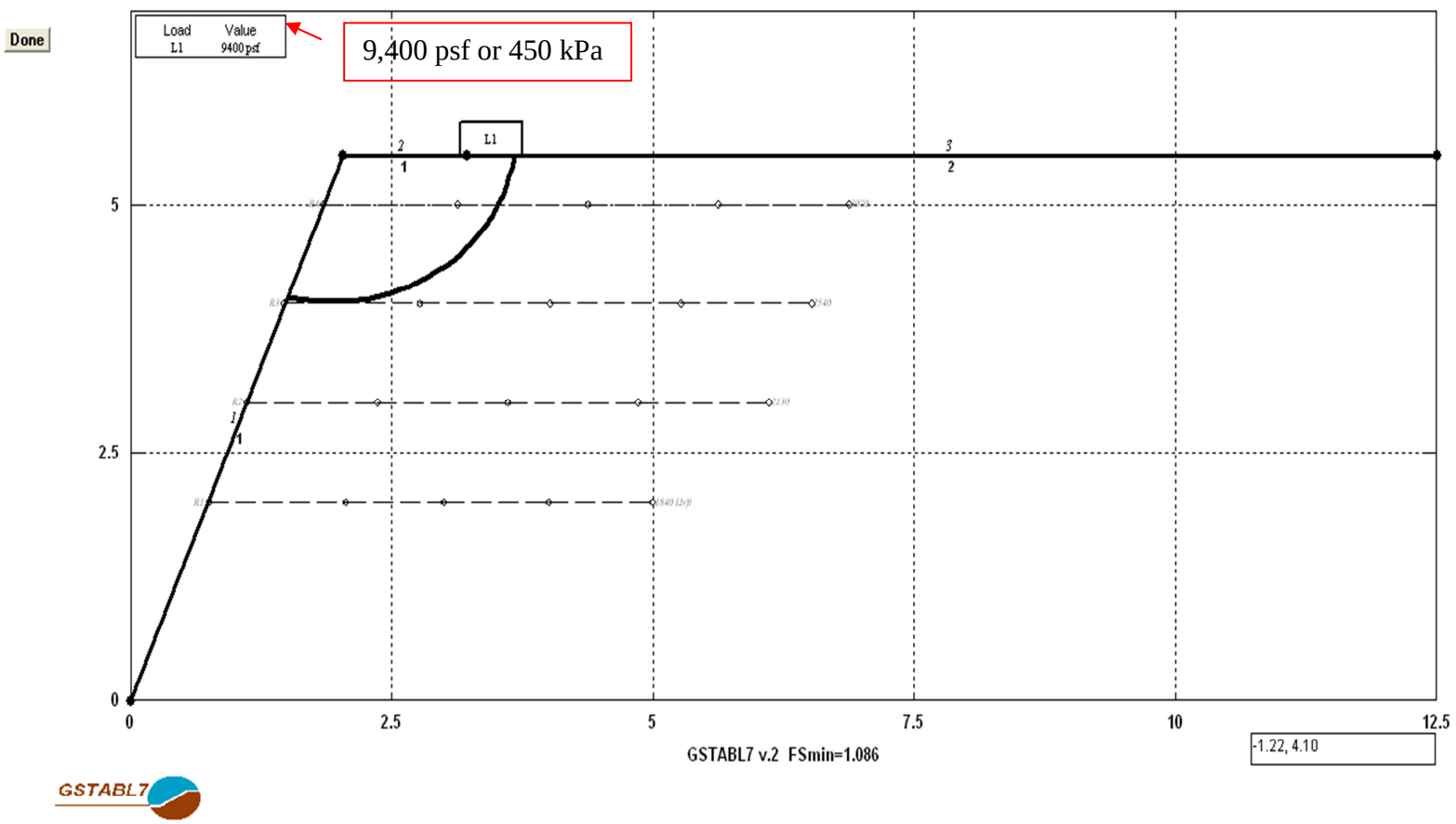
Done
Load
L1
Value
9400 psf
9,400 psf or 450 kPa
L1
5
2.5
0
0
2.5
5
7.5
10
12.5
GSTABL7 v.2 FSmin=1.086
-1.22, 4.10
GSTABL7

(b)

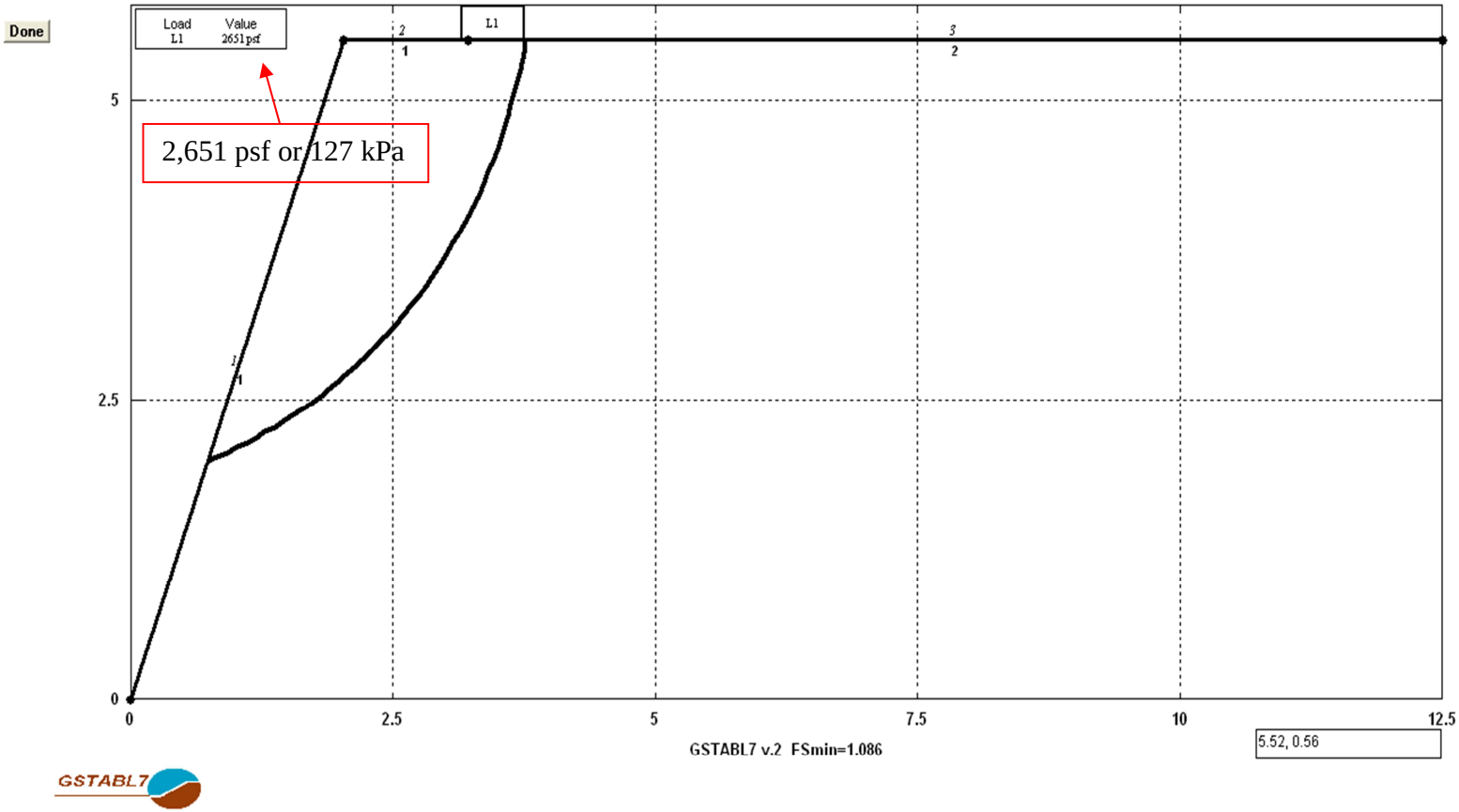

(c)

Figure 9.12. Slope stability analysis of embankment model constructed at OMC-2% using GSTABL: (a) Model geometry, (b) Critical slip surface and factor of safety for reinforced embankment and (c) Critical slip surface and factor of safety for unreinforced embankment

Figure 9.13 shows the results of stability analysis using FLAC/Slope for the embankment built at OMC-2%. The model reinforced embankment was subjected to the actual experimental failure load, and the failure wedge and factor of safety were determined.

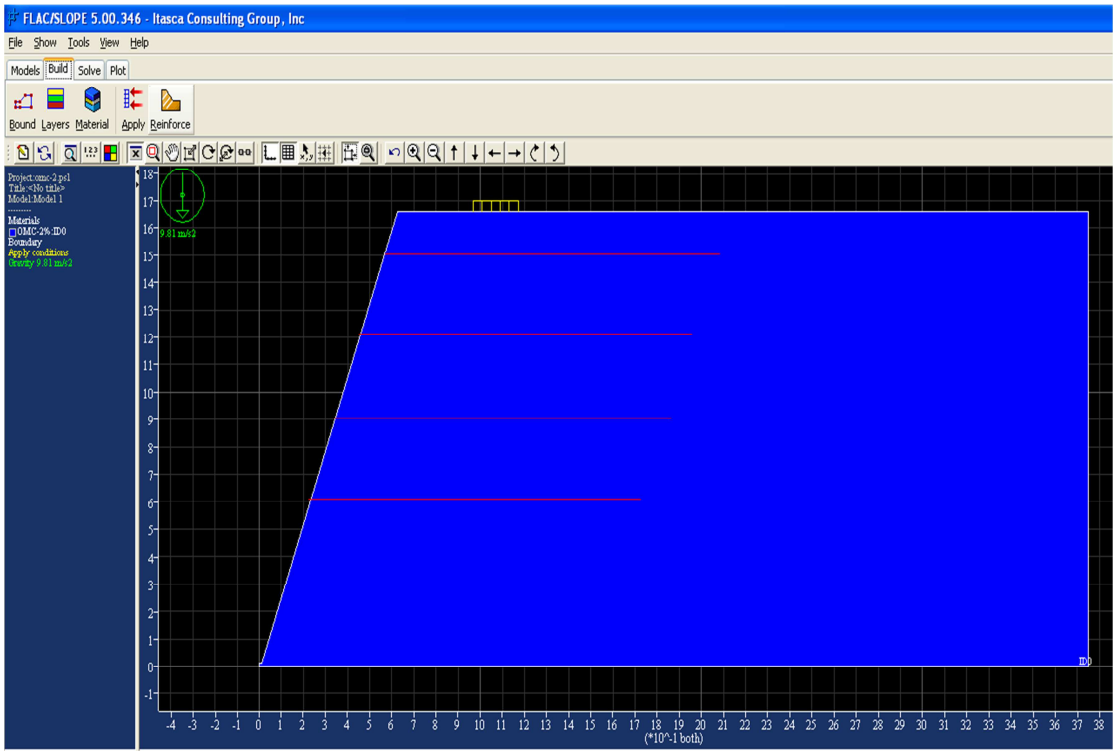

(a)

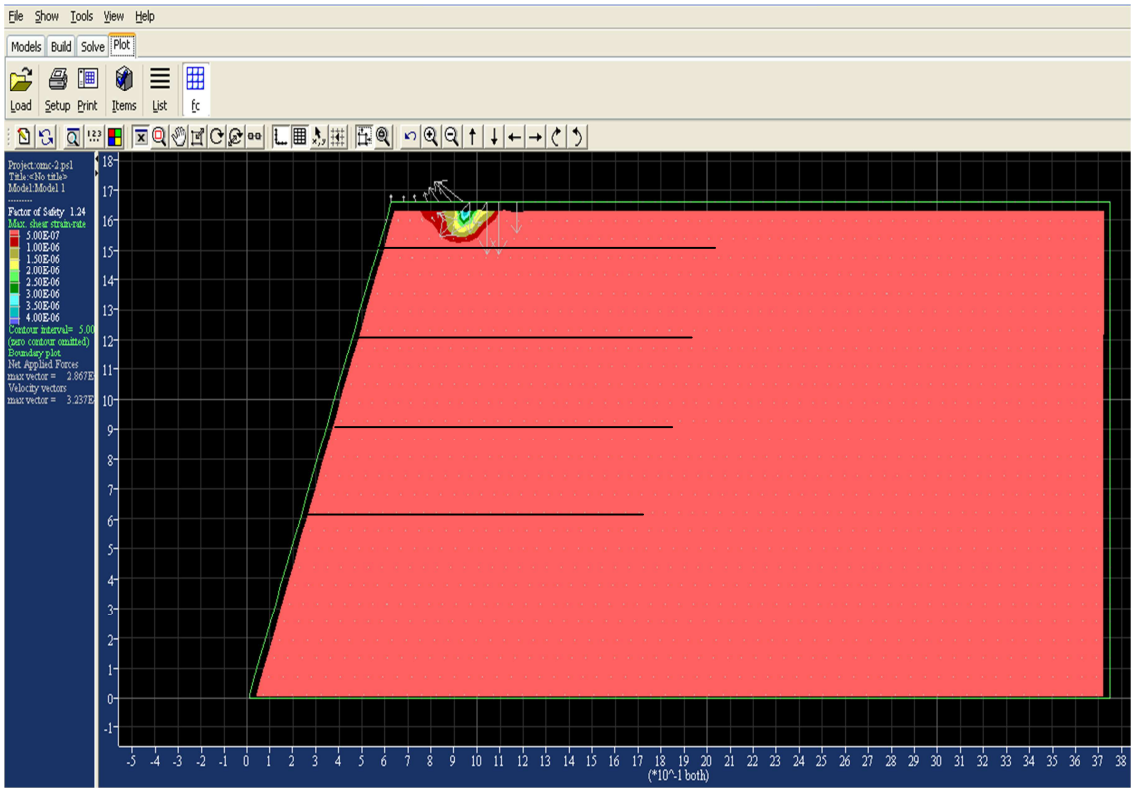

(b)

Figure 9.13. Slope stability analysis using FLAC/SLOPE, (a) Embankment geometry (b) Critical slip plane (FS= 1.24)

Results in Figure 9.13b indicate that the slip plane in the FLAC/SLOPE analysis was formed above the top geotextile layer with the factor of safety of 1.24, which was different from what was observed in the outdoor test. Therefore, it was decided to analyze the stability of reinforced embankment model constructed at OMC+2% using the GSTABL program.

9.6.2. Embankment Model at OMC+2%

Figure 9.14 shows the predicted slip surface and factor of safety within the embankment as it was subjected to the laboratory failure pressure of 450 kPa. Results in Figure 9.14 indicate that the MRF value applied to the soil-geotextile interface lowered the factor of safety from 1.086 to 0.937 and show that the embankment constructed on wet side of optimum would be unstable when subject to the footing pressure of 450 kPa. Figure 9.15 shows that the surcharge load needed to reach the same factor of safety obtained for the OMC-2% model (i.e. FS= 1.086) for the case of embankment constructed at OMC+2% is 320 kPa. The results indicate that when the interface strength of soil-geotextile decrease by 22% (MRF= 0.78) as a result of wetting, the load bearing capacity of the embankment decreases by 30% as compared to the model constructed at OMC-2%.

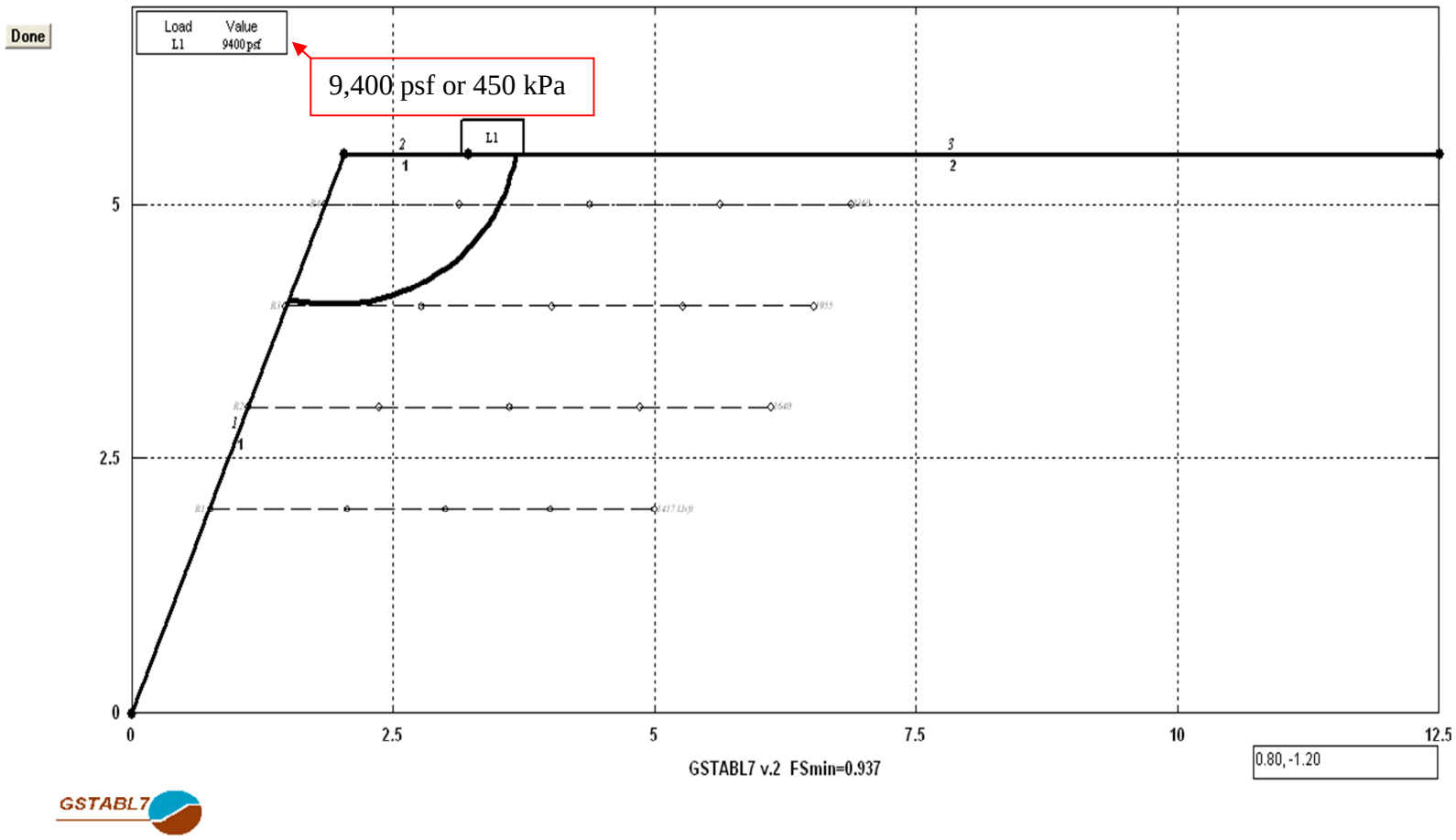

Figure 9.14. Predicted slip plane and factor of safety for the embankment model constructed at OMC+2% from GSTABL analysis

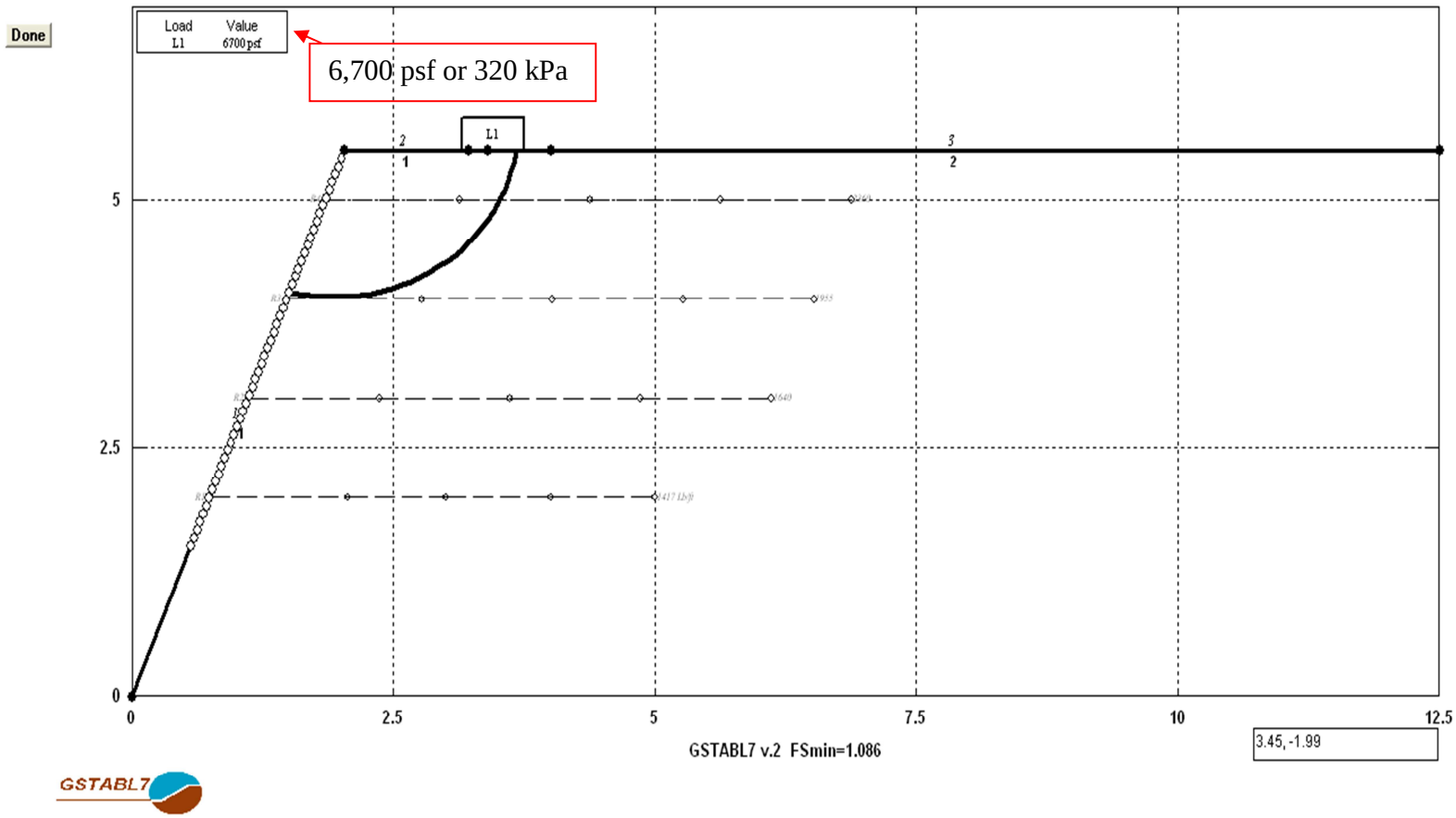

Figure 9.15. Slip plane and bearing capacity of the embankment model constructed at OMC+2% from GSTABL analysis to reach the factor of safety equal to 1.086. Note: White circles on the facing slope indicate the initiation points of possible slip planes formed within the large-scale embankment in GSTABL model.

CHAPTER 10

IMPLICATIONS OF STUDY RESULTS TO DESIGN: MOISTURE REDUCTION FACTOR

Figure 10.1 shows the variations of $\mu(\omega)$ for the Chickasha soil-woven geotextile interface as a function of the soil GWC at different overburden pressures from large-scale and small-scale pullout tests and interface shear tests carried out in this study. In the calculation of $\mu(\omega)$, the pullout resistance and/or interface strength at ω = OMC-2% is taken as the reference value (Hatami et al. 2010a,b).

Results shown in Figure 10.1 indicate that construction of reinforced soil slopes and embankments on the wet side of OMC or wetting of the soil-geotextile interface during construction or service life of the reinforced soil structure (as compared to e.g., the case of OMC-2%) could result in considerably lower pullout resistance of the geotextile reinforcement. The calculated amounts of reduction in interface strength from OMC-2% to OMC+2% as obtained from the large-scale and small-scale test data are between 27% to 36% depending on the test cases. Results shown in Figure 10.1 indicate that the variation of $\mu(\omega)$ with the soil GWC could be approximated as linear for practical purposes for the range of GWC values examined in this study.

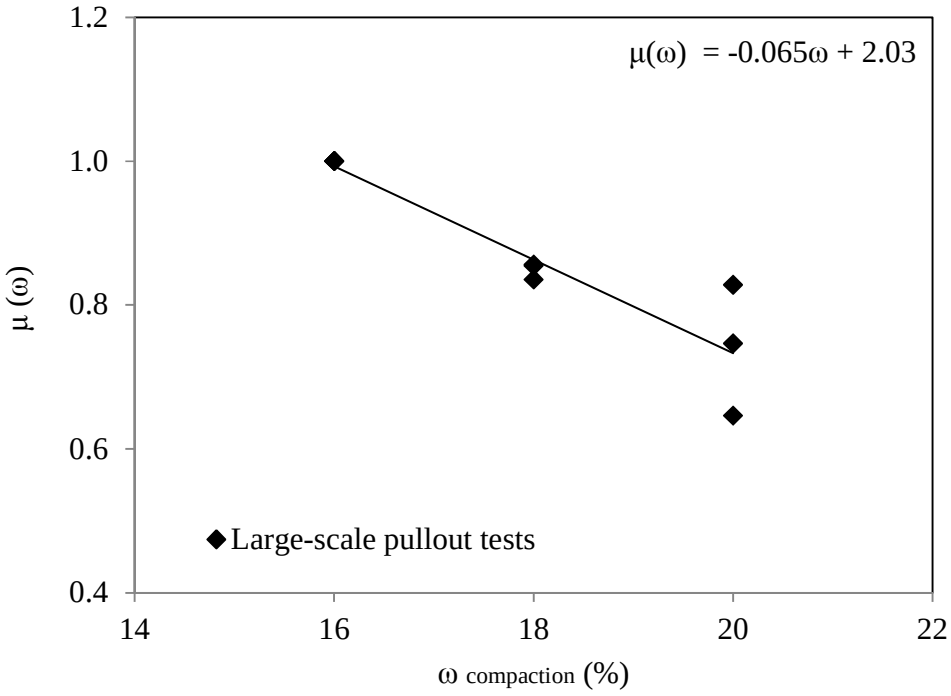
μ(ω) = -0.065ω + 2.03
1.2
1.0
0.8
0.6
0.4
μ (ω)
Large-scale pullout tests
14
16
18
20
22
ω compaction (%)

(a)

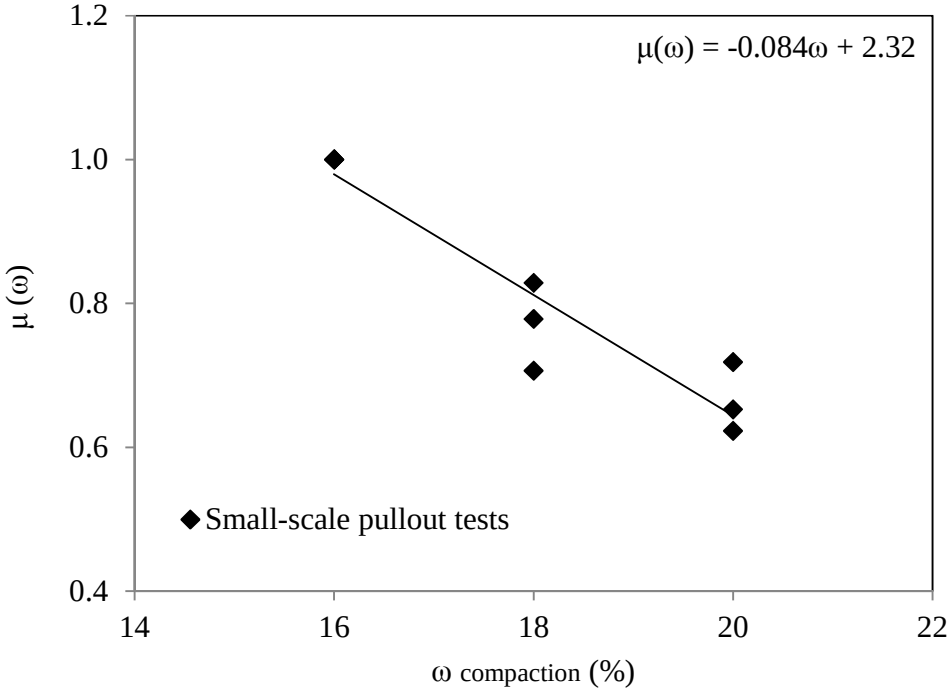
μ(ω) = -0.084ω + 2.32
1.2
1.0
0.8
0.6
0.4
μ (ω)
Small-scale pullout tests
14
16
18
20
22
ω compaction (%)

(b)

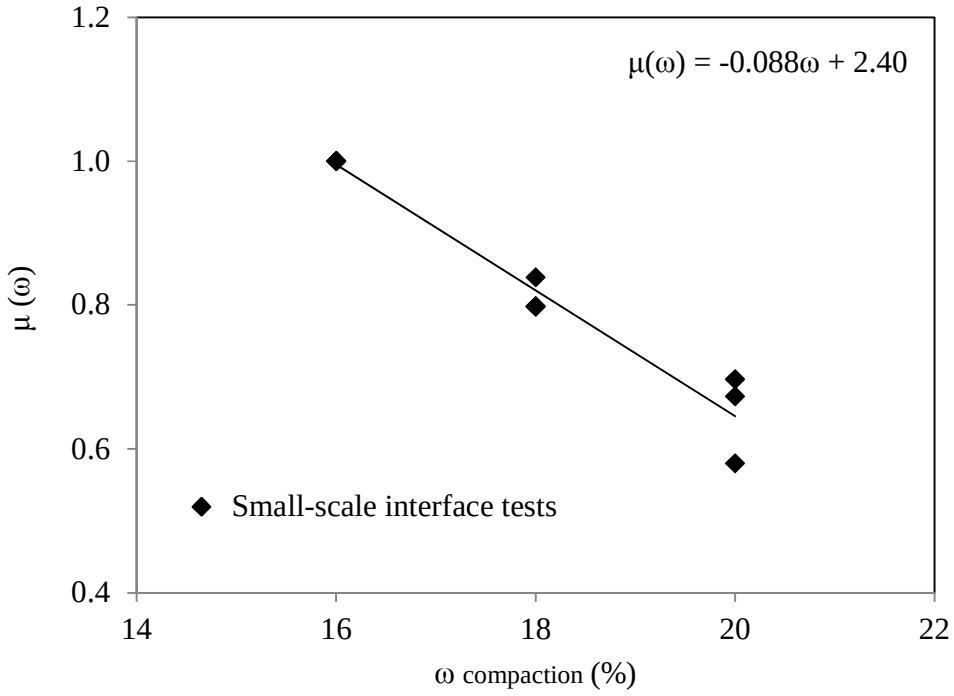

(c)

Figure 10.1. Moisture reduction factor for the woven geotextile in Chickasha soil: (a) Large-scale pullout tests; (b) Small-scale pullout tests; (c) Small-scale interface shear tests

Based on the results of this study, the observed failure wedges in all six reduced-scale embankment test cases involved sliding a sheared block of soil over the geotextile reinforcement with comparatively insignificant pullout behavior (Figure 8.12). Figure 10.2 shows the μ(ω) values (i.e. MRF) for reduced-scale embankment tests calculated from Equation 10.1. The $\sigma_n^{'}$values in Equation 10.1 are determined using the failure loads in Table 8.1.

$$\mu(\omega) = \frac{[(c_a + \sigma_n^{'} \tan\delta) L_{IS}]_{for\ each\ test\ case}}{[(c_a + \sigma_n^{'} \tan\delta) L_{IS}]_{at\ OMC-2\%}} \quad (10.1)$$

Where L_{IS} is the shear length over the length of geotextile reinforcement and is defined in Figure 8.12a. c_a and δ are interface shear strength parameters.

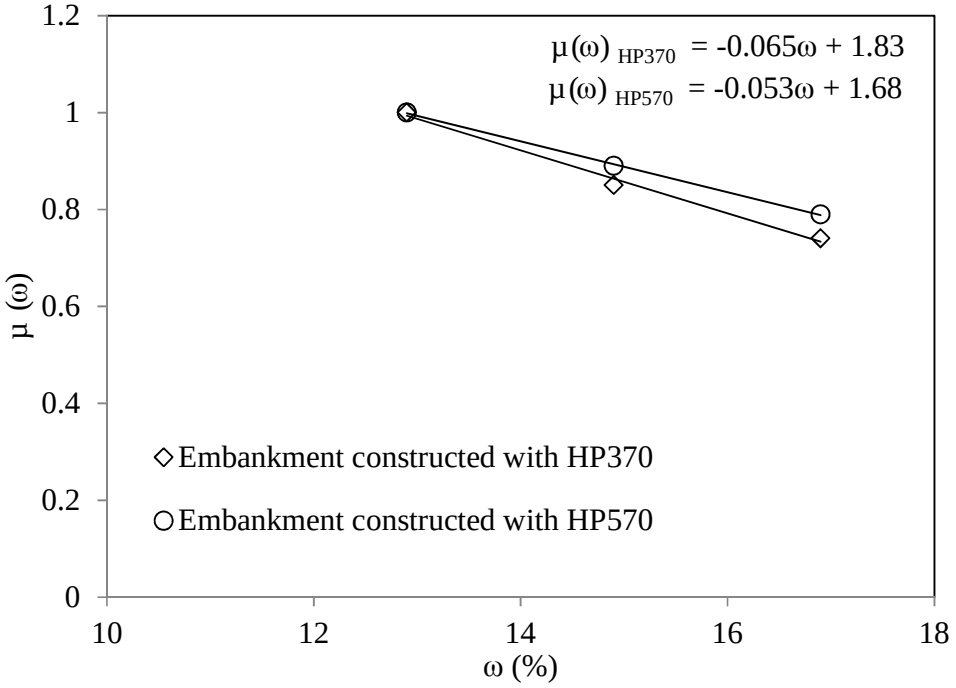

Figure 10.2. Moisture reduction factors for the embankment models constructed with HP370 and HP570 geotextile reinforcement

Results shown in Figure 10.2 for the model embankments indicate that the moisture reduction factors [MRF or $\mu(\omega)$] for the model embankments reinforced with HP370 and HP570 geotextile reinforcement for a change in the soil GWC value from OMC-2% to OMC+2% are approximately 74% and 79%, respectively. Figure 10.3 shows the variation of MRF with soil, geotextile and type of test from current and recent studies (Hatami et al. 2010a,b; 2013; Hatami et al. 2014 and Chan, E. 2014)).

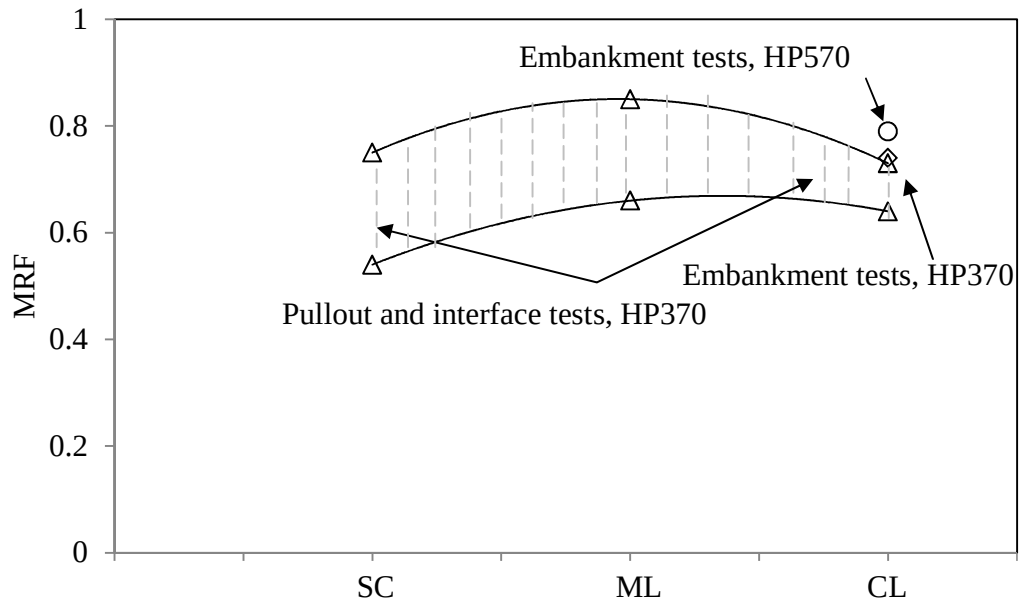

Figure 10.3. MRF values as a function of soil, geotextile and soil type. Note: The MRF values were determined for the moisture content changes from OMC-2% to OMC+2% (i.e. SC $_{pullout/interface}$: 10.6 to 14.6%; ML $_{pullout/interface}$: 10.7 to 14.7%, CL $_{pullout/interface}$: 16 to 20% and CL $_{embankment}$: 12.9 to 16.9%)

CHAPTER 11

CONCLUSIONS AND RECOMMENDATIONS

11.1. Conclusions

The primary objective of this study was to develop a moisture reduction factor [MRF or $\mu(\omega)$] for the pullout resistance and interface shear strength of geotextile reinforcement for the design of reinforced soil structures with marginal soils. Based on the results of this study, the current FHWA design equation for resistance of geotextile reinforcement was modified to account for the influence of the marginal soil moisture content on the pullout resistance of geotextile in reinforced soil structures. The MRF values indicated to what extent the interface shear strength in reinforced embankment models changed from dry side of optimum moisture content to the wet side. Based on the results of this study the following conclusions are made:

1. Results from large-scale and small-scale tests on soil-geotextile interfaces in this study indicated that changes in the soil suction and GWC can have a significant influence on the geotextile reinforcement pullout resistance.
2. Results from large-scale pullout tests showed that strain distribution in the geotextile was nonuniform with the greatest value in its front end and lowest in its tail end. The same results also indicated that geotextile strains were greater in dryer soil (e.g. OMC-2% as compared to OMC+2%) and at higher overburden pressures.
3. Pullout and interface shear tests carried out at different scales showed that the interface adhesion and, consequently, pullout strength of reinforcement

increases with matric suction. Small-scale pullout tests indicated that interface adhesion and friction angle values were 31% and 40% smaller, respectively, in specimens at OMC+2% as compared to those tested at OMC-2%. The interface shear tests also indicated that the interface friction angle was 15% smaller in specimens at OMC+2% as compared to those tested at OMC-2%.

4. Small-scale pullout test results showed greater adhesions than those from corresponding large-scale tests which could be attributed to the smaller size and boundary effects.
5. Adhesion values calculated from pullout tests were greater than those from interface shear tests, which could be attributed to the passive resistance of the fine-grained soil which penetrated into the stretched geotextile when subjected to pullout force.
6. The collective range of MRF values from all the pullout and interface shear tests in this study varied between 64 and 73% depending on the soil GWC and the scale and type of test.
7. The results of embankment tests indicated that the embankment model constructed at OMC-2% resulted in the largest failure load when subjected to a line surcharge load simulating loading from bridge abutments.
8. Failure loads of model embankments constructed with HP370 and HP570 geotextiles at OMC+2% were 40% and 33% smaller respectively, than that of the model compacted at OMC-2%.
9. Earth pressures determined using the Boussinesq method overestimated the measured values in the model embankment tests. Possible reasons were

attributed to deviations in the geometry of the embankments and load transfer through test box sidewalls from the assumptions in the Boussinesq's theoretical approach.

10. Strains in two similar geotextiles that were different in their tensile strength and tensile modulus values were consistently larger in drier model embankments with higher matric suction. The value of peak strain measured in the model that was built with the stronger HP570 woven geotextile at OMC-2% was 3.4%.
11. The MRF values for the case of OMC+2% (using the OMC-2% case as baseline) for the embankment models constructed with HP370 and HP570 geotextiles were 74% and 79%, respectively.

11.2. Recommendations for Future Work

1. The behavior of a marginal soil that is initially placed and compacted at OMC-2% and wetted to OMC+2% is different from that of the same marginal soil placed and compacted at OMC+2%. Therefore, it would be complementary to this study to produce MRF values for soil-geotextile interfaces that are initially set up at OMC-2% and subsequently wetted to OMC, OMC+2% and beyond (e.g. using an irrigation system in the test facility) to simulate field conditions.
2. Extend the results of this study to a larger range of GWC values on the dry and wet sides of optimum (i.e. OMC±4).
3. Extend the results of this study to different types of geotextiles (i.e. woven and non-woven) to investigate the influence of reinforcement properties on the moisture reduction factor.

4. Perform pullout and interface shear tests using a 30 cm × 30 cm DST machine to include medium-scale test results in the database of MRF values produced in this study.
5. Study the influence of front boundary conditions using Styrofoam, cardboard and rubber on the small-scale pullout test results.
6. Investigate the influence of footing setback (footing distance from embankment crest) and reinforcement design on the bearing capacity of embankment and MRF values.
7. Perform embankment tests on various types of marginal soils (i.e. silt and sand) to determine the MRF values and compare them with the data from pullout/IST on the same soil carried out in the author's recent study to find how the embankment geometry would influence the moisture reduction factors.

12. REFERENCES

Abu-Farsakh, M., Farrag, K., Almohd, I. and Mohiuddin, A., 2005, "Bearing and Frictional Contributions to the Pullout Capacity of Geogrid Reinforcements in Cohesive Backfill", *Proceeding of Geo-frontiers, ASCE, Austin, TX*.

Abu-Farsakh M., Coronel J. and Tao M., 2007, "Effect of Soil Moisture Content and Dry Density on Cohesive Soil–Geosynthetic Interactions Using Large Direct Shear Tests", *Journal of Materials in Civil Engineering, ASCE,* Vol. 19, pp. 540-549.

Adams, M. T. and Collin, J. G., 1997, "Large Model Spread Footing Load Tests on Geosynthetic Reinforced Soil Foundations", *Journal of Geotechnical and Geoenvironmental Engineering, ASCE,* Vol. 123, No. 1, pp. 66- 72.

Adanur, S., Gowayed, Y. and Elton, D., 1994,"Design and Characterization of Geotextiles for High Performance Applications", *National Textile Center Research Brief*, September 1994, Auburn University, AL, USA.

American Association of State Highway and Transportation Officials, AASHTO, 2008, "Guide Specifications for Design and Construction of Segmental Concrete Bridges", Second Edition, Washington, DC, http://www.transportation.org/

Anubhav, P.K.B., 2010, "Modeling of Soil-Woven Geotextile Interface Behavior from Direct Shear Test Results", *Geotextiles and Geomembranes*, Vol. 28, No. 4, pp. 403-408.

ASTM International, 2006, "Standard Test Method for Amount of Material in Soils finer than No. 200 (75-μm) Sieve", *American Society for Testing and Materials,* West Conshohochen, PA, USA.

ASTM International, 2007, "Standard Test Method for Particle Size Analysis of Soils", *American Society for Testing and Materials,* West Conshohochen, PA, USA.

ASTM International, 2008, "Standard Test Method for Density and Unit Weight of Soil in Place By the Rubber Balloon Method", *American Society for Testing and Materials*, West Conshohocken, PA, USA.

ASTM D6836, 2008, "Standard Test Methods for Determination of the Soil Water Characteristic Curve for Desorption using a Hanging Column, Pressure Extractor, Chilled Mirror Hygrometer and/or Centrifuge", *American Society for Testing and Materials*, West Conshohochen, PA, USA.

ASTM International, 2009, "Standard Test Method for Tensile Properties of Geotextiles by the Wide-Width Strip Method", *American Society for Testing and Materials,* West Conshohochen, PA, USA.

ASTM International, 2010, "Standard Test Method for Laboratory Determination of Water (Moisture) Content of Soil and Rock by Mass", *American Society for Testing and Materials,* West Conshohochen, PA, USA.

ASTM International, 2010, "Standard Test Method for Measurement of Soil Potential (Suction) Using Filter Paper", *American Society for Testing and Materials,* West Conshohochen, PA, USA.

ASTM D6706, 2010, "Standard Test Method for Measuring Geosynthetic Pullout Resistance in Soil", *American Society for Testing and Materials,* West Conshohochen, PA, USA.

ASTM International, 2011, "Standard Test Method for Direct Shear Tests of Soils Under Consolidated Drained Conditions", *American Society for Testing and Materials*, West Conshohocken, PA, USA.

ASTM International, 2012, "Standard Test Method for Laboratory Compaction Characteristics of Soil Using Modified Effort", *American Society for Testing and Materials*, West Conshohocken, PA, USA.

ASTM D4751, 2012, "Standard Test Method for Determining Apparent Opening Size of Geotextile", *American Society for Testing and Materials,* West Conshohochen, PA, USA.

ASTM International, 2013, "Standard Test Method for Determining the Shear Strength of Soil-Geosynthetic and Geosynthetic-Geosynthetic Interfaces by Direct Shear", *American Society for Testing and Materials*, West Conshohocken, PA, USA.

ASTM D4833, 2013, "Standard Test Method for Index Puncture Resistance of Geomembranes and Related Products", *American Society for Testing and Materials,* West Conshohochen, PA, USA.

ASTM D4632, 2013, "Standard Test Method for Grab Breaking Load and Elongation of Geotextiles", *American Society for Testing and Materials,* West Conshohochen, PA, USA.

ASTM D4491, 2014, "Standard Test Method for Water Permeability of Geotextiles by Permittivity", *American Society for Testing and Materials,* West Conshohochen, PA, USA.

Bathurst, R. J., Blatz, J. A. and Burger, M. H., 2003, "Performance of Instrumented Large-Scale Unreinforced and Reinforced Embankments Loaded by a Strip Footing to Failure," *Canadian Geotechnical Journal,* Vol. 40, No. 6, pp. 1067-1083.

Berg R.B., Christopher, B.R. and Naresh C. Samtani, 2009, "Design and Construction of Mechanically Stabilized Earth Walls and Reinforced Soil Slopes", *Federal Highway Administration, Washington, DC, USA, FHWA-NHI-10-024.*

Bergado, D. T., Long, P. V., Saowapakpiboon, J. and Voottipruex, P., 2008, "Evaluation of Interface Parameters from Pullout Tests in Silty Sand and Weathered Clay," *Proceedings of 4th Asian Regional Conference on Geosynthetics*, China, pp. 139-145.

Bilgin, O., and Kim, H., 2010, “Effect of Soil Properties and Reinforcement Length on Mechanically Stabilized Wall Deformations”, Earth Retention Conference, ASCE, Bellevue, Washington, USA, pp. 556-563.

Bilgin, O., and Mansour,,E., 2014, “Effect of Reinforcement Type on the Design Reinforcement Length of Mechanically Stabilized Earth Walls”, *Geotextiles and Geomembranes*, Vol. 59, pp. 663-673.

Briaud, J.L.**,** 2007, “Spread Footings in Sand: Load Settlement Curve Approach”, *Journal of Geotechnical and Geoenvironmental Engineering*, Vol 133, No. 8, pp. 905-920.

Budhu, M., 2000, *Soil Mechanics and Foundations*, 1st ed., John Wiley & Sons, Inc.

Bueno, B. S., Benjamim, C. V. S. and Zornberg, J. G., 2005, “Field Performance of a Full-Scale Retaining Wall Reinforced with Non-Woven Geotextile,” *Slopes and Retaining Structures Under Seismic and Static Conditions, ASCE*, Geotechnical Special Publication No. 140, Gabr, Bowders, Elton, and Zornberg, Editors, Austin, Texas, pp. 2617-2625.

Campbell, G.S. and W.H. Gardner. 1971, ‘Psychometric Measurement of Soil Water Potential: Temperature and Bulk Density Effects.”, *Soil Science Society of America Proceedings*, Vol.35. pp. 8-11.

Cardoso, R., Romero E., Lima A. and Ferrari A., 2007, “A comparative Study of Soil Suction Measurement Using Two Different High-Range Psychrometers.”, *Experimental Unsaturated Soil Mechanics*, Vol. 112, pp. 79-93.

Cassidy, M.J., Byrne, B.W., and Houlsby, G.T., 2002, “Modelling the Behaviour of Circular Footings under Combined Loading on Loose Carbonate Sand”, *Geotechnique*, Vol. 52, No.10, pp. 705-712.

Cerato, A.B. and Lutenegger, A.J., 2007. “Scale Effects of Shallow Foundations Bearing Capacity on Granular Material”, *Journal of Geotechnical and Geoenvironmental Engineering, ASCE*, Vol. 133, No. 10, pp. 1192-1202.

Castelli, F., and Motta, E., 2010, "Bearing Capacity of Strip Footings Near Slopes", *Geotechnical and Geological Engineering*, Vol. 28, 2010, pp. 187-198.

Chadi, E. M. and Milind, K., 2009, “Vertical Pullout Test for Measurement of Soil-geomembrane Interface Friction Parameters”, *Geotechnical Testing Journal*, ASTM, Vol. 32, No. 4, pp. 1-7.

Chandrakaran, S., Subaida, E. A. and Sankar, N., 2008, “Prediction of Pullout Strength of Woven Coir Geotextiles from Yarn Pullout Resistances”, *the 12th International Conference of International Association for Computer Methods and Advances in Geomechanics*, India, pp. 3735-3742.

Chan, E., 2014. Reduced-Scale Laboratory Investigation of Reinforced Embankments. MSc. Thesis, Norman, Oklahoma.

Chao, K.C., 2007, “Design Principles for Foundations on Expansive Soils”, Dissertation, Colorado State University, Fort Collins, Colorado.

Chua, K.M., Aspar, W., and De La Rocha, A., 1993, "Simulating Failures of Geosynthetics- Reinforced Earth Structures under Saturated Condition", *Geosynthetic'93*. Vancouver, IFAI, St. Paul, 417-430.

Dash, S.K., Rajagopal, K. and Krishnaswamy, N.R., 2007, "Behaviour of Geocell-Reinforced Sand Beds Under Strip Loading", *Canadian Geotechnical Journal*, Vol. 44, 905-916.

Elias, V., Christopher, B.R. and Berg, R.R., 2001, "Mechanically Stabilized Earth Walls and Reinforced Soil Slopes-Design and Construction Guidelines", *Federal Highway Administration, Washington, DC, USA, FHWA-NHI-00-043.*

Ellithy, G., and Gabr, M., 2000, "Compaction Moisture Effect on Geomembrane/Clay Interface Shear Strength", *Geo-Denver, ASCE*, Denver, CO, USA, 39-53.

Farrag, K. and Morvant, M. J., 2004, "Evaluation of Interaction Properties of Geosynthetics in Cohesive Soils: Lab and Field Pullout Tests," *Louisiana Department of Transportation and Development and Louisiana Transportation Research Center*, Baton Rouge, LA, USA, Final Report LTRC 736-99-0658.

Fredlund, D.G., Morgenstern, N.R., and Widger, R.A., 1978, "The Shear Strength of Unsaturated Soils", *Canadian Geotechnical Journal*, Vol. 15, No. 3, pp. 313-321.

Fredlund, D.G., Shuai, F., and Freng, M., 2000, "Use of New Thermal Conductivity Sensor for Laboratory Suction", *Proceedings of the Asian Conference on Unsaturated Soils, Singapore,* pp. 275-280.

Geokon, Inc., 2013, "Earth Pressure Cells, 3500, 4800 Series", *Geokon, Inc.*, Lebanon, NH, USA, http://www.geokon.com/content/datasheets/4800_Series_Earth_Pressure_Cells.pdf

Georgiadis, K., 2010, "Undrained Bearing Capacity of Strip Footings on Slopes", *Journal of Geotechnical and Geoenvironmental Engineering, ASCE*, Vol. 136, No. 5, pp. 677-685.

Germer, K., Farber, A. and Braun, J., 2008, "Studies on Slope Failure Process in a Laboratory Flume," *Geophysical Research Abstracts*, Vol. 10, EGU2008-A-05633, pp. 115-118.

Gill, K.S., Choudhary, A.K., Jha, J.N., and Shukla, S.K., 2013, "Large Model Footing Load Test on Multi Layer Reinforced Coal-Ash Slope", *Geo-Congress 2013, ASCE, San Diego, CA*, pp. 489-498.

Gregory Geotechnical Software, 2003, GSTABLE, Version 2.0

Goodhue, M. J., Edil, T. B. and Benson, C. H., 2001, "Interaction of Foundry Sand with Geosynthetics", *Journal of Geotechnical and Geoenvironmental Engineering*, ASCE, Vol. 127, No. 4, pp. 353-362.

Hamid, T.B. and Miller, G.A., 2009, "Shear Strength of Unsaturated Soil Interfaces", *Canadian Geotechnical Journal*, Vol. 46, pp. 595-606.

Hatami, K., Miller G.A., and Garcia L., 2010a, "Use of MSE Technology to Stabilize Highway Embankments and Slopes in Oklahoma", *Oklahoma Department of Transportation, Tulsa, OK, USA, Final Report OTC REOS7-1-19.*

Hatami K., Garcia L.M. and Miller, G.A., 2010b, "Influence of moisture content on the pullout capacity of geotextile reinforcement in marginal soils", *61st Highway Geology Symposium, Oklahoma City, OK.*

Hatami K., Garcia L.M. and Miller G.A., 2011, "A Moisture Reduction Factor for Pullout Resistance of Geotextile Reinforcement in Marginal Soils", *Geo-Frontiers, Dallas, TX, ASCE Special Publication* No. 211.

Hatami, K., Granados, JE., Esmaili, D. and Miller, GA., 2013, "Influence of Gravimetric Water Content on Geotextile Reinforcement Pullout Resistance in MSE Walls with Marginal Quality Soils," *Journal of Transportation Research Record*, 2363: 66-74.

Hatami, K., Esmaili, D., Chan, EC., and Miller, G.A, 2014, "Laboratory Performance of Reduced-Scale Reinforced Embankments at Different Moisture Content", *International Journal of Geotechnical Engineering*, Vol. 8, No. 3, pp. 260-276.

Hossain, M. Z. and Inoue, S., 2002, "Soil-Reinforcement Interaction Under Laboratory Pullout Tests Using Geosynthetics and Wire Meshes", *Bulletin of the Graduate School of Bioresources*, Mie University, No. 29, pp. 1-20.

Hossain, MZ., and Sakai, T., 2007, "A Study on Pullout Behavior of Reinforcement Due to Variation of Water Content of Soil", *International Commission of Agricultural Engineering: CIGR E-Journal*, Manuscript LW 07 011, Vol. 9.

Huang, C. C., Tatsuoka, F. and Sato, Y., 1994, "Failure Mechanism of Reinforced Sand Slopes Loaded with a Footing", *Soils and Foundations Journal*, Vol. 34, No. 2, pp. 27-40.

Itasca Consulting Group Inc., 2005, FLAC/Slope, Version 5.00.

Kato, S., and Kohashi, H., 2006, "Study on the Monitoring System of Slope Failure Using Optical Fiber Sensors", *Proceedings of ASCE, GeoCongress 2006*, pp. 1-6.

Kawamura, S., Miura, S., Yokohama, S., Kudo, A., and Kaiya, N., 2013, "Field Monitoring of Embankment Constructed by Volcanic Soil and Its Evaluation", *Geo-Congress 2013, ASCE, San Diego, CA*, pp. 373-382

Keller, G.R., 1995, "Experiences with Mechanically Stabilized Structures and Native Soil Backfill", *Transportation Research Record*, 1474: 30-38.

Keskin, M.S., and Laman, M., 2013, "Model Studies of Bearing Capacity of Strip Footing on Sand Slope", KSCE Journal of Civil Engineering, Vol. 17, No. 4, pp.699-711.

Khoury, C.N., Miller, G.A. and Hatami, K., 2011, "Unsaturated Soil-Geotextile Interface Behavior", *Geotextiles and Geomembranes Journal*, Vol. 29, No. 1, pp. 17-28.

Kibria, G., Hossain, S., and Sadik Khan, M., 2014, “Influence of Soil Reinforcement on Horizontal Displacement of MSE Wall”, *International Journal of Geomechanics, ASCE,* Vol. 14, pp. 130-141.

Kim, Y.T, and Lee, J.S., 2013, “Slope Stability Characteristic of Unsaturated Weathered Granite Soil in Korea Considering Antecedent Rainfall”, *Geo-Congress 2013, ASCE, San Diego, CA,* pp. 394-401.

Kumar, A., Ohri, M. L. and, Bansal, R. K., 2007, "Bearing Capacity Tests of Strip Footings on Reinforced Layered Soil," *Geotechnical and Geological Engineering Journal, Springer,* Vol. 25, No. 2, pp. 139-150.

Kumar, A. and Saran, S., 2003, "Closely Spaced Footings on Geogrid-Reinforced Sand", *Journal of Geotechnical and Geoenvironmental Engineering, ASCE,* Vol. 129, No. 7, pp. 660-664.

Lawson, W.D, Jayawickrama, P.W., Wood, T.A., and Surles, J.G., 2013, “Pullout Resistance Factors for Steel Reinforcements Used in TxDOT MSE Walls”, *Proceedings of ASCE, GeoCongress 2013, San Diego,* CA, USA, pp. 44-53.

Lee, H.S., and Bobet, A., 2005, “Laboratory Evaluation of Pullout Capacity of Reinforced Silty Sands in Drained and Undrained Conditions”, *Geotech. Testing Journal* (ASTM), Vol. 28, pp. 370-379.

Lee, K. M. and Manjunath, V. R., 2000, "Experimental and Numerical Studies of Geosynthetic Reinforced Sand Slopes Loaded with a Footing", *Canadian Geotechnical Journal,* Vol. 37, No. 4, pp. 828- 842.

Lee, K. M. and Manjunath, V. R. and Dewaikar, D. M., 1999, "Numerical and Model Studies of Strip Footing Supported by a Reinforced Granular Fill-Soft Soil System", *Canadian Geotechnical Journal,* Vol. 36, No. 5, pp. 793- 806.

Ling, H. I., Pamuk, A., Dechasakulsom, M., Mohri, Y. and Burke, C., 2001, “Interaction of PVC Geomembranes with Cohesive Soils”, *Journal of Geotechnical and Geoenvironmental Engineering, ASCE,* Vol. 127, No. 11, pp. 950-954.

Liu, Y., Scott, J. D., and Sego, D. C., 1994, "Geogrid Reinforced Clay Slopes in a Test Embankment", *Geosynthetics International,* Vol. 1, No. 1, pp. 67-91.

Liu, C. N., Zornberg, J. G., Chen, T. C., Ho, Y. H. and Lin, B. H., 2009, "Behavior of Geogrid-Sand Interface in Direct Shear Mode", *Journal of Geotechnical and Geoenvironmental Engineering, ASCE,* Vol. 135, No. 12, pp. 1863-1871.

Lopes, M. L. and Silvano, R., 2010, “Soil/Geotextile Interface Behavior in Direct Shear and Pullout Movements”, *Geotechnical and Geological Engineering Journal, Springer,* Vol. 28, No. 6, pp. 791-804.

McKeen, R. G., 1992, ‘‘A Model for Predicting Expansive Soil Behavior’’, *Proceedings of International Conference on Expansive Soils, ASCE,* Dallas, TX, Vol. 1, pp. 1-6.

Miller, G.A. and Hamid, T.B., 2005, "Direct Shear Testing of Interfaces in Unsaturated Soil", *Proceedings of EXPERUS, International Symposium on Advances in Experimental Unsaturated Soil Mechanics, Trento, Italy*.

Mofiz, S.A., Sarkar, D.C., Rahman, S., Awall, M.R., Taha, M.R., and Hossain, M.K., 2005, "Instrumentation and Matric Soil Suction Measurement in a Decomposed Granite Soil Slope", *Advanced Experimental Unsaturated Soil Mechanics*, Tarantino, Romero & Cui (eds), Taylor and Francis Group, London, ISBN 0415383374, pp.527-532.

Mohiuddin, A., 2003, "Analysis of Laboratory and Field Pullout Tests of Geosynthetics in Clayey Soils", *Msc. Thesis, Louisiana State University*, USA, 121 pages.

Muhammad Ali, S., 1999, "Interface Frictional Characteristics of Non-Woven Geotextile- Sabkha and Sand Using Pullout Tests", *Msc. Thesis, King Fahad University*, SA, 303 pages.

Myers, B.K. and Scofield, D.H., 2006, "Providing Improved Dam Safety Monitoring Using Existing Staff Resources: Fern Ridge Dam Case Study", http://www.engineeredmonitoringsolutions.com/Automated_Dam_Safety_Monitoring_Fern_Ridge_Dam.pdf

Nam S., Gutierrez M., Diplas P., Petrie J., Wayllace A., Lu N. and Munoz J.J., 2009, "Comparison of Testing techniques and Models for Establishing the SWCC of Riverbank Soils", *Engineering Geology Journal*, Vol. 110, pp. 1-10.

Niemiec, J., 2005, "Investigation of Soil-Geosynthetic Interface Properties," *Msc. Thesis, West Virginia University*, USA, 238 pages.

Ou, F.L., Cox, W. and Collett, L., 1982, "Rock Aggregate Management Planning for Energy Conversation: Optimization methodology", *Transportation Research Record*, No. 872, pp. 63-69.

Palmeira, E.M., 2004, "Bearing Force Mobilization in Pullout Tests in Geogrids, Geotextiles and Geomembranes", *Journal of Geotextiles and Geomembranes*, Vol. 22, pp. 481-509.

Palmeira, E. M., 1987, "The Study of Soil-Reinforcement Interaction by Means of Large-Scale Laboratory Tests" *PhD Thesis, University of Oxford*, UK, 238 pages.

Pan H., Qing Y. and Pei-yong L., 2010, "Direct and Indirect Measurement of Soil Suction in the Laboratory", *Electronic Journal of Geotechnical Engineering*, Vol. 15.

Perera, Y.Y., Padilla, J.M. and Fredlund, D.G., 2004, "Measurement of Soil Suction In Situ using the Fredlund Thermal Conductivity Sensor", *Presentation Material for Mining and Waste Management Short Course, Vail, CO*.

Phoon, K-K. and Kulhawy F.H., 2008, Serviceability Limit State Reliability-Based Design", in: (Phoon, K-K. ed.): Reliability-Based Design in Geotechnical Engineering: Computations and Applications, Taylor & Francis, New York, NY, USA, pp.344-384.

Riccio, M., Ehrlich, M. and Dias, D., 2014, “Field Monitoring and Analyses of the Response of a Block-Faced Geogrid Wall Using Fine-Grained Tropical Soils”, *Geotextiles and Geomembranes*, Vol. 42, pp. 127-138.

Sako K., Kitamura R. and Fukugawa R., 2006, “Study of Slope Failure Due to Rainfall: a Comparison between Experiment and Simulation”, *Proceedings of 4th International Conference on Unsaturated Soils*, Carefree, AZ, 2, pp. 2324-2335.

Sayeed, M.M.A., Ramaiah, B.J., and Rawal, A., 2014, “Interface Shear Characteristics of Jute/Polypropylene Hybrid Non-Woven Geotextiles and Sand Using Large Size Direct Shear Test”, *Geotextiles and Geomembranes Journal*, Vol. 42, No.1, pp. 63-68.

Sawwaf, M. E. and Nazir, A., 2012, "Behavior of Eccentrically Loaded Small-Scale Ring Footings Resting on Reinforced Layered Soil", *Journal of Geotechnical and Geoenvironmental Engineering, ASCE*, Vol. 138, No. 3, pp. 376-384.

Sensor Products Inc., 2013, http://www.sensorprod.com/tactilus.php

Sharma, J. S., Fleming, I. R. and Jogi, M. B., 2007, “Measurement of Unsaturated Soil-Geomembrane Interface Shear Strength Parameters”, *Canadian Geotechnical Journal*, Vol. 44, No. 1, pp. 78-88.

Shiau, J. S., Merifield, R. S., Lyamin, A. V., and Sloan, S. W., 2011, "Undrained Stability of Footings on Slope", *International Journal of Geomechanics*, Vol. 11, pp. 381-390.

Shivashankar, R., and Jayaraj, J., 2013, “Behavior of Prestressed Gesyntehtic Reinforced Granular Beds Overlying Week Soil”, Indian Geotechnical Journal, Vol. 44, No. 1, pp. 26-38.

Subaida, E.A., Chandrakaran, S. & Sankar, N., 2008, “Experimental Investigations on Tensile and Pullout Behaviour of Woven Coir Geotextiles”, *Geotextiles and Geomembranes*, Vol. 26, pp. 384– 392.

Sitharam, T. G., Sireesh, S. and Kumar Dash, S., 2005, "Model Studies of a Circular Footing Supported on Geocell-Reinforced Clay", *Canadian Geotechnical Journal*, Vol. 42, No. 2, pp. 693-703.

Thanapalasingam, J. and Gnanendran, C. T., 2008, “Predicting the Performance of Foundations Near Reinforced Sloped Fills,” *the 12th International Conference of International Association for Computer Methods and Advances in Geomechanics*, India, pp. 3727-3734.

Tohari, A., Nishigaki, M. and Komatsu, M., 2007, "Laboratory Rainfall-Induced Slope Failure with Moisture Content Measurement", *Journal of Geotechnical and Geoenvironmental Engineering, ASCE*, Vol. 133, No. 5, pp. 575-587.

U.S. Department of Agriculture, Natural Resources Conservation Service, Web Soil Survey. http://websoilsurvey.sc.egov.usda.gov/default.aspx

Wescor Inc., 2001, HR-33T Dew Point Microvoltmeter Instruction/Service Manual. *Wescor Inc., Lohan, UT*.

Yang, G.Q., Liu, H., Zhou, Y.T., and Xiong,B.L., 2014, "Post-Construction Performance of a Two-Tiered Geogrid Reinforced Soil Wall Backfilled with Soil-Rock Mixture", *Geotextiles and Geomembranes*, Vol. 42, pp. 91-97.

Yoo, C., 2013, "Effect of Rainfall on Performance of Geosynthetic Reinforced Soil Wall using Stress-Pore Pressure Coupled Analysis ", *Geo-Congress 2013, ASCE, San Diego, CA* , pp. 566-573.

Yoo, H., Kim, H., and Jeon, H., 2007, "Evaluation of Pullout and Drainage Properties of Geosynthetic Reinforcements in Weathered Granite Backfill Soils", *Fiber and Polymers*, Vol. 8, pp. 635-641.

Zhang, Z., Farrag, K., and Morvant, M. J., 2003, "Evaluation of the Effect of Synthetic Fibers and Non-Woven Geotextile Reinforcement on the Stability of Heavy Clay Embankment", *Louisiana Department of Transportation and Development and Louisiana Transportation Research Center*, Baton Rouge, LA, USA, Final Report LTRC 736-99-0760.

Zhan, T.L.T., Ng, C.W.W., and Fredlund, D.G., 2006, "Instrumentation of an Unsaturated Expansive Soil Slope", *Canadian Geotechnical Journal*, Vol. 44, pp. 392-408.

Zornberg, J.G., Kang, Y., 2005, "Pullout of Geosynthetic Reinforcement with In-plane Drainage Capability", *Geosynthetics Research and Development in Progress, Eighteenth Geosynthetic Research Institute Conference* (GRI-18), Austin, Texas, January 26.

APPENDIX I

PRELIMINARY STABILITY ANALYSIS FOR REDUCED-SCALE AND LARGE-SCALE EMBANKMENT MODELS

Several preliminary slope stability analyses were carried out using FLAC/Slope with various types of loading, soil and interface properties, slope angles and geotextile locations to determine the location and geometry of critical failure plane. Figures A-1 and A-2 show sample initial models that were used to design reduced-scale embankments that were set up and tested in this study.

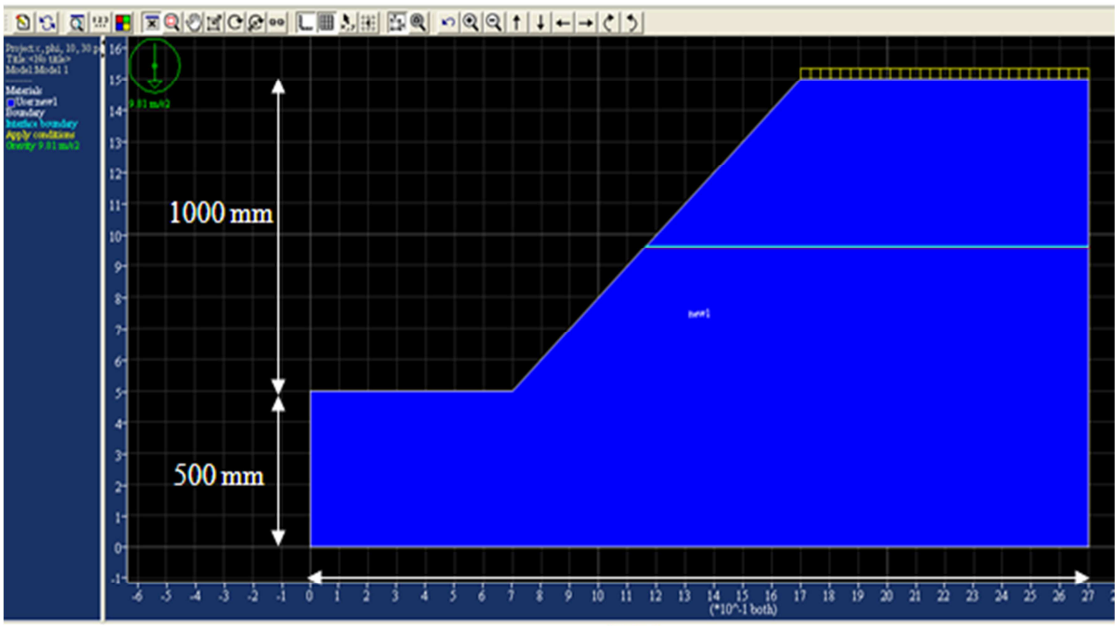

(a)

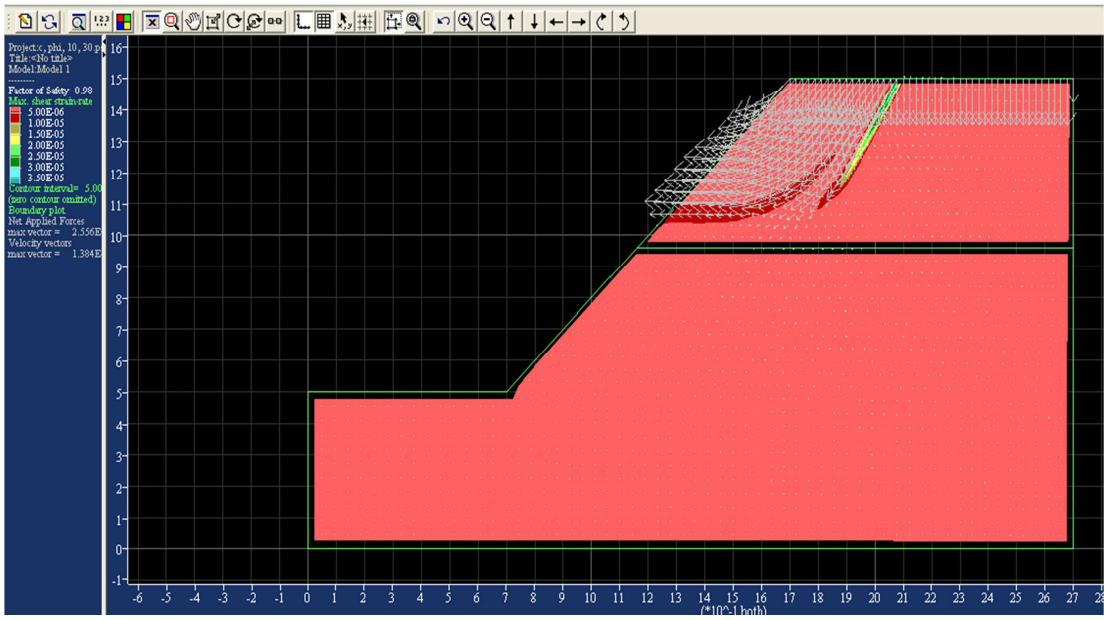

(b)

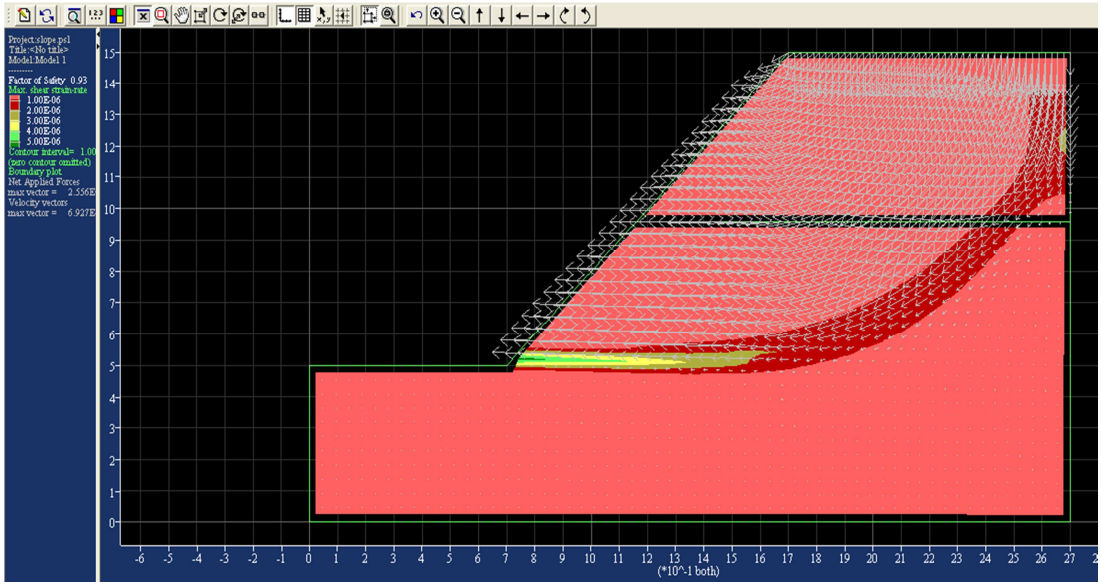

(c)

Figure A-1. Stability analysis of a 45° reduced-scale reinforced embankment slope; (a) Model at the end of construction, (b) Slip plane geometry in the embankment with cohesion = 10 kPa and friction angle = 30°, (c) Slip plane geometry in the embankment with cohesion = 30 kPa and friction angle = 5°

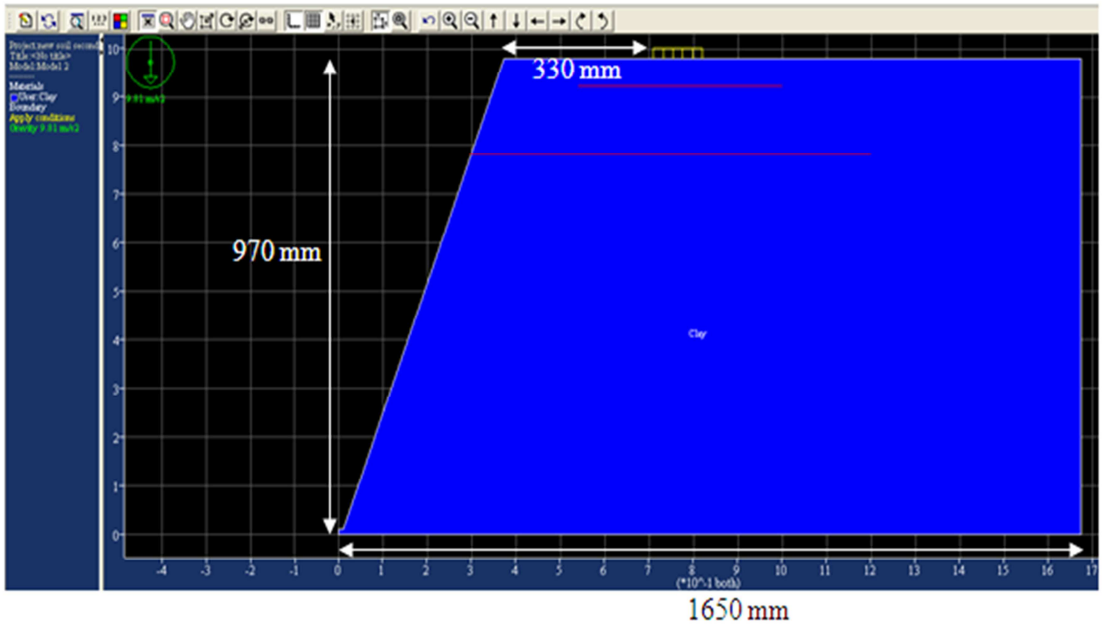

(a)

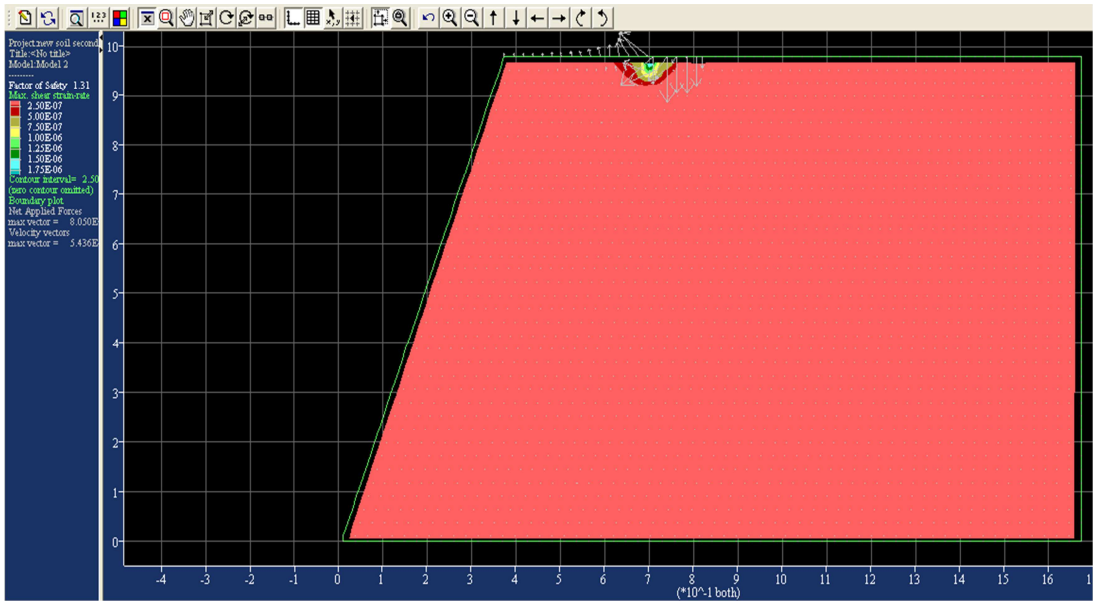

(b)

Figure A-2. Stability analysis of a 69.5° reduced-scale reinforced embankment slope; (a) Model at the end of construction, (b) Slip plane geometry in the embankment with cohesion = 20 kPa and friction angle = 27°

Various test cases were also modeled for outdoor reinforced embankments to find the appropriate height for the test box. The models were different from one another in the location of loading beam, geotextile arrangements and geometry of embankment (Figure A-3).

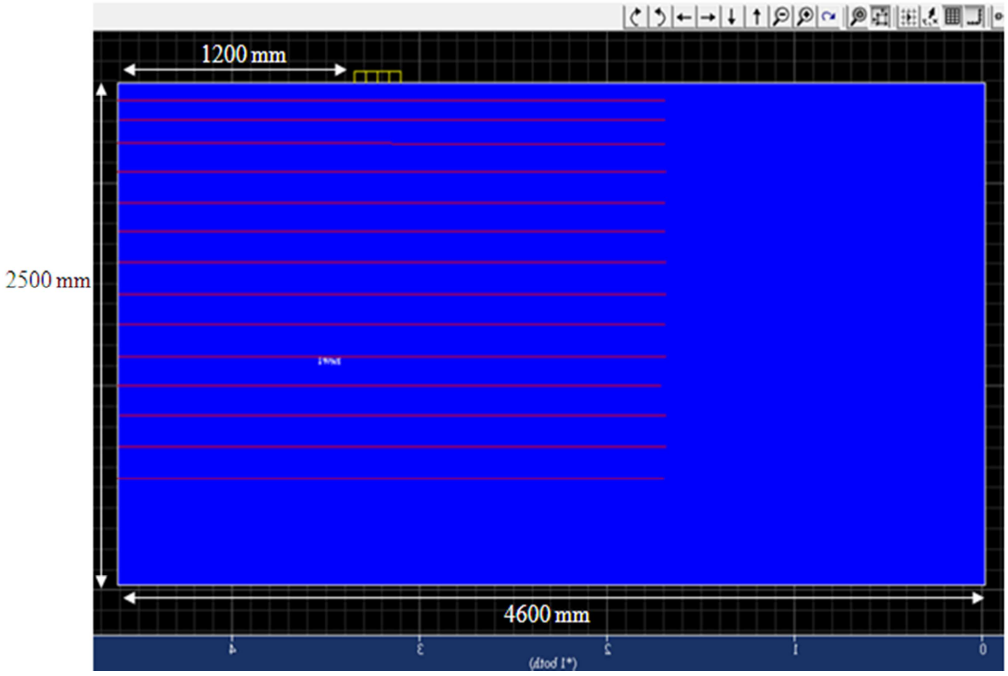

(a)

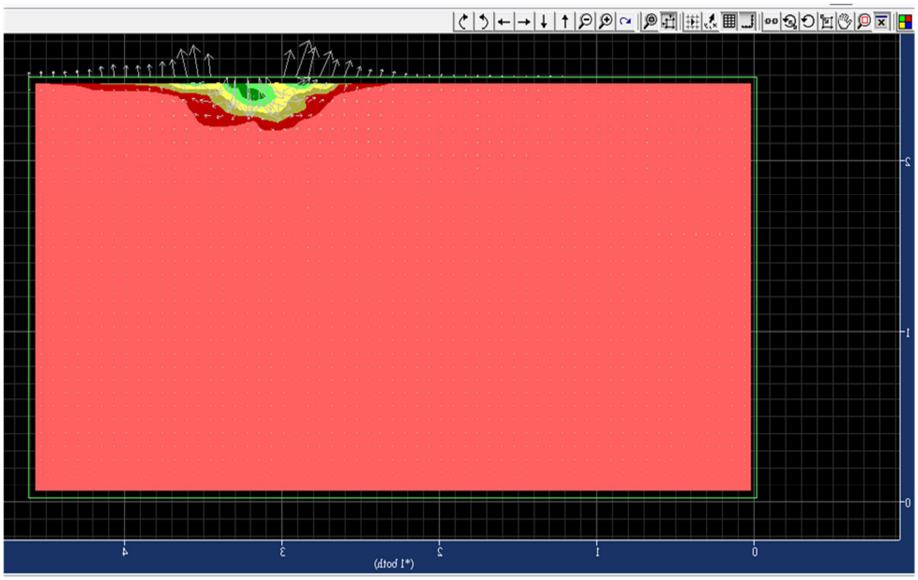

(b)

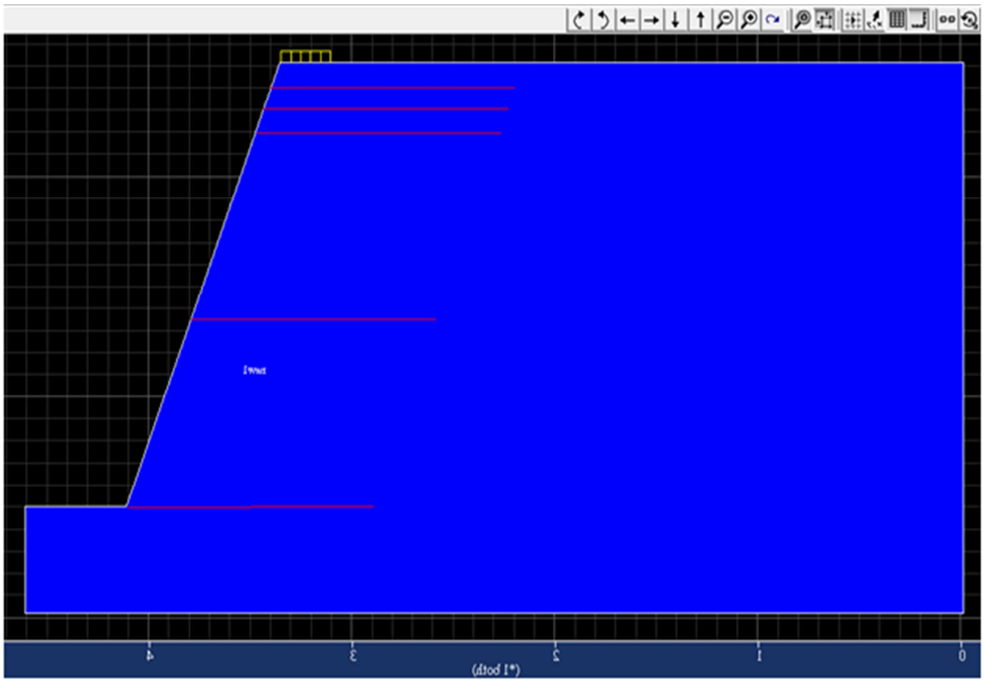

(c)

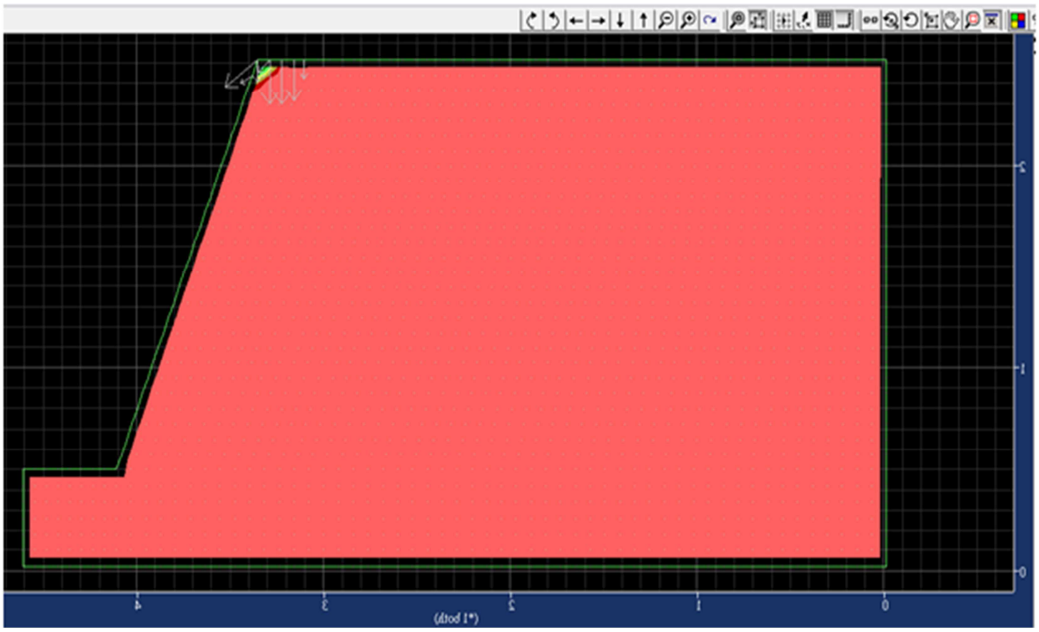

(d)

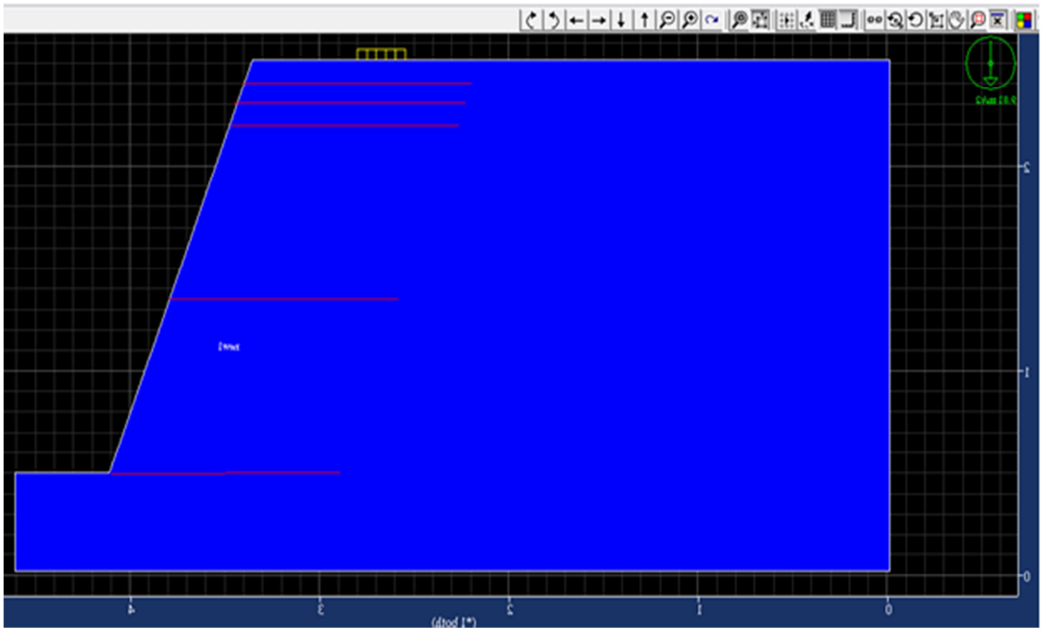

(e)

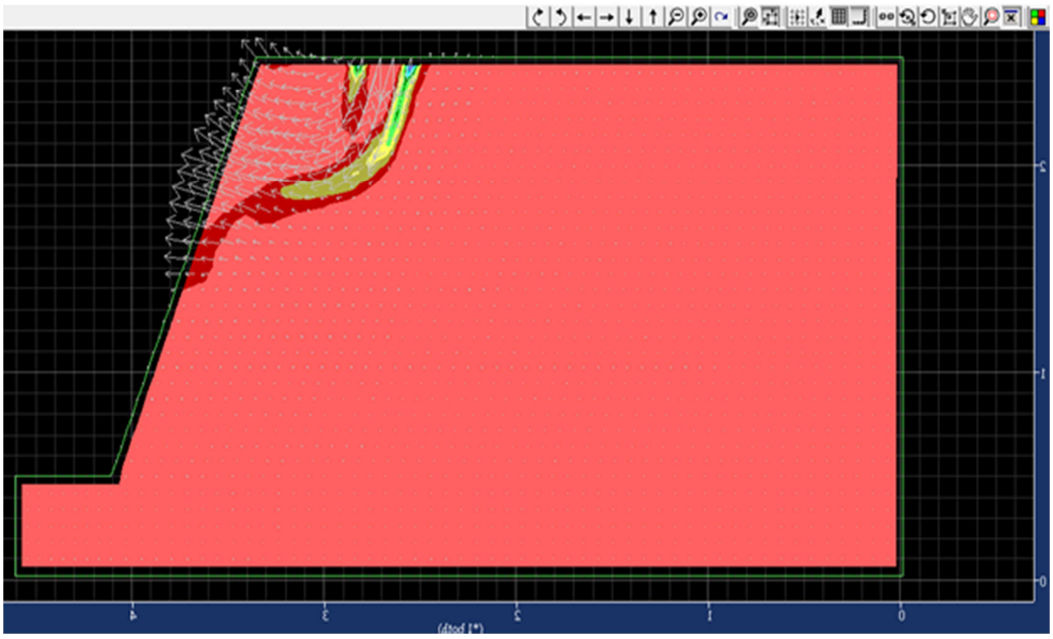

(f)

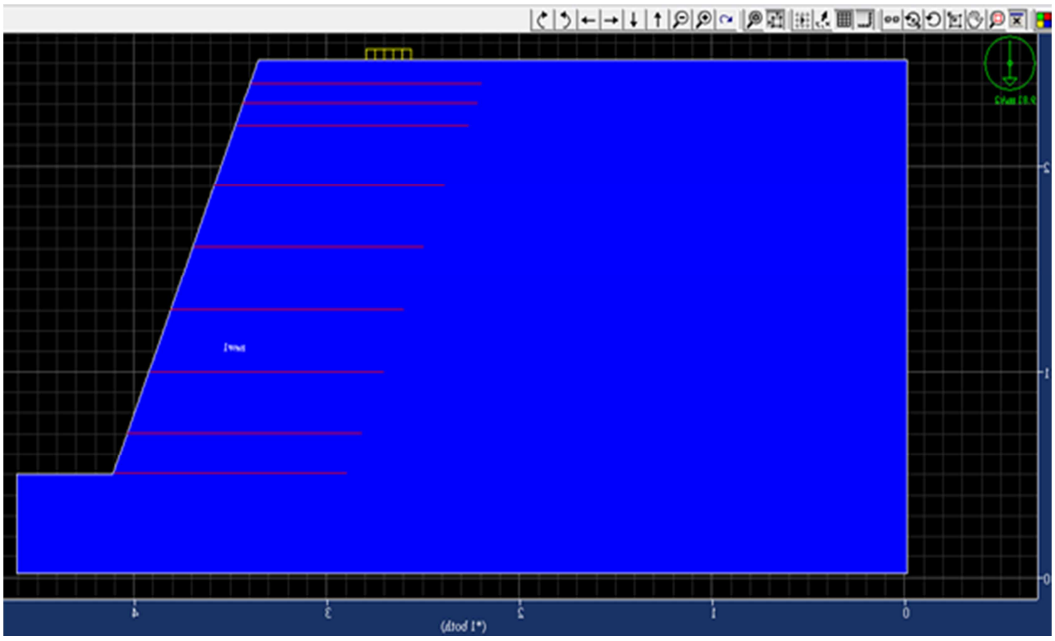

(g)

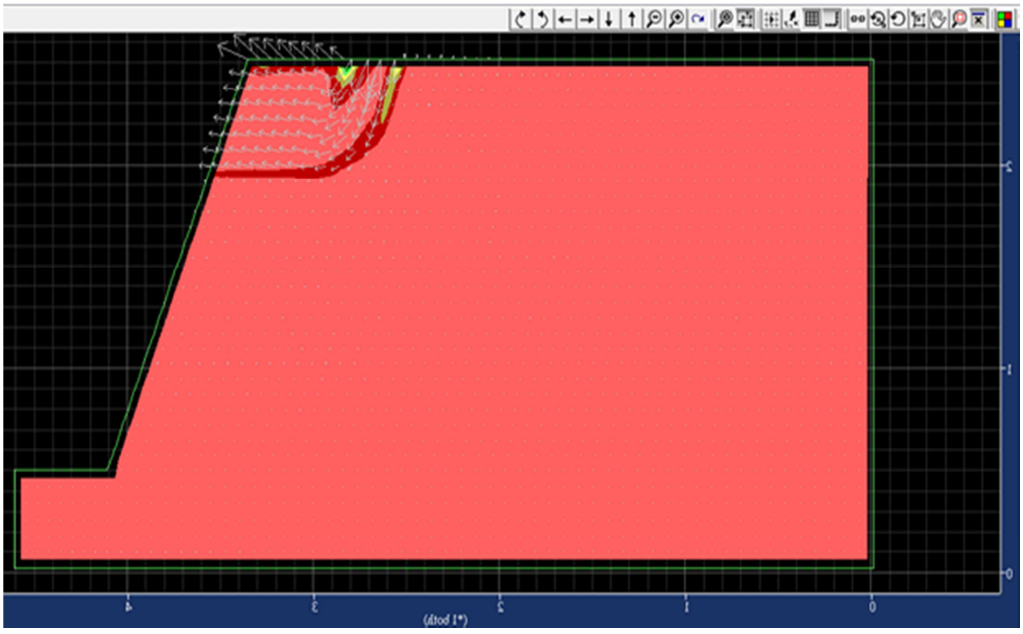

(h)

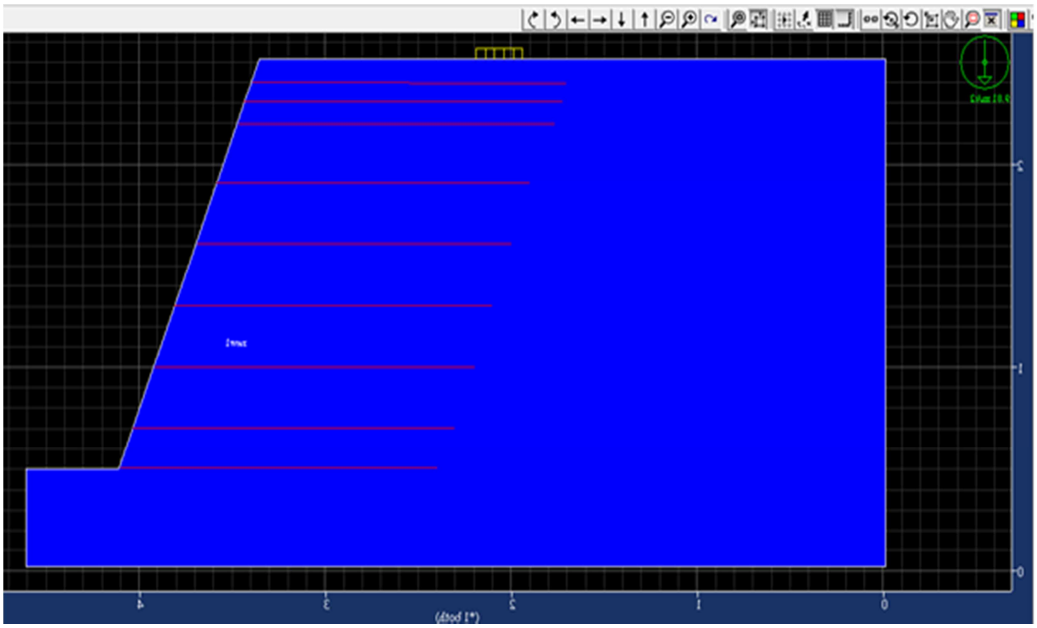

(i)

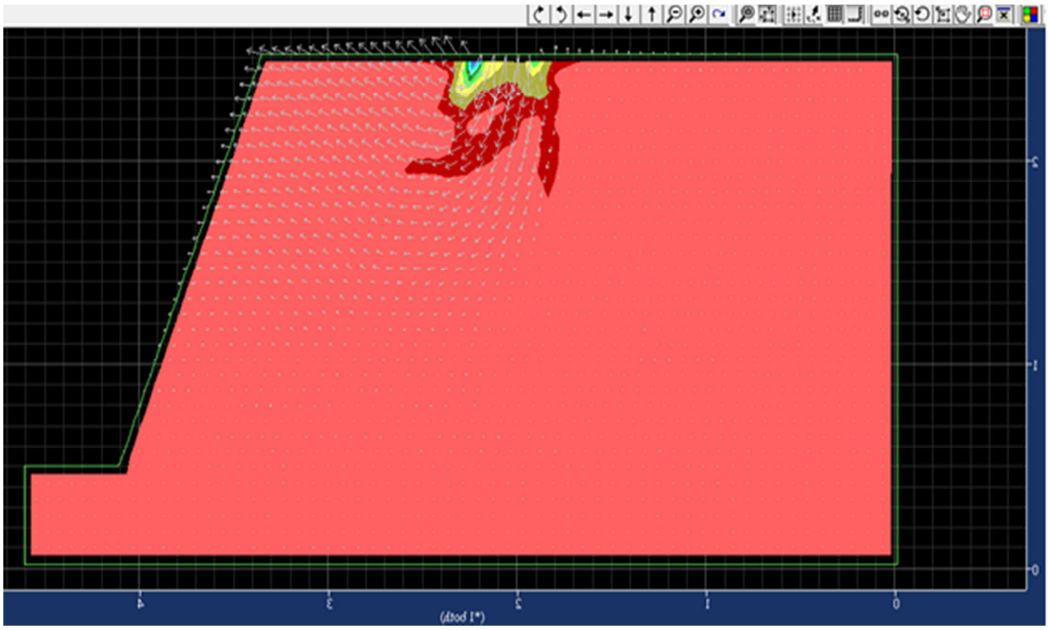

(j)

Figure A-3. Stability analysis of a MSE wall and embankment models (cohesion = 60 kPa, friction angle = 25°); (a)-(b) MSE wall at the end of construction and slip plane geometry (uniform vertical geotextile spacing = 150 mm), (c)-(f) Embankment at the end of construction and slip plane geometry (non-uniform vertical geotextile spacing: 100 mm at top and 850 mm at bottom), (g)-(j) Embankment at the end of construction and slip plane geometry (non-uniform vertical spacing = 100 mm at top and 300 mm at bottom)

At the beginning of the outdoor project, it was decided to design and build the test box using steel frames which was changed to reinforced concrete after more investigations. Frame 3-D program was utilized to model and design preliminary steel outdoor test box (Figure A-4a) and its maximum deflection was found to be 1.7 mm (0.067 inch) (Figure A-4b). Table A-1 summarizes the design output of the box.

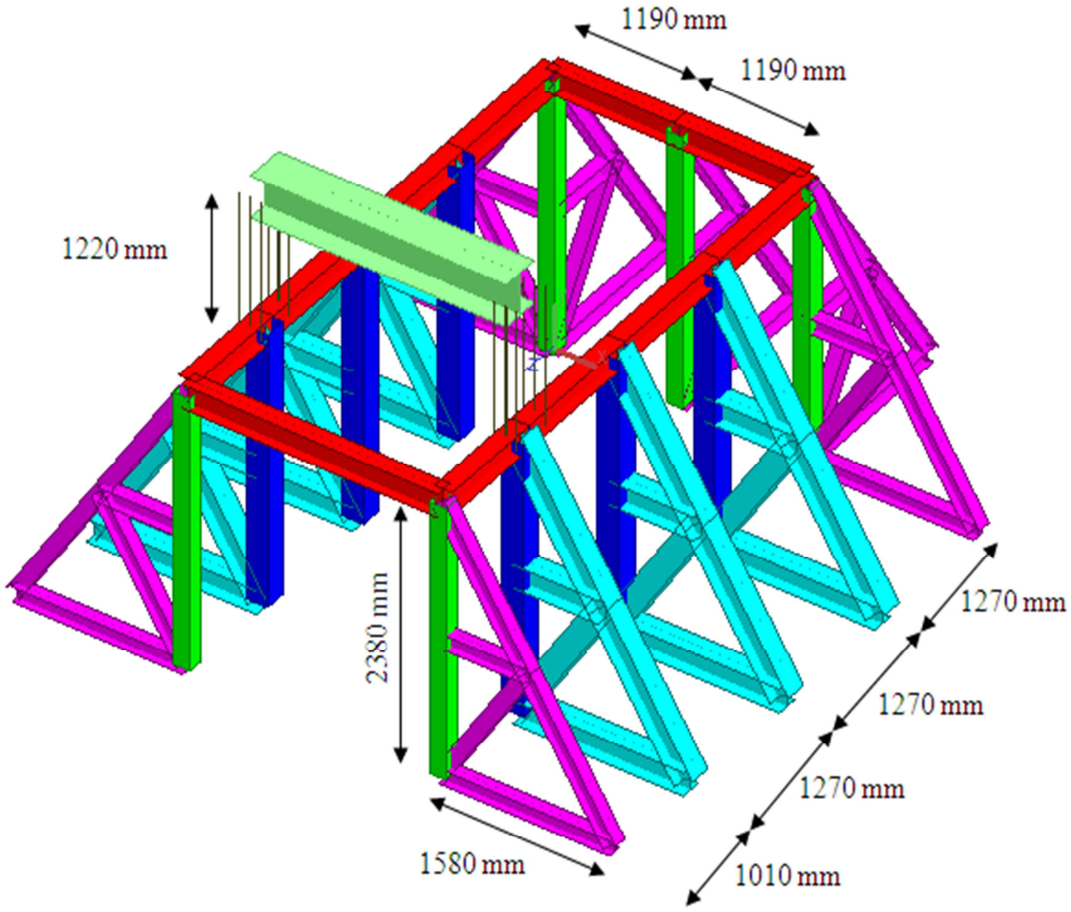

(a)

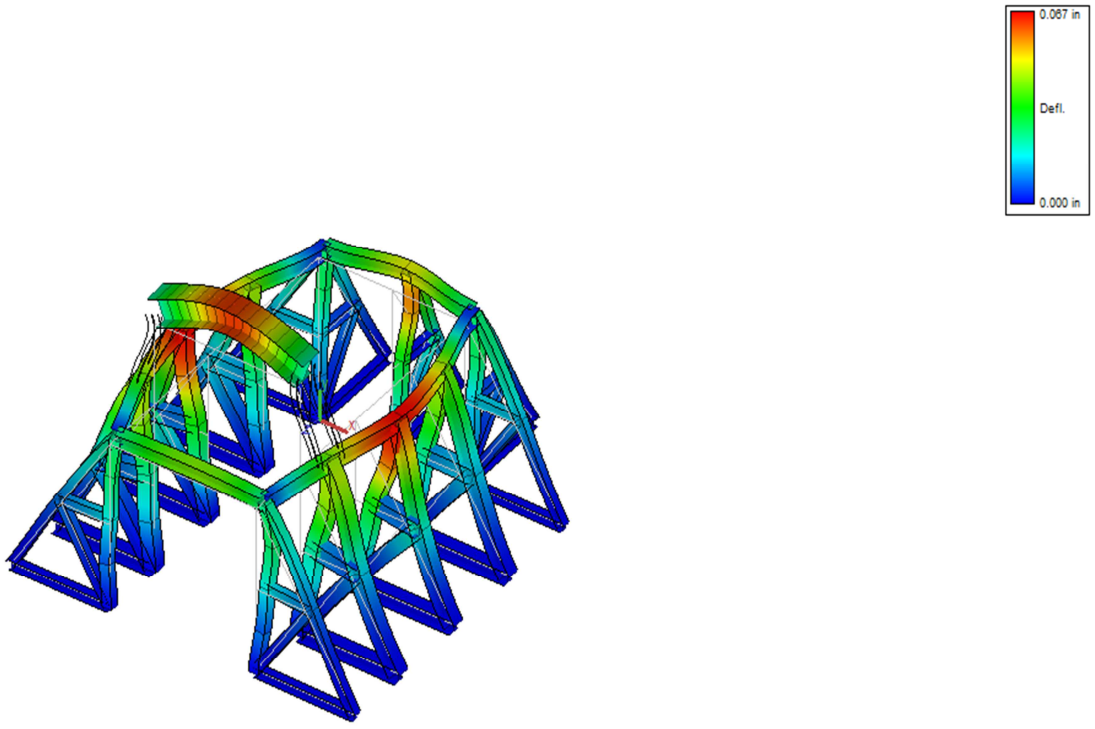

(b)

Figure A-4. Modeling outdoor test box in Frame 3-D program, (a) Box dimensions, (b) Box deflections

Table A-1. Results of structural design for outdoor test box

Member color/name	**Profile section**
Red	W 8×28
Green	TS 6×6×5/16
Chromatic blue	TS 8×8×5/16
Light blue	W 8×31
Pink	W 5×19
Reaction beam	W 14×120
Frame columns	Double C 15×50 + 4mm plate welded in flange and 2 mm plate in web.